Bacterial indole-3-acetic acid production: a key mediator of plant-microbe interactions between *Phaseolus vulgaris* and the foliar epiphyte *Pantoea agglomerans* 299R

by

Tracy Kathleen Powell

A dissertation submitted in partial satisfaction of the

requirements for the degree of

Doctor of Philosophy

in

Plant Biology

in the

Graduate Division

of the

University of California, Berkeley

Committee in charge:

Professor Steven E. Lindow, Chair
Professor Lew Feldman
Professor Ellen Simms

Spring 2011

Bacterial indole-3-acetic acid production: a key mediator of plant-microbe interactions between *Phaseolus vulgaris* and the foliar epiphyte *Pantoea agglomerans* 299R

by Tracy Kathleen Powell

Abstract

Bacterial indole-3-acetic acid production: a key mediator of plant-microbe interactions between *Phaseolus vulgaris* and the foliar epiphyte *Pantoea agglomerans* 299R

by

Tracy Kathleen Powell

Doctor of Philosophy in Plant Biology

University of California, Berkeley

Professor Steven E. Lindow, Chair

The phyllosphere epiphyte *Pantoea agglomerans* 299R synthesizes indole-3-acetic acid (IAA), an important plant hormone. IAA production was previously shown to confer a small but significant fitness advantage to *Pa*299R cells inoculated onto bean (*Phaseolus vulgaris*) leaves, but the mechanism by which bacterial IAA exerts this effect is unknown. In this work, we investigated several hypotheses regarding how bacterial IAA enhances the growth and survival of leaf epiphytic microbes such as *Pa*299R.

We first tested the hypothesis that bacterial IAA enhances the availability of plant sugars to phyllosphere bacteria, thereby relieving carbon limitation of bacterial growth on the leaf surface (Chapter Two). We inoculated sucrose- and fructose-inducible biosensor bacteria onto bean leaves, and investigated the effects of auxin availability on sugar sensing. We manipulated auxin availability in two ways: we compared sugar sensing by wild-type *Pa*299R (IAA^+) biosensors to that of the isogenic, IAA^- mutant *Pa*MX149; and sugar sensing by *Pa*MX149 bacteria inoculated with exogenous NAA to bacteria inoculated without NAA. The presence of auxin—whether endogenously synthesized or exogenously applied—was associated with a significant decrease in sucrose sensing, and a small but significant increase in fructose sensing. Additionally, *in vitro* assays demonstrated that *Pa*299R initiates growth more rapidly when using glucose or fructose as a sole carbon source than when using sucrose. Together, this suggests that IAA biosynthesis may function as a resource conversion strategy to enhance carbon acquisition and rapid bacterial growth in an oligotrophic, environmentally dynamic phyllosphere.

In addition to its role in carbon acquisition, we also investigated several alternative hypotheses of bacterial IAA production in the phyllosphere (Chapter Three). We demonstrated that bacterial IAA exerts no measurable impact on resistance of *Pa*299R to environmental stress. We also found that bacterial IAA does not affect the autofluorescence of substrate leaf epidermal cells that support large bacterial aggregates of *Pa*299R. Finally, we describe unsuccessful efforts to determine the role of bacterial IAA in another foliar epiphyte and compatible bean pathogen, *Pseudomonas syringae* pv. *syringae* B728a.

For Sky,
who never got to finish his;

and for my grandmother,
who doubtless would have preferred great-grandchildren.

Table of Contents

Acknowledgments

In the darker, more pessimistic moments of producing a dissertation, the whole enterprise seems cruelly solitary. But here at the end, with the completed document printed out and stacked at my elbow, relief and hindsight are conspiring to offer a rosier (and more accurate) perspective: I can't help but reflect on the many, many people whose intellectual and emotional support sustained me through the past eight years. I'm very pleased to have this space to acknowledge their contributions, and offer my thanks.

Perhaps the greatest influence on my research and scientific development was my graduate mentor and committee chair, Prof. Steve Lindow, whose breadth of knowledge, attention to experimental detail, and years of thoughtful feedback have guided my research since the beginning. Even as my research veered towards narrow, abstract scientific questions, he continually exposed me to wide range of other research—by organizing field trips to count walnuts and pick apples for his applied research projects, by discussing kaleidoscopically diverse microbiological research in his journal clubs and academic courses, and by maintaining exceptionally broad programs of ecology, plant pathology, and applied agricultural research in the lab. This constant churning of outside ideas and influences helped make science seem vital, even when the narrowness of my individual topic threatened to stagnate my thinking. And of course, he is uniquely generous among professors in acknowledging the needs of the body as well as the mind: the research presented here was fueled largely by a bottomless supply of bulk caramels, mixed nuts, and fun-sized candy bars provided *gratis* by Steve. (It may seem like a trivial kindness, but when awakening on the graduate lounge couch for a 4am timepoint, there's nothing quite like a consolatory fistful of M&Ms to make life seem *almost* worth living.) And to counteract all those snackborne calories, he was wonderfully proactive about organizing regular hikes and snowshoe trips; in addition to furthering my scientific education, I must therefore also thank him for making sure I ventured beyond the lab and enjoyed California's spectacular terrain during my time as a graduate student.

I'd also like to thank my other doctoral committee members—Prof. Lew Feldman, for his thoughtful insights into auxin biology, as well as for setting an inspiring example of pedagogical excellence; and Prof. Ellen Simms, for her ecological expertise and crucial instruction in analyzing quantitative data. Their experimental suggestions and feedback on this manuscript significantly improved the finished work. It was my privilege to work with these two scholars, whose time and efforts helped me to become a more rigorous thinker and a more confident, thoughtful scientist.

My comrades-in-arms in the Lindow lab have provided the most immediate, day-to-day source of technical knowhow, critical feedback, and professional support throughout my graduate career. For their collaboration and scientific expertise over the years, I'd therefore like to thank Adrien Burch, Clelia Baccari, Scott Blitch, Subhadeep Chatterjee, Juliana Cho, Kristen DeAngelis, Glenn Dulla, Kevin Hockett, Renee Koutsoukis, Karyn Newman, Audrey Parangan-Smith, Beatriz Quinones, Eugenia Ramos, Sky Rashby, Betsy Roberts, Russell Scott, Ryan Shepherd, Alessandra Souza, Nian Wang, and Gale Wichmann.

Beyond the intellectual and professional support lent by my committee members and fellow labmates, many others within the Berkeley community have also helped me grow, both professionally and intellectually. Oficially, graduate school hinges on academic research, but these individuals furnished me with a parallel education that went beyond the laboratory and extended into the broader disciplines of teaching and communicating about science. I consider these lessons as important to my career as anything I accomplished at the bench. For helping expand my scientific abilities beyond the laboratory, I'd therefore like to thank Professors Mike Freeling and Peggy Lemaux, who both gave me opportunities to talk about science with individuals from outside the research community, as did my fellow biology instructors in the San Quentin Prison Education Program. Additionally, my friends and comrades at the *Berkeley Science Review* have provided some of the most constructive and stimulating discussions I've ever had about science, as well as critical feedback that allowed me to grow as a writer and editor.

Alongside these colleagues, a host of friends have conspired to keep me sane throughout the sometimes satisfying, often demoralizing travails of graduate school. I would not have survived intact without Marie Abe and Jennifer Callaghan, each of whom logged more trans-continental air miles and late-night, long-distance telephone hours in service to our friendship than I'll ever be able to thank them for; Eugenia Ramos, my "work wife" and scientific sister-in-arms, whose daily companionship and support made it worth going to lab in the morning; and Betty Gilbert, international woman of (mycological) mystery, fellow connoisseur of trashy media, and stalwart traveling companion.

It would take a tome of dissertative proportions to thank everyone properly, but I must at least mention Scott Blitch, Gale Wichmann, Sarah Brown, and Kamal Gandhi, who have been not only colleagues but also generous friends; and also Sasha Clayton, Howard Connell, Kim Hooper, and the assorted housemates, landlords, and neighbors who made Berkeley feel like home over the past eight years. My thanks to Adam Bliss and Lara Mercurio (*et al.*) for hosting Thursday Game Nights, and to Andrew Main and Bryan Vodden (*et al.*) for hosting Friday Geek Nights—you folks made the rest of the week worth slogging through. Thanks also to my "first-year" PMB cohort for sharing the foxhole with me these many long years—particularly Karelyn Cruz Martinez, Shannon Peters Schechter, Thomas Sharpton, Jenne Stonaker, Phoi Tran, Ian VanTrump, and Val Wong. For their friendship, support, and advice over the years, I also thank Kam Woods, Wendy Hansen, and my honorary aunts Kathleen Donelli and Maureen Mitchell.

Finally, I'd like to thank my family. In addition to their material and financial support while I finished writing this dissertation, my dad and stepmom have been an unstinting source of love and encouragement. They're at the core of whatever resilience I've developed through all of this, and I'll never be able to thank them enough. My brothers Teague and Ryan and sister Mahriah were also very supportive over the years, and I only wish that I could have come home to visit them (or had them out to visit me) more often. I love you all, and I would never have been able to do it without you.

Chapter I. Introduction

A remarkable range of plant-associated microorganisms is capable of synthesizing the auxin indole-3-acetic acid (IAA) (Spaepen *et al*., 2007; Patten *et al.*, 1996). When expressed endogenously by the plant, this important growth hormone has been implicated in a variety of fundamental plant developmental processes, including cell growth and division (Tromas *et al*., 2010), vascularization (Avsian-Kretchmer *et al*., 2002), organ initiation (Benkova *et al*., 2003; Reindhardt *et al*, 2000), apical dominance, and various tropisms, (reviewed in Woodward & Bartel *et al*., 2005). When expressed exogenously by a microbial partner, IAA's effects may be equally diverse—but in many cases are less well understood. In this dissertation, I have therefore attempted to characterize *why* microbes produce IAA. What, exactly, does microbial IAA do to the host plant, and how does this benefit the bacteria? Due to the taxonomic and ecological diversity of IAA-producing microbes, I have generally limited the scope of my investigation to IAA production by the gram-negative, plant foliar epiphyte *Pantoea agglomerans*.

Rationale for study of bacterial IAA

The adaptive function of bacterial IAA deserves attention for several reasons. On an immediate, practical level, microbial IAA production has important agricultural implications—both positive and negative. This renders the broader phenomenon of bacterial IAA important to economic productivity, food security, and agroecology.

For example, IAA plays an important role in the disease etiology of many agriculturally important pathogens (reviewed in Kazan *et al.*, 2009), including *Agrobacterium tumefaciens* (Gafni *et al.*, 1995), *Pseudomonas savastanoi* (Iacobellis *et al*., 1994), *Pantoea agglomerans* pv. *gypsophilae* (Barash *et al.*, 2009), *Pseudomonas syringae* pv. *syringae* (Mazzola *et al.*, 1994), as well as many pathogenic fungi (Maor *et al*., 2004; Gravel *et al*., 2007). When produced by such organisms, IAA may help suppress plant defense responses (Shinshi *et al*., 1987; Jouanneau *et al*., 1991; Navarro *et al.*, 2006), initiate and shape the architecture of plant galls (Lee *et al.*, 2009; Gafni *et al.*, 1995), and/or contribute to the pathogen's epiphytic fitness on the plant surface (Manulis *et al*., 1998). In addition to mediating such plant-pathogen interactions, bacterial IAA may also act as an endogenous regulatory signal, coordinating expression of bacterial virulence factors (Yang *et al*., 2007; Mazzola *et al.*, 1994) or enhancing resistance to environmental stress (Bianco *et al*., 2006; Bianco *et al*., 2009). Due to its importance in pathogenesis, a better understanding of bacterial IAA production could offer new strategies for combating plant disease.

In contrast to its role in disease, IAA can actually be beneficial to plants when presented by microbial partners in other ecological contexts. In particular, inoculating crops with IAA-producing plant growth promoting rhizobacteria (PGPR) can enhance agriculturally important traits such as disease resistance (Van Wees *et al*., 2008; Conrath *et al*., 2006); lateral root and root hair formation (Dobbelaere *et al*., 1999; Patten *et al*., 2002); uptake of nitrate and other mineral ions (Mantelin *et al.*, 2004); and resistance to drought, salt, and other abiotic stresses (Yang *et al*., 2008). Such gains aren't due solely to IAA—in addition to affecting plant growth by secretion of IAA and other phytohormones, PGPR can suppress disease (by stimulating plant

systemic resistance, competitively excluding pathogens, or secreting antibiotic compounds) and biofertilize host plants (by enhancing the availability or plant uptake of N, P, Fe, or other minerals) (Van Wees *et al.*, 2010; Dodd *et al*, 2010). Bacterial IAA production is therefore only one component of a complex, additive phenomenon (Bashan *et al*., 1997). It is, however, a very important component: Khalid *et al*. (2004) found that auxin production was a powerful predictor of a PGPR strain's ability to promote wheat yields, and more than 80% of members of some important PGPR genera produce auxin (Ahmad *et al.*, 2008).

Like these ectorhizal PGPR, root-nodulating bacteria commonly produce IAA (Spaepen *et al*., 2007). Together with regulation of plant auxin transporters such as PIN proteins and AUX1 in infected tissue, microbial IAA is believed to help coordinate the initiation and architecture of nodules (Mathesius *et al.*,2008); this function has been demonstrated in both leguminous (Camerini *et al*., 2008) and actinorhizal nodules (Perrine-Walker *et al*., 2010). Mycorrhizal fungi have also been reported to synthesize IAA (Ek *et al*., 1983; Splivallo *et al*., 2009).

Thus, in both ectorrhizal plant growth promotion and the more intimate chemical exchanges of root nodulation and mycorrhizal colonization, bacterial IAA plays an important role in beneficial plant-microbe interactions. A better understanding of how to manipulate these auxin-mediated interactions could therefore suggest new, reduced-input strategies for fertilization, pest and pathogen control, and yield enhancement (Berg, 2009). Furthermore, IAA-producing PGPR have been shown to enhance plant extraction of a variety of heavy metal contaminants (Khan *et al*., 2009), indicating that IAA production by beneficial bacteria may foster enhanced remediation strategies for toxic compounds, as well as agricultural improvements.

Based on auxin's important roles in both plant pathogenesis and plant growth promotion, the practical incentive for researching bacterial IAA production is clear. However, in many of the examples mentioned above, IAA production is carried out by pathogens or root-associated bacteria—model systems which are already active areas of study. In the research described in this dissertation, I have focused instead on IAA production by foliar epiphytes, a class of organisms in which the effects of IAA production are less well understood; the direct agricultural utility of the phenomenon has therefore not been established.

Nonetheless, a case can be made for the importance of studying the auxin-mediated interactions of foliar epiphytes. Competitive exclusion of foliar pathogens by non-pathogenic phyllosphere bacteria is an established method of disease control (Lindow, 1987); to the extent that IAA facilitates establishment of epiphytic bacterial communities on leaf surfaces, it could represent an agriculturally useful microbial biodefense trait. Conversely, IAA production by some foliar pathogens has been shown to specifically facilitate growth during the epiphytic colonization stage (Manulis *et al*., 1998). Understanding how IAA affects the fitness of both desirable and undesirable epiphytic microbes could therefore assist in manipulating foliar populations of bacteria to achieve desirable agricultural outcomes.

More broadly, leaf epiphytic *P. agglomerans* may prove a useful model to understand the function of IAA in other plant-microbe systems, including those in the rhizosphere or pathogenic systems. Previous work in the Lindow lab established an extensive preliminary dataset regarding the production, regulation, and adaptive importance of IAA production by *Pa*299R in the phyllosphere of the common bean (*Phaseolus vulgaris*). My research capitalizes on these earlier

efforts, further extending our knowledge of this model system for IAA-mediated plant-microbe interactions.

Finally, the rationale for studying bacterial IAA production extends beyond the immediate practical imperatives of translational research. It is an intriguing phenomenon in its own right, and understanding it better could have interesting implications in the fields of microbial ecology. In one sense, IAA appears to function as an inter-kingdom signal: although strict definitions limit the term "signaling" to noncoercive social interactions such as quorum sensing (Diggle *et al*., 2007), generous definitions of "chemical signaling" include the deployment of bacterial chemicals to coerce responses from individuals of another species or kingdom (Atkinson *et al*., 2009; Pacheco *et al*., 2009; Hughes *et al*., 2008). In this broader sense, bacterial IAA may be an intriguing example of how bacteria deploy chemical messages to manipulate plant signal cascades and elicit favorable responses from the host plant. IAA could also prove an interesting example of how small diffusible molecules function in intra- and inter-specific competition between microbes on the leaf.

Auxin signaling in plants

In order to delve into how bacterially derived IAA might be capable of impacting plant behavior, it is worth reviewing the general details of how plants respond to auxin. Briefly, in plants, IAA triggers two important response pathways (Figure 1). The first is mediated by Auxin-Binding Protein 1 (ABP1), and is still poorly understood; the second, more intensively studied pathway is mediated by Transport Inhibitor Resistant 1/Auxin F-Box (TIR1/AFB) protein.

Upon application of IAA, early responses occur primarily at the plant cell surface: IAA activates Auxin-Binding Protein 1 (ABP1) proteins at the plasma membrane, which in turn stimulates activity of proton ATPases (Tromas *et al*., 2010). As these enzymes pump protons into the extracellular space, the resulting drop in apoplastic pH facilitates cell wall loosening, as cell wall expansins with low pH optima begin to catalyze hydrolysis or lateral slippage of the cross-linking polysaccharides that immobilize cellulose microfibrils (Cosgrove, 2000; Sanchez-Rodriguez *et al*., 2010). As this cell wall remodeling occurs, inward-rectifying K^+ channels are activated at the plasma membrane in order to accommodate apoplastic acidification; in turn, this activates aquaporins, driving water uptake into the cell and providing increased turgor pressure to fuel cell expansion (Tromas *et al*, 2010). By 20-30 minutes after IAA exposure, further cell wall remodeling occurs and soluble sugars and xyloglucans begin to accumulate in the apoplast (dos Santos *et al.*, 2004; Hoson, 1993; Badescu *et al.*, 2006; Sanchez-Rodriguez *et al.*, 2010). ABP1 is therefore believed to orchestrate short-term, plasma membrane-localized responses to IAA—particularly the combined cell wall loosening and turgor-driven cell expansion of the "acid growth response," as described above. ABP1 may also help to regulate cell division (Chen *et al.*, 2001; David *et al*., 2007) and downstream expression of auxin-responsive genes (Braun *et al*., 2008), but these putative functions remain poorly understood.

As ABP1-mediated events unfold at the cell surface, IAA also crosses the plasma membrane—either by passive diffusion or via the auxin influx transporter AUX1. Once inside the cell, a second auxin response pathway is engaged: IAA binds and stabilizes the cytoplasmic auxin receptor TIR1, which in turn functions as part of the ubiquitin E3 ligase complex SCF^{TIR1}

(Dharmasiri *et al*., 2005; Kepinski *et al.*, 2005). In the presence of IAA, SCF^{TIR1} ubiquitinates AUX/IAA repressor proteins, targeting them for degradation by the 26S proteasome. Upon AUX/IAA degradation, Auxin Response Factors (ARFs) are free to initiate transcription of auxin-inducible genes at promoter sites characterized by Auxin Response Elements (AREs) (Chapman *et al*., 2009). The TIR1-mediated auxin response is therefore responsible for orchestrating changes in gene expression in the plant nucleus (though, as described above, downstream signaling from ABP1 may also exert some influence on gene regulation).

Interestingly, from a single, generic hormone stimulus, the TIR1-mediated signal cascade generates a surprisingly broad array of developmentally and tissue-specific responses. Differential spatial and temporal regulation of genes within the functional signaling classes (TIRs, AUX/IAAs, and ARFs) is believed to generate the diversity and specificity of IAA responses. In addition to TIR1/AFB, for example, an additional four F-box genes can act as auxin receptors in *Arabidopsis thaliana*; the gene family of Aux/IAA repressors contains 29 members, and the ARF gene family contains 23 (Lokerse *et al*., 2009). These same mechanisms that generate temporally, developmentally, and tissue-specific reactions to auxin stimuli are also presumed to generate the diversity of plant responses to IAA provided by microbial partners at different times, locations, and concentrations.

A brief introduction to bacterial IAA production on plant surfaces

The bacterial species investigated in this research, *P. agglomerans* 299R, is only one of a large, taxonomically and ecologically diverse group of auxin-producing bacteria (excellently reviewed in Spaepen *et al*., 2007). As described above, IAA-producers range from gall-forming pathogens such as *Pseudomonas savastanoi* (Iacobellis *et al*., 1994) and *Pantoea agglomerans* pv. *gypsophila* (Barash *et al*., 2009), both of which produce IAA directly; and *Agrobacterium tumefaciens* (Akiyoshi *et al*., 1983), in which IAA production is encoded on the Ti plasmid; to phytopathogens such as *Pseudomonas syringae* pv. *syringae* (Glickmann *et al*., 1998). Beneficial IAA-producers include the majority of PGPR (Ahmad *et al.*, 2008), including the model species *Pseudomonas fluorescens* (Kochar *et al.*, 2011), *Azospirillum brasilense* and *Enterobacter cloacae*; and root-nodulating bacteria such as *Rhizobium*, *Bradyrhizobium*, and *Frankia* (Perrine-Walker *et al.*, 2010; Spaepen *et al*., 2007).

Though bacterial biosynthesis of IAA can occur by a variety of pathways, the hormone is generally synthesized from a tryptophan precursor (Figure 2). Two pathways are particularly relevant to this research: the indole-3-acetamide (IAM) and indole-3-pyruvate (IPyA) pathways. In the IAM pathway, the tryptophan precursor is first transformed to IAM by indole-2-monooxygenase (IaaM), then hydrolyzed to IAA by IaM hydrolase (IaaH) (Spaepen *et al*., 2007). This pathway is employed by the foliar pathogen *Pseudomonas syringae* pv. *syringae*; it is discussed in this context in Chapter 3.

The IPyA pathway entails transamination of tryptophan to IPyA, followed by decarboxylation to an indole-3-acetaldehyde (IAAld) intermediate. This decarboxylation represents the limiting step in IAA biosynthesis and is catalyzed by the enzyme indolepyruvate decarboxylase (IpdC). In the final step, IAAld is oxidized to IAA (Spaepen *et al*., 2007). In addition to being the predominant plant pathway for synthesizing endogenous auxin, the IPyA pathway is one of the most common

bacterial biosynthetic pathways—including in the model foliar epiphyte *Pantoea agglomerans* (Brandl *et al*., 1996).

Previous work has implicated the indolepyruvate pathway of IAA biosynthesis in the leaf epiphytic fitness of foliar bacteria (described below). These findings comprise the experimental basis for my own research into the adaptive role of IAA production by *P. agglomerans* 299R.

The prevalence of IAA production among plant-associated bacteria suggests that it plays a useful adaptive role: as many as 60% of bacteria from field-grown lettuce leaves (Kim *et al*., 2011), and more than 50% isolated from pear leaves and fruits (Lindow *et al*., 1998), produce IAA. An adaptive value of IAA has also been demonstrated directly in some species. Manulis *et al,* (1998) found that *ipdC*-deficient knockouts of the pathogen *Erwinia herbicola* pv. *gypsophilae* exhibited significantly reduced growth relative to wild-type bacteria when inoculated onto the leaf surface of *Gypsophila paniculata*, its plant host, but no difference in its ability to cause disease once inside the plant. (Interestingly, *E. gypsophila* also synthesizes IAA via the indole-3-acetamide pathway; knocking out IAM biosynthesis affected pathogenesis but not epiphytic survival, suggesting that the two pathways act in distinct phases of the microbe's life cycle.) Similar results were obtained in *P. agglomerans* 299R, in which *ipdC*$^-$ bacteria also exhibited reduced fitness relative to wild-type bacteria—a trend observed both on *Phaseolus vulgaris* leaves and in pear flowers (Brandl *et al*., 1998). In *Pa*299R, relative fitness was significantly correlated with net bacterial growth, indicating that IAA production probably enhanced bacterial proliferation on plant surfaces.

In a hint at the underlying mechanism of IAA-mediated fitness enhancement, the hormone's ability to improve bacterial growth was highly localized: when *ipdC*$^-$ mutants were co-inoculated onto leaves with varying ratios of wild-type bacteria, the mutant's fitness did not increase along with the proportion of IAA-producing cells (Brandl *et al*., 1998). This lack of *trans*-complementation indicates that bacterial IAA does not alter the plant environment on the scale of an entire leaf or even leaf region; instead, it suggests that bacterial IAA acts at a single-cell or subcellular scale to improve bacterial fitness. Further study of *ipdC* indicated that this rate-limiting IAA biosynthetic gene was heterogeneously expressed on the leaf surface, with 65% of cells on the plant leaf exhibiting some transcriptional induction and 10% exhibiting strong induction (Brandl *et al.*¸ 2001). Upregulation occurred in response to *in vitro* water limitation (including salt and matric stress), and these cues may play a role in triggering induction on the leaf surface (Brandl *et al*., 1997).

Cumulatively, the data indicate that the majority of *Pa*299R cells on the leaf surface are equipped to synthesize IAA via the IPyA pathway, though transcriptional activation is heterogeneous within the phyllosphere population. The resulting IAA facilitates bacterial growth on plant surfaces in a highly localized fashion. The mechanism by which this localized growth enhancement occurs is unknown, but many researchers have suggested that IAA somehow modifies plant behavior so as to facilitate bacterial proliferation.

Plants respond to microbial IAA

Although bacterial IAA may sometimes act as an endogenous regulatory signal, in many cases bacterial IAA is believed to diffuse into the host plant, where it interacts with the native auxin response machinery to influence host physiology. Decades of observation support this basic model. Early research by Libbert *et al*. (1970a) demonstrated that corn coleoptiles that were either nonsterile or specifically inoculated with IAA-producing bacteria contained significantly more free IAA than axenic coleoptiles; subsequent inoculations with ^{14}C-labeled bacteria showed that this excess IAA was bacterial in origin (Libbert *et al*., 1970b). In the ensuing decades, research demonstrated that auxin-producing bacteria affected a variety of plant behaviors in an IAA-dependent manner, including root growth and architecture (Loper *et al*., 1986; Persello-Cartieaux *et al.*, 2001), and plant defense responses (Shinshi *et al*., 1987; Jouanneau *et al*., 1991). In more recent years, molecular evidence for engagement of the plant auxin response has also accumulated. When IAA-producing bacteria were inoculated onto *Arabidopsis thaliana* plants carrying the auxin-inducible IAA2:GUS transcriptional reporter, upregulation occurred in response to bacterial colonies on the root (O'Callaghan *et al*., 2001), and Persello-Cartieaux and colleagues (2001) used a mutant screen to confirm that plant auxin-response genes were necessary for PGPR-induced changes to root architecture. Microarray studies have also demonstrated upregulation of several auxin response genes in *A. thaliana* plants inoculated with either *Pseudomonas fluorescens* FPT9601-T5 (Wang *et* al., 2005) or with *Pseudomonas thivervalensis* MLG45 (Cartieaux *et al*., 2003).

Clearly, bacterial IAA is capable of triggering plant auxin responses under experimental conditions. However, the extent to which it does so under ecologically relevant conditions is likely subject to environmental constraints, including precursor availability and diffusional limitations.

For example, *in vitro* assays of bacterial IAA production indicate that high-producing strains such as *P. agglomerans* and *Pseudomonas spp*. can generate more than 100µg/mL IAA (Lindow *et al*., 1998). Based on estimates from radish root-inhibition assays, *Pa*299R produces local IAA concentrations equivalent to 50µM IAA when inoculated onto roots (Brandl and Lindow, 1998). But these assays are typically conducted under optimal conditions for IAA biosynthesis—in particular, with the addition of the IAA precursor tryptophan to assay media. When cultured in the absence of supplemental tryptophan, bacterial IAA production is typically several fold lower (Spaepen *et al.*, 2007; Glickmann *et al*., 1998). The effective local concentration of IAA produced by bacteria *in planta* is therefore highly dependent upon availability of tryptophan to plant-associated microbes—an observation supported by Kravchenko *et al*. (2004), who demonstrated that the phytostimulatory ability of IAA-producing rhizobacteria depended upon the concentration of tryptophan exuded from the roots of the host plant.

Although tryptophan is found in plant exudates, its quantity can vary by species and cultivar—ranging, for example, from ≈3 ng/day for tomato roots to ≈300 ng/day for radish roots (Kravchenko *et al.*, 2004). Tryptophan exudates also display heterogeneous distribution across the surface of an individual plant. Jaeger *et al*. (1999), for example, reported localized tryptophan levels in excess of 10^{-4}M on mature root tissues of the annual grass *Avena barbata*, but 10-fold lower concentrations near the root tip. Tryptophan has also been reported in leaf-surface washings (Morgan *et al*., 1964; Derridj, 1996). Although rigorous estimates of leaf-surface tryptophan concentrations are difficult to find, Steinbauer *et al*. (2009) reported foliar concentrations of up to 10 ng/cm^2 on eucalyptus leaves and Soldaat *et al* (1996) reported roughly

26 umol/m^2 (0.53ng/cm^2) on leaves of four *Senecio* species. These observations suggest that, although highly variable, leaf surface tryptophan might be sufficient to support IAA biosynthesis in some microhabitats. Additional tryptophan may also be provided by exudates from diazotrophic phyllosphere bacteria (Pati *et al.*, 1994), epiphytic bryophytes (Wanek *et al*., 2005), or other leaf-dwelling organisms.

Even if tryptophan is sufficiently available for bacterial production of IAA, for the hormone to influence the plant, it must also diffuse into the plant and engage the host's auxin-reponse machinery. Unlike the root surface, across which diffusion of bacterial IAA into the plant tissue is relatively unimpeded, the leaf cuticle represents an additional barrier between bacteria and putative IAA targets in the leaf interior. Although, cuticular diffusion has been demonstrated for synthetic auxin compounds (Riederer *et al*., 1985; Baker *et al*., 2008), partitioning of IAA through the cuticle is likely to depend on the pH of the leaf surface (Kramer *et al.*, 2006). Diffusion may also be enhanced by bacterial production of surfactants—amphipathic molecules that can facilitate transfer of compounds across the waxy cuticle (Liu *et al*., 2004; Schonherr *et al.*, 1996).

In summary, IAA generated by many plant-associated bacteria is capable of engaging the host plant's native auxin response machinery. Depending on the concentration of the bacterial IAA stimulus—as well as the species, exposed tissue, and developmental stage of the host plant—a variety of responses can be elicited. However, the ability of bacteria to synthesize IAA is limited by the availability of exogenous tryptophan. Once synthesized, the ability of bacterial IAA to engage the host plant may also be limited by diffusion into host tissue. Although much work suggests that bacterial IAA overcomes these environmental constraints in roots, the extent to which they limit the effect of bacterial IAA in foliar tissue remains largely unstudied.

The adaptive function of bacterial IAA in the plant phyllosphere

As described above, auxin can incite a variety of responses in the plant host depending on the timing, location, and concentration of IAA produced by the bacterial partner. In my research, I sought to understand how bacterial IAA produced by *P. agglomerans* 299R might enhance bacterial fitness in the phyllosphere. I tested two hypotheses that are not mutually exclusive: first, that IAA production by *Pa*299R directly affects bacterial cells on the leaf surface, and second, that bacterial IAA produced by *Pa299R* indirectly enhances microbial fitness by engaging the plant auxin response.

In the first hypothesis, IAA production by *Pa*299R does not affect the host plant at all, but rather exerts a purely endogenous effect on bacterial cells. This hypothesis derives predominantly from work by Bianco *et al*. (2006), who found that application of exogenous IAA to (non-auxin producing) *E. coli* K12 cells triggered upregulation of several genetic and biochemical stress response pathways, with an accompanying increase in bacterial survival under a variety of *in vitro* stress conditions. Subsequent experiments found similar effects in *Sinorhizobium meliloti* when IAA was applied exogenously or overexpressed from a plasmid (Bianco *et al.*, 2009). If the response of *P. agglomerans* to IAA were similar to that of *E. coli* or *S. meliloti*, it might suggest that IAA production increases epiphytic fitness of *P. agglomerans* 299R by promoting resistance

to stressful conditions in the phyllosphere. Experiments testing this hypothesis are described in Chapter 3.

The second hypothesis proposes that bacterial IAA produced by *P. agglomerans* 299R acts exogenously to modify behavior of the plant host in order to benefit the bacterium. As described above, a wealth of prior research suggests that bacterial IAA engages the plant auxin response in disease and PGPR model systems. In the phyllosphere, a plant-modification interpretation was also favored by Monier *et al*. (2005), who found that in an artificial inoculation system, proximity to established *Pa*299R colonies promoted the survival of immigrant cells arriving in the phyllosphere; this suggested beneficial modification of the local environment by colonies of IAA-producing cells. A similar explanation was proposed by Brandl *et al*. (1998) to explain the growth-correlated fitness advantage enjoyed by wild-type 299R cells over an IAA-deficient mutant derivative in the phyllosphere.

The majority of the research described in this dissertation therefore focuses on the hypothesis that bacterial IAA benefits the microbe by somehow modifying the host plant or influencing its behavior. One particular host cell characteristic that bacterial IAA has been proposed to modify is cellular autofluorescence: Monier *et al*. (2005) reported the qualitative observation that *P. vulgaris* leaf epidermal cells carrying large colonies of 299R exhibited increased blue-green autofluorescence. If true, such epidermal cell fluorescence might be used as a proxy measure for bacterial modification of the local plant environment. Efforts to quantitatively test whether this association exists—and whether changes in plant cell autofluorescence are mediated by IAA—are therefore reported in Chapter 3.

A more compelling possibility is that bacterial IAA stimulates the release of sugars from the host plant. Carbon limitation is a primary obstacle to bacterial growth in the phyllosphere (Mercier *et al*., 2000); this, combined with the observation that IAA-producing cells exhibited the greatest fitness advantage over IAA^- competitors during periods of rapid growth (Brandl *et al*., 1998), implicate nutrient acquisition as a likely fitness strategy.

Hypothesis: Bacterial IAA increases partitioning of plant sugars to the leaf surface

In order to increase sugar availability on the leaf surface, phyllosphere bacteria would have to increase partitioning of plant-derived carbon to the apoplast, from where it can leak or diffuse to the phylloplane (Figure 3). When bacteria colonize plant species that undergo apoplastic phloem-loading (including *P. vulgaris* and *A. thaliana*), this could be accomplished by two means: 1) increasing the amount of photosynthate arriving into the apoplast (by increasing the influx of sugars from photosynthetically active mesophyll source cells); or 2) decreasing the amount of sugar exported from the apoplast (by decreasing the efflux of sugar to the plant vasculature or re-uptake by mesophyll cells) (Voitsekhovskaja *et al.*, 2000). In another possible mechanism, 3) bacteria could increase diffusion of apoplastic sugars across the cuticle onto the leaf surface.

As a powerful plant growth regulator, IAA could potentially act at any of these three levels to divert plant photosynthate to phyllosphere bacteria (Morris, 1996).

For example, IAA has been reported to influence the activity of key sucrose biosynthetic enzymes in photosynthetic source cells. Sakalo *et al*. (2004) found that application of IAA to sugar beet shoots significantly increased foliar activity of sucrose phosphate synthase, an enzyme that catalyzes a critical step of sucrose biosynthesis and acts as a branchpoint away from starch biosynthesis. IAA might therefore increase flux of photosynthate from mesophyll cells to the apoplast by diverting photoassimilates from intracellular storage pathways (starch) to export pathways (sucrose). IAA application also appeared to prolong leaf productivity by delaying breakdown of chlorophyll during senescence (Jin *et al.*, 2009; Sakalo *et al.*, 2004), suggesting that IAA could act to prolong photosynthetic productivity of host plant cells—and by extension, the supply of leaked photosynthate to nearby bacteria.

Alternatively, bacterial IAA could also increase the rate of sugar efflux from mesophyll cells into the apoplastic compartment by enhancing transport activity. Although the mechanism of cellular sugar efflux remains a source of speculation, Chen *et al*. (2010) recently identified a class of glucose antiporters dubbed SWEET proteins that may fulfill this function (though the export path for sucrose, the primary photosynthate, remains uncertain). The effect of plant hormones on SWEET activity was not studied, but the researchers did find that the compatible bacterial pathogen *Pseudomonas syringae* pv. *tomato* DC3000 stimulated transcriptional upregulation of *AtSWEET* mRNA in an effector-dependent manner, suggesting that sugar efflux proteins may be a common target for bacterial nutrient acquisition in the plant apoplast.

In contrast to increasing the flux of photosynthate out of source cells, IAA might also increase apoplastic sugar retention by preventing sugar efflux from the apoplast. For example, application of IAA was shown to stimulate rapid, localized accumulation of sugars in foliar and stem tissues (Petzold *et al*., 1992; Patrick *et al.*, 1973; Morris *et al.*, 1987). These changes in sink strength were typically associated with stimulation of increased cell-wall invertase (*cwinv)* activity (Morris *et al.*, 1984; Morris *et al.*, 1986). Such increased cell wall invertase activity could result either from IAA-induced expression of *cwinv* genes (Long *et al.,* 2002), or as a result of increased enzyme activity following IAA-mediated apoplastic acidification, which favors the invertase's low pH optimum (Roitsch *et al.*, 2004). In either case, higher cell wall invertase activity is believed to promote localized sink strength by irreversibly cleaving apoplastic sucrose into its component monosaccharides, glucose and fructose.

In symplastically isolated sink tissues such as pollen, developing grains, or some root tissues, conversion of sucrose into hexose sugars permits carbon uptake from the apoplast into sink cells via monosaccharide transporters, while maintaining the sucrose diffusion gradient for phloem unloading (Roitsch *et al.*, 2003). In source tissues such as leaves, in which transport machinery is geared towards export rather than import of sugars, the net effect of increased apoplastic invertase activity is somewhat harder to predict. One possibility is that increased invertase activity might prevent phloem loading by sucrose-specific transporter proteins, resulting in increased local carbohydrate availability (Kocal *et al*., 2008). This hexose accumulation could help the plant fuel energy-intensive defense or stress responses (Roitsch *et al*., 2004); from a bacterial perspective, the net increase in apoplastic sugars would translate into increased leakage of sugars to the leaf surface—and thus a net increase in phyllosphere carbon availability.

Given that both plant hormones and plant sugars are embedded in fiendishly complex webs of metabolic and signaling regulation (Leon *et al*., 2003; Gibson 2003), this relatively clean-cut

hypothesis is highly simplistic. Due to downstream sugar-signaling effects, for example, increased apoplastic carbon concentrations could instigate feedback repression of primary photosynthetic productivity and sugar export by source cells (Rolland *et al*., 2002; reviewed in Roitsch, 1999), negating any initial increases in apoplastic sugars. Nonetheless, this hypothetical working model represents a useful starting point for thinking about IAA-mediated sugar interactions at the foliar surface. Furthermore, several plant-associated microbes alter local invertase activity of host plants (Blee *et al.* 2002; Chopra *et al*., 2004; Berger *et al*., 2007), suggesting that this represents a common strategy by which microbes manipulate host carbon partitioning (Biemelt *et al.*, 2006).

Having discussed possible ways in which bacterial IAA might promote influx of carbon to the apoplast from source cells—or prevent efflux of carbon from the apoplast to sink cells—it is worth mentioning a final mechanism by which the hormone might increase nutrient acquisition by phyllosphere bacteria: enhancing diffusion of carbon across the cuticle. Given that the leaf cuticle represents the major barrier to carbon diffusion from the plant apoplast to the phylloplane, increasing its permeability to plant sugars could enhance carbon acquisition by epiphytic microbes. Assuming that bacterial IAA activates apoplastic invertases, this might enhance epiphytic carbon bioavailability by stimulating transformation of less diffusible sucrose into glucose, to which the cuticle is more permeable (Derridj, 1996). Alternatively, pH has been shown to affect cuticular permeability to solutes (Arand *et al*., 2010; Knoche *et al*., 2000); IAA-mediated acidification of the apoplast might therefore enhance outward diffusion of carbon by altering physicochemical properties of epicuticular waxes.

Clearly, there are many possible mechanisms by which bacterial IAA could elicit carbon release from the host plant. Combined with previous reports suggesting that bacterial IAA enhances bacterial fitness in a highly localized, growth-dependent manner, it seemed highly plausible that the hormone played a role in phyllosphere carbon acquisition. This hypothesis was therefore a major focus of my research.

Experimental approach and challenges

Based on the lines of reasoning described above, my dissertation focused primarily on investigating the hypothesis that IAA production by *Pa*299R enhances bacterial fitness by facilitating carbon acquisition in the phyllosphere. To test this hypothesis, I employed single-cell sugar biosensors—*Pa*299R cells expressing sucrose- or fructose-inducible reporter genes (Miller *et al.*, 2001; Leveau *et al.*, 2001a)—to test whether bacteria sensed more carbon *in planta* when IAA was present than when it was absent.

Naturally, the body of this dissertation focuses on the results of these biosensor experiments, rather than technical details of their execution. However, pursuing a biosensor-based approach posed methodological challenges, requiring experimentation, optimization, and troubleshooting of a variety of techniques. In particular, developing methods for high-throughput quantification of single-cell reporter activity is central to both this research and other areas of contemporary environmental microbiology (Remus-Emsermann *et al*., 2010; Leveau *et al*., 2002; Jansson, 2003; van der Meer *et al*., 2010). This is because single-cell measures enable much greater understanding of population dynamics and inter-organismal variability than aggregate reporter

measures such as ice nucleation or mean population fluorescence. Unfortunately, such single-cell approaches pose several challenges—particularly when applied to environmental samples.

One of the challenges to effective quantification of single-celled fluorescent reporters is interpreting patterns of biosensor expression. For example, the maturation and decay rates of the chosen reporter protein contribute to varying intensities of cellular GFP fluorescence, as does the rate of cell division in the bacterial biosensor (Leveau *et al.*, 2001b). Additionally, in the case of *Pa*299R sugar biosensors, the bacteria metabolize the inducer molecule; bioreporter fluorescence is therefore a sensitive but *dynamic* measure of "real-time" intracellular carbon consumption, rather than a static measure of environmental carbon concentration. As a result, the kinetics of bacterial sugar import and metabolism complicate the interpretation of fluorescence data. For example, dose-response curves for both the sucrose and fructose biosensors indicate that increasing carbon concentration does not always yield uniform increases in cellular fluorescence throughout the population. Rather, populations can exhibit a bimodal, induced/uninduced induction pattern, in which elevated carbon concentrations are reported as a higher proportion of induced cells. In the case of a short-half-life GFP reporter, elevated carbon concentrations can also be indicated by a longer *duration* of induction, as cells take longer to consume the available sugar before dropping back to an uninduced state (Leveau *et al.*, 2001a). Attempting to compare reporter induction between two experimental populations is therefore not necessarily a simple question of comparing mean fluorescence; it may instead require comparing the proportion of induced cells, or dynamic changes in reporter induction over time.

Given these quantitative demands, identifying an optimal technological platform for quantifying single-cell fluorescence represents another major challenge. The small size and dim fluorescence of bacterial cells call for powerful, precise optics; coupled with the inherently high level of background debris generated by environmental samples, the signal-to-noise ratio is often unfavorable. Generating meaningful experimental data can tax standard microscopic or flow cytometric platforms. Methodological investigations addressing both platform optimization and interpretation of fluorescence data are therefore discussed in Appendix 1.

Summary and Overview

In summary, my research investigates the adaptive role of bacterial IAA production by the phyllosphere epiphyte *Pantoea agglomerans*.

In Chapter 1, I address the hypothesis that IAA relieves bacterial carbon limitation by facilitating carbon acquisition from the host plant. The putative role of plant cell wall invertase as a target for bacterial IAA receives particular attention. Additionally, methods developed to conduct these experiments—specifically, flow cytometric and microscopic techniques for quantifying single-cell biosensor fluorescence—are discussed in Appendix 1.

In Chapter 2, I test additional hypotheses regarding bacterial IAA production. The role of bacterial IAA in enhancing environmental stress resistance is investigated, as well as its ability to induce cellular autofluorescence in epidermal substrate cells of the host plant. Finally, attempts to characterize the role of IAA in foliar growth and pathogenesis of *Pseudomonas syringae* pv. *syringae* are described.

LITERATURE CITED

Ahmad, F., I. Ahmad, M.S. Khan. (2008) Screening of free-living rhizospheric bacteria for their multiple plant growth promoting activities. *Microbiological Research*. **163**: 173-181.

Akiyoshi, D.E., R.O Morris, R. Hinz, B.S. Mischke, T. Kosuge, D.J. Garfinkel, M.P. Gordon, & E.W. Nester. (1983) Cytokinin-auxin balance in crown gall tumors is regulated by specific loci in the T-DNA. *Proceedings of the National Academy of Sciences*. **80**(2): 407-411.

Arand, K., D. Stock, M. Burghardt, & M. Riederer. (2010) pH-dependent permeation of amino acids through isolated ivy cuticles is affected by cuticular water sorption and hydration shell size of the solute. *Journal of Experimental Botany*. **61**(14): 3865-3873.

Atkinson, S., & P. Williams. (2009) Quorum sensing and social networking in the microbial world. *Journal of the Royal Society Interface.* **6**(40): 959-978.

Avsian-Kretchmer, O., J. Cheng, L. Chen, E. Moctezuma, & Z.R. Sung. (2002) Indole acetic acid distribution coincides with vascular differentiation pattern during Arabidopsis leaf ontogeny. *Plant Physiology*. **130**(1): 199-209.

Baker, E.A., & M.J. Bukovac. (2008) Characterization of the components f plant cuticles in relation to the penetration of 2,4-D. *Annals of Applied Biology*. **67**(2): 243-253.

Barash, I., & S. Manulis-Sasson. (2009) Recent evolution of bacterial pathogens: the gall-forming *Pantoea agglomerans case*. *Annual Reviews of Phytopathology*. **47**: 133-152.

Bashan, Y., & G. Holguin. (1997) Azospirillum-plant relationships: environmental and physiological advances. *Canadian Journal of Microbiology*. **43**: 103-121.

Benkova, E., M. Michniewicz, M. Sauer, T. Teichmann, D. Seifertova, G. Jurgens, & J. Friml. (2003) Local, efflux-dependent auxin gradients as a common module for plant organ formation. *Cell*. **151**: 591-602.

Berg, G. (2009) Plant-microbe interactions promoting plant growth and health: perspectives for controlled use of microorganisms in agriculture. *Applied Microbiology and Biotechnology*. **84**: 11-18.

Berger, S., A.K. Sinha, & T. Roitsch. (2007) Plant physiology meets phytopathology: plant primary metabolism and plant-pathogen interactions. *Journal of Experimental Botany*. **58** (15/16): 4019-4026.

Blee, K.A, & A.J. Anderson (2002) Transcripts for genes encoding soluble acid invertase and sucrose synthase accumulate in root tip and cortical cells containing mycorrhizal arbuscules. *Plant Molecular Biology.* **50** (2): 197-211.

Brandl, M., and S. Lindow. (1998) Contribution of indole-3-acetic acid production to the epiphytic fitness of *Erwinia herbicola*. *Applied and Environmental Microbiology*. **64** (9): 3256-3263.

Brandl, M.T., B. Quinones, & S.E. Lindow. (2001) Heterogeneous transcription of an indoleacetic acid biosynthetic gene in *Erwinia herbicola* on plant surfaces. *Proceedings of the National Academy of Sciences.* **98**(6): 3454-3459.

Brandl, M., E.M. Clark, and S.E. Lindow. (1996) Characterization of the indole-3-acetic acid (IAA) biosynthetic pathway in an epiphytic strain of *Erwinia herbicola* and IAA production *in vitro*. *Canadian Journal of Microbiology*. **42**: 586-592.

Brandl, M.T., and S.E. Lindow. (1997) Environmental signals modulate the expression of an indole-3-acetic acid biosynthetic gene in *Erwinia herbicola*. *Molecular Plant Microbe Interactions*. **10**(4): 499-505.

Braun, N., J. Wyrzykowska, P. Muller, K. David, D. Couch, C. Perrot-Rechenmann, A.J. Fleming. (2008) Conditional repression of AUXIN BINDING PROTEIN 1 reveals that it coordinates cell division and cell expansion during postembryonic shoot development in *Arabidopsis* and Tobacco. *Plant Cell.* **20** (10): 2746-2762.

Camerini, S., B. Senatore, E. Lonardo, E. Imperlini, C. Bianco, G. Moschetti, G.L. Rotino, B. Campion, R. Defez. (2008) Introduction of a novel pathway for IAA biosynthesis to rhizobia alters vetch root nodule development. *Archives of Microbiology*. **190**: 67–77

Cartieaux, F., M.C. Thibaud, L. Zimmerli, P. Lessard, C. Sarrobert, P. David, A. Gerbaud, C. Robaglia, S. Somerville, L. Nussaume. (2004) Transcriptome analysis of *Arabidopsis* colonized by a plant-growth promoting rhizobacterium reveals a general effect on disease resistance. *The Plant Journal*. **36**(2): 177-188.

Chapman, E.J., & M. Estelle. 2009) Mechanism of auxin-regulated gene expression in plants. *Annual Reviews in Genetics*. **43**:265-285.

Chen, J.G., H. Ullah, J.C. Young, M.R. Sussman, & A.M. Jones. (2001) ABP1 is required for organized cell elongation and division in *Arabidopsis* embryogenesis. *Genes and Development*. **15**: 902-911.

Chen, L., B. Hou, S. Lalonde, H. Takanaga, M.L. Hartung, X., Qu, W. Guo, J. Kim, W. Underwood, B. Chaudhuri, D. Chermak, G. Antony, F.F. White, S.C. Somerville, M.B. Mudgett, & W.B. Frommer. (2010) Sugar transporters for intercellular exchange and nutrition of pathogens. *Nature.* **468**: 527-532.

Chopra, J., N. Kaur, A.K. Gupta. (2003) Changes in sugar content and activities of sucrose metabolizing enzymes in roots and nodules of lentil. *Biologia Plantarum* **46**(1): 89-93.

Conrath, U., G.J.M. Beckers, V. Flors, P. Garcia-Agustin, G. Jakab, F. Mauch, M. Newman, C.M.J. Pieterse, B. Poinssot, M.J. Pozo., A. Pugin, U. Schaffrath, J. Ton, D. Wendehenne, L. Zimmerli, & B. Mauch-Mani. (2006) Priming: getting ready for battle. *Molecular Plant Microbe Interactions*. **19**(10): 1062-1071.

Cosgrove, D. (2000) Loosening of plant cell walls by expansins. *Nature.* **407**: 321-326.

David, K.M., D. Couch, N. Braun, S. Brown, J. Grosclaude, & C. Perrot-Rechenmann. (2007) The auxin-binding protein 1 is essential for the control of cell cycle. *Plant Journal*. **50**: 197-206.

Derridj, S. (1996) Nutrients on the leaf surface. In *Aerial Plant Surface Microbiology*, Ed. Morris *et al*., Plenum Press, New York.

Diggle, S.P., A. Gardner, S.A. West, A.S. Griffin. (2007) Evolutionary theory of bacterial quorum sensing: when is a signal not a signal. *Philsophical Transactions f the Royal Society of London B.* **362**(1483): 1241-1249.

Dobbelaere, S., A. Croonenborghs, A. Thys, A.V. Broek, & J. Vanderleyden. (1999) Phytostimulatory effect of *Azospirillum brasilense* wild type and mutant strains altered in IAA production on wheat. *Plant and Soil*. **212**: 155-164.

Dodd, I.C., N.Y. Zinovkina, V.I. Safronova, & A.A. Belimov. (2010) Rhizobacterial mediation of plant hormone status. *Annals of Applied Biology*. **157**(3): 361-379.

Ek, M., P.O. Ljungquist, & E. Stenstrom. (1983) Indole-3-acetic acid production by mycorrhizal fungi determined by gas chromatography-mass spectrometry. *New Phytologist*. **94**: 401-407.

Gafni, Y., M. Icht, B.Z. Rubinfeld. (1995) Stimulation of *Agrobacterium tumefaciens* virulence with indole-3-acetic acid. *Letters in Applied Microbiology*. **20**(2): 98-101.

Gibson, S.I. (2003) Sugar and phytohormone response pathways: navigating a signaling network. *Journal of Experimental Botany*. **55**(395): 253-264.

Glickmann, E., L. Gardan, S. Jacquet, S. Hussain, M. Elasri, A. Petit, & Y. Dessaux. (1998) Auxin production is a common feature of most pathovars of *Pseudomonas syringae. Molecular Plant Microbe Interactions*. **11**(2): 156-162.

Gravel, V., H. Antoun, & R.J. Tweddell. (2007) Effect of indole-acetic acid (IAA) on the development of symptoms caused by *Pythium ultimum* on tomato plants. *European Journal of Plant Pathology*. **119**(4): 457-462.

Hughes, D.T., & V. Sperandio. (2008) Inter-kingdom signaling: communication between bacteria and their hosts. *Nature Reviews Microbiology*. **6**(2): 111-120.

Iacobellis, N.S., A. Sisto, G. Surico, A. Evidente, & E. Dimaio. (1994) Pathogenicity of *Pseudomonas syringae* subsp. *Savastanoi* mutants defective in phytohormone production. *Journal of Phytopathology*. **140**(3): 238-248.

Jaeger, C.H., S.E. Lindow, S. Miller, E. Clark, M.K. Firestone. (1999) Mapping of sugar and amino acid availability in soil around roots with bacterial sensors of sycrose and tryptophan. *Applied and Environmental Microbiology*. **65**(6): 2685-2690.

Jansson, J.K. (2003) Marker and reporter genes: illuminating tools for environmental microbiologists. *Current Opinion in Microbiology*. **6**(3): 310-316.

Kazan, K., & J.M. Manners. (2009) Linking development to defense: auxin in plant-pathogen interactions. *Trends in Plant Science*. **14**(7): 373-382.

Khalid, A., M. Arshad, Z.A. Zahir. (2004) Screening plant growth-promoting rhizobacteria for improving growth and yield of wheat. *Journal of Applied Microbiology.* **96**(3): 473-480.

Khan, M.S., A. Zaidi, P.A. Wani, M. Oves. (2009) Role of plant growth promoting rhizobacteria in the remediation of metal contaminated soils. *Environmental Chemical Letters*. **7**:1-19.

Kim, Y.C., J. Leveau, B.B.M. Gardener, E.A. Pierson, L.S.Pierson, & C. Ryu. (2011) The multifactorial basis for plant health promotion by plant-associated bacteria. *Applied and Environmental Microbiology*. **77**(5): 1548-1555.

Knoche, M., & M.J. Bukovac. (2000) Finite dose diffusion studies: II. Effect of concentration and pH on NAA penetration through isolated tomato fruit cuticles. *Pest Management Science*. **56**(12): 1016-1022.

Kochar, M., A. Upadhyay, & S. Srivastava. (2011) Indole-3-acetic acid biosynthesis in the biocontrol strain *Pseudomonas fluorescens* Psd and plant growth regulation by hormone overexpression. *Research in Microbiology*. **162**(4): 426-435.

Kokal, N., U. Sonnewald, & S. Sonnewald. (2008) Cell wall-bound invertase limits sucrose export and is involved in symptom development and inhibition of phososynthesis during compatible interaction between tomato and *Xanthomonas campestris* pv *vesicatoria*. *Plant Physiology*. **148**: 1523-1536.

Kramer, E.M, & M.J. Bennett. (2006) Auxin transport: a field in flux. *Trends in Plant Science.* **11**(8): 382-386.

Kravchenko, L.V., T.S. Azarova, N.M. Makarova, & I.A. Tikhonovich. (2004) The effect of tryptophan present in plant root exudates on the phytostimulating activity of rhizobacteria. *Microbiology.* **73**(2): 156-158.

Lee, C.W., M. Efetova, J.C. Engelmann, R. Kramell, C. Wasternack, J. Ludwig-Muller, R. Hedrich, & R. Deeken. (2009) *Agrobacterium tumefaciens* promotes tumor induction by modulating pathogen defense in *Arabidopsis thaliana*. *Plant Cell*. **21**(9): 2948-2962.

Leon, P., & J. Sheen. (2003) Sugar and hormone connections. *TRENDS in Plant Science.* **8**(3): 110-116.

Leveau, J.H.J, and S.E. Lindow. (2001a) Appetite of an epiphyte: Quantitative monitoring of bacterial sugar consumption in the phyllosphere. *Proceedings of the National Academy of Sciences.* **98**(6): 3446-3453.

Leveau, J.H.J., and S.E. Lindow. (2001b) Predictive and interpretive simulation of green fluorescent protein expression in reporter bacteria. *Journal of Bacteriology*. **183**(12): 6752-6762.

Leveau, J.H.J, & S.E. Lindow. (2002) Bioreporters in microbial ecology. *Current Opinion in Microbiology*. **5**(3): 259-265.

Libbert, E. & Manteuffel, R. (1970) Interactions between plants and epiphytic bacteria regarding their auxin metabolism VII. The influence of the epiphytic bacteria on the amount of diffusible auxin from corn coleoptiles. *Physiologia Plantarum* 23: 93-98.

Libbert, E. & Silhengst, P. (1970) Interactions between plants and epiphytica bacteria regarding their auxin metabolism VIII. Transfer of ^{14}C-Indoleacetic acid from epiphytic bacteria to corn coleoptiles. *Physiologia Plantarum* 23: 480-487.

Lindow, S.E. (1987) Competitive exclusion of epiphytic bacteria by ice$^-$ *Pseudomonas syringae* mutants. *Applied and Environmental Microbiology.* **53**(10): 2520-2527.

Lindow, S.E., C. Desurmont, R. Elkins, G. McGourty, E. Clark, & M.T. Brandl. (1998) Occurrence of indole-3-acetic acid-producing bacteria on pear trees and their association with fruit russet. *Phytopathology* **88** (11):1149-1157.

Lindow, S.E., and M.T. Brandl. (2003) Microbiology of the Phyllosphere. *Applied and Environmental Microbiology*. **69**(4): 1875-1883.

Lindow, S.E., C. Desurmont, R. Elkins, G. McGourty, E. Clark, and M. Brandl. (1998) Occurrence of indole-3-acetic acid-producing bacteria on pear trees and their association with fruit russet. *Phytopathology*. **88**(11): 1149-1157.

Liu, Z.Q., R.E. Gaskin, J.A. Zabkiwicz. (2004) Visualization of the effect of a surfactant on the uptake of xenobiotics into plant foliage by confocal laser scanning microscopy. *Weed Research*. **44**(3): 237-243.

Lokerse, A.S., & D. Weijers. (2009) Auxin enters the matrix—assembly of response machineries for specific outputs. *Current Opinion in Plant Biology*. **12**: 520-526.

Long, J.C., W. Zhao, A.M. Rashotte, G.K. Muday, and S.C. Huber. (2002) Gravity-stimulated changes in auxin and invertase gene expression in maize pulvinal cells. *Plant Physiology*. **128**(2): 591-602.

Loper, J.E., & M.N. Schroth (1986) Influence of bacterial sources of indole-3-acetic acid on root elongation of sugar beet. *Phytopathology*. 76 (4): 386-389.

Mantelin, S., & B. Touraine. (2004) Plant growth-promoting bacteria and nitrate availability: impacts on root development and nitrate uptake. *Journal of Experimental Botany*. **55** (394): 27-34.

Manulis, S., A. Haviv-Chesner, S.E. Lindow, I. Barash. (1998) Differential involvement of indole-3acetic acid biosynthetic pathways in pathogenicity and epiphytic fitness of *Erwinia herbicola* pv. *gypsophilae. Molecular Plant-Microbe Interactions.* **11**(7): 634-642.

Maor, R., S. Haskin, H. Levi-Kedmi, & A. Sharon. (2004) *In planta* production of indole-3-acetic acid by *Colletotrichum gloeosporioides* f. sp aeschynomene. *Applied and Environmental Microbiology*. **70**(3): 1852-1854.

Mathesius, U. (2008) Auxin: at the root of nodule development? *Functional Plant Biology*. **35**: 651–668.

Mazzola, M., and F.F. White. (1994) A mutation in the indole-3-acetic acid biosynthesis pathway of *Pseudomonas syringae* pv. *syringae* affects growth in *Phaseolus vulgaris* and syringomycin production. *Journal of Bacteriology.* **176**(5): 1374-1382.

Mercier, J., and S.E. Lindow. (2000) Role of leaf surface sugars in colonization of plants by bacterial epiphytes. *Applied and Environmental Microbiology.* **66**(1): 369-374.

Miller, W.G., M.T. Brandl, B. Quinones, and S.E. Lindow. (2001) Biological sensor for sucrose availability: relative sensitivities of various reporter genes. *Applied and Environmental Microbiology*. **67**(3): 1308-1317.

Monier, J.M., and S.E. Lindow. (2005) Aggregates of resident bacteria facilitate survival of immigrant bacteria on leaf surfaces. *Microbial Ecology*. **49**: 343-352.

Morgan, J.V., & H.B. Tukey. (1964) Characterization of leachate from plant foliage. *Plant Physiology*. **39**(4): 590-593.

Morris, D.A., and E.D. Arthur. (1984) Invertase and auxin-induced elongation in intermodal segments of *Phaseolus vulgaris*. *Phytochemistry*. **23** (10): 2163-2167.

Morris, D.A. (1996) Hormonal regulation of source-sink relationships: an overview of potential control mechanisms. In *Photoassimilate Distribution in Plants and Crops: Source-Sink Relationships.* Ed. E. Zamski and A.A. Schaffer. CRC Press/Marcel Dekker, Inc.. New York, NY.

Morris, D.A., and E.D. Arthur. (1986) Stimulation of acid invertase activity by indol-3yl-acetic acid in tissues undergoing cell expansion. *Plant Growth Regulation*. **4**: 259-271.

Morris, D.A., and E.D. Arthur. (1987) Auxin-induced assimilate translocation in the bean stem (*Phaseolus vulgaris* L.). *Plant Growth Regulation.* **5**: 169-181.

O'Callaghan, K.J., R.A. Dixon, and E.C. Cocking. (2001) *Arabidopsis thaliana*: a model for studies of colonization by non-pathogenic and plant-growth-promoting rhizobacteria. *Australian Journal of Plant Physiology*. **28**: 975-982.

Pacheco, A.R., & V. Sperandio. (2009) Inter-kingdom signaling: chemical language between bacteria and host. *Current Opinion in Microbiology*. **12**(2): 192-198.

Patten, C., & B. Glick. (2002) Role of *Pseudomonas putida* indoleacetic acid in development of the host plant root system. *Applied and Environmental Microbiology*. **68**(8): 3795-3801.

Pati, B.R., S. Sengupta, & A.K. Chandra. (1994) Studies on the amino-acids released by phyllosphere diazotrophic bacteria. *Microbiological Research.* **149** (3): 287-290.

Patrick, J.W., and P.F. Wareing. (1973) Auxin-promoted transport of metabolites in stems of *Phaseolus vulgaris* L. *Journal of Experimental Botany*. **24** (83): 1158-1171.

Patten, C.L., & B. Glick. (1996) Bacterial biosynthesis of indole-3-acetic acid. *Canadian Journal of Microbiology*. **42**: 207-220.

Patten, C.L., & B. Glick. (2002) Role of *Pseudomonas putida* indoleacetic acid in development of the host plant root system. *Applied and Environmental Microbiology*. **68**(8): 3795-3801.

Perrine-Walker, F., P. Doumas, M. Lucas, V.Vaissayre, N.J. Beauchemin, L.R.Band J. Chopard, A. Crabos, G. Conejero, B. Peret, J.R. King, J. Verdeil, V. Hocher, C. Franche, M.J. Bennett, L.S. Tisa, & L. Laplaze. (2010) Auxin carriers localization drives auxin accumulation in plant cells infected by *Frankia* in *Casuarina glauca* actinorhizal nodules.*Plant Physiology*. **154**: 1372-1380.

Persello-Cartieaux, F. P. David, C. Sarrobert, M.C. Thibaud, W. Achouak, C. Robaglia, & L. Nussaume. (2001) Utilization of mutants to analyze the interaction between *Arabidopsis thaliana* and its naturally root-associated *Pseudomonas*. *Planta* 212: 190-198.

Petzold, U., S. Peschel, I. Dahse, and G. Adam. (1992) Stimulation of source-applied ^{14}C-sucrose export in *Vicia faba* plants by brassinosteroids, GA_3 and IAA. *Acta Botanica Neerlandia*. **41**(4): 469-479.

Reinhardt, D., T. Mandel, & C. Kuhlemeier. (2000) Auxin regulates the initiation and radial position of plant lateral organs. *Plant Cell*. **12**: 507-518.

Remus-Emsermann, M.N.P., & J.H.J. Leveau. (2010) Linking environmental heterogeneity and reproductive success at single-cell resolution. *ISME Journal*. **4**: 215-222.

Riederer, M., & J. Schonherr. (1985) Accumulation and transport of (2,4-dichlorophenoxy)acetic acid in plant cuticles: II. Permeability of the cuticular membrane. *Ecotoxicology and Environmental Safety.* **9**(2): 196-208.

Roitsch, T. (1999) Source-sink regulation by sugar and stress. *Current Opinion in Plant Biology*. **2**: 198-206.

Rolland, F., B. Moore, & J. Sheen. (2002) Sugar sensing and signaling in plants. *The Plant Cell*. Supplement 2002: S185-S205.

Schaarschmidt, S., J. Kopka, J. Ludwig-Muller, & B. Hause. (2007) Regulation of arbuscular mycorrhization by apoplastic invertases: enhanced invertase activity in the leaf apoplast affects the symbiotic interaction. *The Plant Journal*. **51**: 390-405.

Schonherr, J., & P. Baur. (1996) Cuticle Permeability Studies. In *Aerial Plant Surface Microbiology*, Ed. Morris *et al*., Plenum Press, New York.

Sanchez-Rodriguez, C., I. Rubio-Somoza, R. Sibout, & S. Persson. (2010) Phytohormones and the cell wall in *Arabidopsis* during seedling growth. *Trends in Plant Science*. **15**(5): 291-301.

Simon, S., & J. Petrasek. (2011) Why plants need more than one type of auxin. *Plant Science* **180**: 454-460.

Soldaat, L.L., J-P. Boutin, & S. Derridj. (1996) Species-specific composition of free amino acids on the leaf surface of four *Senecio* species. *Journal of Chemical Ecology*. **22**(1): 1-12.

Spaepen, S., J. Vanderleyden, R. Remans. (2007) Indole-3-acetic acid in microbial and microorganism-plant signaling. *FEMS Microbiology Reviews*. **31**(4): 425-448.

Splivallo, R., U. Fischer, C. Gobel, I. Feussner, & P. Karlovsky. (2009) Truffles regulate plant root morphogenesis via the production of auxin and ethylene. *Plant Physiology*. **150**(4): 2018-2029.

Steinbauer, M.J., N.W. Davies, C. Gaertner, & S. Derridj. (2009) Epicuticular waxes and plant primary metabolites on the surfaces of juvenile *Eucalyptus globules* and *E. nitens* (Myrtaceae) leaves. *Australian Journal of Botany*. **57**: 474-485.

Tromas, A., I. Paponov, & C. Perrot-Rechenmann. (2010) Auxin Binding Protein 1: functional and evolutionary aspects. *Trends in Plant Science*. **15**:436-446.

Van der Meer, J.R., S. Belkin. (2010) Where microbiology meets microengineering: design and applications of reporter bacteria. *Nature Reviews Microbiology*. **8**:511-522.

Van Wees, S.C.M, S. Van der Ent, & C. M.J. Pieterse. (2008) Plant immune responses triggered by beneficial microbes. *Current Opinion in Plant Biology*. **11**: 443-448.

Voitsekhovskaja, O.V., M.V. Pakhomova, A.V. Syutkina, Y.V. Gamalei, and U. Heber. (2000) Compartmentation of assimilate fluxes in leaves. *Plant Biology **2**.* 103-112.

Wanek, W., & K. Portl. (2005) Reciprocal transfer of nitrogen between epiphyllous liverworts and host plants in the understorey of a lowland tropical wet forest in Costa Rica. *New Phytologist*. **166** (2): 577-588.

Wang, Y., Y. Ohara, H. Nakayashiki, Y. Tosa, & S. Mayama. (2005) Microarray analysis of the gene expression profile induced by the endophytic plant growth-promoting rhizobacteria, *Pseudomonas fluorescens* FPT9601-T5 in *Arabidopsis. Molecular Plant Microbe Interactions*. **18**(5): 385-396.

Yang, J., J. W. Kloepper, & C. Rya. (2008) Rhizosphere bacteria help plants tolerate abiotic stress. *Trends in Plant Science*. **14**(1): 1-4.

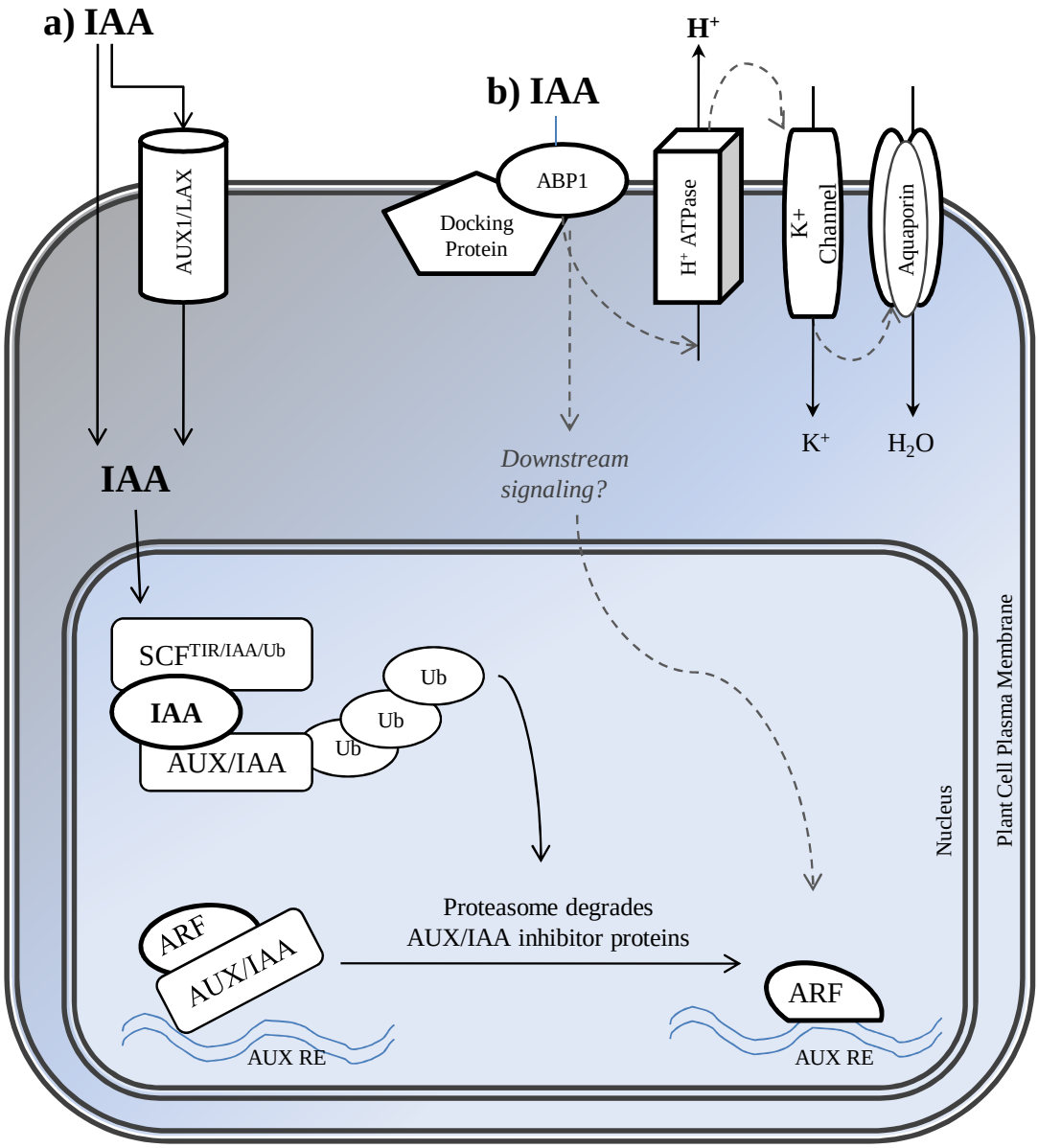

Figure 1. Diagram of IAA response pathways in the plant cell (figure modified from Simon *et al*., 2010; Tromas *et al.* 2010). Major response pathways include TIR1-mediated intracellular signaling (A), which mediates IAA-induced transcriptional changes, and the ABP1-mediated signaling pathway (B), which is believed to mediate rapid responses to IAA at the plasma membrane, as well as downstream cellular effects.

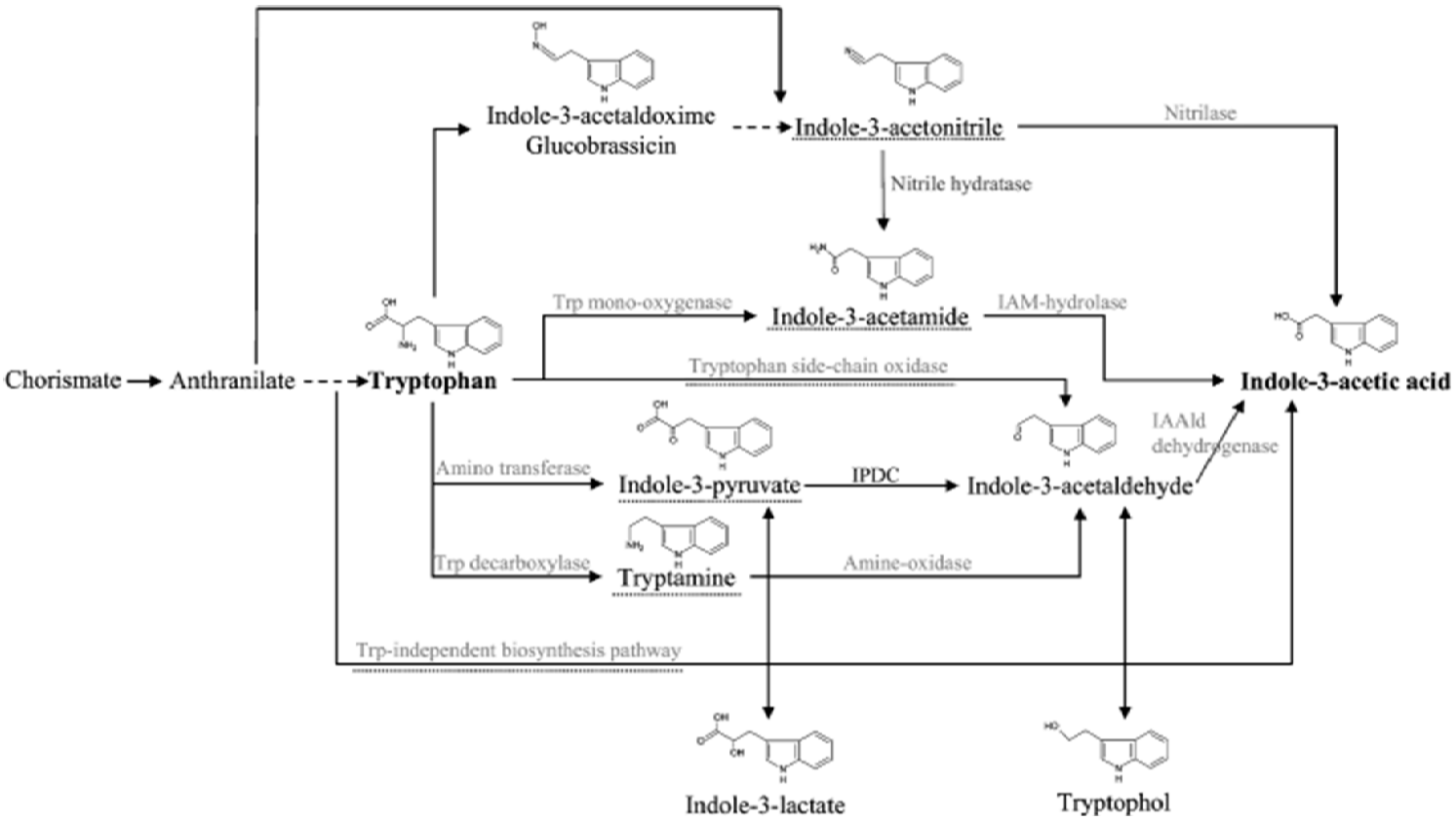

Figure 2. Microbial biosynthetic pathways of IAA (figure from Spaepen *et al*., 2007). "The intermediate referring to the name of the pathway or the pathway itself is underlined with a dashed line. IAAld, indole-3-acetaldehyde; IAM, indole-3-acetamide; IPDC, indole-3-pyruvate decarboxylase; Trp, tryptophan." The indolepyruvate decarboxylase pathway and indoleacetamide pathway are particularly relevant to this work.

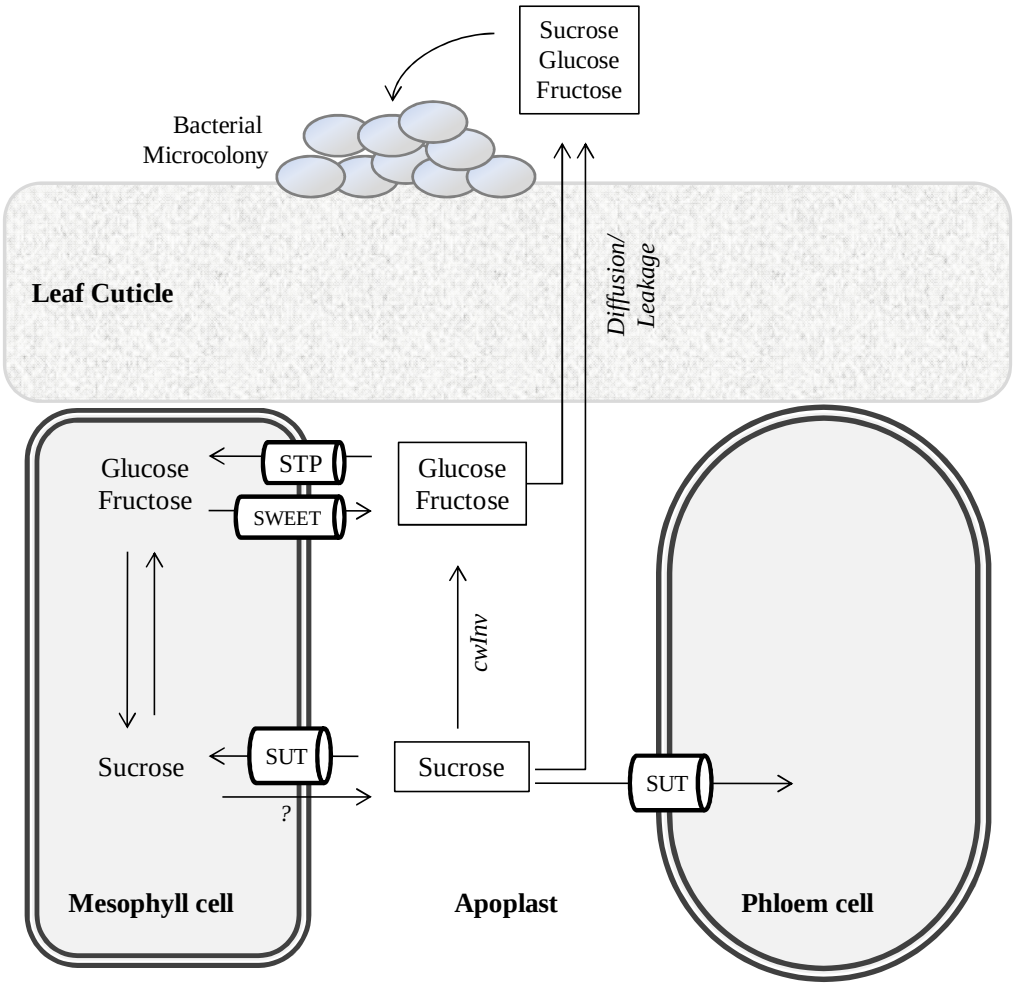

Figure 3. Diagram of carbon partitioning in the phyllosphere. Leaf surface sugars arrive via diffusion or leakage from the leaf interior. In turn, apoplastic sugar content derives from dynamic fluxes of photosynthate (sucrose) and its component monosaccharides (glucose and fructose), which transit between the photosynthetically active source cells of the leaf mesophyll, the apoplastic compartment, and the sink cells of the phloem. SUT=sucrose transporter; STP=monosaccharide sugar transporter; cwInv=cell wall invertase; SWEET=putative sugar efflux transporter

Chapter II. Bacterial auxin production facilitates resource conversion and carbon acquisition by the phyllosphere epiphyte *Pantoea agglomerans*

Abstract

The phyllosphere epiphyte *Pantoea agglomerans* 299R synthesizes indole-3-acetic acid (IAA), an important plant hormone. IAA production was previously shown to confer a small but significant fitness advantage to *Pa*299R cells inoculated onto bean leaves, but the mechanism by which bacterial IAA exerts this effect is unknown. Here, we investigate the hypothesis that bacterial IAA enhances the availability of plant sugars, thereby relieving carbon limitation of bacterial growth on the leaf surface. Sucrose- and fructose-inducible biosensor bacteria were inoculated onto bean leaves, and the effects of auxin availability on sugar sensing investigated. When reporter activity of wild-type *Pa*299R (IAA^+) biosensors was compared to that of the isogenic, IAA^- mutant *Pa*MX149, endogenous auxin was found to stimulate a significant decrease in sucrose availability, while fructose sensing was increased by a small but significant amount. Coinoculation of biosensor bacterial with exogenous NAA also decreased sucrose sensing and increased fructose sensing. *In vitro* assays demonstrate that *Pa*299R growth begins more rapidly when using glucose or fructose as a sole carbon source than when using sucrose. This suggests that IAA biosynthesis may function as a resource conversion strategy to enhance carbon acquisition in an oligotrophic, environmentally dynamic phyllosphere.

Introduction

A remarkable range of plant-associated microorganisms are capable of synthesizing indole-3-acetic acid (IAA), a plant growth hormone that controls endogenous developmental processes such as cell growth and division (Tromas *et al*., 2010), vascularization (Avsian-Kretchmer *et al*., 2002), organ initiation (Benkova *et al*., 2003; Reindhardt *et al*, 2000), apical dominance, and various tropisms, (reviewed in Woodward & Bartel *et al*., 2005). Several studies have shown that between 50-60% of bacteria isolated from foliar surfaces produce auxin (Kim *et al*., 2011; Lindow *et al.*, 1998). This enrichment for auxin-producing species suggests that the ability to produce phytohormones might enhance bacterial fitness in some way, and therefore be selected for in a plant environment. However, the precise nature of this fitness benefit—exactly what bacterial auxin does to the plant, and how this benefits bacteria—is the target of much speculation and a growing body of research.

Here, we attempt to identify the mechanism by which IAA biosynthesis enhances fitness of the leaf epiphyte *Pantoea agglomerans* (formerly *Erwinia herbicola*), a common environmental bacterium that synthesizes IAA via the indole-3-pyruvate (*ipdC*) pathway (Brandl *et al.*, 1996).

Previous work has shown that IAA production confers a small but significant fitness advantage to *P. agglomerans* on leaf surfaces (Brandl *et al.*, 1998). When coinoculated onto bean leaves with an isogenic, IAA^- mutant, wild-type *P. agglomerans* exhibited a selection rate constant of 0.067 per cell generation. This relative fitness advantage accrued primarily during phases of active growth—particularly the initial 10-15 hours after inoculation, as epiphytic cell populations

expanded rapidly on the plant leaf. A similar trend was observed when *Pa*299R was inoculated onto pear flowers, where regression analysis indicated a significant positive correlation between the rate of net bacterial population growth and the rate at which the wild-type strain outgrew the IAA^- mutant. In both leaf and floral environments, the relative proportion of IAA-producing cells stabilized or dropped when bacterial populations stopped expanding, suggesting that bacterial auxin confers fitness during periods of colonization or rapid cell growth, but does little to enhance bacterial survival during stationary intervals or population contractions (Brandl *et al.*, 1998).

It is worth noting that the periods of epiphytic proliferation in which IAA production confers a fitness advantage correspond to periods in which transcription of IAA biosynthetic genes were found to be upregulated (Brandl *et al.*, 1997). A promoter-reporter fusion construct demonstrated that indolepyruvate decarboxylase (*ipdC*), the gene encoding the rate-limiting enzyme of IAA biosynthesis, is rapidly induced upon inoculation onto tobacco leaves, reaching maximal, 32-fold induction by 20 hours post-inoculation (*hpi*). Combined with the relative success of wild-type *P. agglomerans* over IAA^- mutants, this transcriptional pattern clearly implicates IAA biosynthesis in enhancing bacterial fitness in the phyllosphere, particularly during the initial phase of leaf surface colonization.

The exact nature of this fitness enhancement has never been addressed directly. However, the observation that IAA's fitness effect is growth-dependent suggests that bacterial IAA may act by relieving constraints on bacterial proliferation. Carbon limitation has been shown to be a primary impediment to microbial proliferation in the phyllosphere (Mercier *et al*., 2000), implicating bacterial IAA in carbon acquisition. Additionally, Mercier and Lindow (2000) demonstrated a significant positive correlation between total leaf surface sugars before inoculation (mono- and disaccharides, as determined by HPLC) and final bacterial carrying capacity, further suggesting that carbon availability limits bacterial proliferation. Based on this hypothesis, Brandl *et al*. (1998) estimated that, in order to sustain the additional growth observed in the wild-type strain relative to the IAA^- mutant, bacterial IAA would have to make 7% more nutrients available to bacteria—approximately 1microgram of extra phylloplane carbon per leaf.

Previous reports have demonstrated that auxin can promote localized increases in carbon availability. For example, the hormone enhanced localized sink strength in roots, developing grains, seeds, and fruits (Roitsch *et al.*, 2003; Jin *et al.*, 2009) by increasing invertase activity. More relevant to phyllosphere bacteria, auxin has also been shown to stimulate accumulation of sugars in foliar and stem tissues. Application of IAA to *Vicia fava* leaves elicited transport of ^{14}C-labeled photoassimilates to the site of application within 4 hours of incubation (Petzold *et al*., 1992; Patrick *et al.*, 1973). And when *Phaseolis vulgaris* internodes were exposed to 10µM exogenous IAA, localized accumulation of hexose sugars and sucrose was detected within 24 hours (Morris *et al.*, 1987). These changes in sink strength are typically associated with stimulation of increased cell-wall invertase activity (Morris *et al.*, 1984; Morris *et al.*, 1986; Roitsch *et al.*, 2004; Long *et al.*, 2002).

Here, we test the hypothesis that microbial IAA facilitates carbon acquisition by phyllosphere bacteria. In addition to being a well-studied model of bacterial IAA production, *Pa*299R has also been used extensively as a bacterial biosensor to monitor environmental concentrations of sucrose (Miller *et al.*, 2001) and fructose (Leveau *et al*, 2001a). By mobilizing sugar-inducible

biosensor plasmids into *Pa*299R and its IAA$^-$ mutant derivatives, *Pa*MX149 and *Pa*XYLE, we sought to compare the nutrient status of phyllosphere bacteria in the presence or absence of bacterial IAA.

In particular, we sought to characterize the distribution of sugar sensing among individual cells of the population. Though average, population-level shifts in sugar availability are informative, they can obscure important patterns in nutrient acquisition. For example, a small, change in mean sucrose sensing in a phyllosphere population could represent a steep change in sucrose acquisition by a few cells, or a modest change in sucrose acquisition by many cells. Similarly, changes in sugar availability might be experienced mainly by slow-growing bacteria experiencing low-carbon, oligotrophic conditions or, alternatively, by bacteria dwelling in carbon-rich "nutrient oases" and experiencing relatively rapid growth (Lindow and Brandl, 2003). Understanding which bacterial subpopulations are affected by auxin production and how patterns of sugar availability change in response to bacterial IAA could illuminate the mechanisms by which bacterial auxin biosynthesis improves evolutionary fitness.

Materials and Methods

Culture Conditions

For routine culturing, all bacteria were grown in LB liquid or agar medium with appropriate antibiotics (Kanamycin C_F=50µg/mL, Tetracycline=15µg/mL, Rifampicin=100µg/mL, Natamycin=43µg/mL, Cycloserine=25µg/mL, Streptomycin=20µg/mL). Unlessotherwise specified, *E. coli* were grown at 37°C, and *P. agglomerans* at either 28°C (in liquid culture) or 37° (on agar plates).

For *in vitro* carbon growth comparisons, virgin glass culture tubes were acid-washed, rinsed repeatedly with freshly distilled water, filled with D_i water, then autoclaved to remove any residual carbon. The tubes were then emptied, rinsed repeatedly in D_i water, inverted, and dried at 50°C before autoclaving to sterilize. All liquid media components were prepared in similarly cleaned glassware, with autoclaved D_i water. During each experiment, a single colony of freshly streaked *Pa*299R was inoculated into Minimal-A medium (Miller *et al*., 1972) amended with Rifampicin, Natamycin, and 0.4% Galactose; the inoculum was grown overnight with shaking at 300rpm. The overnight culture was inoculated into 1x MinA medium at C_F=1x10^4 cells/mL, divided into tubes, and amended with various concentrations of carbon. Tubes were incubated at 28°C with shaking at 300rpm. At designated intervals, liquid samples were removed, diluted, and spiral plated onto LB plates amended with Rifampicin and Natamycin. Colonies were enumerated by manual or laser counting after approximately 24 hours' growth at 37°C.

Plant Materials and Growth Conditions

P. vulgaris plants (cv. Bush Blue Lake 274) were grown in a greenhouse under mixed natural and artificial lighting. Where indicated, average daily solar radiation was estimated using the NASA atmosphere-ocean model for insolation in Berkeley, CA (GPS 37.87, -122.27) (http://aom.giss.nasa.gov/srlocat.html). Experimental estimates of incident light intensity

represent three measurements of photon flux density collected over a 5-minute period with a Li-Cor light meter.

For experiments in which light intensity was manipulated, plants were grown either in full sunlight, or under tents of four layers of cheesecloth. For experiments in which temperature intensity was manipulated, plants were grown in chambers set to 12 hours light/12 hours dark, with temperature set to either 30°C (high-temperature conditions) or 20°C (low-temperature conditions).

For experiments using *Arabidopsis thaliana* ec. Col-0, seeds for the wild-type and homozygous mutant lines *At*068113c (*cwinv2*), *At*094878c (*cwinv4*), and *At*007233c (*cwinv1*) were acquired from the Salk Institute (Alonso *et al*., 2003). Plants were grown under long-day, greenhouse conditions as prescribed (ARBC, 2004).

Plant Inoculation and Harvest

In plant inoculation experiments, a single, freshly streaked bacterial colony was inoculated into Minimal-A medium (Miller *et al*., 1972) amended with appropriate antibiotics, 0.4% Galactose, and 2.5mM tryptophan. The inoculum was grown overnight with shaking at 300rpm, then resuspended at 10^7/mL in 100mM KPO_4 buffer. Immediately before inoculation, samples were amended as appropriate with 6.25mM sucrose and either 100µM NAA in EtOH or an equal volume of EtOH alone. Healthy, 2-3-week-old Blue Bush Bean plants with undamaged leaves were chosen and spray-inoculated until water ran off the ab- and adaxial surfaces of all leaves. Each plant was then loosely covered with a plastic bag fastened at the base with a rubber band (to maintain humidity) and placed in an illuminated growth chamber at room temperature.

After the designated period of incubation on the plant surface, bacteria were harvested from leaves. For microscopic analysis, two healthy primary leaves (as opposed to trifoliates) were chosen from each pot, severed, and immersed in 20mL of KPO_4 buffer; for flow cytometric analysis 15-20 leaves were immersed in a beaker of 200mL KPO_4 buffer. In each case, leaves were sonicated for 5 minutes, vortexed for 30 seconds, and then removed. Where indicated, leaves were blotted and weighed (to normalize foliar populations) before discarding.

To concentrate harvested cells, leaf washate samples were centrifuged at 5000 x *g* for 10 minutes at 4°C in a Sorvall centrifuge. The supernatant was carefully removed by pipetting, and the cells resuspended in approximately 2mL of KPO_4 buffer. To remove leaf debris, each sample was syringe-filtered through a 5µm TMTP filter (Millipore Isopore filter, CAT# TMTP02500). Filtered samples were once again concentrated by tabletop centrifugation at 5000 x *g* for 10 minutes at 4°C. (At this step, microscopy samples were resuspended in 25µL KPO_4 buffer and stained with 4',6-diamidino-2-phenylindole (DAPI, C_F=2.5µg/mL) for 10 minutes in the dark at room temperature, then snap-frozen on dry ice before fixation.)

All samples were fixed overnight at 4°C after resuspension/addition of 1mL 4% paraformaldehyde. After fixation, samples were washed with buffer and resuspended for analysis. To prevent sample degradation, all samples were analyzed via microscopy or flow cytometry within one week of harvest.

Bacterial inoculation of *A. thaliana* plants was performed as described above, with two exceptions: inocula included 0.05% Silwet surfactant to reduce beading of the inoculum and increase bacterial dispersal on *A. thaliana*'s waxy leaves, and inoculum was sprayed onto the plants using an airbrush. At harvest, three large, undamaged primary leaves were selected from each pot and placed into 1mL tubes of 10mM phosphate buffer with 0.05% Silwet.

Ice nucleation assays

To quantify sucrose availability to phylloplane bacteria, the sucrose-inducible bacterial biosensor *Pa*299R (p61RYice) was inoculated onto bean leaves. To harvest, two healthy primary leaves (as opposed to trifoliates) were chosen from each pot, severed, and immersed in 20mL of KPO_4 buffer. Leaves were then sonicated for 5 minutes, vortexed for 30 seconds, and removed. Mean bacterial reporter induction in inocula and leaf harvest samples was measured by ice nucleation assay (Loper *et al.*, 2002) and normalized to CFU counts derived from hand- or laser-counting of spiral-plated samples.

Microscopy and Image Processing

Fixed cell samples were diluted as needed, spotted onto ProbeOn Plus (Fisher Scientific, cat#22-230-900) slides in 20µL droplets, and dried at 37°C for 30-45 minutes. Samples were then covered with Aqua PolyMount anti-fade mounting reagent (Polysciences, cat#18606) and a #1 cover slip. Bacteria were viewed and photographed at 1000x magnification using a Roper Quantix camera attached to a Zeiss AxioImager M1 microscope equipped with standard DAPI and EndowGFP filter cubes. Optimum views, in which cells were abundant but not clumped together, were photographed. For each treatment, 5-25 images were acquired using iVision software (BioVision, 2010). For each view photographed, tandem DAPI and GFP images were captured using the Multi-D Acquire function. The same exposure settings were used throughout a single experiment; exposure times ranged between 200-300ms for DAPI and 300-500ms for GFP.

For quantitative image analysis, the iVision FlatField function was applied to every image to correct for uneven microscope illumination across the field of view (BioVision); all subsequent image analysis was performed on these corrected images. Bacterial cells were identified by using the iVision segmentation function to separate DAPI-stained cells from the background. The selection threshold was manually adjusted such that segment masks wrapped tightly along cell boundaries as defined by DAPI staining. All segments with a size smaller than 40 pixels and greater than 300 pixels were omitted, to avoid debris and large cell aggregates. The resulting segment mask was pasted onto the corresponding GFP image and manually aligned to ensure that no drift occurred between images. The mean GFP pixel intensity of each segmented cell object was quantified using the "Measure Segments" function and exported to an Excel file. To correct for variation in background fluorescence between images, mean pixel intensity was calculated for three haphazardly selected background areas from each image. Mean background pixel intensity of these three areas was calculated, then subtracted from the mean pixel intensity of every measured object in the image.

Background-corrected pixel intensity data were imported into Statistica (Version 9.1, StatSoft), which was used to generate basic descriptive statistics, histograms, and normal probability plots.

To calculate the GFP-positive proportion of each population, the 90th percentile of the 0-hour GFP intensity was calculated for each strain; at all subsequent time points, cells that exceeded this strain-specific threshold induction value were considered GFP-positive.

Flow Cytometry

Flow cytometry was performed using a Partec CyFlow small-particle analyzer. Particles were excited using a 480nm laser, GFP fluorescence was detected with a 520nm band pass filter (FL1), and red fluorescence using 570nm long-pass filter (FL2). Data were acquired and mean relative GFP induction analyzed using FCS Express software (DeNovo).

To ensure sensitive detection of bacteria, forward-scatter (FS) and sidescatter (SS) gain settings were always adjusted to ensure optimum particle separation and identification of bacterial subpopulations. Fluorescence gain was set such that 99% of non-fluorescent control bacteria fell within the first decade of a single-parameter fluorescence histogram; cells exceeding this threshold were considered GFP-positive. For samples harvested from leaves, a constitutive GFP-positive control strain was used to identify the biosensor cell population in each experiment: by selectively gating on GFP-positive fluorescent events, the biosensor cell subpopulation was identified from a complex mix of particles on the FS/SS scatterplot. A gate was drawn around this putative biosensor population, and all subsequent analyses of leaf washate samples restricted to this defined subpopulation.

Statistical Analyses

Basic data analysis and calculations were performed in Microsoft Excel (2007). Statistical analyses were performed using Statistica (Version 9.1, StatSoft). Normality of cellular fluorescence within a given population was assessed by normal-probability plots. Where indicated, biosensor reporter induction was compared between treatments using one-way or multifactorial ANOVA followed by post-hoc analysis using planned contrast coefficients or Tukey's HSD test. Ice nucleation experiments were assessed via ANCOVA, with estimated insolation on the day of experiment as the continuous variable, and with treatment and experimental replicate date as the categorical variables.

Results

Light intensity increases phyllosphere sucrose availability

To help control for inter-experiment variability in basal levels of phyllosphere sugars, the effect of seasonal environmental conditions on leaf-surface sugar availability was investigated. In 6 replicate experiments conducted between June 2009 and January 2010, greenhouse-grown bean plants were inoculated with the sucrose-inducible biosensor strain *Pantoea agglomerans* MX149 (p61RYice). Inoculated plants were then incubated under controlled conditions for 7 hours before harvesting and assaying bacteria for sucrose-induced ice nucleation activity (Figure 3). When a downward trend was noted in mean sucrose sensing within the same treatment across replicate experiments, analyses were undertaken to establish whether these declines were significant (Table 1). A significant, negative correlation ($r=-0.57$, $p\leq0.01$) was observed between *Pa*MX149 (p61RYice) biosensor induction and experimental date (expressed as the number of

days from the initial experiment), suggesting that seasonal changes in basal sucrose availability occur in the phyllosphere. A similar negative correlation was observed in the 100µM sucrose positive control ($r=-0.73$, $p\leq0.01$), but was absent in both auxin treatments (*Pa*299R: $r=-0.21$, $p=0.45$; NAA^+: $r=-0.15$, $p=0.55$). The negative control exhibited minimally detectable ice nucleation activity throughout all experiments (data not shown).

To confirm the initial observation that seasonal conditions contribute to experimental variation in sucrose availability, two experiments were conducted. In the first, 2-week-old bean plants were transferred either to a warm, long-day greenhouse ("summer" conditions) or a cool, short-day greenhouse ("winter" conditions). *Pa*MX149 (p61RYice) reported significantly higher levels of sucrose on summer-grown plants than winter-grown plants ($t=-17.23$, $df=4$, $p<0.001$). This trend persisted even in a positive control treatment in which sucrose biosensor bacteria were co-inoculated onto the plants with 100 µM exogenous sucrose, though the difference was no longer significant ($t=-2.32$, $df=4$, $p=0.08$) (Figure 1a).

To further explore seasonal effects, bacterial sucrose sensing was compared on host plants pre-adapted to different temperature and light intensity conditions. Two-week-old bean plants were maintained in either high- or low-intensity light in the same greenhouse for 1 week prior to experimentation; photon flux density under low-light intensity was approximately 25% of the high-intensity treatment (data not shown). As part of the same experiment, 2-week-old bean plants were moved into high-temperature (30°C) or low-temperature (20°C) incubators and maintained under similar light conditions for 3 days prior to experimentation. On the day of the experiment, biosensor bacteria were inoculated onto all plants, incubated under uniform, standard experimental conditions, and harvested at 7hpi to measure reporter induction (Figure 1b). Biosensors on plants grown under high-intensity light reported significantly higher sucrose exposure than plants grown under low-intensity light ($t=3.10$, $df=8$, $p=0.015$). Temperature exerted no measurable effect on sucrose sensing ($t=0.99$, $df=8$, $p=0.35$).

Based on these results, seasonal variations in light intensity or other environmental conditions appear to influence the basal amount of phyllosphere sucrose available to bacterial epiphytes, with summer conditions yielding higher quantities of leaf-surface sugar. Estimated insolation on the date of each experiment was therefore included as a statistical covariate to account for variations in baseline sucrose sensing across experiments performed at different times of year (Table 2).

The presence of auxin decreases sucrose availability to phyllosphere bacteria

As a preliminary test of whether bacterial auxin production alters sucrose availability in the phyllosphere, bacterial auxin levels were manipulated by coinoculation of a sucrose-inducible bacterial biosensor with exogenous naphthalene acetic acid (NAA), a synthetic auxin. Bean leaves were spray-inoculated with the IAA^- *P. agglomerans* strain MX149 bearing the plasmid p61RYice, a sucrose-inducible *inaZ* bioreporter with a range of sensitivity between 10^{-6} and 10^{-3}M sucrose (Miller *et al*., 2001). Biosensor bacteria were inoculated with or without NAA, then recovered from the plant at 3, 7, and 24 hours post-inoculation (hpi) and assayed for ice nucleation activity (Figure 2).

Negative control bacteria lacking the *inaZ* reporter exhibited negligible ice nucleation activity throughout the experiment (data not shown), whereas positive control biosensors inoculated with

6.25mM exogenous sucrose reported consistently elevated induction (Figure 2). Sucrose-inducible biosensors in all treatments responded to leaf surface sugars with a sharp initial increase in sucrose sensing at 3hpi. Multifactorial ANOVA confirmed this temporal induction pattern, showing a significant effect of time on reporter induction ($F_{(3,12)}$=68.58, p<0.001); the test also found a marginally significant, overall treatment effect of NAA coinoculation on sucrose sensing ($F_{(1,12)}$=6.60, p=0.025) (Table 3). Planned contrast comparisons between the NAA+ and NAA- treatments at each timepoint indicated that marginally significant differences emerged at 7 hpi, with auxin-inoculated cells reporting lower sucrose exposure (t=2.68, p=0.020, df=1); this trend persisted at 24hpi, but was no longer statistically significant (Table 4). Based on these results, samples were harvested at only the 7hpi timepoint in subsequent replicates of the experiment.

The experiment was repeated a total of six times, though one replicate was omitted due to failed induction of the positive control (Figure 3). Using plant insolation as a covariate to explain inter-experimental variability in baseline sucrose availability, ANCOVA analysis suggested a significant treatment effect of NAA coinoculation on sucrose sensing across the remaining five experiments ($F_{(2,53)}$=77.696, p<0.001) (Figure 3; Table 5). To test the *a priori* hypothesis that NAA coinoculation reduced sucrose availability across all five experiments, post-hoc comparisons of NAA^+ and NAA^- treatments were performed using contrast coefficients; these confirmed that the presence of exogenous auxin significantly decreased sucrose availability to phyllosphere bacteria ($F_{(1,53)}$=15.32, p<0.001) (Figure 4b; Table 6).

We also investigated whether physiologically relevant levels of endogenous bacterial auxin could reduce phyllosphere sucrose availability. As part of the same set of experiments described above, bean leaves were spray-inoculated with the wild-type sucrose biosensor strain *Pa*299R (p61RYice) or its auxin-deficient mutant derivative, *Pa*MX149 (p61RYice). At 7hpi, bacteria were recovered from the plants and assayed for ice nucleation activity (Figure 3). Though relative differences in sugar sensing were smaller between IAA^+ and IAA^- bacteria than between exogenous NAA^+ and NAA^- treatments, the same trend persisted: when auxin was present, bacteria reported less sucrose. Using plant insolation as a covariate to control for variations in basal sucrose levels, ANCOVA analysis suggested a significant net treatment effect of bacterial auxin status on sucrose sensing across the four experiments ($F_{(2,44)}$=50.226, p<0.001) (Figure 3; Table 7). Using contrast coefficients, post-hoc comparisons of mean sucrose sensing by 299R and MX149 confirmed the *a priori* hypothesis that wild-type bacteria experienced significantly less sucrose on bean leaves than isogenic, IAA^- mutants ($F_{(1,44)}$=7.44, P<0.01) (Figure 4a; Table 8).

Auxin-dependent decreases in sucrose availability are minimally detectable using a fluorescent bioreporter

To complement sucrose-sensing experiments performed using an ice nucleation reporter, similar experiments were performed using *P. agglomerans* bacteria bearing the plasmid p61RYtir, a sucrose-inducible *gfp* bioreporter with a range of sensitivity between 10^{-5} and 10^{-2} M fructose (Miller *et al*., 2001). These results were inconsistent with those achieved using the ice nucleation reporter, perhaps because the fluorescent reporter was tenfold less sensitive.

In an initial experiment, fluorescent biosensor induction was quantified using flow cytometry. Sucrose bioreporter strain *Pa*299R (p61RYtir) and its isogenic, IAA$^-$ derivatives MX149 and XYLE were inoculated onto bean plants. At 24hpi, the bacteria were harvested and their GFP fluorescence measured via flow cytometry (Figure 5). Due to variable, GFP-negative background, it was impossible to distinguish uninduced reporter cells from background particulates, so the proportion of induced versus uninduced cells could not be calculated (see Appendix 1 for a discussion of background contamination in flow cytometry). However, GFP-positive cell populations were easily identified, and the mean cellular fluorescence of induced cells was compared between the experimental strains (Figure 6). In one experimental replicate, a one-way ANOVA showed a significant treatment effect of bacterial strain on sucrose sensing ($F_{(2, 5742)}$=78.746, p<0.001) (Figure 7). Post-hoc Tukey HSD comparisons (Table 9) of the three strains found significant (p<0.001) differences in sucrose sensing between all three strains, with *Pa*MX149 sensing the most sucrose (x=1224.2, S.D.=195.8, n=2419), *Pa*XYLE sensing an intermediate concentration (x=1178.9, S.D.=222.7, n=1806), and the wild-type *Pa*299R sensing the least (x=1138.2, S.D.=223.78, n=1520). However, attempts to replicate these results, or to coinoculate the sucrose GFP biosensors with exogenous NAA, suffered from failed or inconsistent biosensor induction (data not shown).

In an effort to gain more reliable results using the fluorescent sucrose biosensor, leaf inoculation experiments were repeated using microscopy and digital image analysis to quantify cellular GFP content. Wild-type and IAA$^-$ *P. agglomerans* sucrose biosensors were spray-inoculated onto bean plants, harvested at varying intervals, and their induction measured via microscopy. As part of the same experiment, bacterial auxin status was also manipulated by co-inoculating MX149 (p61RYtir) and XYLE (p61RYtir) with or without exogenous NAA.

Neither endogenous nor exogenous auxin exerted a consistent impact on bacterial sucrose sensing of p61RYtir strains as quantified by microscopy (Figure 8). As with the flow cytometry experiments, this was due largely to failed induction of the biosensors: after 1.5 and 5 h on the leaf surface, neither the mean cellular fluorescence of harvested biosensors nor the proportion of GFP-positive cells exceeded that of the inoculum. The only exception was the *Pa*299R treatment, which exhibited both a higher proportion of GFP-positive cells and a significantly higher mean cellular fluorescence at 1.5 hpi. However, this induction appeared spurious—positive control treatments in which 299R and other p61RYtir biosensor strains were co-inoculated with exogenous sucrose showed no significant induction, nor did any other treatment.

Exogenous auxin increases fructose availability to phyllosphere bacteria

To complement experiments performed with a sucrose-inducible biosensor and further test how auxin affects carbon availability in the phyllosphere, the effect of auxin on fructose-inducible GFP biosensor strains was tested.

In an initial time course experiment, bean leaves were spray-inoculated with the IAA$^-$ *P. agglomerans* strain MX149 bearing the plasmid pFru44, a fructose-inducible *gfp* reporter (Leveau *et al.*, 2001a). Bacteria were inoculated onto plants with or without exogenous NAA, then recovered from the plant and assayed for GFP cellular fluorescence at 3, 7, and 24hpi using flow cytometry (Figure 9). A multifactorial ANOVA found no significant net treatment effect of NAA coinoculation across time points, but did report a significant treatment-by-time-point

interaction ($F_{(3,8)}$=1402.29, p<0.001) (Table 10). *Post-hoc* analysis using contrast coefficients to compare NAA^+ and NAA^- treatments at each timepoint found that NAA-coinoculated cells sensed marginally more sugar at 7 hpi, but significantly less at 24 hpi (Table 11). The experiment was repeated two additional times, with reporter activity assayed by flow cytometry at 24 hpi only. Results were inconsistent: the second experiment suggested that NAA^+ cells experienced significantly more fructose than NAA^- cells (t=-4.57, p=0.01, df=4; Figures 10-11a), while the third experiment showed that they experienced no significant difference (t=0.823, p=0.46, df=4; Figure 11b).

Because it expresses the relatively stable ASV protein variant of GFP, the rate of cell growth (*i.e.* how quickly GFP is diluted from individual cells) exerts a significant effect on cellular pFru44 fluorescence (Leveau *et al*., 2001b). This complicates interpretation of 24hpi fluorescence data, and may have contributed to the indeterminate results achieved using the pFru44 reporter construct. To simplify interpretation of fluorescence data, subsequent experiments were performed with bioreporter strains bearing the fructose-inducible pFru46 construct, which uses the less stable AAV GFP variant as a reporter. With a half-life of only 60 minutes when expressed in *E. coli* (versus 110 minutes for ASV), the AAV variant offers a more sensitive measure of real-time fructose availability (Leveau *et al.*, 2001b; Andersen *et al*., 1998; Appendix 1).

NAA coinoculation experiments were repeated on bean plants using the MX149 (pFru46) bioreporter, and GFP induction measured via microscopy at 0, 1, 3, and 5 hpi. A negative control strain, wild-type *Pa*MX149, remained GFP-negative throughout the experiment (<10% GFP positive at all time points), while *Pa*MX149 (pKTbla), the constitutive-GFP control strain, remained consistently induced (>92% GFP-positive at all time points) (Figure 12). Although all pFru46 biosensor treatments showed strong induction upon foliar inoculation, cells coinoculated with exogenous NAA or sucrose showed more rapid induction, with >90% of the population becoming GFP-positive by 1 hpi; in contrast, only 29% of biosensors inoculated with buffer alone became induced by 1 hpi (Figure 13). By 3-5 hpi, all treatments showed similarly high proportions of induced cells. (Data are summarized in Figure 14a)

In addition to the proportion of induced cells in each treatment, we also sought to measure the strength of induction of the biosensor population; mean cellular fluorescence intensity was therefore calculated for the GFP-positive bacterial subpopulation of each treatment. Negative *Pa*MX149 control cells displayed minimal fluorescence, with mean fluorescence pixel intensities of <90; positive control cells remained consistently GFP-positive throughout the experiment (Figure 12). As expected, mean fluorescence pixel intensity of biosensor cells increased significantly upon foliar inoculation: multifactorial ANOVA confirmed this effect, indicating that time of observation exerted a significant effect on GFP fluorescence ($F_{(3,1736)}$=70.90, p<0.001) (Table 12). Despite early differences in the *proportion* of GFP-positive cells in NAA^+ versus NAA^- treatments, mean *fluorescence* intensity of the induced cells was indistinguishable at 1 hpi and 3 hpi (p>0.1). However, the ANOVA indicated a significant treatment-by-timepoint interaction ($F_{(3, 1736)}$=17.37, p<0.001); post-hoc analysis with Tukey's HSD test indicated that at 5 hpi, the induced population of NAA-coinoculated cells displayed significantly higher fluorescence than buffer-inoculated cells (p<0.001), with the NAA^- treatment sensing only 72% as much sucrose as the NAA^+ treatment. (Table 13; Data are summarized in Figure 14b)

Native bacterial IAA production increases fructose availability in the phyllosphere

Exogenous NAA appeared to transiently enhance fructose availability to phyllosphere bacteria; to test whether fructose availability was similarly affected by physiological levels of native bacterial IAA, bean leaves were inoculated with pFru46 biosensor strains of IAA-deficient *Pa*MX149 or *Pa*XYLE, the wild-type *Pa299R,* or *Pa*299R (pMB2), which carries an extra, plasmid-borne copy of the *ipdC* gene under its native promoter. At 24hpi, bacteria were harvested and their GFP expression analyzed via flow cytometry (Figure 15). Nonfluorescent, *Pa*299R negative control cells were consistently GFP-negative, and *Pa*299R (pKTbla) positive control cells exhibited consistently elevated GFP expression—although once again, high levels of nonfluorescent background particles made it difficult to differentiate between induced and uninduced cell populations. The experimental biosensor strains exhibited fluorescent induction on leaves, and distributions of GFP-positive cells were approximately normal (Figure 16). One-way ANOVA showed a significant effect of bacterial strain on fructose sensing ($F_{(3,10,644)}$=162.27, p<0.001) (Figure 17). Tukey's HSD comparisons of the four strains at the p<0.001 level suggested that *Pa*299R (pMB2) (x=3554.1, S.D.= 379.0, n=3432) sensed significantly more fructose than all other strains, while *Pa*299R (x=3406.6, S.D.= 502.6, n=3418) and *Pa*XYLE (x=3395.3, S.D.=428.7, n=1638) sensed approximately equal amounts of fructose. *Pa*MX149 sensed significantly less fructose than any other strain (x=3294.3, S.D.=458.0, n=2160)—96.7% as much sugar as wild-type *Pa*299R, and only 92.7% as much as *Pa*299R (pMB2).)

To complement these flow cytometric data, a similar experiment was performed using microscopic quantification of fluorescent fructose biosensors. Bean leaves were inoculated with wild-type *Pa*299R (pFru46) or its isogenic, IAA-deficient mutant *Pa*MX149 (pFru46)*;* non-fluorescent *Pa*MX149 were used as a negative control, and constitutively GFP-positive *Pa*MX149 (pKTbla) cells as a positive control. Cells were harvested at 0, 1, 3, and 10 hpi, and GFP fluorescence assessed by fluorescence microscopy and subsequent digital image analysis.

Negative controls exhibited minimal fluorescence at all timepoints, whereas *Pa*MX149 (pKTbla) cells were consistently fluorescent throughout the experiment (Figure 18). Uninduced fructose biosensors were nonfluorescent at t=0 (fluorescence thresholds were set such that 10% of cells from the 0-hour inocula were GFP-positive) (Figure 19), with a right-hand-skewed distribution (Figure 20). By 1-3 hpi, biosensors had rapidly shifted to a normally distributed population of induced cells (>95% GFP-positive); by 10 hpi, as leaf-surface sugar supplies were exhausted, both strains had returned to a right-hand-skewed distribution, with only 24% GFP-positive cells. Similar proportions of MX149 and 299R cells were induced at all time points. (Data are summarized in Figure 21.)

To compare the fluorescence intensity of induced cells, mean cellular fluorescence was calculated for the GFP-positive bacterial subpopulation of each sample. Multifactorial ANOVA confirmed a significant initial increase in fluorescence induction across all treatments, with the number of hours after inoculation exerting a significant effect on biosensor induction ($F_{(3,\ 2302)}$=300.42, p<0.001) (Figure 21a). Although there was no overall difference in induction between the 299R and MX149 bacterial strains, a significant strain-by-timepoint interaction was detected ($F_{(3,\ 2303)}$=13.86, p<0001); post-hoc analysis with Tukey's HSD test indicated that at 1 hpi, *Pa*299R experienced significantly higher fructose induction than *Pa*MX149 (p<0.001). At

this time point, cellular fluorescence intensity of the IAA^+ strain *Pa*299R (x=2037.20, S.D.=830.87, n=273) was 21% higher than the IAA^- mutant *Pa*MX149 (x=1618.26, S.D.=701.38, n=342). There was no significant difference in fluorescence between the two strains at other time points ($p>0.05$)

Individual plant cell wall invertases do not mediate bacterial effects on phyllosphere sugar availability in A. thaliana

The observed trends in bacterial sugar sensing in the phyllosphere, which indicated that IAA increases fructose availability but decreases sucrose availability, suggested that IAA may activate plant invertases. To probe the role of plant cell wall invertases in bacterial carbon acquisition, auxin-mediated behavior of bacterial biosensors was investigated on *Arabidopsis thaliana* invertase mutants. (The experiment was also intended to test whether trends in bacterial sugar sensing would persist on host plants other than *P. vulgaris*.) In addition to wild-type *A.t.* Columbia-0 controls, *cwinv1* (At3g13790), *cwinv2* (At2g36190), and *cwinv4* (At3g52600) mutant plants were inoculated with sucrose biosensors (*Pa*MX149 (p61RYtir)) or fructose biosensors (*Pa*MX149 (pFru46)) in the presence or absence of exogenous NAA. After 1.5 hours on the leaf surface, bacteria were harvested and assayed by fluorescence microscopy to determine the proportion of GFP+ cells and the mean fluorescence of the induced cell population.

NAA-mediated changes in sugar sensing observed on wild-type *A.t.* Col-0 plants did not conform to those observed on *P. vulgaris*. No significant differences in sucrose availability were detected between NAA^+ and NAA^- treatments: a similar proportion of p61RYtir biosensors were GFP-positive in both treatments (Figure 22a), and mean cellular fluorescence was statistically indistinguishable between the populations (Figure 22b; Table 15). Trends in fructose sensing on wild-type *A.thaliana* were opposite those observed in *P. vulgaris*: mean cellular fluorescence was significantly higher in the NAA-coinoculated pFru46 cell population than the buffer-inoculated population (Table 15); the proportion of GFP-positive cells was also higher than buffer-inoculated cells (Figure 23a).

Sugar sensing trends on the *cwinv4* (*At094878c*) and *cwinv1* (*At007233c*) mutants were similar to those noted on wild-type *A. thaliana*. In contrast, the *cwinv2* mutant (*At068113c*) supported trends in sugar sensing that resembled those observed on *P. vulgaris*. Though mean cellular fluorescence of the p61RYtir sucrose biosensor was similar between NAA^+ and NAA^- treatments, a lower proportion of cells became GFP-positive in the NAA-coinoculated population (Figure 22). Conversely, NAA coinoculation yielded both a higher proportion of GFP-positive pFru46 cells and a significantly higher mean cellular fluorescence (Figure 23; Table 15), suggesting increased fructose availability in the presence of auxin.

P. agglomerans 299R *growth is induced more quickly using glucose or fructose as a carbon source than sucrose*

Experimental data suggested that bacterial IAA increased availability of monosaccharides (fructose) while decreasing availability of disaccharides (sucrose). To test whether such a shift in carbon availability might enhance bacterial growth, a series of *in vitro* experiments was conducted to compare growth of *Pa*299R on sucrose, glucose, and fructose.

Bacteria were cultured in Minimal A liquid medium with varying concentrations of sucrose, glucose, or fructose as a sole carbon source, and cell populations measured at various times after inoculation. No growth differences were evident at 4hpi, but by 8-24hpi glucose- and fructose-grown cells exhibited higher growth than cells cultured in similar concentrations of sucrose (Figures 24-25a). By 48 and 72hpi, carbon-dependent growth differences were no longer evident (differences between carbon treatments were occasionally present, but were inconsistent between experiments) (Figure 25b-26). These results suggest that although net growth of *Pa*299R is equal on all carbon sources, glucose and fructose confer a transient growth advantage, as they support a more rapid induction of bacterial growth than sucrose.

To further characterize patterns of *Pa*299R carbon utilization, *in vitro* growth experiments were repeated in the presence of cycloserine, an antibiotic that selectively kills actively growing cells. Under these culture conditions, a high proportion of surviving cells indicates minimal cell growth on a given carbon source, while a drop in the number of surviving cells indicates the onset of cell growth. After 4.5 hours of growth, glucose- and fructose-grown cell populations had fewer surviving cells than sucrose-grown cells at all carbon concentrations greater than 0.05 mg/L, indicating that a greater proportion of cells had undergone cell division (Figure 27). This trend persisted weakly at 10hpi, but by 30hpi cells had died in all treatments.

Discussion

Sugar-specific bioreporter induction in the foliar epiphyte *Pa*299R revealed that auxin alters carbon availability on the leaf surface of the model host plant *P. vulgaris*. Contrary to expectation, the change was not simply an overall increase in sugar availability. Rather, auxin elicited a decrease in phyllosphere sucrose, and an increase in fructose.

Reduced sucrose in response to IAA

Comparison of induction data to published dose-response curves suggests that the *Pa*MX149 (p61RYice) sucrose biosensor experienced mean local sugar concentrations of approximately $3x10^{-5}$M sucrose—similar to those previously reported on bean leaves, and below the limit of detection of the p61RYtir GFP sucrose reporter (Miller *et al*., 2001). Our data, however, indicate that phyllosphere bacteria sense lower concentrations of sucrose in the presence of auxin. Wild-type (IAA^+) *Pa*299R biosensors and cells co-inoculated with exogenous NAA both detected significantly less sucrose than the IAA^- *Pa*MX149 mutant (88% and 84%, respectively). Based on the aggregate nature of these ice nucleation bioreporter data, it was unclear whether auxin-induced declines were attributable to a small, population-wide decrease in sucrose availability or to a large decrease in sucrose availability to a smaller subpopulation of cells.

In an attempt to differentiate between these hypotheses, the p61RYtir green fluorescent protein (GFP) biosensor was used to probe how auxin affected biosensor induction at the single-cell level. Unfortunately, differences in sucrose detected by the GFP biosensor were inconsistent across experiments. In the single flow cytometric experiment in which all treatments became significantly induced, the data confirmed the trend noted in ice nucleation experiments: after 24 hours on bean leaves, the IAA^- mutants *Pa*MX149 and XYLE both sensed significantly more sucrose than did wild-type 299R. However, in subsequent experiments employing both flow

cytometric and microscopic evaluations, biosensors often failed to become induced (*i.e.* become GFP-positive after arrival on the leaf); no significant differences were detected in either the mean GFP fluorescence or the proportion of GFP-induced cells between the auxin and auxin-free treatments.

These inconsistent results with the p61RYtir reporter do not necessarily undermine the findings of the p61RYice reporter. Given that the mean sucrose concentrations detected by the inaZ reporter fell below the threshold of sensitivity for p61RYtir (Figure 28), the fluorescent bioreporter's failure to detect auxin-dependent changes in sucrose—or even to become consistently induced when inoculated onto bean leaves—may simply reflect its limited range of sensitivity. Variation in basal quantities of sucrose from one experiment to the next, possibly due to difference in light intensity experienced by the plant, could also have contributed to inconsistent data trends.

Data from the GFP-based sucrose sensor were also inherently difficult to interpret due to the sensor's pattern of induction. Sucrose dose-responsiveness of the p61RYtir biosensor does not arise simply from uniform, population-wide shifts in cellular fluorescence. Rather, bacterial cells can exhibit heterogeneous responses to increasing inducer concentrations—for example, a bimodal "induced-versus-uninduced" distribution, in which increasing sugar concentrations yield an increasing proportion of induced cells, versus a more traditional, dose-responsive induction, in which increasing sugar concentrations yield uniform increases in individual cellular fluorescence. (Appendix 1; Miller *et al*., 2001; Leveau *et al.*, 2001a). Interpreting leaf-surface sucrose reporter data can therefore depend very heavily on accurately measuring the ratio between induced and uninduced biosensor cells on the leaf surface, as well as the mean fluorescence of the biosensor population. Due to highly variable numbers of GFP-negative particles contaminating flow cytometric data (ranging from 25-89% of the total putative cell count), these calculations were not possible using flow cytometry. In contrast, microscopic quantification reduced the proportion of background contamination (typically <10% of putative bacterial particles). Unfortunately, microscopy experiments could not acquire the same large sample sizes as are available from flow cytometry. That, combined with the persistently low number of induced cells on the leaf surface, reduced statistical power for analyzing the proportion of induced p61RYtir bioreporter cells on the leaf surface.

With these limitations in mind, tentative interpretation of data from the p61RYtir experiments suggests no major auxin-dependent differences in either the proportion of cells fluorescing or the population mean fluorescence of induced sucrose biosensor cells. As p61RYtir is presumably only detecting the top 5% of most induced cells (Leveau *et* al., 2001a), this argues against the hypothesis that auxin alters sucrose availability to strongly induced cells (which would have been detectable as a further reduction in the already small proportion of GFP-positive cells). The 12-16% decline in sucrose availability detected by p61RYice bioreporters in the presence of auxin is therefore likely due to decreased sucrose availability to the estimated 95% of phylloplane cells that fall below the p61RYtir detection threshold. This interpretation suggests that bacterial IAA may primarily benefit *Pa*299R occupying nutritionally marginal, C-limited sites on the leaf surface, rather than the small proportion of foliar epiphytes that land in sucrose-rich nutrient "oases" capable of inducing the p61RYtir biosensor.

Increased fructose in response to bacterial IAA

When fructose-inducible biosensors were used to explore how auxin affects fructose availability on the leaf surface, they reported a trend opposite to that observed from sucrose sensing: in the presence of auxin, bacteria sensed more fructose.

In all treatments, biosensors became induced within 1-3 hours after inoculation, and remained fluorescent until initial sugar reservoirs were depleted, ca. 7-10 hours after inoculation. This observation conforms to a previous report using this biosensor (Leveau *et al*., 2001a), which found that the majority of bacteria consumed initial leaf sugar reserves of ≈ 0.15-4.6 pg/cell within 7 hours of arrival on the leaf surface.

Although experiments with the stable-gfp pFru44 gave a null result after 24 hours on the leaf (possibly due to the confounding effects of promoter induction and bacterial cell division), microscopy experiments with the short-half-life pFru46 bioreporter suggested that in the presence of auxin, bacteria experience an initial burst of elevated sugar after inoculation on the leaf. When co-inoculated with 100µM NAA in microscopy experiments, a much higher proportion of bacteria became induced after one hour on the leaf surface (90%, versus 29% of NAA^- cells); by five hpi, similar proportions of the bacterial population in each treatment had become induced, but the population mean fluorescence of NAA^+ cells remained significantly (28%) higher than that of NAA^- cells. When wild-type *Pa*299R cells were compared to auxin-deficient mutants, population mean fluorescence of induced 299R cells was significantly (21%) higher than that of the NAA^- strain *Pa*MX149 at one hpi, though the proportion of induced cells was similar. In each case, auxin treatments displayed a transient advantage in sugar acquisition between 1-5 hours, but this relative advantage disappeared by 10-24 hpi, as initial sugar reserves were consumed and the biosensor populations of both $auxin^+$ and $auxin^-$ treatments returned to a GFP-negative state.

Although microscopy experiments showed no significant differences between auxin and auxin-deficient treatments at later experimental time points, a flow cytometry experiment (which benefited from much higher sample sizes) suggested that subtle differences in sugar availability may persist even beyond the first few hours after inoculation. When observed after 24 hours on bean leaves, population mean fluorescence of wild-type *Pa*299R was 4% lower than that of bacteria expressing an extra copy of the *ipdC* gene under its native promoter; in turn, the *PaMX149* mutant reported 3% lower mean induction than did the wild-type. These empirical observations are in the range of the 7% net carbon advantage predicted by Brandl *et al.* (1998), and roughly mirror the 7% decline in sucrose sensing detected by the p61RYice biosensor in the presence of auxin.

Given the specificity and range of the pFru46 bioreporter, it is unsurprising that only small differences in fructose availability were detected between $auxin^+$ and $auxin^-$ treatments. Although the sensor is exquisitely responsive to fructose availability *in vitro* (with sensitivity reaching as low as ≈2µM fructose), it is also induced by other sugars—particularly sucrose, which induces the reporter with only 2-fold less sensitivity than fructose (Figure 29; Leveau *et al*., 2001a). Thus, although pFru46 is a good reporter of overall carbon availability, it is a sub-optimal tool for elucidating dynamic partitioning between sucrose and fructose on the leaf surface. In mixed-substrate environments such as the leaf surface, increases in fructose availability could be obscured by unrelated fluctuations in sucrose availability—or, crucially, offset by IAA-induced *declines* in sucrose availability. Given that we observed an increase in fructose sensing despite

the observed decreases in sucrose sensing indicated by the p61RYice bioreporter, we are reasonably confident in asserting that phyllosphere fructose availability increases in the presence of auxin. However, follow-up studies that employ more detailed chemical techniques to track changes in leaf surface sugar profiles could generate more precise quantitative estimates of how bacterial IAA modifies carbon availability in the microbial habitat.

Bacterial IAA facilitates carbon acquisition by resource conversion

Cumulatively, the experimental data presented here support the hypothesis that bacterial IAA production by phyllosphere epiphytes decreases bioavailability of sucrose, but increases bioavailability of fructose. In conjunction with previous reports that auxin stimulates rapid, localized plant apoplastic invertase activity (Roitsch *et al.*, 2004; Morris *et al.*, 1984; Morris *et al.*, 1986), this pattern suggests that bacterial auxin may activate plant invertases, driving cleavage of the disaccharide sucrose into its component monosaccharides, glucose and fructose.

This begs the question of why bacteria would expend cellular resources to produce IAA, simply to transform one metabolizable sugar (sucrose) into another (fructose or glucose). In addition to the energy, carbon, and amino acids required to induce transcription and translation of the indolepyruvate decarboxylase enzyme, subsequent IAA biosynthesis would deplete pools of tryptophan in the cell—making auxin biosynthesis a potentially costly metabolic boondoggle.

Several hypotheses could explain the adaptive value of IAA-mediated resource conversion. Perhaps the most obvious is that invertase-mediated cleavage of apoplastic sucrose prevents phloem loading by sucrose-specific transporter proteins, thereby increasing sugar concentrations in the apoplastic compartment. Decreasing vascular sink strength via cold girdling, which also impedes phloem loading, was found to increase the concentration of apoplastic sugars within 30-60 minutes of application in *Vicia faba* (Ntsika and Delrot, 1986), *Spinacea oleracea*, and *Symphytum officinale* leaves (Voitsekhovskaja *et al.*, 2000). Furthermore, a variety of fungal and bacterial pathogens stimulate activity of extracellular invertases during pathogenesis, which promotes source-to-sink transition and improves local access to photoassimilates (Biemelt *et al.*, 2006). It remains unclear whether invertase activity is orchestrated by the invading pathogen for its own benefit, or is induced by the plant to provide a ready source of hexose to fuel energy-intensive defense responses and provide metabolic feedback signals to the host plant (Essmann *et al.*, 2008; Kocal *et al.*, 2008; Bonfig *et al.*, 2010). Nonetheless, cell wall invertases play a crucial role in determining source/sink balance and apoplastic sugar availability, and may therefore represent a carbon acquisition strategy for epiphytic organisms, as well as endophytic pathogens.

Another possibility is that monosaccharides may diffuse more easily than can sucrose from the plant apoplast to the leaf surface. Derridj (1996) reported that glucose could cross the maize leaf cuticle fivefold more quickly than sucrose. Given that cuticle permeability poses a significant barrier to carbon diffusion from the plant apoplast to the leaf surface (Derridj, 1996), IAA may enhance epiphytic carbon bioavailability by stimulating transformation of less diffusible plant photoassimilates into glucose, to which the cuticle is more permeable. A resource conversion strategy may therefore support more effective mobilization of carbon towards bacteria. (This could also explain why bacteria would employ the small, diffusible molecule IAA to stimulate plant invertases across the cuticle, rather than simply producing their own invertase, which would be unable to diffuse into the apoplast.) Interestingly, this hypothesis would suggest that

the effectiveness of bacterial IAA production may be environmentally conditional, as solute mobility through the plant cuticle is temperature-dependent, increasing 5- to 10-fold for each 10°C increase in temperature (Schonherr *et al.*, 1996). As such, both diffusion of IAA into the apoplast and the reciprocal diffusion of apoplastic solutes to the leaf surface would be higher at elevated temperatures. Bacterial IAA production may therefore be adaptive at higher, but not lower temperatures.

Alternatively, bacteria may simply be able to use glucose and fructose as a carbon source more efficiently than they can use sucrose. Experiments described here suggest that, although net bacterial growth after 48 hours is similar on all three carbon sources, either glucose or fructose supports more rapid induction of bacterial cell division than does sucrose, with differential growth most pronounced during the initial 6-24h after inoculation. This period of enhanced *in vitro* proliferation is similar to the period during which the majority of bioavailable sugars are consumed by phyllosphere bacteria *in planta* (Miller *et al.*, 2001), as well as the period during which wild-type *Pa*299R cells experience enhanced fitness relative to an IAA-deficient mutant when growing on leaves (Brandl *et al.*, 1998).

The relatively rapid induction of *Pa*299R growth using fructose or glucose as a carbon source may result from regulatory differences between the metabolic pathways used to break down these sugars versus sucrose. As a close relative of *E. coli*, *Pa*299R likely absorbs glucose and fructose via PEP-phosphotransferase (PTS)-mediated uptake under the control of global metabolic regulators (Deutscher *et al*., 2006). Sucrose is also presumed to be absorbed via PTS-mediated uptake, as *Pa*299R was found to harbor a functional, genomic *scr* operon (data not shown). But, rather than being under the control of global regulators, the *scr* operon is only conditionally induced: based on characterization in *Klebsiella pneumoniae, Salmonella typhimurium* and *Erwinia amylovora* (Cowan *et al*., 1991; Aulkemeyer *et al*., 1991; Bogs *et al*., 2000), the *scrKYABR* operon is autoinductively regulated—selectively derepressed in the presence of the sucrose metabolite fructose-6-phosphate. The *scr* genes are believed to exhibit similar autoinductive regulation in *Pa*299R, based both on strong homology to *scr* operons in better-studied organisms and on the induction pattern of *scr*-based P61RYtir sucrose biosensors, which exhibit a strongly bimodal distribution in the presence of sucrose. This was interpreted to be a result of a dose-dependent proportion of cells rapidly becoming fully induced in response to sucrose, while the remainder of the cell population remained uninduced (Miller *et al*., 2001). During *in vitro* growth experiments, *Pa*299R's initial growth delay may therefore be attributable to an operon induction lag, as *scr* gene transcription and translation is initiated on a low-frequency, stochastic basis within the cell population. By later time points, either the entire population would eventually become induced, or the *scr*-induced subpopulation would have time to consume all of the sucrose. In either case, net bacterial cell doublings would ultimately be comparable between sucrose-grown cells and the more rapidly consumed fructose- or glucose-grown cells. Future monitoring of *scr* gene expression during bacterial growth on various carbon substrates could be undertaken to test this hypothesis.

In addition to operon induction lag, another possibility not directly investigated in this work is catabolite repression (Deutscher, 2008). In *Staphylococcus xylosus*, glucose was shown to repress *scr*-mediated sucrose utilization via the global catabolite control protein A (CcpA), ensuring preferential consumption of glucose in mixed-substrate environments (Jankovic *et al*., 2007). Glucose is an important component of bean leaf-surface carbon reservoirs (Mercier *et al.*,

2000); assuming that *Pa*299R exhibits similar patterns of catabolite repression, the ability to consume sucrose might be repressed in the phyllosphere. Although catabolite repression has not been studied directly in *P. agglomerans,* the *scr* operon of the related enterobacterial strain *Erwinia amylovora* exhibits catabolite repression in the presence of glucose (Bogs *et al.*, 2000), and the related eucalyptus pathogen *Pantoea ananatis* contains a CcpA homolog (Maayer *et al.*, 2010). Assuming that the presence of glucose suppresses sucrose metabolism on the leaf, auxin-mediated resource conversion may ensure that sucrose reserves that would otherwise go unused in a mixed-carbon environment can be accessed rapidly. In the future, *in vitro* experiments with mixed carbon sources could establish whether catabolite repression occurs in *Pa*299R, and how it might affect growth on the leaf surface.

In a phyllosphere context, the results presented here suggest that sucrose represents a less-accessible carbon source for *Pa*299R during the initial hours of arrival on the leaf surface, perhaps due to catabolite repression or induction lag of the sucrose metabolic operon. Thus, although bacteria with access to disproportionately more glucose or fructose would not experience any net growth advantage over long periods of time, they would derive a short-term advantage by inducing growth more rapidly upon onset of growth-permissive conditions. Classic r-selection theory suggests that IAA-mediated resource conversion would be adaptive under high-disturbance conditions where rapid, opportunistic proliferation was favored (Andrews *et al*., 1986). With its rapid shifts in temperature, UV exposure, water availability, and other environmental conditions, the phyllosphere fits this description. For example, Axtell *et al.* (2002) showed that freshly inoculated bacteria experienced decreased water availability within 5-30 minutes after inoculation onto *P. vulgaris* leaves. With growth constrained by such brief intervals of environmental hospitality, adaptations that effectively reduce lag phase by conferring earlier, more rapid initial proliferation can be expected to contribute significantly to fitness (Lenski, 1998).

Proposed model

Based on these observations, we propose the following model (Figure 30). Phyllosphere bacteria synthesize IAA, which diffuses into the plant across the leaf cuticle or along continuous aqueous films into nearby stomata. In the plant apoplast, microbially derived IAA interacts with auxin-specific plant receptors such as ABP1 at the plasma membrane. The resulting activation of H^+ ATPases is both rapid and localized—acidifying the apoplast, stimulating activity of cell wall invertases, and driving hydrolysis of sucrose into glucose and fructose. Apoplastic sugars diffuse onto the leaf surface, where the shift in carbon content—increased monosaccharide availability at the expense of sucrose—enhances bacterial fitness. This adaptive advantage may arise by favoring more diffusible sugars, thereby enhancing carbon transit to the phylloplane; by shifting the bioavailable carbon profile away from sucrose to more rapidly metabolizable resources (glucose and fructose); or by altering the plant environment in some other manner.

Future research might directly probe this model by testing the involvement of putative plant targets using knockout mutants. Although study of the putative auxin receptor ABP1 was long hampered by embryo lethality of null mutants, generation of inducible RNAi knockdown mutants in *N. tobacco* now facilitates such investigation (Siemens *et al*., 2010; Essmann *et al*., 2008). If bacterial IAA elicits plant responses via ABP1, then auxin-dependent differences in

carbon availability and bacterial fitness should disappear when bacteria are inoculated onto ABP1$^-$ leaves.

Similarly, a variety of plant invertase knockout mutants are now available. Though preliminary inoculations of sugar biosensors onto three different *A. thaliana* cell-wall invertase mutants revealed no robust IAA-mediated effects on *Arabidopsis* Col-0, this observation does not rule out the role of leaf invertases in mediating bacterial carbon acquisition. With six putative homologs in the *A.t.* cell wall invertase (*AtcwINV)* gene family (Sherson *et al.*, 2003), functionally redundant homologs could complement individual gene knockouts. (Indeed, the very fact that single-gene knockout plants exhibit only mild phenotypic irregularities suggests that complementation may occur.) Based on published reports, complementation seems somewhat unlikely—the six genes have spatially and developmentally distinct expression patterns, and only *AtcwINV1* (At3g13790), *AtcwINV3* (At1g55120), and *AtcwINV6* (At5g11920) were reported to be expressed in leaves (Sherson *et al.*, 2003); of these three genes, *AtcwINV3* and *AtcwINV6* were found to be fructan exohydrolases with no invertase activity (de Coninck *et al*., 2004). (A single-knockout mutant of the only remaining foliar-expressed candidate gene, *AtcwINV1*, was tested here, as were the largely flower- and seed-expressed *AtcwINV2* and *4*.) However, despite this apparent lack of expression overlap, *AtcwINV4* was also reported to exhibit low levels of expression in seedlings; gene complementation remains a formal possibility. Multiple-knockout mutants should therefore be tested to see whether IAA-dependent changes in sugar sensing emerge when functionally redundant plant genes are eliminated.

Alternatively, *Nicotiana tabacum* lines with inducible, RNAi-mediated silencing of cell wall invertases have been generated and used to investigate plant-pathogen interactions (Siemens, *et al*., 2010; Essmann *et al*., 2008); these plants might also be used to probe trends in carbon acquisition by IAA-producing bacteria. Exogenous chemical inhibitors could also be employed to interfere with invertase activity (Huang *et al*., 2007).

IAA-mediated fitness benefits may be context-dependent

Other questions raised by sugar-sensing experiments on *A. thaliana* include the extent to which IAA-mediated bacterial interactions vary depending on the plant host, or on environmental conditions.

Regarding host specificity, preliminary results suggested that auxin-mediated trends in sugar sensing detected on *P. vulgaris* plants were not sustained on the wild-type *A.thaliana* ecotype Columbia-0. One possible explanation for this result is the presence of 14 putative cwINV inhibitor proteins in the *A. thaliana* genome (Huang *et al.*, 2007). At least one of these proteins has been shown to localize to the apoplast, where, under acidic conditions (maximum activity at pH=4.5), it inhibits invertase activity by competitively excluding sucrose from the enzyme's active site (Hothorn *et al*., 2010). Although the presence of invertase inhibitors has not been studied in *P. vulgaris*, similar proteins were described in tobacco and tomato (Greiner *et al.*, 2000). Variation in the presence or regulation of invertase inhibitors between different plant species could therefore alter the dynamics of bacterial IAA-mediated invertase activation in the plant host. Inter-species variation in the kinetics of carbon transit through the apoplast may also explain differences in IAA-mediated carbon acquisition. *A. thaliana,* for example, appears to clear perfusions of exogenous carbon from its intercellular spaces much more rapidly than does

P. vulgaris (E. Ramos, pers. comm.). Such overall reductions in sugar availability could minimize the effect of bacterially derived IAA on bacterial carbon acquisition in plant species with rapid clearance of apoplastic nutrients.

In addition to being host-dependent, fitness benefits derived from bacterial auxin production may also be seasonally dependent. Our data indicated seasonal fluctuations in the baseline amount of sucrose available to microbes on the leaf surface, with repeated leaf-inoculation experiments reporting progressively lower sugar concentrations as summer progressed into winter (Figure 3). (Based on follow-up experiments, declines in light availability seem particularly likely to yield diminishing concentrations of leaf-surface sugars.) As phyllosphere carbon content is presumed to arise from passive diffusion of apoplastic solutes, seasonal changes at the leaf surface probably reflect underlying shifts in apoplastic carbon content.

It is unclear whether such shifts in apoplastic carbon concentration arise from seasonal declines in source cell productivity (*i.e.* a decline in sucrose export from mesophyll cells to the apoplast) or from increased export to sink tissues (*i.e.* increased uptake of photosynthate from the apoplast into the vasculature). However, it is intriguing that, although co-inoculation with 6.25mM sucrose was expected to maximally induce the biosensor across all experiments, the treatment instead exhibited significant seasonal declines (Figure 1a; Figure 3). Essentially, plants appeared to absorb exogenous sucrose more strongly in the winter than in the summer, yielding lower biosensor induction at the leaf surface; this suggests that vascular sink strength may increase during the winter months, perhaps to improve scavenging of photosynthate needed to sustain sink organs during periods of reduced primary productivity.

Increased sink strength could be caused by increased activity of sucrose transporters responsible for phloem-loading at major and minor veins of the leaf. Although seasonal fluctuations of sucrose transporter activity has not been investigated specifically, several researchers have reported environmental regulation of proton-sucrose symporter proteins in leaves. For example, transcription of the SUT1 and SUT4 transporters was shown to exhibit diurnal oscillations in *Solanum tuberosum*, with maximal expression during the middle of the light period (Chincinska *et al*., 2007); similar results were obtained in tobacco and tomato (Kuhn *et al*., 1997). Additionally, light was required for activation of AtSUC2 during major vein development in *N. tabacum* (Wright *et al.*, 2003), indicating that in addition to environmental regulation, light may play a broader developmental role in orchestrating the source-to-sink transition in leaf vasculature. Environmental conditions may therefore influence the activity of the phloem-loading machinery, perhaps increasing activity during the fall and winter.

Seasonal changes in phloem uptake capacity might therefore explain why the *Pa*MX149 sucrose biosensor detected less sugar on winter-grown bean leaves: as phloem sink strength increased, apoplastic sucrose concentrations decreased, along with the quantity of sucrose diffusing to the leaf surface. But what accounts for the *absence* of seasonal sucrose declines on leaves treated with auxin? (NAA-treated cells, for example, consistently reported around 10^{-4} ice nuclei/cell, or roughly $2x10^{-5}$M sucrose, yielding no significant decline across experiments.) The explanation most likely lies in auxin-mediated stimulation of invertase activity: in the presence of NAA, whatever apoplastic sucrose is present (whether high concentrations in the summer or low concentrations in the winter) is cleaved to glucose and fructose, minimizing subsequent induction of bacterial sucrose biosensors. The presence of weakly inductive, non-target sugars

(Miller *et al.*, 2001) plus residual leaf surface sucrose could account for the remaining, low induction values observed across seasons. As with exogenous NAA, the relatively lower concentrations of IAA generated by wild-type *Pa299R* appeared sufficient to drive hydrolysis of excess sucrose in the summer months, negating any seasonal decline in sucrose sensing (though a shallow decline was discernable, it was not statistically significant). In contrast, the auxin-deficient mutant *Pa*MX149 was unable to modify basal sucrose availability via plant invertase activation, and therefore experienced high levels of sucrose during the summer months, which declined significantly in the winter.

This interpretation suggests that, in the context of auxin-mediated resource conversion, seasonal declines in sucrose availability might render IAA production maladaptive during the dimmer winter months. Although the presence of auxin resulted in large declines in sucrose sensing relative to the *Pa*MX149 mutant on sucrose-rich summer plants, relative differences between $auxin^+$ and $auxin^-$ treatments progressively shrank as baseline sucrose levels fell, eventually declining below significance late in the season. This suggests that the metabolic expense of IAA production yields progressively smaller effects as sucrose availability declines—presumably because plant cell wall invertases targeted by bacterial IAA have less available substrate to convert to fructose and glucose.

Summary

By observing reporter activity of sugar-inducible *Pa*299R biosensors inoculated with or without auxin onto *P. vulgaris* leaves, we found that bacterial IAA alters carbon availability to phyllosphere bacteria. Whether provided by endogenous bacterial IAA biosynthesis or co-inoculation of exogenous NAA, auxin reduced sucrose availability and increased fructose availability to biosensors on the leaf surface. These complementary trends suggest that bacterial auxin may activate plant cell wall invertases to promote conversion of sucrose to glucose and fructose, although preliminary experiments testing this hypothesis using *A. thaliana* invertase mutants were inconclusive. Such a resource conversion strategy might benefit bacteria by increasing carbon availability during crucial early hours of growth, as *in vitro* experiments suggested that *Pa*299R can initiate growth more rapidly when using glucose or fructose as a sole carbon source than when using sucrose. Alternatively, increasing the monosaccharide/sucrose ratio may increase local apoplastic carbon concentrations by preventing export of sugars via sucrose-specific phloem loading. However, invertase activation may represent a conditionally adaptive approach, as environmental factors, including seasonal conditions, light intensity, host plant identity, and the frequency of environmental disruption, are all expected to impact the success of IAA-mediated resource conversion as a strategy for carbon acquisition.

Acknowledgments

Great thanks to Steve Ruzin and Denise Schichnes, of the College of Natural Resources Biological Imaging Facility, for their instruction and advice on fluorescence microscopy and the IVision software package; also to Mietche Remus-Emsermann for his feedback and helpful suggestions on microscopic image analysis of biosensor cells. Thanks to the Arkin laboratory for the generous use of their Partec flow cytometer, and to Denise Wolf and Jolyn Twelves for instruction on how to operate it. Thanks also to Hector Nolla of the CNR flow cytometry core

facility, for technical advice and assistance running samples on the cell sorters. This work was supported by a Graduate Research Fellowship awarded by the National Science Foundation.

LITERATURE CITED

Alonso, J.M., A.N. Stepanova, T.J. Leisse, C.J. Kim, H. Chen, P. Shinn, D.K. Stevenson, J. Zimmerman, P. Barajas, R. Cheuk, C. Gadrinab, C. Heller, A. Jeske, E. Koesema, C.C. Meyers, H. Parker, L. Prednis, Y. Ansari, N. Choy, H. Deen, M. Geralt, N. Hazari, E. Hom, M Karnes, C. Mulholland, R. Ndubaku, I. Schmidt, P. Guzman, L. Aguilar-Henonin, M. Schmid, D. Weigel, D. E. Carter, T. Marchand, E. Risseeuw, D. Brogden, A. Zeko, W.L. Crosby, C.C. Berry, and J.R. Ecker. (2003) Genome-wide insertional mutagenesis of *Arabidopsis thaliana*. *Science*. **301**(5633): 653-657.

Andersen, J.B., C. Sternberg, L.K. Poulsen, S.P. Bjorn, M. Givskov, & S. Molin. (1998) New unstable variants of green fluorescent protein for studies of transient gene expression in bacteria. *Applied Environmental Microbiology*. **64**(6): 2240-2246.

Andrews, J.H., and R.F. Harris. r-selection and K-selection and microbial ecology. *Advances in Microbial Ecology*. **9**: 99-147.

Arabidopsis Biological Resource Center. (2004) Handling Arabidopsis Plants and Seeds: Methods used by the Arabidopsis Biological Resource Center. http://abrc.osu.edu/abrc_handling_mw2004.pdf. Accessed 05/01/2011.

Axtell, C.A., and G.A. Beattie. (2002) Construction and characterization of a *proU-gfp* transcriptional fusion that measures water availability in a microbial habitat. *Applied and Environmental Microbiology*. **68**(9): 4604-4612.

Aulkemeyer, P., R. Ebner, G. Heilenmann, K. Jahreis, K. Schmid, S. Wrieden, and J.W. Lengeler. (1991) Molecular analysis of two fructokinases involved in sucrose metabolism of enteric bacteria. *Molecular Microbiology*. **5** (12): 2913-2922.

Bedescu, G.O., and R. M. Napier. (2006) Receptors for auxin: will it all end in TIRs? *TRENDS in Plant Science*. **11**(5):1360-1385.

Biemelt, S., and U. Sonnewald. 2006) Plant-microbe interactions to probe regulation of plant carbon metabolism. *Journal of Plant Physiology*. **163**: 307-318.

BioVision Technologies, Inc. (2010) IVision (image analysis software). http://www.biovis.com/ivision.htm.

Bogs, J., and K. Geider. (2000) Molecular analysis of sucrose metabolism of *Erwinia amylovora* and influence on bacterial virulence. *Journal of Bacteriology*. **182** (19): 5351-5358.

Bonfig, K.B., A. Gabler, U.K. Simon, N. Luschin-Ebengreuth, M. Hatz, S. Berger, N. Muhammad, J. Zeier, A.K. Sinha, and T. Roitsch. (2010) Post-translational derepression of invertase activity in source leaves via down-regulation of invertase inhibitor expression is part of the plant defense response. *Molecular Plant*. **3**(6): 1037-1048.

Brandl, M., and S. Lindow. (1998) Contribution of indole-3-acetic acid production to the epiphytic fitness of *Erwinia herbicola*. *Applied and Environmental Microbiology*. **64** (9): 3256-3263.

Brandl, M., E.M. Clark, and S.E. Lindow. (1996) Characterization of the indole-3-acetic acid (IAA) biosynthetic pathway in an epiphytic strain of *Erwinia herbicola* and IAA production *in vitro*. *Canadian Journal of Microbiology*. **42**: 586-592.

Brandl, M.T., and S.E. Lindow. (1997) Environmental signals modulate the expression of an indole-3-acetic acid biosynthetic gene in *Erwinia herbicola*. *Molecular Plant Microbe Interactions*. **10**(4): 499-505.

Chen, L., B. Hou, S. Lalonde, H. Takanaga, M.L. Hartung, X. Xu, W. Guo, J. Kim, W. Underwood, B. Chaudhuri, D. Chermak, G. Antony, F.F. White, S. C. Somervile, M.B. Mudgett, and W. B. Frommer. (2010) Sugar transporters for intercellular exchange and nutrition of pathogens. *Nature*. **468**: 527-534.

Chincinska, I.A., J. Liesche, U. Krugel, J. Michalska, P. Geigenberger, B. Grimm, and C. Kuhn. (2007) Sucrose transporter StSUT4 from potato affects flowering, tuberization, and shade avoidance response. *Plant Physiology*. **146** (2): 515-528.

Cowan, P.J., H Dagesha, L. Leonard, J.L. Howard, and A.J. Pittard. (1991) Characterization of the major promoter for the plasmid-encoded sucrose genes *scrY*, *scrA*, and *scrB*. *Journal of Bacteriology*. **173** (23): 7464-7470.

De Maayer, P., W.Y. Chan, S.N. Venter, I.K. Toth, P.R. Birch, F. Joubert, and T.A. Coutinho. (2010) Genome sequence of *Pantoea ananatis* LMG20103, the causative agent of Eucalyptus blight and dieback. *Journal of Bacteriology*. **192**(11): 2936-2937.

De Novo Software. (2009). FCS Express (flow cytometry analysis software), version 3. http://www.denovosoftware.com/site/FCSExpress.shtml

Derridj, S. (1996) Nutrients on the leaf surface. In *Aerial Plant Surface Microbiology*, Ed. Morris *et al*., Plenum Press, New York.

Deutscher, J. (2008) The mechanisms of carbon catabolite repression in bacteria. *Current Opinion in Microbiology*. **11**: 97-93.

Dharmasiri, H., S. Dharmasiri, and M. Estelle. (2005) The F-box protein TIR1 is an auxin receptor. *Nature*. **435**:441-445.

Dos Santos, H.P., E. Purgatto, H. Mercier, and M.S. Buckeridge. (2004) The control of storage xyloglucan mobilization in cotyledons of *Hymenaea courbaril*. *Plant Physiology*. **135**: 287-299.

Essmann, J., I. Schmitz-Thom, H. Schon, S. Sonnewald, E. Weis, and J. Scharte. (2008) RNA interference-mediated repression of cell wall invertase impairs defense in source leaves of tobacco. *Plant Physiology*. **147**: 1288-1299.

Gutierrez, C.K., G.Y. Matsui, D.E. Lincoln, and C.R. Lovell. (2009) Production of the phytohormone indole-3-acetic acid by estuarine species of the genus *Vibrio*. *Applied and Environmental Microbiology*. **75**(8): 2252-2258.

Hoson, T. (1993) Regulation of polysaccharide breakdown during auxin-induced cell wall loosening. *Journal of Plant Research*. **106**: 369-381.

Huang, L., P.N. Bocock, J.M. Davis, and K.E. Koch. (2007) Regulation of invertase: a 'suite' of transcriptional and post-transcriptional mechanisms. *Functional Plant Biology*. **34**: 499-507.

Jaeger, C.H., S.E. Lindow, S. Miller, E. Clark, M.K. Firestone. (1999) Mapping of sugar and amino acid availability in soil around roots with bacterial sensors of sycrose and tryptophan. *Applied and Environmental Microbiology*. **65**(6): 2685-2690.

Jankovic, I., and R. Bruecker. (2007) Carbon catabolite repression of sucrose utilization in *Staphylococcus xylosus*: Catabolite control protein CcpA ensures glucose preference and autoregulatory limitation of sucrose utilization. *Journal of Molecular Microbiology and Biotechnology*. **12**(1-2):114-120.

Jin, Y., D. Ni, and Y. Ruan. (2009) Posttranslational elevation of cell wall invertase activity by silencing its inhibitor in tomato delays leaf senescence and increases seed weight and fruit hexose level. *The Plant Cell*. **21**: 2072-2089.

Kepinski, S., and O. Leyser. (2005) The *Arabidopsis* F-box protein TIR1 is an auxin receptor. *Nature*. **435**: 446-451.

Kim, Y.C., J. Leveau, B.B.M. Gardener, E.A. Pierson, L.S.Pierson, & C. Ryu. (2011) The multifactorial basis for plant health promotion by plant-associated bacteria. *Applied and Environmental Microbiology*. **77**(5): 1548-1555.

Kocal, N., U. Sonnewald, and S. Sonnewald. (2008) Cell wall-bound invertase limits sucrose export and is involved in symptom development and inhibition of photosynthesis during compatible interaction between tomato and *Xanthomonas campestris* pv *vesicatoria*. *Plant Physiology.* **148**: 1523-1536.

Kuhn, C., V.R. Franceschi, A. Schulz, R. Lemoine, and W.B. Frommer. (1997) Macromolecular trafficking indicated by localization and turnover of sucrose transporters in enucleate sieve elements. *Science*. **275** (5304): 1298-1300.

Lenski, R.E., J.A. Mongold, P.D. Sniegowski, M. Travisano, F.Vasi, P.J. Gerrish, and T.M. Schmidt. (1998) Evolution of competitive fitness in experimental populations of *E. coli*: What makes one genotype a better competitor than another? *Antonie van Leeuwenhoek* **73**: 35-47.

Leveau, J.H.J, and S.E. Lindow. (2001a) Appetite of an epiphyte: Quantitative monitoring of bacterial sugar consumption in the phyllosphere. *Proceedings of the National Academy of Sciences.* **98**(6): 3446-3453.

Leveau, J.H.J., and S.E. Lindow. (2001b) Predictive and interpretive simulation of green fluorescent protein expression in reporter bacteria. *Journal of Bacteriology*. **183**(12): 6752-6762.

Lindow, S.E., and M.T. Brandl. (2003) Microbiology of the Phyllosphere. *Applied and Environmental Microbiology*. **69**(4): 1875-1883.

Lindow, S.E., C. Desurmont, R. Elkins, G. McGourty, E. Clark, and M. Brandl. (1998) Occurrence of indole-3-acetic acid-producing bacteria on pear trees and their association with fruit russet. *Phytopathology*. **88**(11): 1149-1157.

Long, J.C., W. Zhao, A.M. Rashotte, G.K. Muday, and S.C. Huber. (2002) Gravity-stimulated changes in auxin and invertase gene expression in maize pulvinal cells. *Plant Physiology*. **128**(2): 591-602.

Mercier, J., and S.E. Lindow. (2000) Role of leaf surface sugars in colonization of plants by bacterial epiphytes. *Applied and Environmental Microbiology.* **66**(1): 369-374.

Miller, J.H. (1972) *Experiments in Molecular Genetics.* Cold Spring Harbor Laboratory, Cold Spring Harbor, NY.

Miller, W.G., M.T. Brandl, B. Quinones, and S.E. Lindow. (2001) Biological sensor for sucrose availability: relative sensitivities of various reporter genes. *Applied and Environmental Microbiology*. **67**(3): 1308-1317.

Morris, D.A., and E.D. Arthur. (1984) Invertase and auxin-induced elongation in intermodal segments of *Phaseolus vulgaris*. *Phytochemistry*. **23** (10): 2163-2167.

Morris, D.A. (1996) Hormonal regulation of source-sink relationships: an overview of potential control mechanisms. In *Photoassimilate Distribution in Plants and Crops: Source-Sink Relationships.* Ed. E. Zamski and A.A. Schaffer. CRC Press/Marcel Dekker, Inc.. New York, NY.

Morris, D.A., and E.D. Arthur. (1986) Stimulation of acid invertase activity by indol-3yl-acetic acid in tissues undergoing cell expansion. *Plant Growth Regulation*. **4**: 259-271.

Morris, D.A., and E.D. Arthur. (1987) Auxin-induced assimilate translocation in the bean stem (*Phaseolus vulgaris* L.). *Plant Growth Regulation.* **5**: 169-181.

Ntsika, G., and S. Delrot. (1986) Changes in apoplastic and intracellular leaf sugars induced by the blocking of export in *Vicia faba*. *Physiologia Plantarum*. **68** (1):145-153.

Patrick, J.W. (1987) Are hormones involved in assimilate transport? In *Hormone Action in Plant Development: A Critical Appraisal*. Ed. G.V. Hood, J.R. Lenton, M.B. Jackson, and R.K. Alli. Butterworths, London.

Patrick, J.W., and P.F. Wareing. (1973) Auxin-promoted transport of metabolites in stems of *Phaseolus vulgaris* L. *Journal of Experimental Botany*. **24** (83): 1158-1171.

Petzold, U., S. Peschel, I. Dahse, and G. Adam. (1992) Stimulation of source-applied ^{14}C-sucrose export in *Vicia faba* plants by brassinosteroids, GA_3 and IAA. *Acta Botanica Neerlandia*. **41**(4): 469-479.

Rolland, F., E. Baena-Gonzalez, and J. Sheen. (2006) Sugar sensing and signaling in plants: conserved and novel mechanisms. *Annual Reviews in Plant Biology*. **57**: 675-709.

Sakalo, V.D., and V.M. Kurchii. (2004) Hormonal control of sucrose phosphate synthase and sucrose synthase in sugar beet. *Russian Journal of Plant Physiology*. **51**(2): 183-188.

Schonherr, J., and P. Baur. (1996) Cuticle permeability studies: a model for estimating leaching of plant metabolites to leaf surfaces. In *Aerial Plant Surface Microbiology*, Ed. Morris *et al*., Plenum Press, New York.

Sherson, S.M., H.L Alford, S.M. Forbes, G. Wallace, and S.M. Smith. (2003) Roles of cell-wall invertases and monosaccharide transporters in the growth and development of *Arabidopsis*. *Journal of Experimental Botany*. **54**(382): 525-531.

Siemens, J., M. Gonzalez, S. Wolf, C. Hofmann, S. Greiner, Y. Du, T. Rausch, T. Roitsch, and J. Ludwig-Muller. (2010) Extracellular invertase in involved in the regulation of clubroot disease in *Arabidopsis thaliana*. *Molecular Plant Pathology*.

Voitsekhovskaja, O.V., M.V. Pakhomova, A.V. Syutkina, Y.V. Gamalei, and U. Heber. (2000) Compartmentation of assimilate fluxes in leaves. *Plant Biology **2***. 103-112.

Wright, C.A., and G.A. Beattie. 2004) *Pseudomonas syringae* pv. *tomato* cells encounter inhibitory levels of water stress during the hypersensitive response of *Arabidopsis thaliana*. *Proceedings of the National Academy of Sciences*. **101**(9): 3269-3274.

Wright, K.M., A.G. Roberts, H.J. Martens, N. Sauer, and K.J. Oparka. (2003) Structural and functional vein maturation in developing tobacco leaves in relation to *AtSUC2* promoter activity. *Plant Physiology*. **131**(4): 1555-1565.

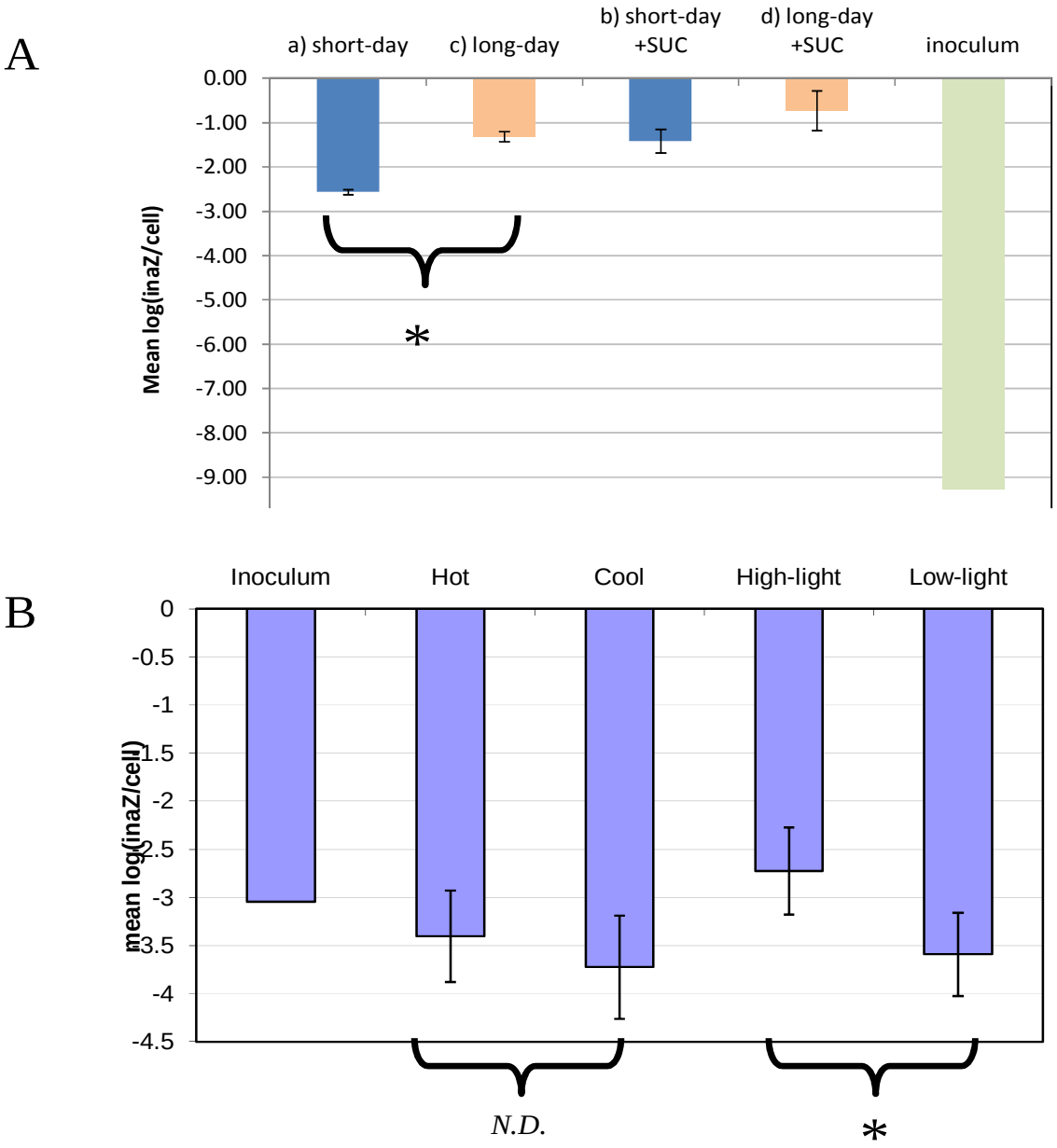

Figure 1. Phylloplane sugar availability is affected by environmental variables. Sucrose availability to bacterial biosensors was higher on leaves grown under long-day (summer) conditions than under short-day (winter) conditions (A). In another experiment, sucrose availability was significantly higher under high-light conditions than low-light conditions, but exhibited no significant difference between hot and cool conditions (B).

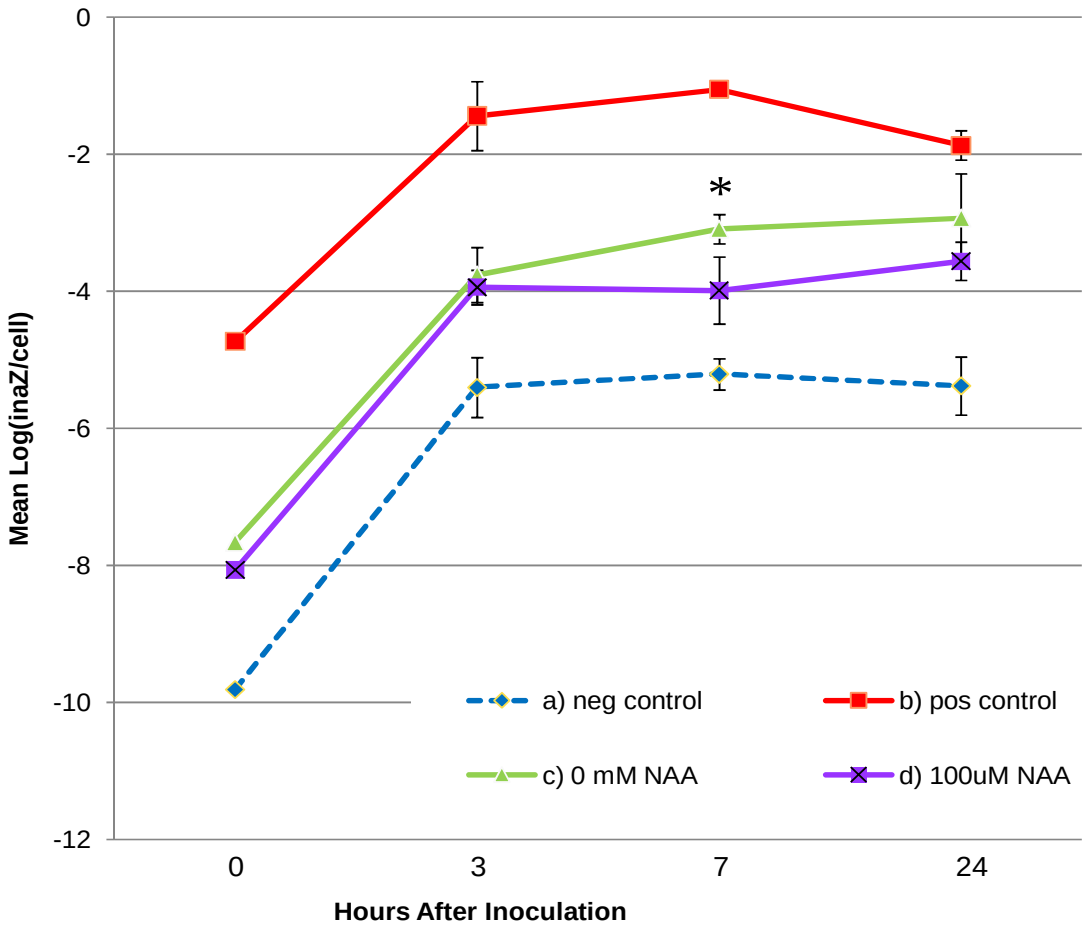

Figure 2. Timecourse of *Pa*MX149 *p61RYice* sucrose biosensor cells inoculated onto bean leaves with or without 100uM NAA. Each point is the mean of 3 replicates ± 1 S.D.; *= significant differences (p=0.02) between NAA+ and NAA- treatments at a given time point.

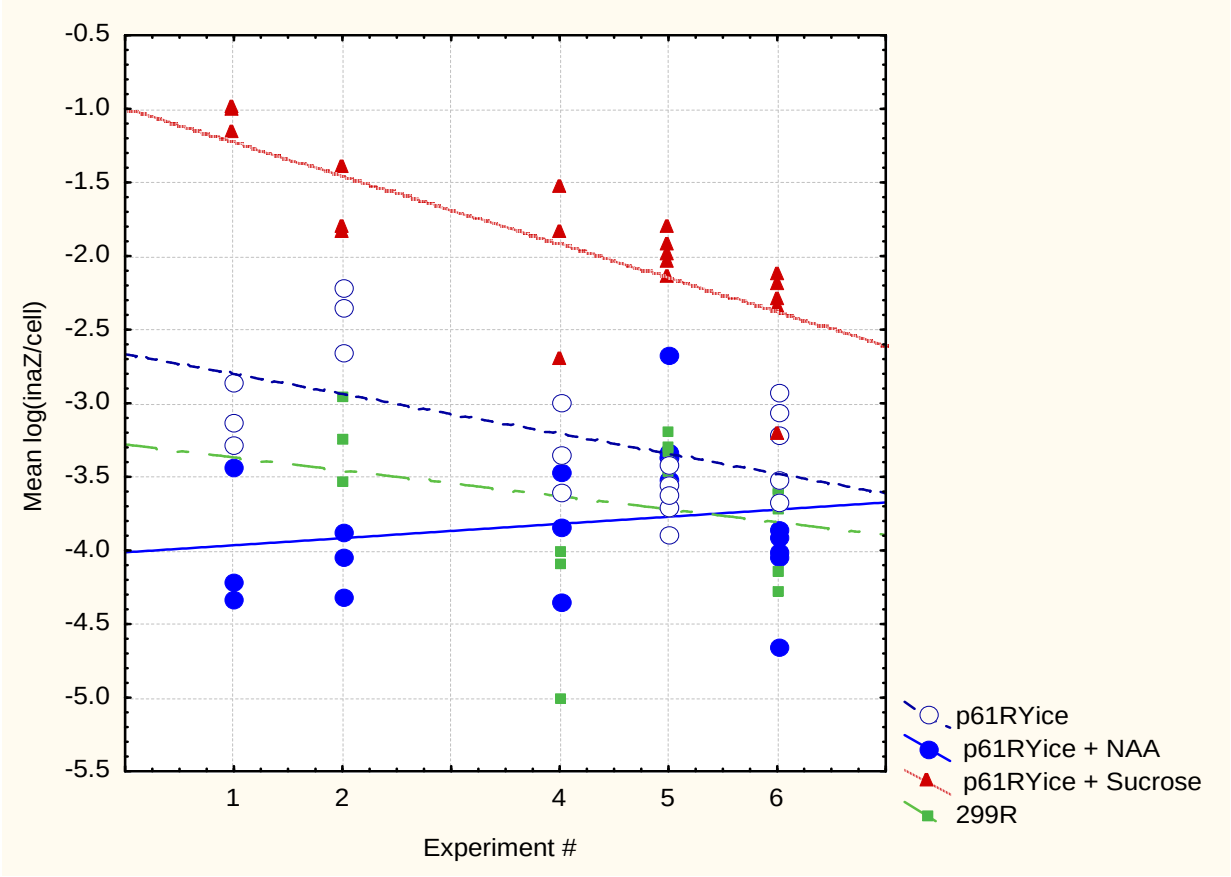

Figure 3. The presence of auxin decreases sugar availability to sucrose-inducible bacterial biosensors in the phyllosphere. Reporter activity of the IAA-deficient mutant *Pa*MX149 (open circles), *Pa*MX149 co-inoculated with 100uM NAA (closed circles), and the wild-type *Pa*299R were compared (squares); MX149 co-inoculated with exogenous sucrose was used as a positive control (triangles). Reporterless *Pa*MX149 was used as a negative control and exhibited minimal activity in all experiments (data not shown). Results from 5 experiments are summarized, arranged by experimental date (A). Each data point represents a single leaf.

A

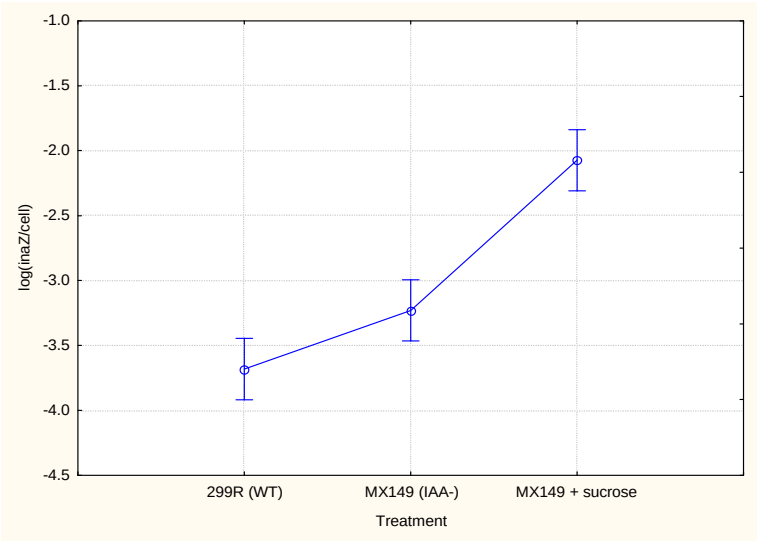

B

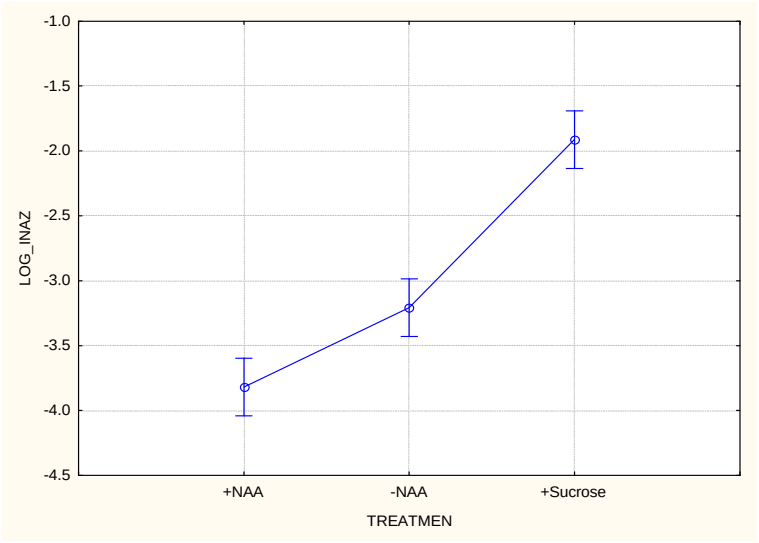

Figure 4. Bacterial sucrose biosensors inoculated onto bean leaves experience significantly less sucrose in the presence of exogenous NAA (A) or endogenous IAA production (B). Mean values after covariate adjustment for plant insolation are shown for the auxin, auxin-free, and positive control treatments across five independent experiments. Vertical bars denote 95% confidence intervals.

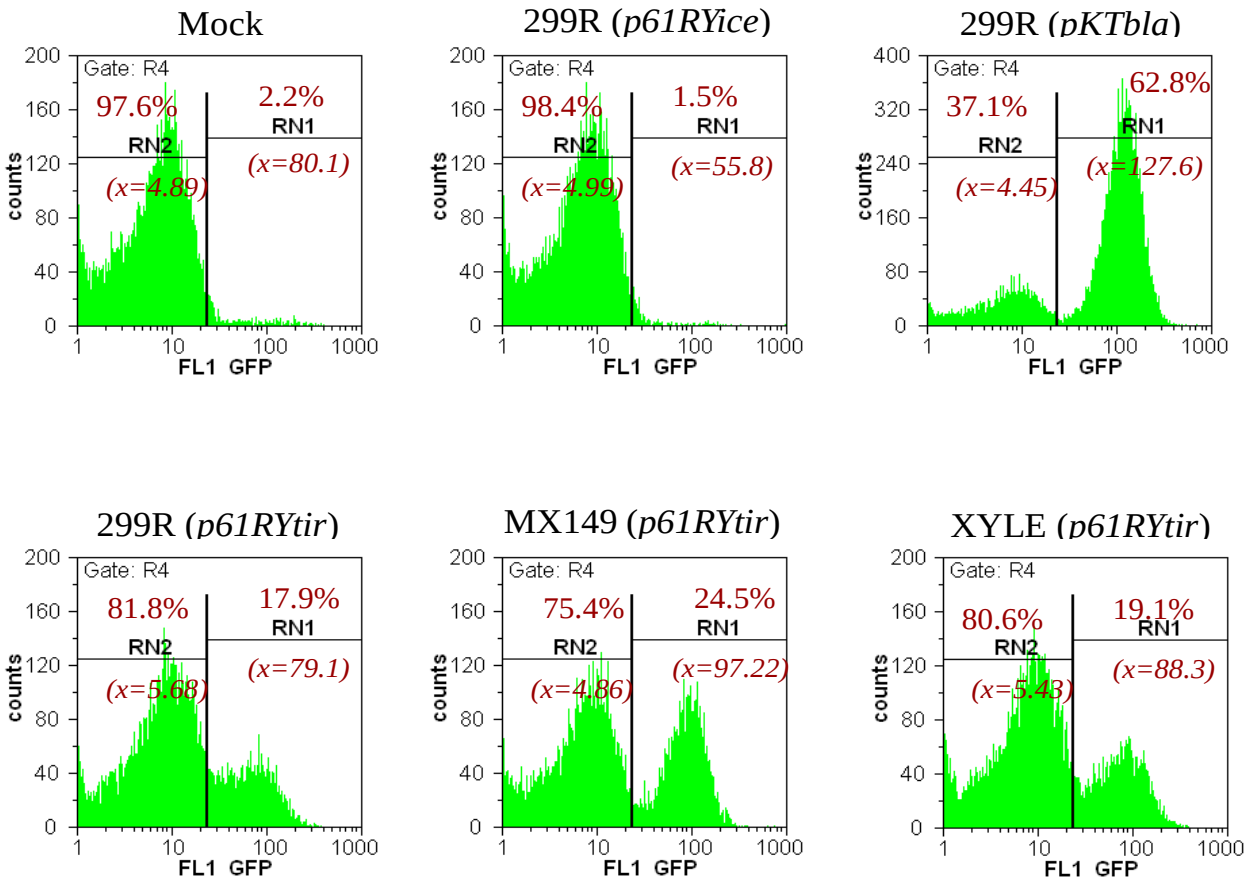

Figure 5. *P. agglomerans* (p61RYtir) sucrose biosensor strain 299R (or its isogenic, IAA- mutant derivatives MX149 and XYLE) were inoculated onto bean leaves, then assayed by flow cytometry for *gfp* induction at 24hpi. Buffer-inoculated leaves, a nonfluorescent 299R (p61RYice) negative control, and constitutive-GFP 299R (pKTbla) positive control are also shown. For each treatment, the percentage of GFP-negative (RN2) and GFP-positive (RN1) particles in each population is indicated; mean GFP fluorescence (x) of each peak is depicted in parentheses.

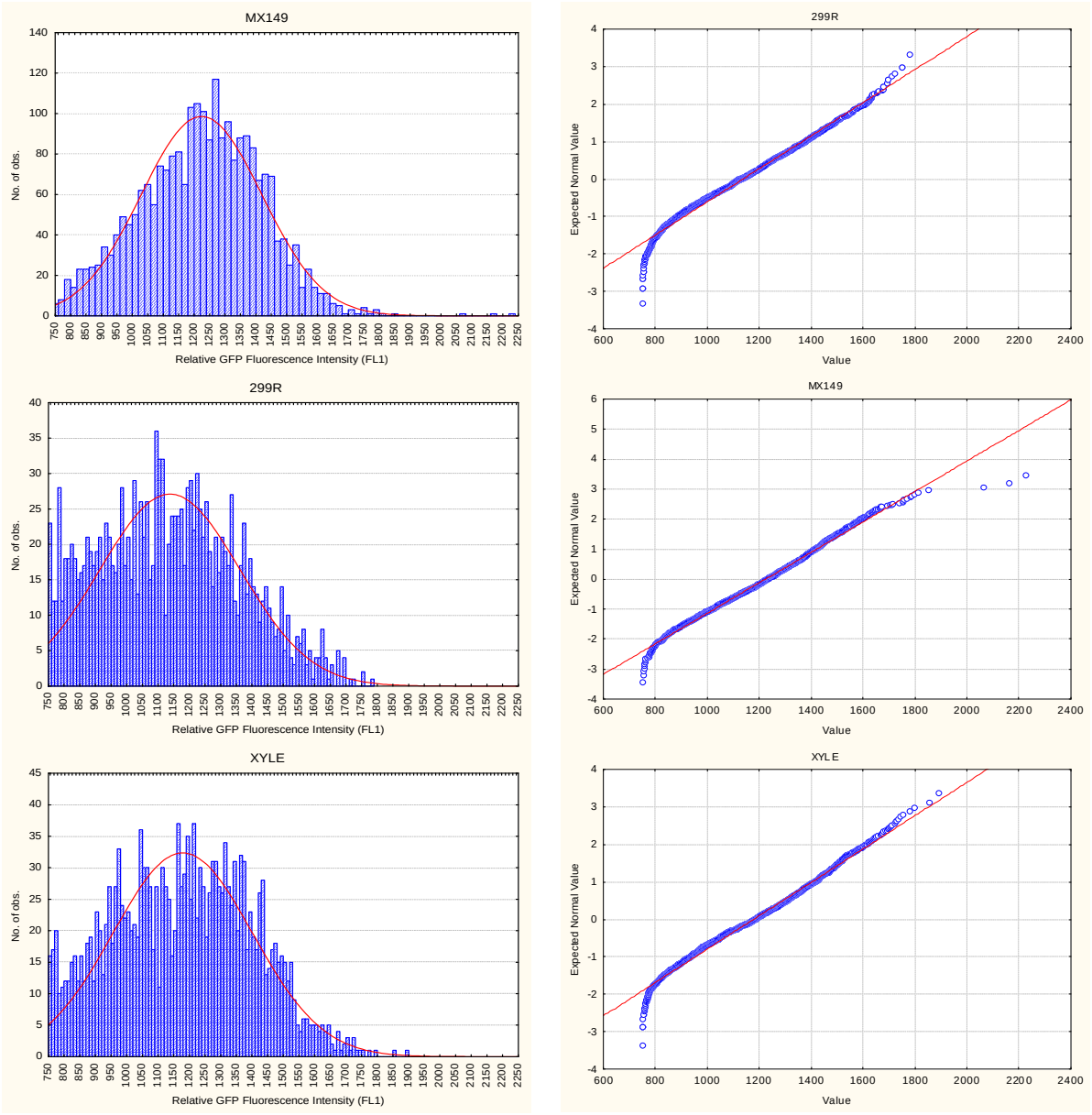

Figure 6. (p61RYice) sucrose biosensor strains of *Pa*299R, *Pa*MX149, and *Pa*XYLE harvested after 24 hpi on bean leaves and assayed by flow cytometry. Cell-fluorescence histograms (left) and normal probability plots (right) are shown for the GFP-positive cell population of each strain.

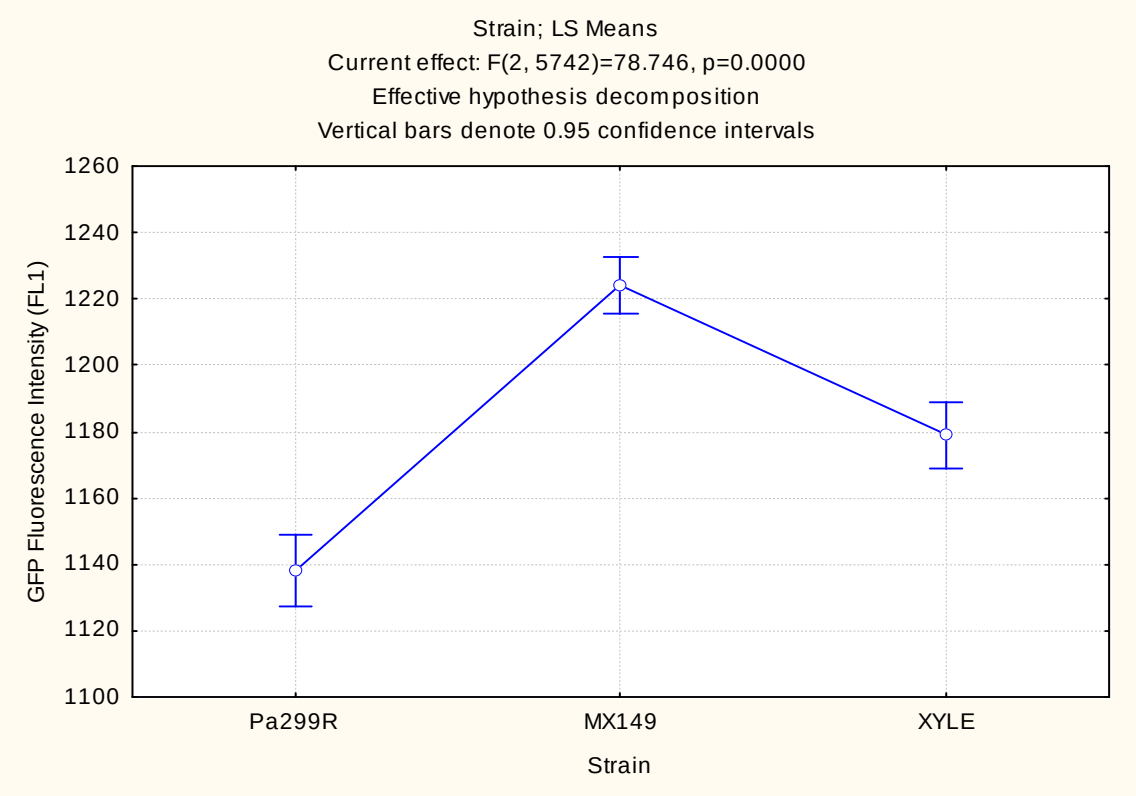

Figure 7. IAA-deficient mutants of *Pa*299R sense significantly more sucrose thanafter 24 hours on bean leaves. Mean cellular fluorescence of each strain's GFP-positive cell populations are shown with 95% confidence intervals; one-way ANOVA results of sucrose sensing flow cytometry are shown above.

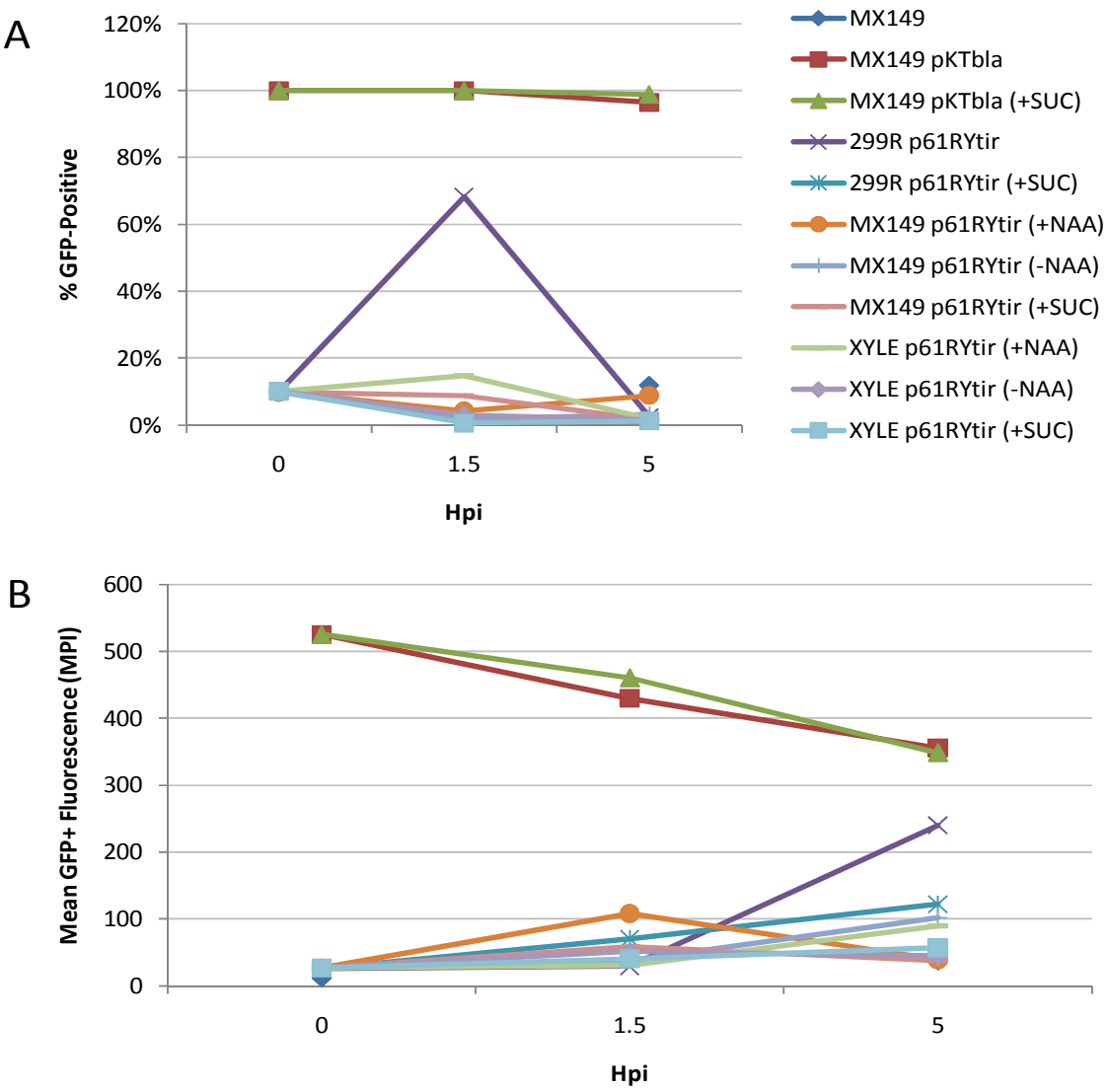

Figure 8. Neither endogenous nor exogenous auxin exerted a consistent effect on sucrose sensing by *P. agglomerans* bacteria, due largely to failed induction of the *p61RYtir* biosensor. Percent GFP-positive cells (A) and mean GFP fluorescence intensity of the GFP-positive population (±S.D.) (B) are shown for auxin-deficient *Pa*MX149 and *Pa*XYLE bacteria and the wild-type *Pa*299R parent strain, each coinoculated with buffer, NAA, or exogenous sucrose (legend at top right); negative control (MX149) and constitutively fluorescent positive control (pKTbla) treatments are also indicated.

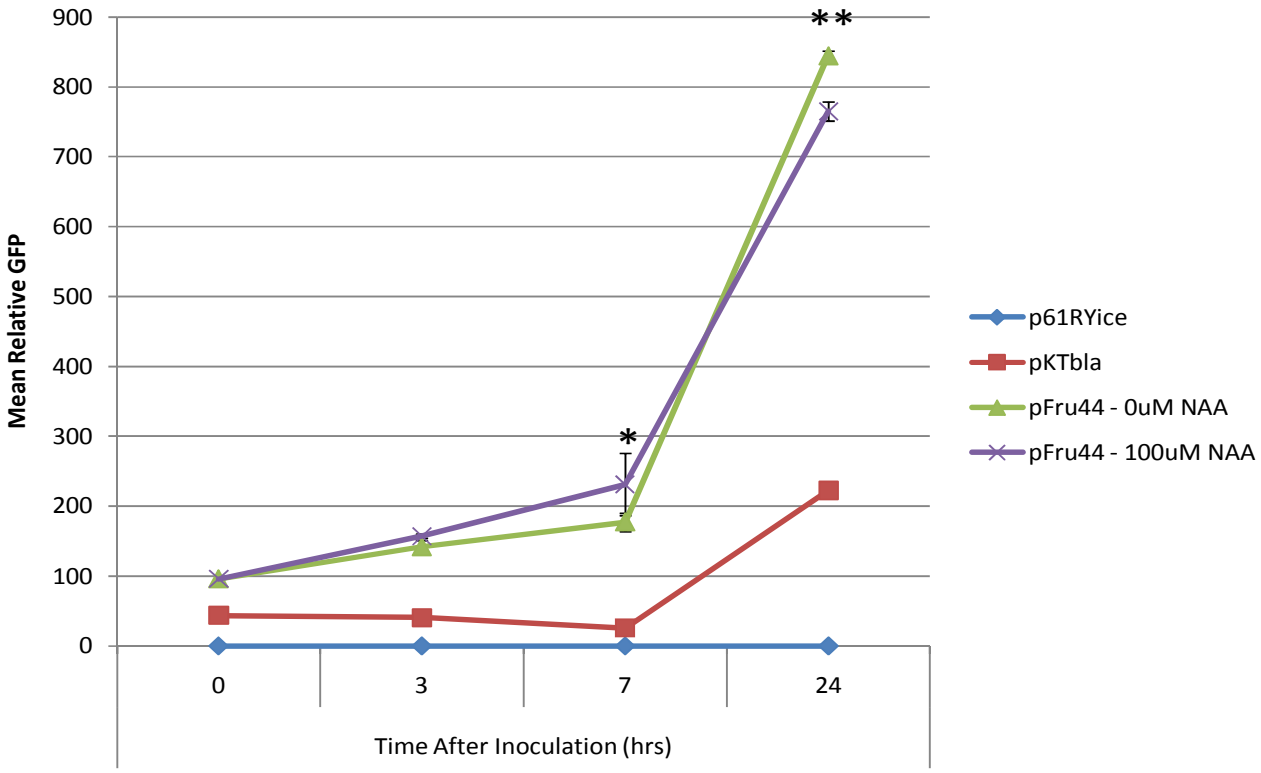

Figure 9. Experimental induction of the fructose biosensor 299R (pFru44) inoculated with or without NAA on bean plants. Each point is the mean of two biological replicates ± 1 S.D.. (*= significant difference between NAA+ and NAA- treatments at $p<0.02$; **$p<0.005$)

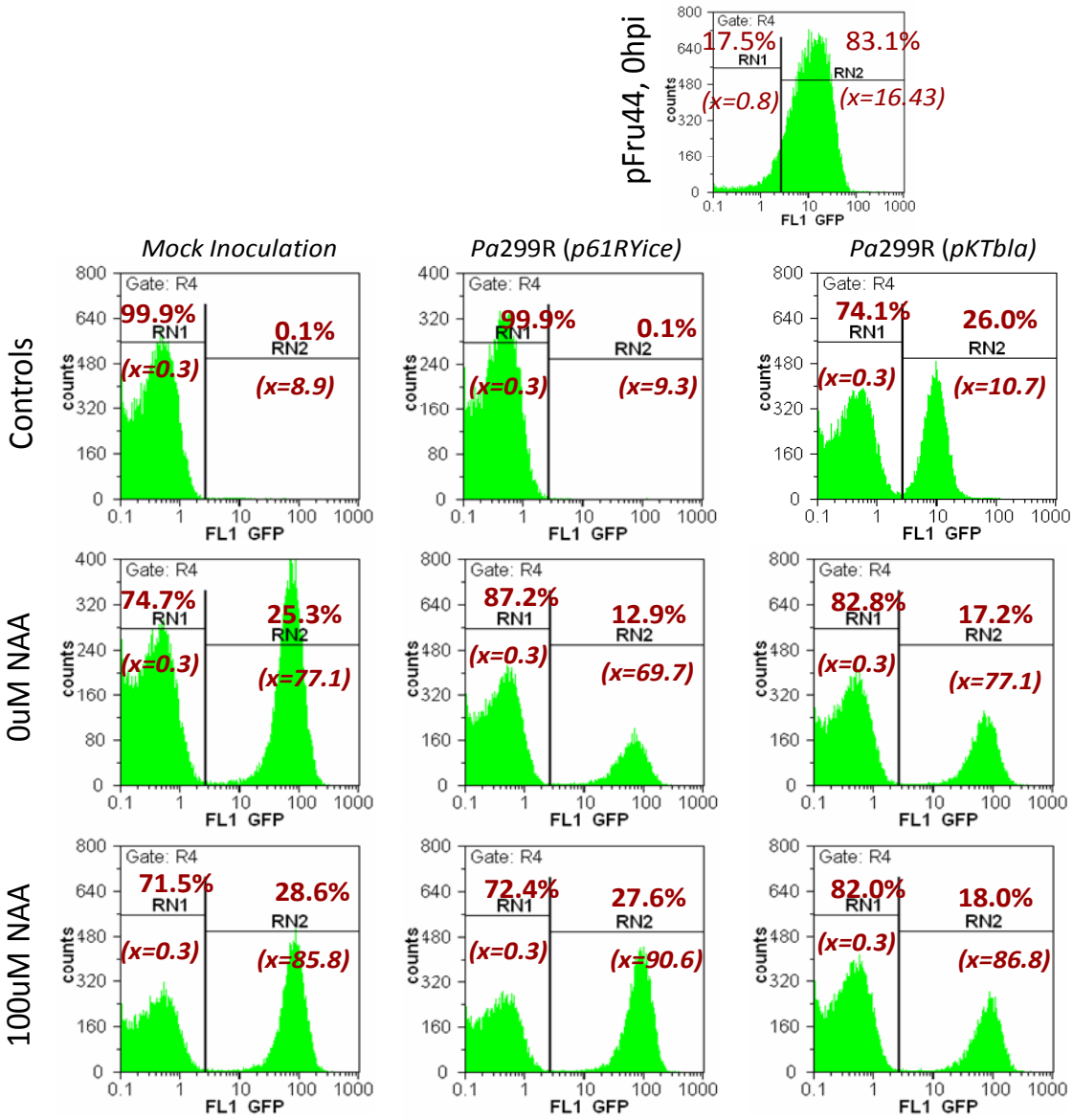

Figure 10. Sample flow cytometry data from one experiment, in which the *Pa*299R (pFru44) fructose biosensor was inoculated onto bean leaves with or without 100uM NAA. Histograms of cellular fluorescence are shown for the 0-hour pFru44 biosensor inoculum; and at 24 hpi for positive and negative controls, 3 replicate inoculations with 0uM NAA, and 3 replicate inoculations wth 100uM NAA. The percentage of GFP-negative (RN1) and GFP-positive (RN2) particles in each population is indicated; mean GFP fluorescence (x) of each peak is depicted in parentheses.

A

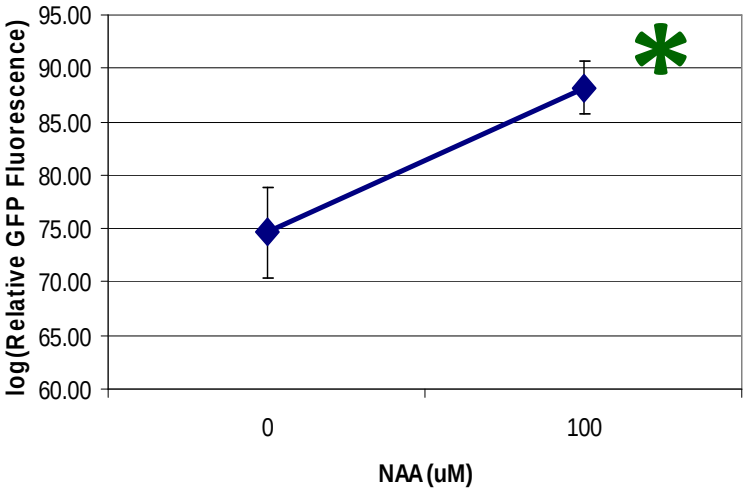

B

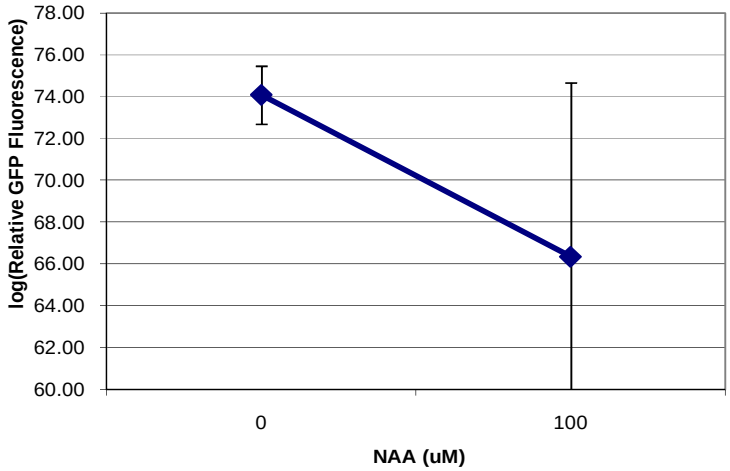

Figure 11. Bioreporter activity of *Pa*299R (pFru44) inoculated onto bean leaves, with or without 100uM NAA, after 24 hours of incubation. Each data point represents the mean of 3 biological replicates, ±1 S.D.; results from two independent experiments are shown (A-B). *=statistically significant difference ($p<0.01$)

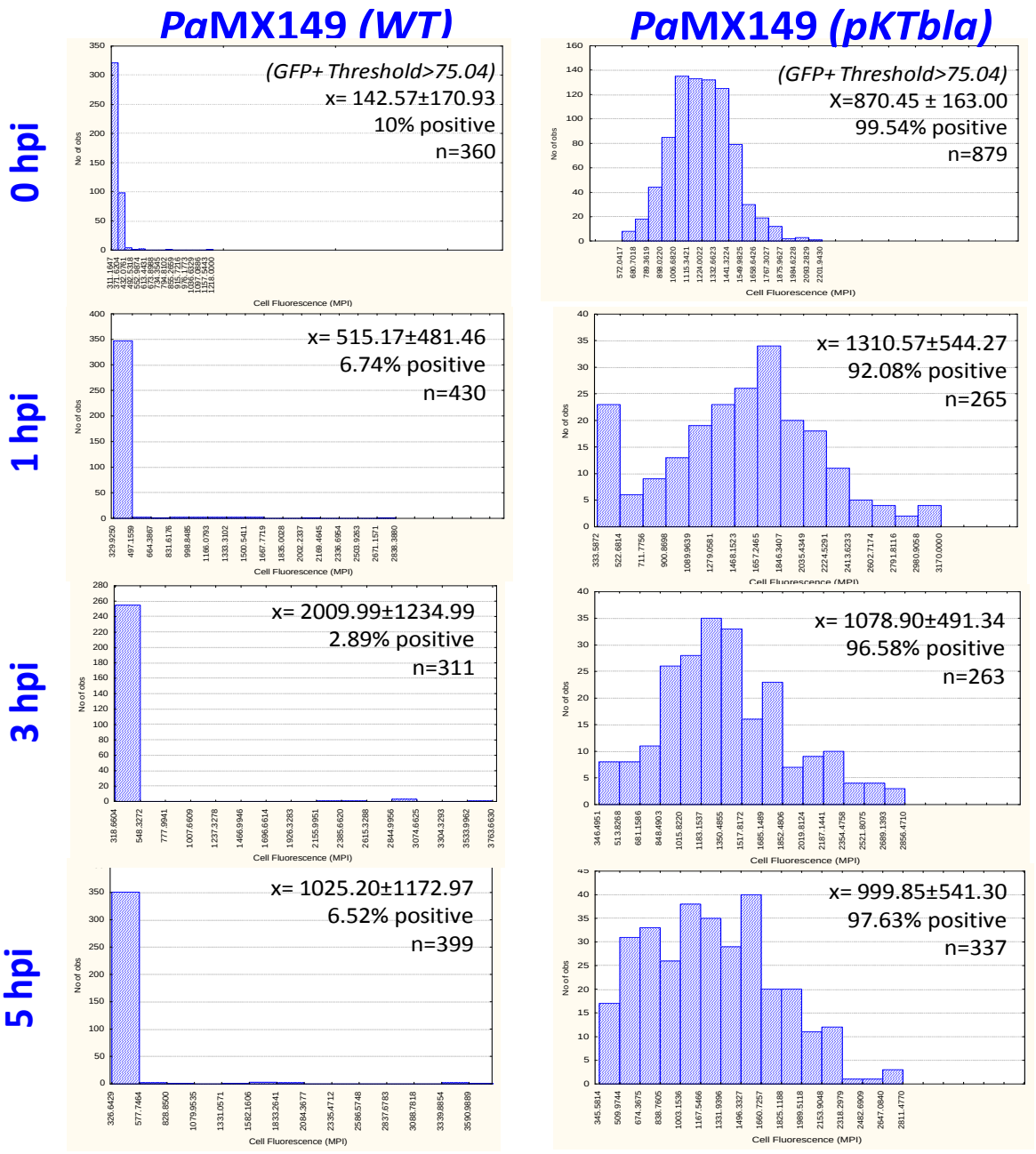

Figure 12. Distribution of cellular fluorescence in nonfluorescent negative and constitutively fluorescent (pKTbla) positive controls cells harvested from bean leaves. Mean cellular fluorescence, % of GFP-positive cells in the population, and the number of harvested cells are indicated to the right of each histogram.

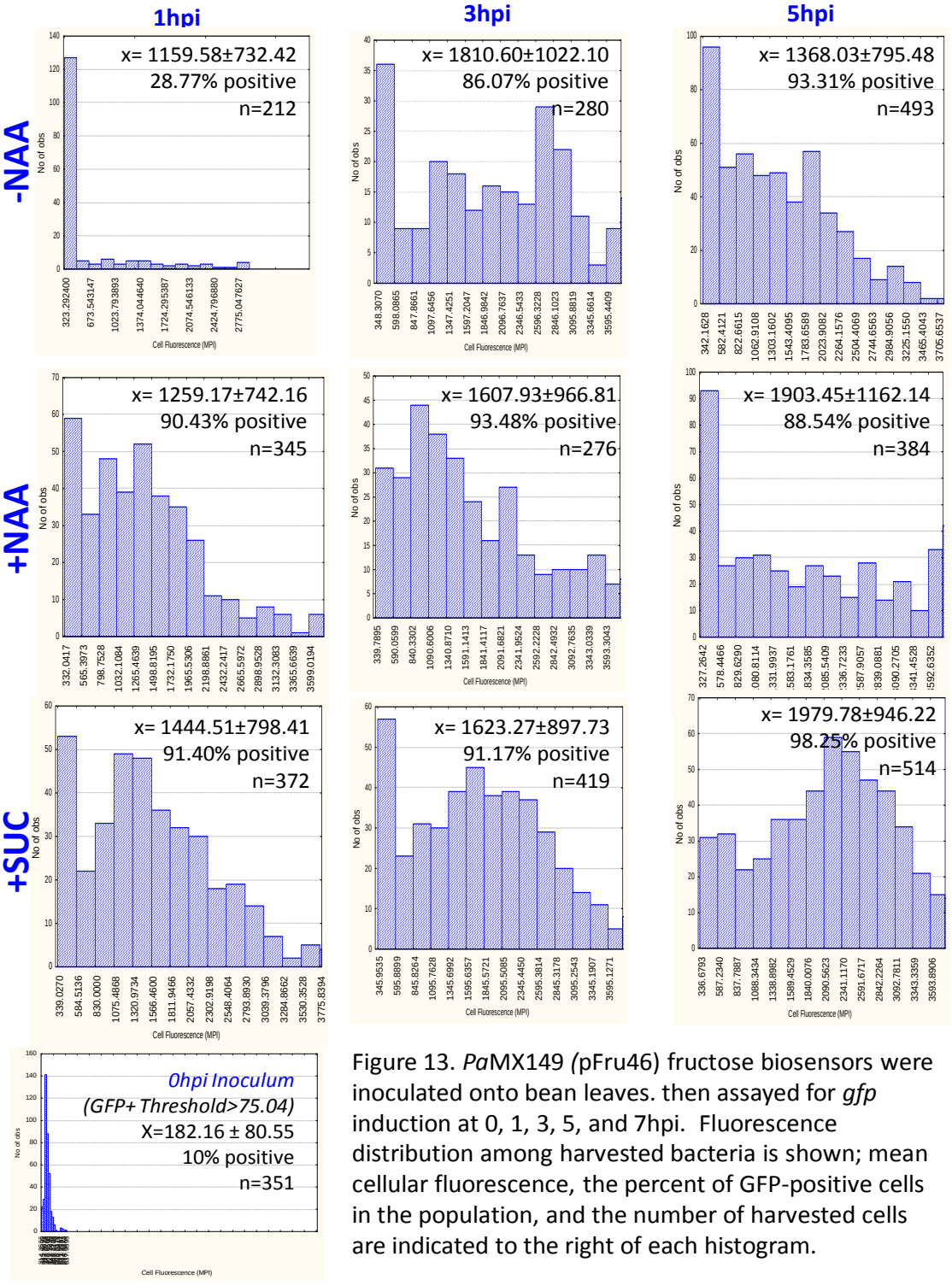

Figure 13. *Pa*MX149 (pFru46) fructose biosensors were inoculated onto bean leaves. then assayed for *gfp* induction at 0, 1, 3, 5, and 7hpi. Fluorescence distribution among harvested bacteria is shown; mean cellular fluorescence, the percent of GFP-positive cells in the population, and the number of harvested cells are indicated to the right of each histogram.

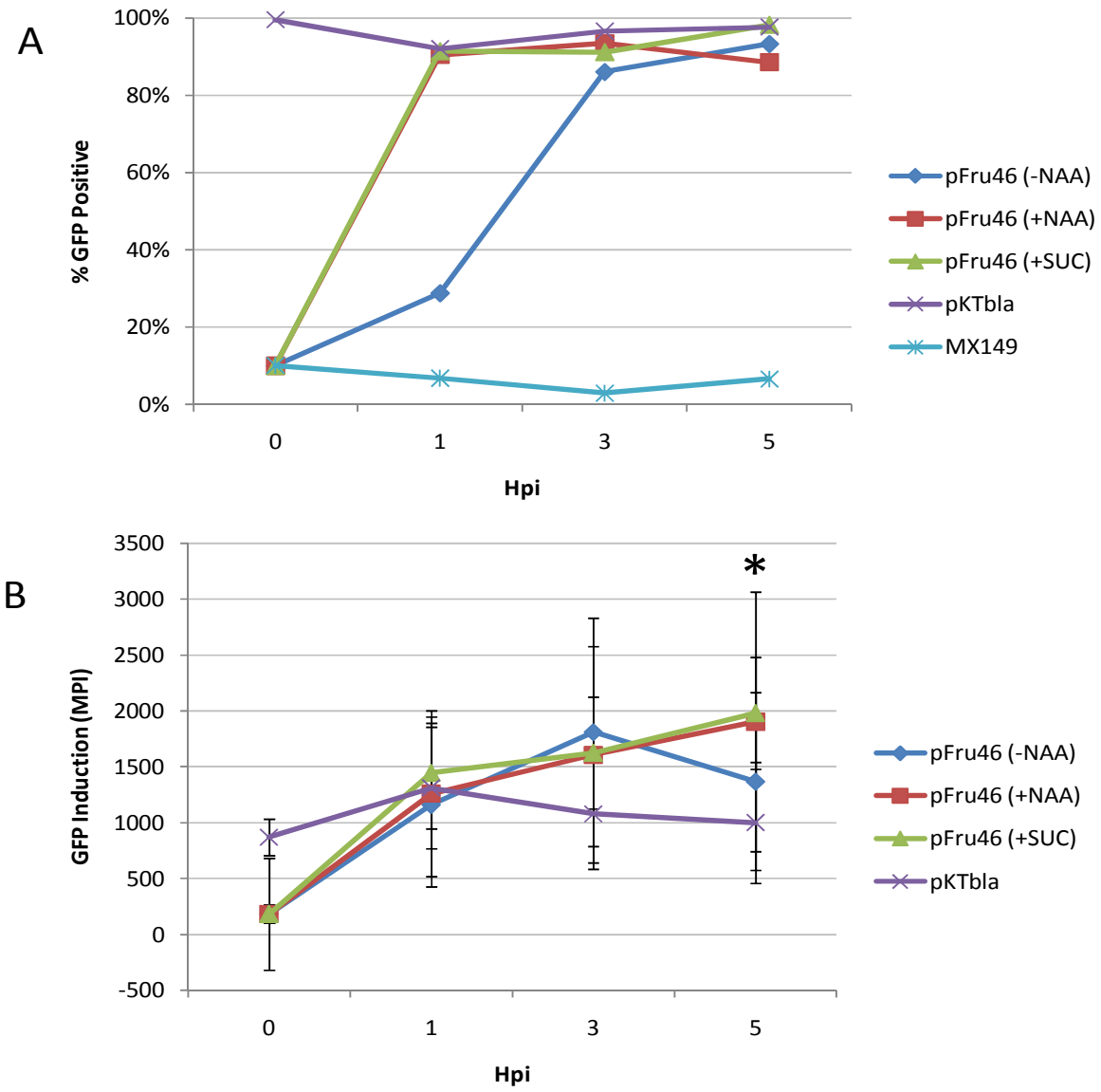

Figure 14. Coinoculation with exogenous NAA allows faster access to phyllosphere sugars by fructose biosensor bacteria. Percent GFP-positive cells (A) and mean GFP fluorescence intensity of the GFP-positive population (±S.D.) (B) are shown for auxin-deficient *Pa*MX149 (pFru46) bacteria coinoculated with buffer, NAA, or exogenous sucrose; negative control (MX149) and constitutively fluorescent positive control (pKTbla) treatments are also indicated. Mean ± 1 S.D. are indicated; *= a statistically significant difference between NAA+ and NAA- treatments ($p<0.001$).

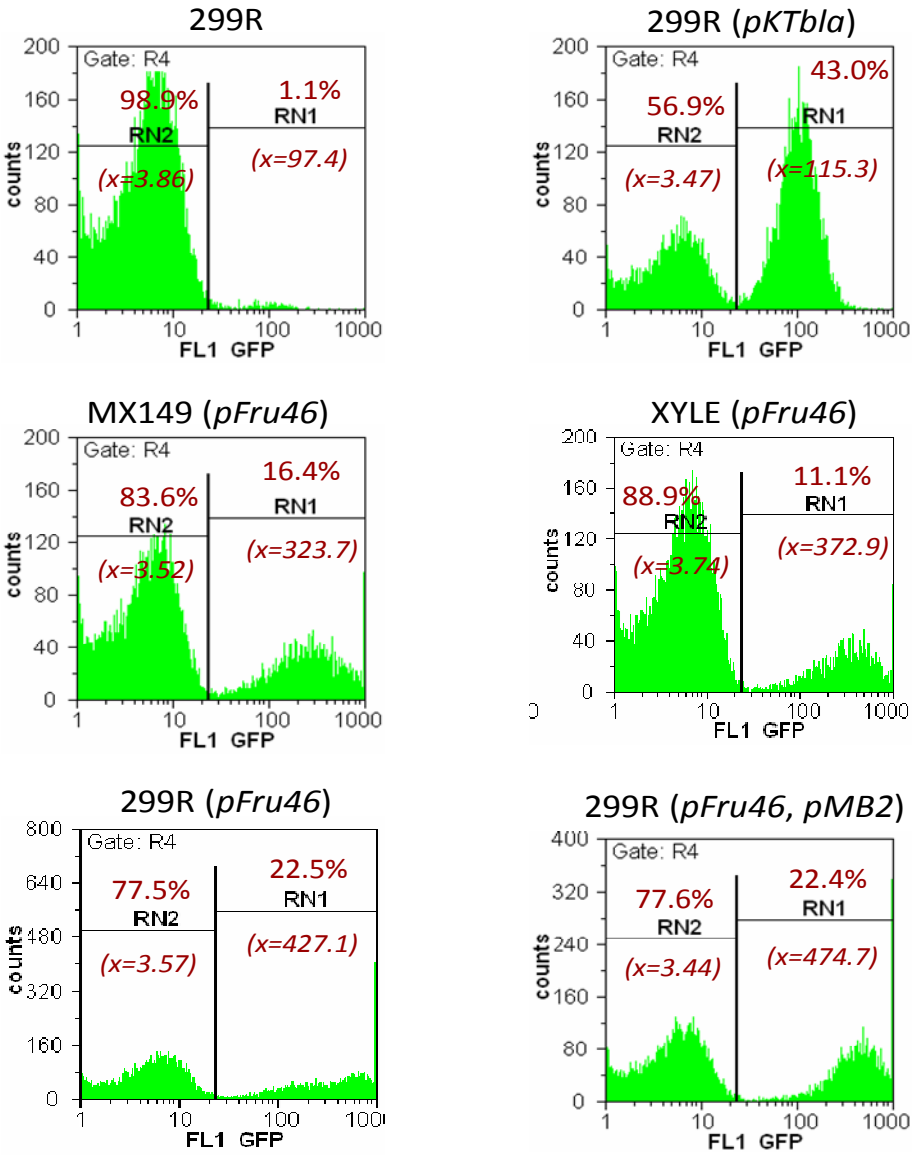

Figure 15. The *Pa*299R (pFru46) fructose biosensor strain (or its isogenic, IAA- mutant derivatives MX149 and XYLE) was inoculated onto bean leaves., then assayed by flow cytometry for *gfp* induction at 24hpi. For each treatment, the percentage of GFP-negative (RN2) and GFP-positive (RN1) particles is indicated; mean GFP fluorescence (x) of each peak is listed in parentheses.

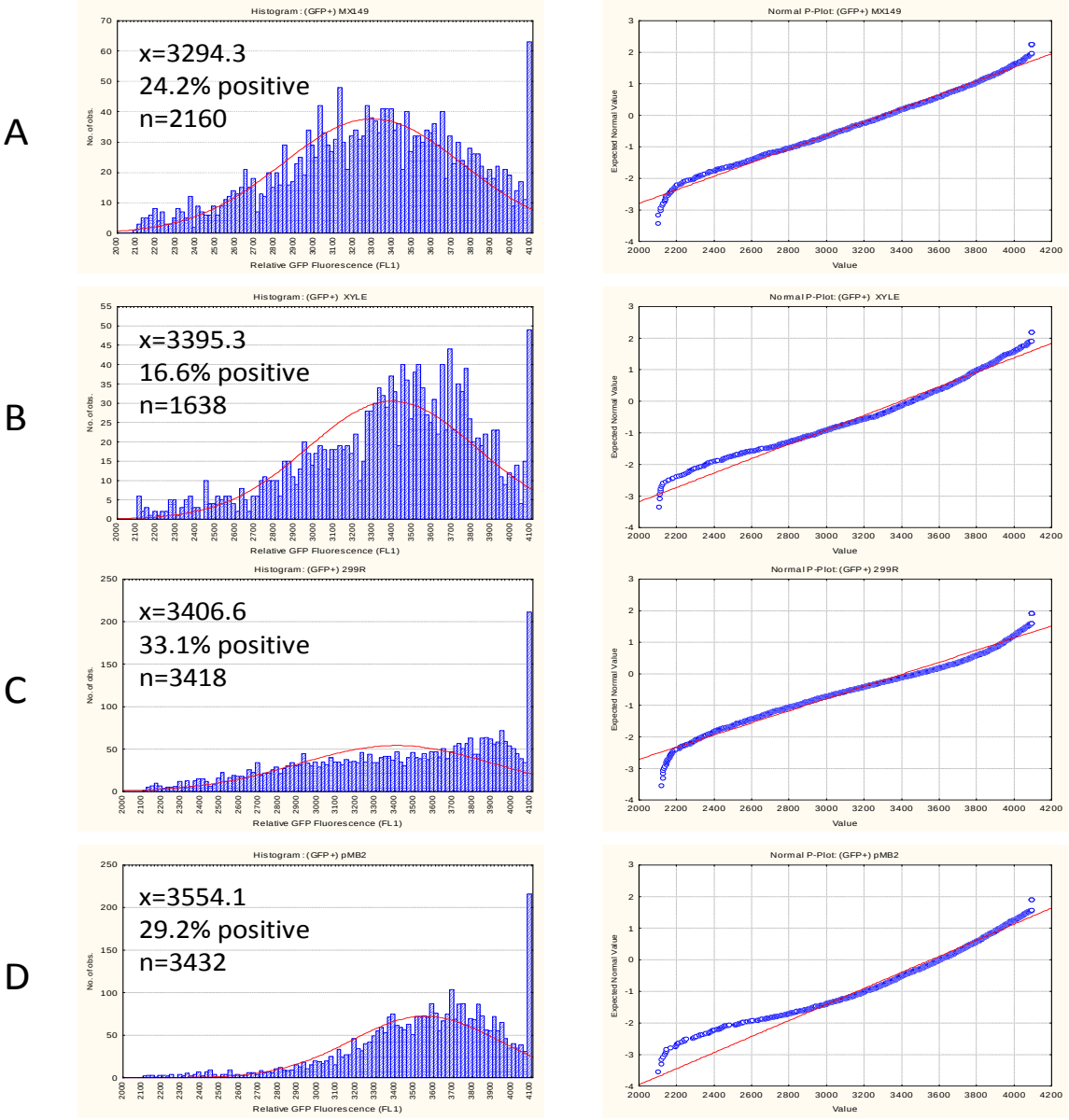

Figure 16. Distribution histograms (left) and normal probability plots (right) of relative GFP fluorescence intensity among individual GFP-positive cells harvested from bean leaves at 24hpi (GFP-negative particles not shown). The fructose-inducible GFP reporter pFru46 was expressed in the auxin-deficient mutants *Pa*MX149 (A) and *Pa*XYLE (B), wild-type *Pa*299R (C) and *Pa*299R *pMB2*, which bears an extra copy of the *ipdC* gene under its native reporter (D).

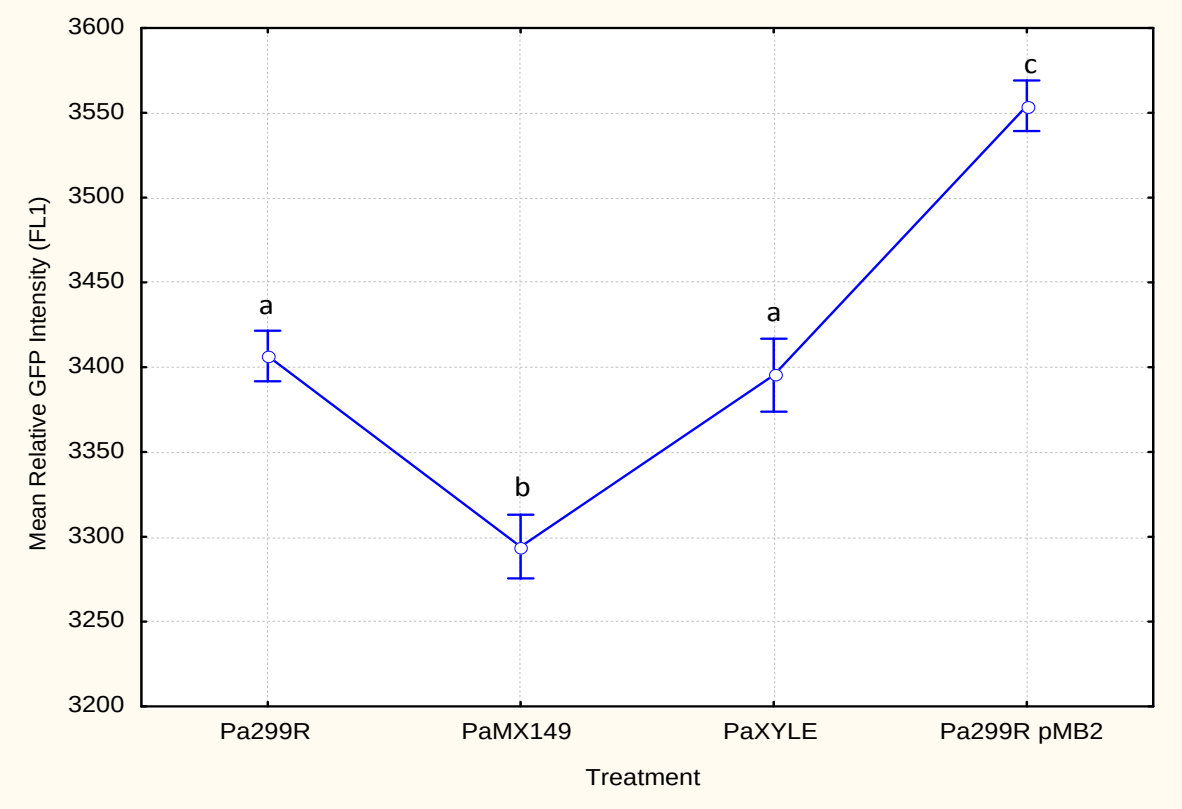

Figure 17. At 24 hpi, bacterial strain exerts a significant effect on mean fluorescence induction in pFru46 fructose biosensors inoculated onto bean leaves. Mean cellular fluorescence of GFP-positive cells (as measured by flow cytometry) and 95% confidence intervals are shown for wild-type *Pa*299R, its IAA-deficient mutant derivatives MX149 and XYLE, and the IAA-overexpressor 299R (pMB2); letters indicate significantly different mean GFP inductions.

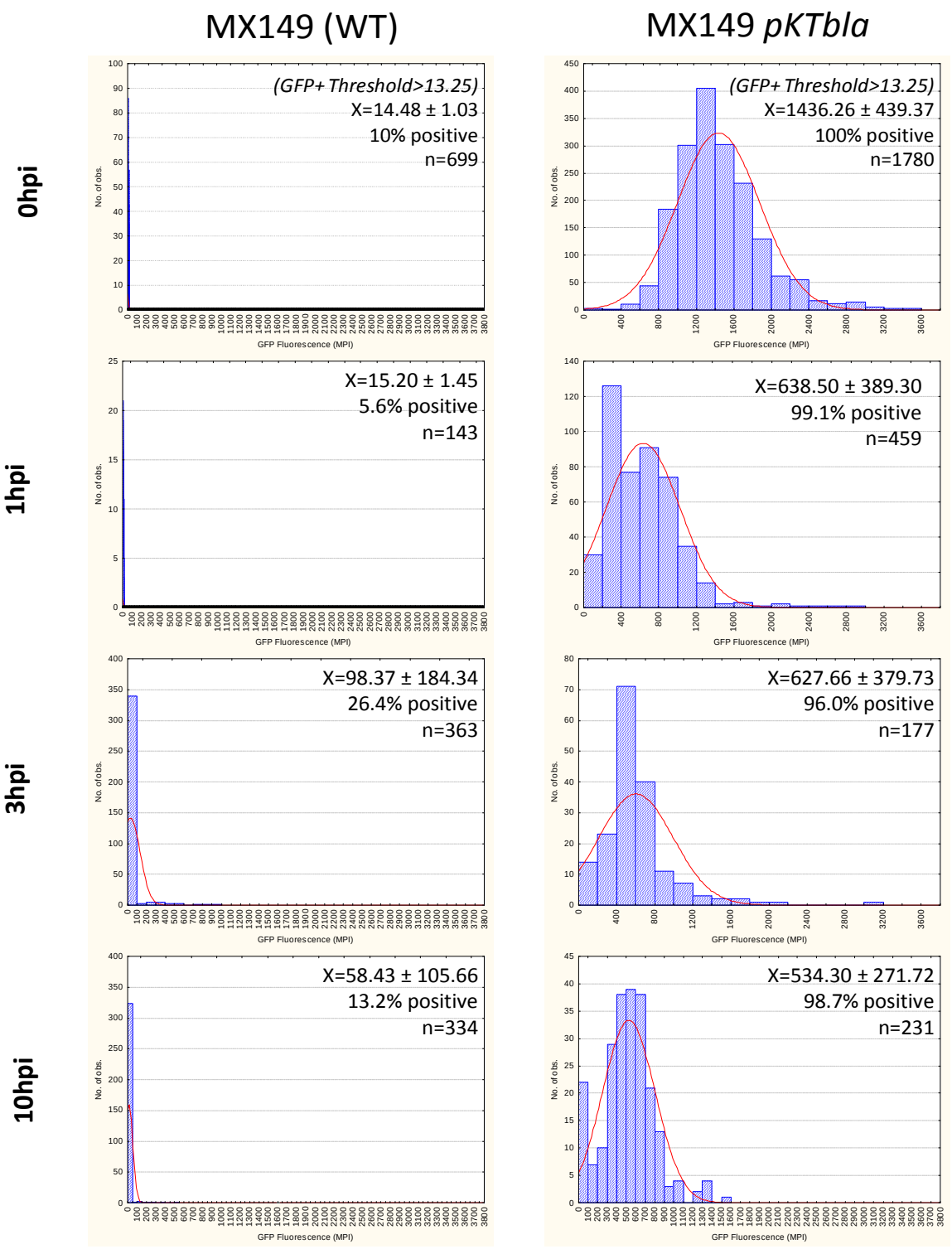

Figure 18. Histograms describe the distribution of GFP fluorescence intensity among *Pa*MX149 (WT) and *Pa*MX149 (pKTbla) cells inoculated onto bean leaves. The fluorescence threshold for GFP-positive cells is indicated (top right, 0hpi of each treatment). For each sample, the total N, % GFP-positive cells, and mean±S.D. of the GFP-positive population are shown. The curve represents the calculated normal distribution.

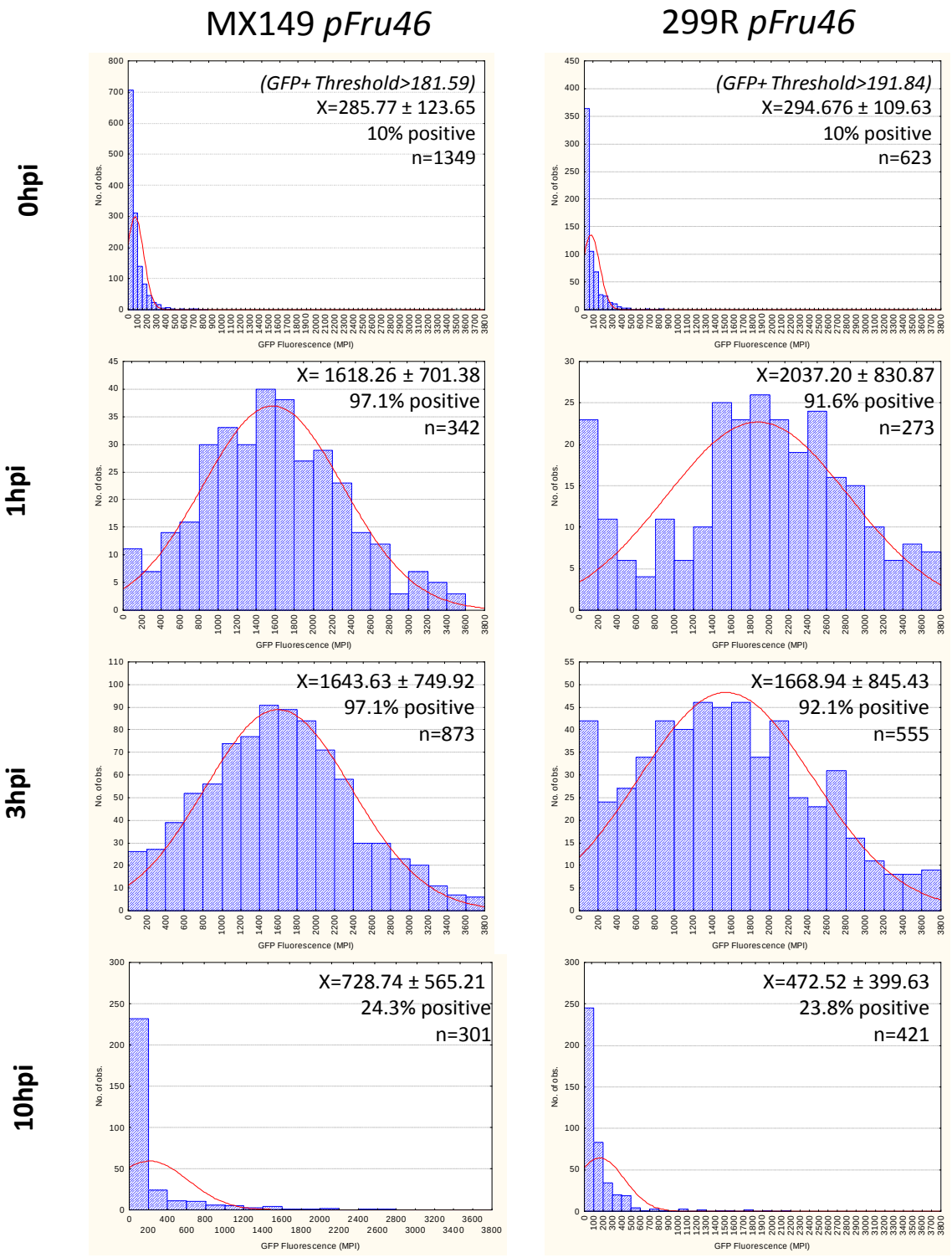

Figure 19. Histograms describing the distribution of GFP fluorescence intensity among *Pa*MX149 (pFru46) and *Pa*299R (pFru46) cells inoculated onto bean leaves. The fluorescence threshold for GFP-positive cells is indicated (top right, 0hpi of each treatment). For each sample, the total N, % GFP-positive cells, and mean±S.D. of the GFP-positive population are indicated. The curve represents the calculated normal distribution.

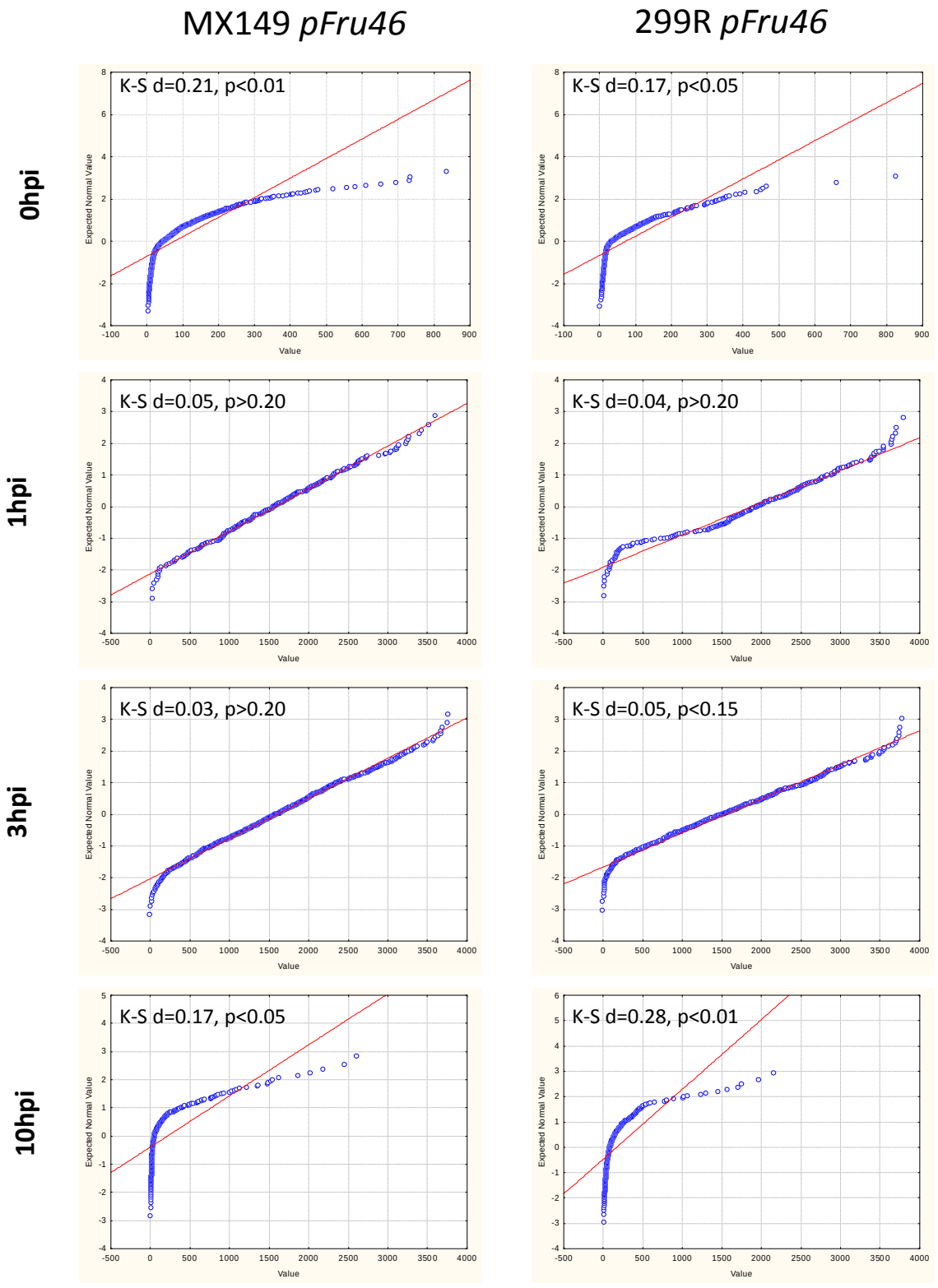

Figure 20. Normal probability plots of the distribution of GFP fluorescence intensity among *Pa*MX149 (pFru46) and *Pa*299R (pFru46) inoculated onto bean leaves. Normality of the GFP-positive cell population only (data not shown) was assessed via the Kolmogorov-Smirnov test; results are shown in the top-left of each plot.

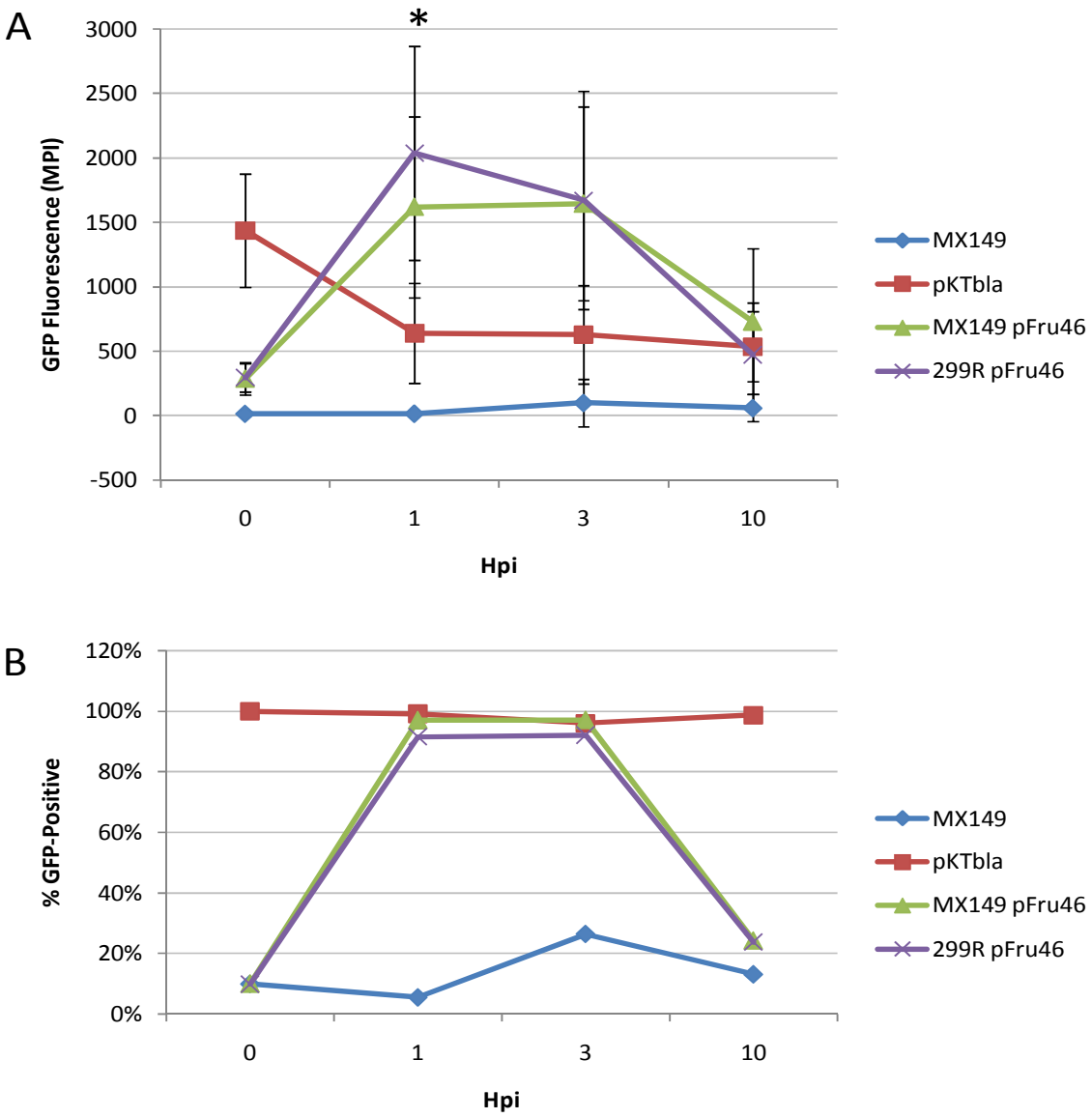

Figure 21. Endogenous IAA increases access to phyllosphere sugars by fructose biosensor bacteria at 1 hpi. Mean GFP fluorescence intensity of the GFP-positive cell population (±S.D.) (A) and the percentage GFP-positive cells(B) are shown for *Pa*299R (pFru46) and its auxin-deficient mutant derivative *Pa*MX149 (pFru46); negative control (MX149) and constitutively fluorescent positive control (pKTbla) treatments are also indicated. Means ± 1 S.D. are indicated; *= a statistically significant difference between MX149 and 299R ($p<0.001$).

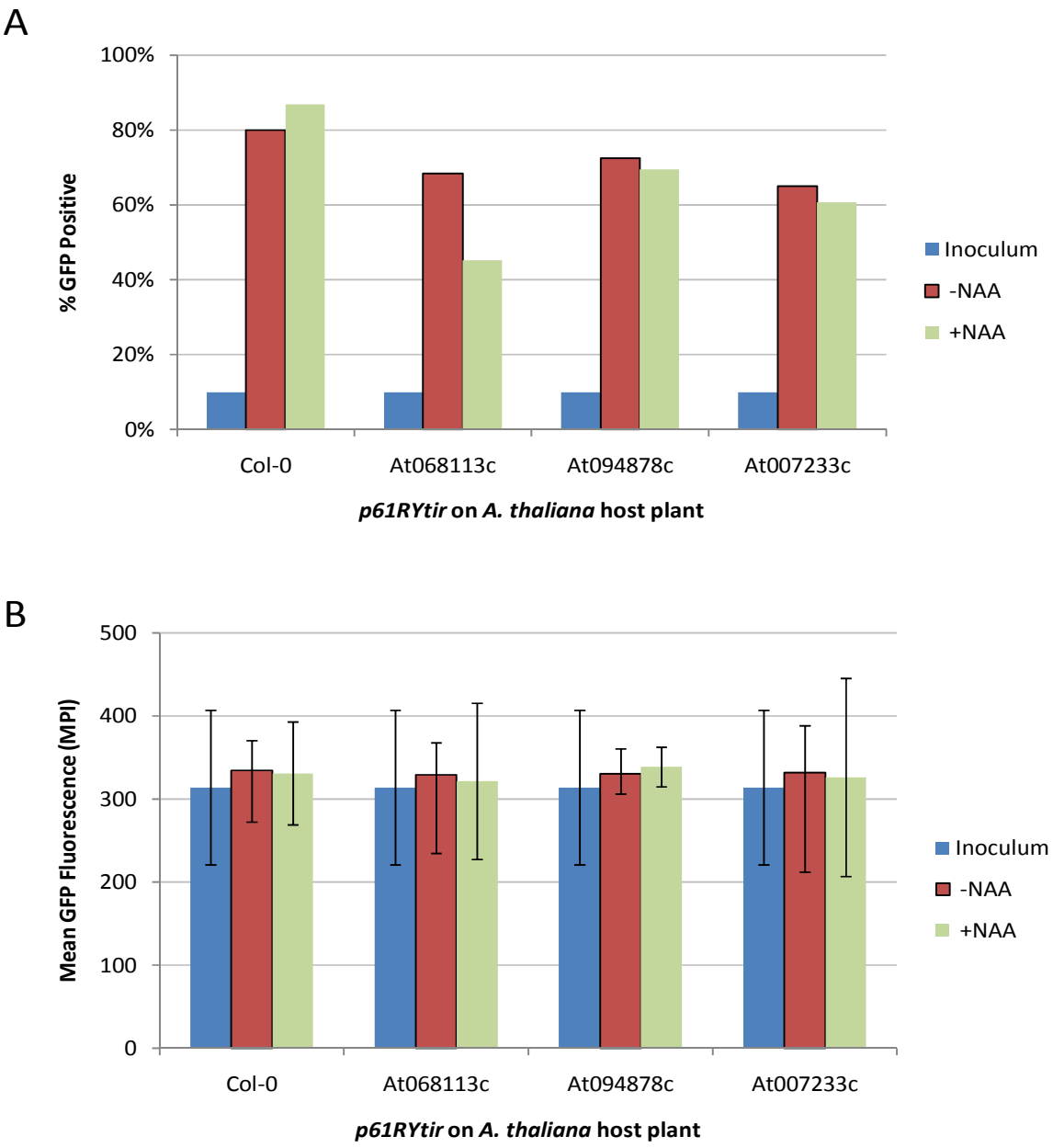

Figure 22. Induction of *Pa*MX149 (p61RYtir) fluorescent sucrose biosensor bacteria inoculated with or without NAA onto wild-type *Arabidopsis thaliana* or 3 *A.t.* cell wall invertase mutants. The proportion of GFP-positive cells (A) and mean cellular fluorescence ±1S.D. (B) are shown.

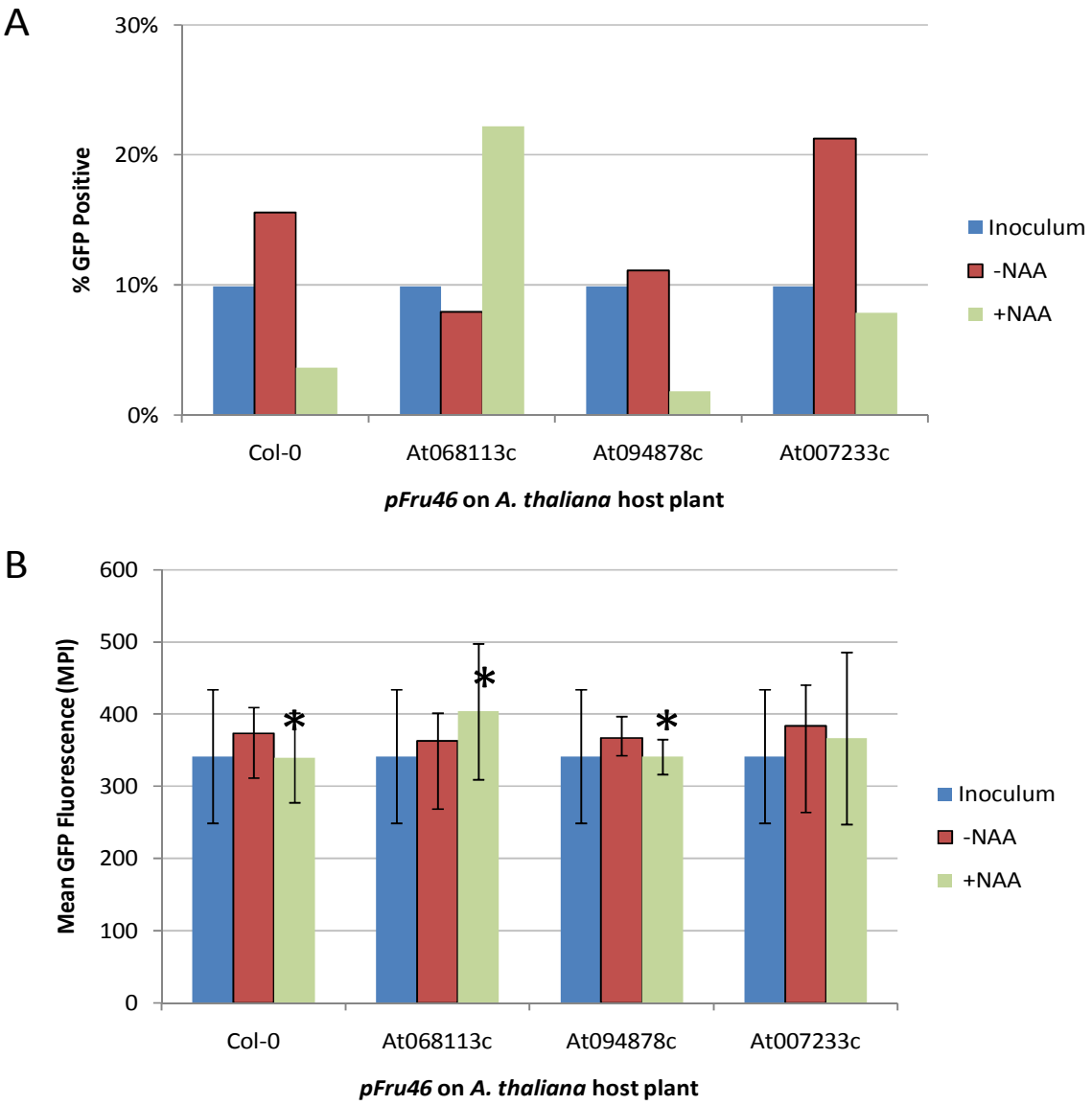

Figure 23. Induction of *Pa*MX149 (pFru46) fluorescent fructose biosensor bacteria inoculated with or without NAA onto wild-type *Arabidopsis thaliana* or 3 *A.t.* cell wall invertase mutants. The proportion of GFP-positive cells (A) and mean cellular fluorescence ±1S.D. (B) are shown. *= a significant ($p<0.01$) difference between NAA+ and NAA- treatments on a given host plant.;

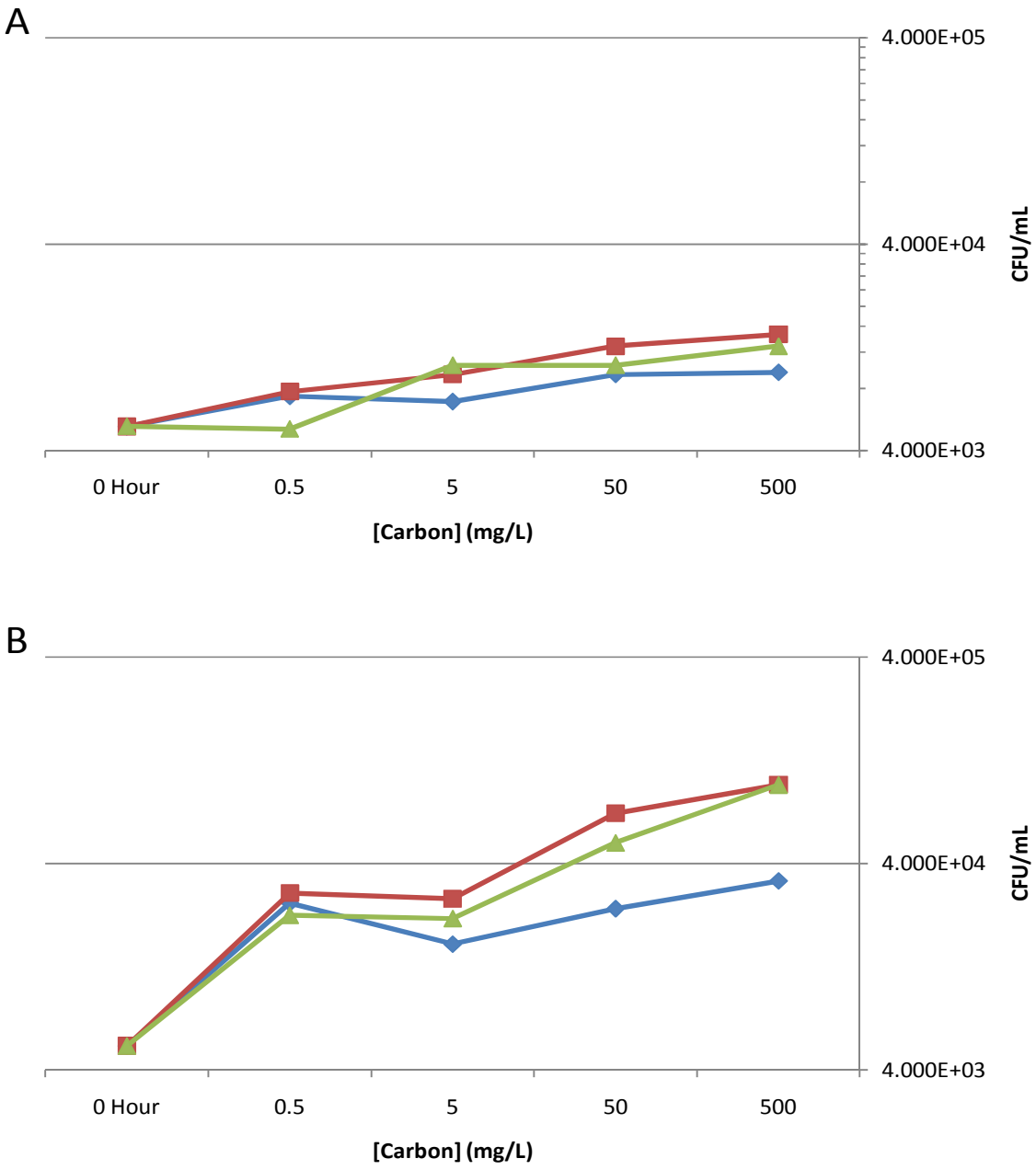

Figure 24. Growth of *Pa*299R cells grown in varying concentration of sucrose, glucose, or fructose after 4.5(A) or 8 hours in culture (B). (n=1)

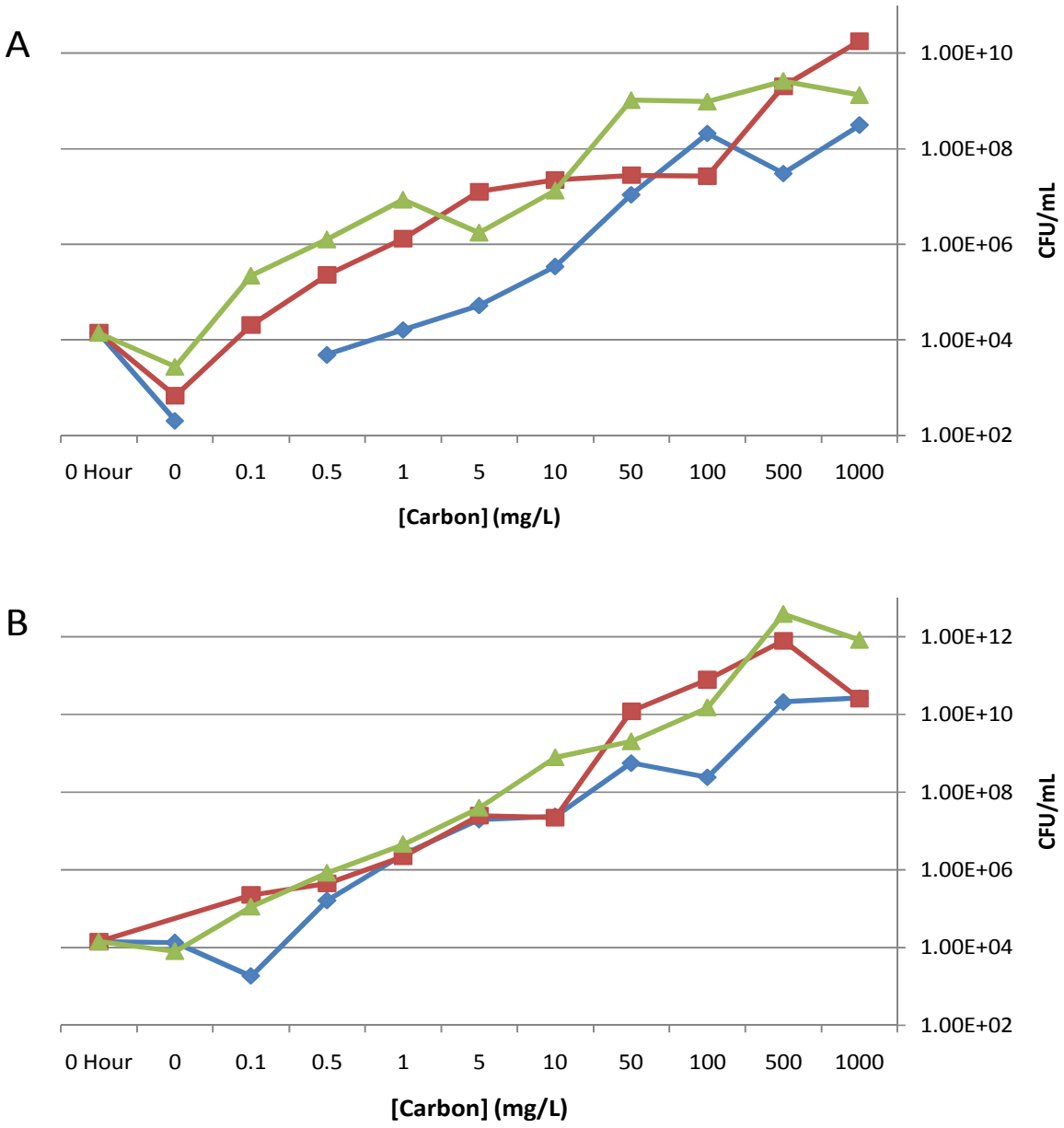

Figure 25. Growth of *Pa*299R cells grown in varying concentration of sucrose, glucose, or fructose after 24 (A) or 48 hours in culture (B). Graphs depict mean ± 1 standard deviation (n=3).

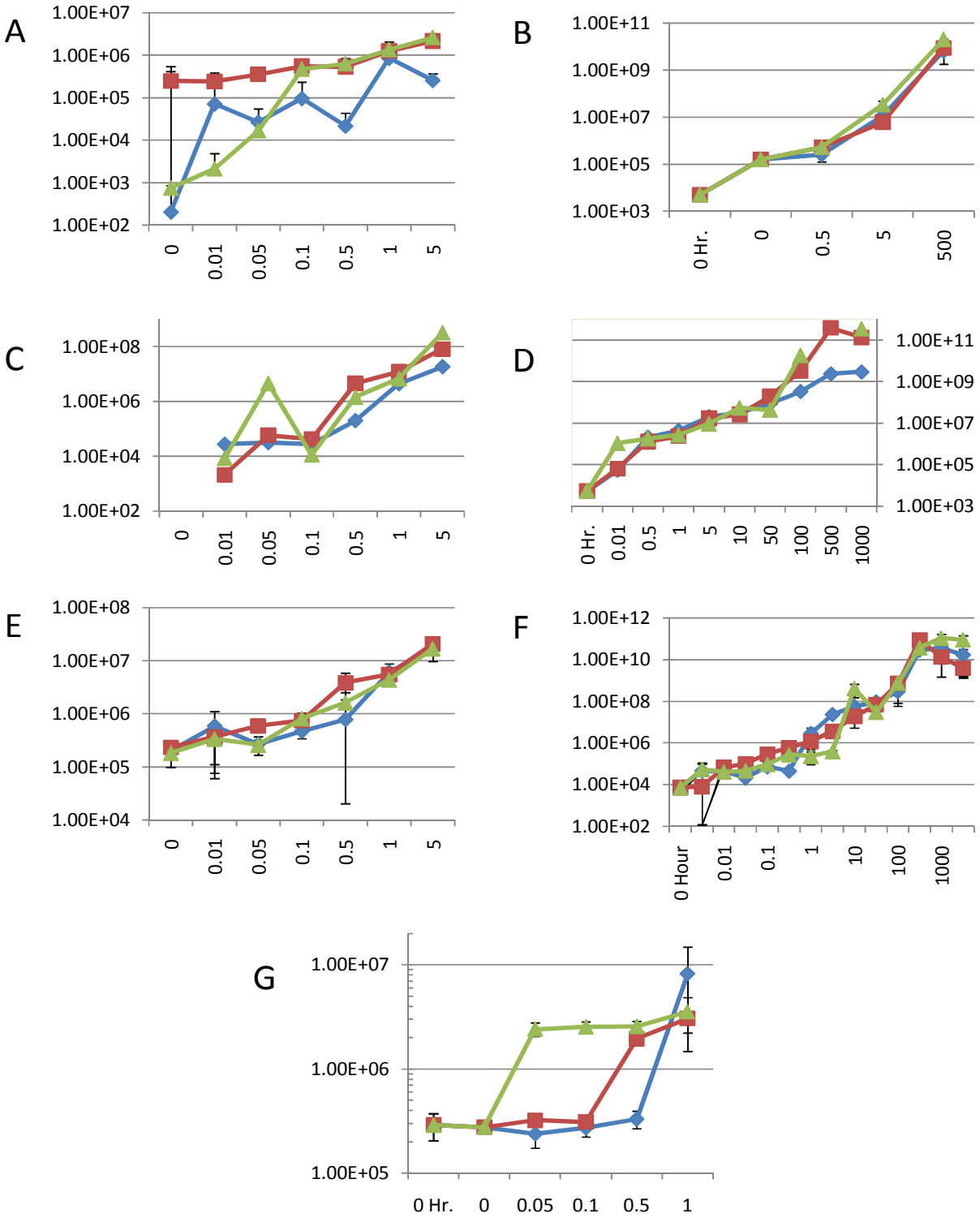

Figure 26. Growth of *Pa*299R cells grown in varying concentration of sucrose, glucose, or fructose for 72 hours. Graphs depict mean ± 1 standard deviation (n=3); each graph represents an independent experiment. (A-G)

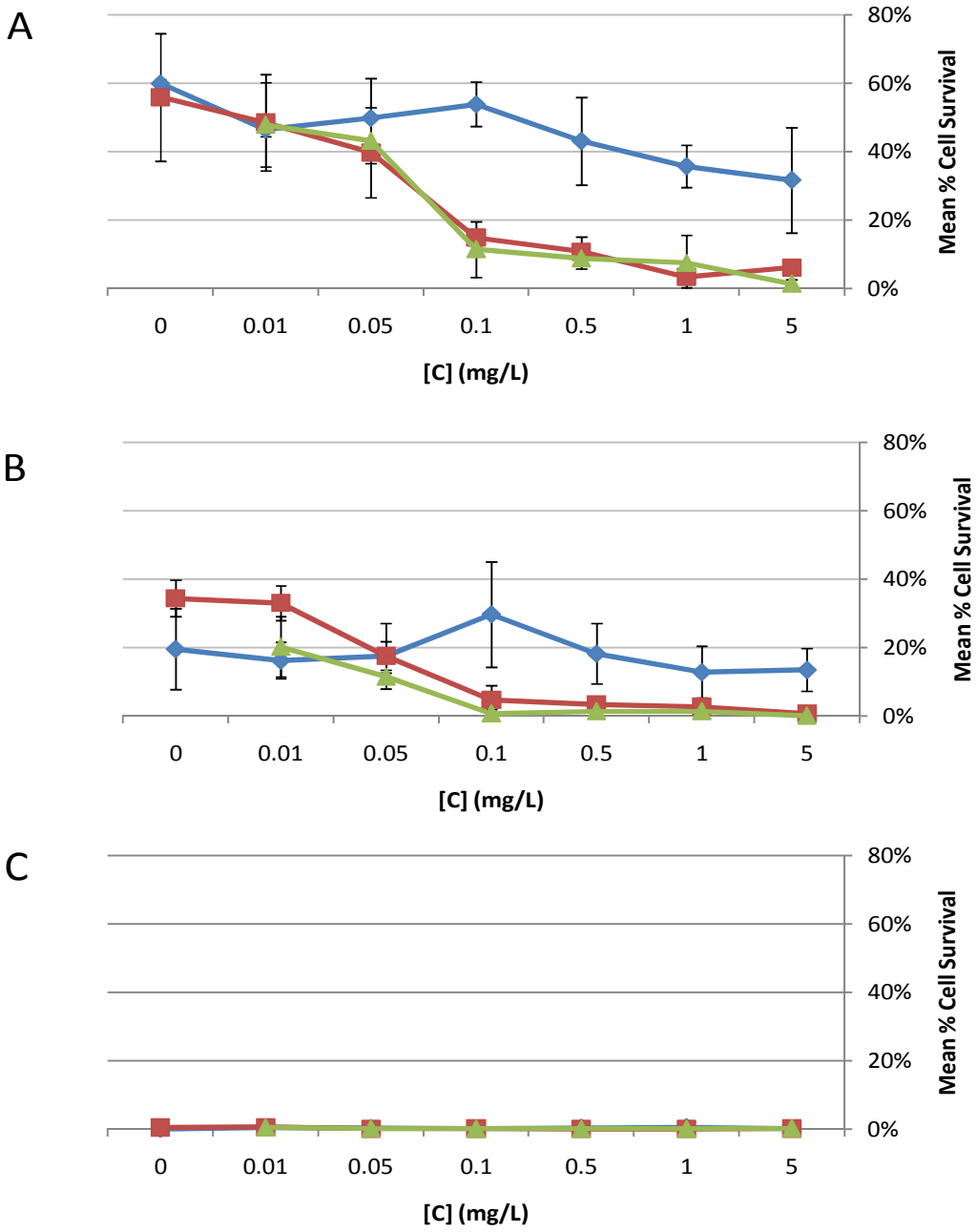

Figure 27. Survival of *Pa*299R cells cultured in the presence of cycloserine with varying concentrations of sucrose, glucose, or fructose after 6.5 (A), 12 (B), or 30 (C) hours of culture.

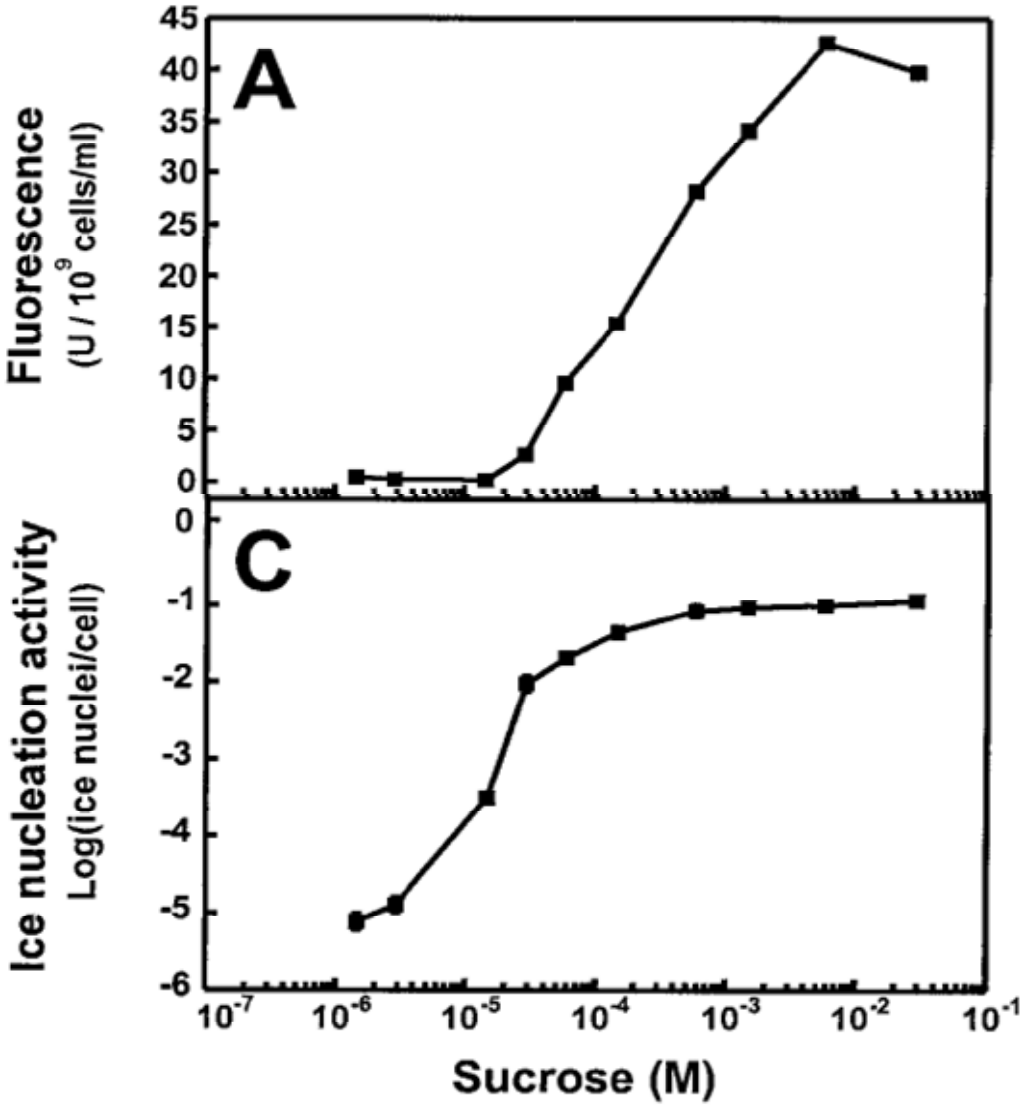

Figure 28. Miller *et* al. (2001) reported differing sensitivities of the *Pa*299R *(*p61RYice) ice nucleation bioreporter and the *Pa*299R (p61RYtir) GFP bioreporter to sucrose.

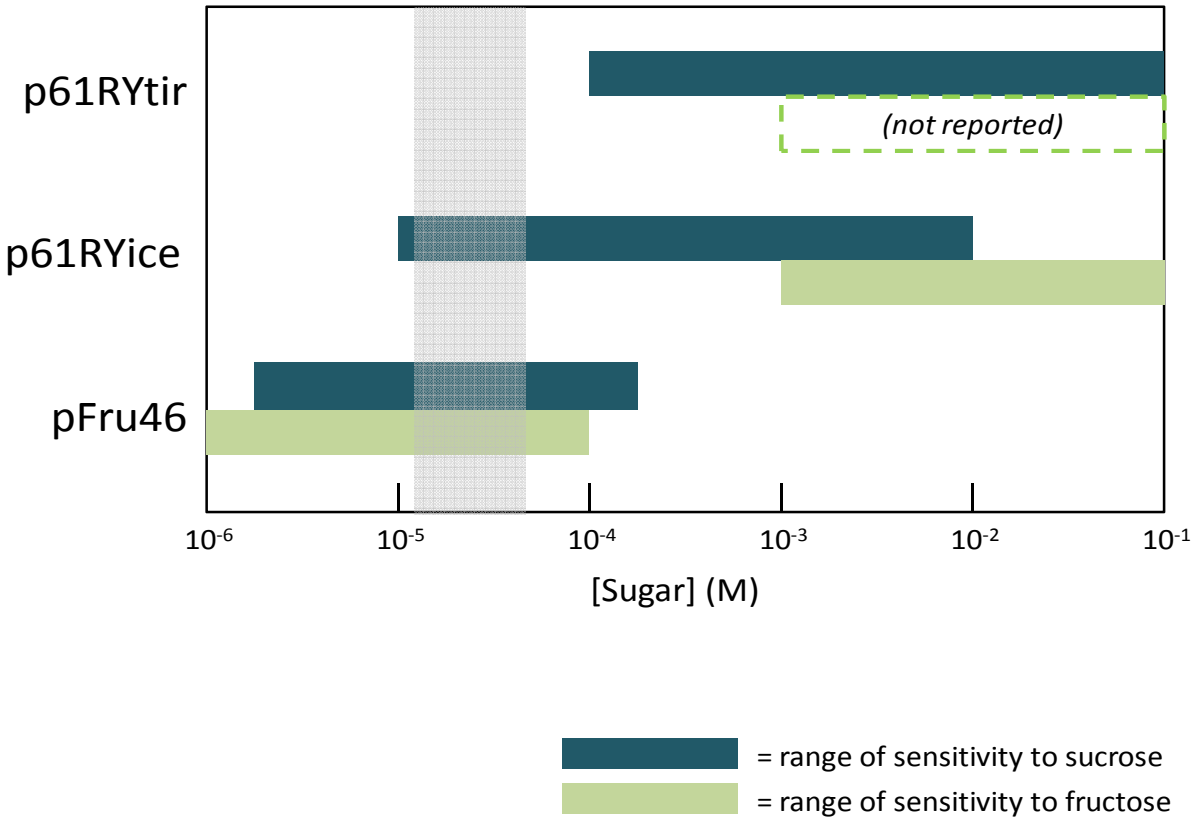

Figure 29. Dynamic ranges of the p61RYtir and pFru46 biosensors to sucrose and fructose (Miller *et al.*, 2001; Leveau *et al.*, 2001a). The anticipated range of IAA-induced changes in sugar availability is indicated as a gray vertical bar.

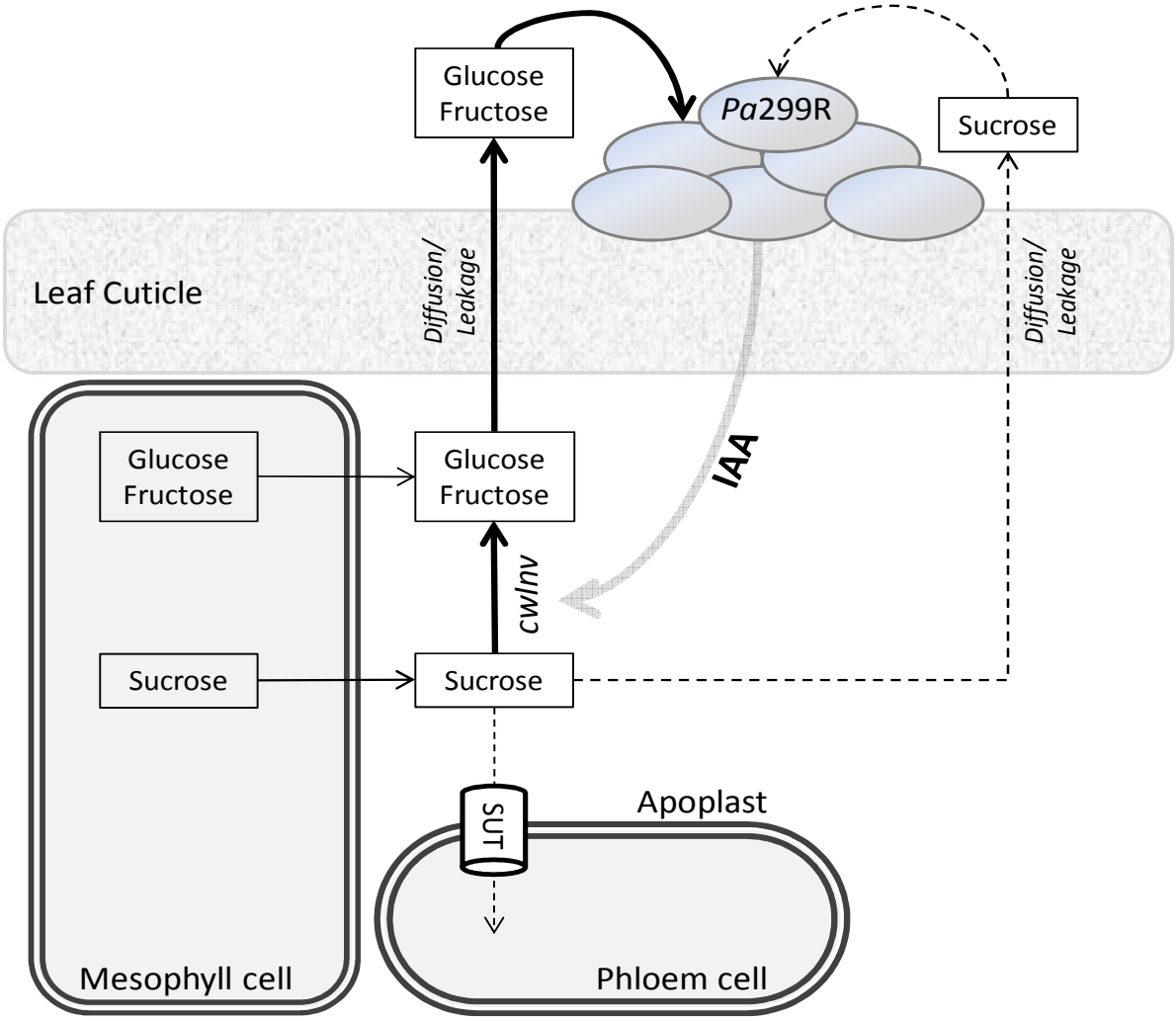

Figure 30. Proposed model of bacterial auxin action in the phyllosphere. Bacterial IAA diffuses across the cuticle into the plant apoplast, where it activates apoplastic cell wall invertases (cwinv). Invertases cleave apoplastic sucrose as it transits from source mesophyll cells into the vasculature. By converting photosynthate into glucose and fructose, invertases divert transport photosynthates into monosaccharide pools before they can be loaded into the phloem by sucrose-specific transporter proteins (SUTs). The altered ratio of apoplastic sugars yields a relative increase in the proportion of glucose and fructose that diffuses to the leaf surface (bold arrows), and a relative decrease in the proportion of sucrose available for diffusion or phloem loading (dashed arrows).

Treatment	Slope	r	p	r^2
p61RYice + Sucrose	-0.005	-0.73	<0.001	0.53
p61RYice	-0.003	-0.57	0.010	0.33
299R	-0.001	-0.21	0.445	0.04
p61RYice +NAA	0.001	0.15	0.550	0.02

Table 1. Correlation and regression analysis of mean sucrose sensing versus time across five replicate experiments.

Experiment #	Experiment (mm/dd/yyyy)	Estimated Insolation (W/m^2)
1	06/12/2009	483.53
2	06/16/2009	484.19
4	09/16/2009	456.89
5	11/18/2009	201.53
6	01/21/2010	200.22
Figure Xa	05/03/2010	445.61
Figure Xb	09/19/2010	349.75

Table 2. Estimated insolation on the day of experiment and mean temperature in the weak preceding to plant-inoculation experiments. Insolation values were used as covariates for ANCOVA analysis of biosensor experiments using the ice nucleation sucrose bioreporter.

Effect	Univariate Results for Each DV (Spreadsheet1) Sigma-restricted parameterization Effective hypothesis decomposition Degr. of Freedom	mean log(inaz/cell) SS	mean log(inaz/cell) MS	mean log(inaz/cell) F	mean log(inaz/cell) p
Intercept	1	341.8745	341.8745	2029.107	0.000000
Treatment	1	1.1127	1.1127	6.604	0.024554
Hpi	3	34.6642	11.5547	68.580	0.000000
Treatment*Hpi	3	0.4068	0.1356	0.805	0.514979
Error	12	2.0218	0.1685		
Total	19	38.6182			

Table 3. Multivariate ANOVA of *Pa*MX149 (p61RYice) Biosensor Induction on Bean Leaves Over Time

Contrast	Contrast Estimates (Spreadsheet1) Dependent variable: mean log(inaz/cell)					
	Estimate	Std.Err	t	p	-95.00% Cnf.Lmt	+95.00% Cnf.Lmt
0hpi (NAA+ vs NAA-)	0.403	0.580	0.694	0.501	-0.862	1.668
3hpi (NAA+ vs NAA-)	0.180	0.335	0.537	0.601	-0.550	0.910
7hpi (NAA+ vs NAA-)	0.898	0.335	2.679	*0.020	0.168	1.628
24hpi (NAA+ vs NAA-)	0.629	0.335	1.876	0.085	-0.101	1.359

Table 4. Contrast Estimates of *Pa*MX149 (p61RYice) Biosensor Induction on Bean Leaves at Individual Time Points

Effect	D.F.	log(inaZ/cell) SS	log(inaZ/cell) MS	log(inaZ/cell) F	log(inaZ/cell) p
Intercept	1	92.80726	92.80726	399.9879	0.000000
Insolation (W/m^2)	1	1.21496	1.21496	5.2363	0.026136
Treatment	2	36.05479	18.02739	77.6959	0.000000
Error	53	12.29733	0.23203		
Total	56	49.56741			

Table 5. ANCOVA analysis of four experiments comparing sucrose sensing of the IAA^- strain *Pa*MX149 (p61RYice) inoculated onto bean plants with or without 100uM NAA

Source	Sum of Squares	D.F.	Mean Square	F	p
Effect	3.55455	1	3.554555	15.32039	0.000261
Error	12.29678	53	0.232015		

Table 6. Planned comparison between NAA+ and NAA- sucrose biosensor samples using contrast coefficients

Effect	D.F.	Log(inaZ/cell) SS	Log(inaZ/cell) MS	log(inaZ/cell) F	Log(inaZ/cell) p
Intercept	1	83.14162	83.14162	379.3471	0.000000
Insolation (W/m^2)	1	0.89938	0.89938	4.1036	0.048883
Treatment	2	22.01594	11.00797	50.2257	0.000000
Error	44	9.64349	0.21917		
Total	47	32.55882			

Table 7. ANCOVA analysis of four experiments comparing sucrose sensing by wild-type *Pa*299R with its isogenic, IAA^- knockout strain *Pa*MX149

Source	Sum of Squares	D.F.	Mean Square	F	p
Effect	1.630371	1	1.630371	7.438833	0.009135
Error	9.643493	44	0.219170		

Table 8. Planned comparison between 299R (p61RYice) and MX149 (p61RYice) biosensor activity on bean leaves using contrast coefficients

Tukey HSD test; variable GFP Fluorescence Intensity (FL1) (Spreadsheet1)
Approximate Probabilities for Post Hoc Tests Error: Between MS = 44986., df = 5742.0

	Strain	{1}	{2}	{3}
1	Pa299R		0.000022	0.000022
2	MX149	0.000022		0.000022
3	XYLE	0.000022	0.000022	

Table 9. One-way ANOVA of sucrose sensing flow cytometry; post-hoc analysis with Tukey's HSD test showed significant ($p<0.001$) differences between all treatments

Effect	Univariate Tests of Significance for mean log(inaz/cell) Sigma-restricted parameterization Effective hypothesis decomposition				
	SS	Degr. of Freedom	MS	F	p
Intercept	1572572	1	1572572	5046.028	0.000
Treatment	27	1	27	0.087	0.776
Hpi	1311049	3	437016	1402.287	0.000
Treatment*Hpi	9451	3	3150	10.109	0.004
Error	2493	8	312		

Table 10. Multivariate ANOVA of *Pa*299R (pFru44) Biosensor Induction on Bean Leaves

Contrast	Contrast Estimates (6.12.09 NAA coinoculation spreadsheet.stw) Dependent variable: mean log(inaz/cell)					
	Estimate	Std.Err	t	p	-95.00% Cnf.Lmt	+95.00% Cnf.Lmt
3hpi (NAA+ vs NAA-)	-15.3850	17.65349	-0.87150	0.408873	-56.0940	25.3240
7hpi (NAA+ vs NAA-)	-53.8400	17.65349	-3.04982	0.015825	-94.5490	-13.1310
24hpi (NAA+ vs NAA-)	79.6400	17.65349	4.51129	0.001972	38.9310	120.3490

Table 11. Contrast Estimates of *Pa*299R (pFru44) Biosensor Induction on Bean Leaves at Individual Time Points

Effect	Univariate Tests of Significance for MPI (GFP+ Only) (4.22.10 Best Statistica spreadshe Sigma-restricted parameterization Effective hypothesis decomposition				
	SS	Degr. of Freedom	MS	F	p
Intercept	1.015635E+09	1	1.015635E+09	1221.706	0.000000
Hpi	1.768148E+08	3	5.893826E+07	70.897	0.000000
Treatment	2.116903E+06	1	2.116903E+06	2.546	0.110726
Hpi*Treatment	4.331958E+07	3	1.443986E+07	17.370	0.000000
Error	1.443180E+09	1736	8.313249E+05		

Table 12. Multifactorial ANOVA results of fructose biosensor induction on bean leaves

	Tukey HSD test; variable MPI (GFP+ Only) (4.22.10 Best Statistica spreadsheet - FF area background correct.sta) Approximate Probabilities for Post Hoc Tests Error: Between MS = 8313E2, df = 1736.0									
Cell No.	Hpi	Treatment	{1} 180.46	{2} 180.46	{3} 1159.6	{4} 1259.2	{5} 1810.6	{6} 1607.9	{7} 1368.0	{8} 1903.5
1	0	C		1.000000	0.000040	0.000032	0.000032	0.000032	0.000032	0.000032
2	0	D	1.000000		0.000040	0.000032	0.000032	0.000032	0.000032	0.000032
3	1	C	0.000040	0.000040		0.994139	0.000047	0.012914	0.701816	0.000032
4	1	D	0.000032	0.000032	0.994139		0.000032	0.000172	0.733410	0.000032
5	3	C	0.000032	0.000032	0.000047	0.000032		0.203312	0.000032	0.929455
6	3	D	0.000032	0.000032	0.012914	0.000172	0.203312		0.016472	0.002212
7	5	C	0.000032	0.000032	0.701816	0.733410	0.000032	0.016472		0.000032
8	5	D	0.000032	0.000032	0.000032	0.000032	0.929455	0.002212	0.000032	

Table 13. Post-hoc analysis of fructose biosensor induction on bean leaves

Strain	A. Thaliana host plant	T	Df	P	NAA- Mean (±S.D.), *n*	NAA+ Mean (±S.D.), *n*
*Pa*MX149 *pFru46*	Col-0	5.80	354	**<0.001***	373.36 (±36.39) *n=135*	339.39 (±61.78) *n=221*
	*At*068113c	3.22	133	**0.002***	362.65 (±38.79) *n=63*	403.58 (±94.00) *n=72*
	*At*094878c	5.39	134	**<0.001***	366.93 (±29.93) *n=81*	340.86 (±23.98) *n=55*
	*At*007233c	0.92	134	0.36	383.75 (±57.05) *n=47*	366.78 (±119.29) *n=89*
*Pa*MX149 *p61RYtir*	Col-0	1.08	126	0.28	334.05 (±20.49) *n=60*	330.83 (±12.71) *n=68*
	*At*068113c	1.87	67	0.07	328.88 (±17.45) *n=38*	321.52 (±14.68) *n=31*
	*At*094878c	-1.50	74	0.13	330.27 (±19.29) *n=40*	338.71 (±29.31) *n=36*
	*At*007233c	1.26	71	0.32	331.45 (±19.55) *n=40*	326.10 (±15.96) *n=33*

Table 14. T-tests of Arabidopsis-inoculated Sugar Biosensors

Organism/Strain	Description	Reference
Phaseolus vulgaris	Common bean, cv. Bush Blue Lake 274	*n/a*
Arabidopsis thaliana	Wild-type, Columbia-0 ecotype	*n/a*
*At*068113c (*cwinv2*) *At*094878c (*cwinv4*) *At*007233c (*cwinv1*)	Homozygous mutants of Col-0; T-DNA insertions in various cell wall invertase homologs	Alonso *et al*., 2003
Pantoea agglomerans 299R	Spontaneous Rif^R mutant of *P.a.* (formerly *Erwinia herbicola*)	*n/a*
*Pa*MX149	IAA-deficient derivative of *Pa*299R; Tn3-Spice insertion in *ipdC*; Sp/St^R	Brandl *et al*., 1996
*Pa*XYLE	IAA-deficient derivative of *Pa*299R; *xyle* insertion in *ipdC*	Brandl *et al*., 1998

Plasmid	Description	Reference
pFru44	*gfp*.ASV reporter (half-life≈110 min) driven by a fructose-inducible X promoter	Leveau *et al*., 2001b
pFru46	*gfp*.AAV reporter (half-life≈60 min) driven by a fructose-inducible X promoter	Leveau *et al*., 2001a
p61RYice	*inaZ* reporter gene driven by the sucrose-inducible *scrY* promoter	Miller *et al*., 2001
p61RYtir	*gfp* reporter gene driven by the sucrose-inducible *scrY* promoter	Miller *et al*., 2001
pKTbla	*gfp* reporter gene driven by weak constitutive *bla* promoter	Miller *et al*., 2001

Table 15. Table of Experimental Organisms and Constructs

Effect	Univariate Results for Each DV (9.21.10 Plant Fructose Sensing - GFP only Spreadsheet.sta) Sigma-restricted parameterization Effective hypothesis decomposition Degr. of Freedom	MPI SS	MPI MS	MPI F	MPI p
Intercept	1	1.333101E+09	1.333101E+09	2521.259	0.000000
Hpi	3	4.765393E+08	1.588464E+08	300.422	0.000000
Treatment	1	6.699091E+05	6.699091E+05	1.267	0.260451
Hpi*Treatment	3	2.198458E+07	7.328195E+06	13.860	0.000000
Error	2302	1.217169E+09	5.287442E+05		
Total	2309	1.762323E+09			

Table 16. Multifactorial ANOVA of fructose biosensor induction on bean leaves

Chapter III. Indole-3-acetic acid production by phyllosphere bacteria: Alternative hypotheses.

Abstract

Many plant-associated bacteria produce the plant hormone indole-3-acetic acid (IAA), including symbiotes, both gall-forming and systemic pathogens, and epiphytes (Spaepen *et al*., 2007). Due to the wide variety of lifestyles such bacteria pursue, IAA may act by different mechanisms in different contexts; diverse hypotheses have therefore been proposed to explain why bacteria devote metabolic resources to synthesizing this auxin. Much of this dissertation has investigated a single hypothesis: that bacterial IAA enhances carbon acquisition by phyllosphere epiphytes (Chapter 2). However, a number of other possible hypotheses were also examined. These include the role of bacterial IAA in 1) enhancing stress resistance of the leaf epiphyte *Pantoea agglomerans* 299R; 2) modifying the autofluorescence of epidermal leaf cells that support large bacterial aggregates of *Pa*299R; and 3) facilitating growth or virulence of the compatible pathogen *Pseudomonas syringae* pv. syringae on the common bean (*Phaseolus vulgaris*). These alternative investigations are summarized here. Briefly, bacterial IAA was found to exert no measurable impact on stress resistance, or on the autofluorescence profile of substrate leaf cells. Efforts to abolish auxin biosynthesis by knocking out *Psyr1536*, the putative *iaaM* biosynthetic gene of *P. syringae,* were unsuccessful; the monooxygenase gene *Psyr4667* is postulated to be a functionally redundant homolog, and it was found to be upregulated on leaf surfaces.

I. Native IAA biosynthesis exerts no measurable effect on resistance of *Pantoea agglomerans* 299R to environmental stress

Introduction

Though *Escherichia coli* strain K12 does not synthesize its own auxin, work by Bianco *et al*. (2006) suggests that application of exogenous IAA can nonetheless improve its resistance to environmental stress. When K12 cells were cultured for two hours in the presence of sub-inhibitory (0.5mM) IAA, microarray analysis showed significant shifts in gene transcription relative to an untreated control. Several of the upregulated genes were stress-related, including *yggB*, a solute channel which helps protect cells against lysis during osmotic shock, and *cfa*, which encodes a cylopropane fatty acid biosynthetic enzyme involved in protection against a variety of stressful environmental conditions. IAA also stimulated upregulation of the DnaK chaperone, cellular accumulation of the protective osmolyte trehalose, and increased lipopolysaccharide (LPS) secretion—all of which have been implicated in bacterial stress resistance. Finally, Bianco *et al*. demonstrated that these transcriptional and physiological changes accompanied increased bacterial resistance to acidic pH, hyperosmotic conditions, cold and heat, oxidative stress, and UV radiation. Subsequent work has demonstrated similar effects in the nodulating rhizobacterium *Sinorhizobium meliloti*, which exhibits enhanced survival under

a variety of abiotic stresses when IAA is applied exogenously or overexpressed on a plasmid (Bianco *et al.*, 2009).

In each of these cases, it is unclear whether IAA acts as a specific regulator of stress resistance, or if incubation with any weak acid might be sufficient to induce a similar response—an indole-only negative control failed to trigger stress resistance (Bianco *et al*. 2006), but an alternate weak-acid control has not been reported.

Nonetheless, there seems a compelling possibility that bacterial IAA synthesis by plant-associated microorganisms may not simply mediate interactions with the host plant, but may instead (or additionally) regulate bacterial physiological responses. For example, previous work by Brandl *et al*. (1998) demonstrated that wild-type (IAA^+) *Pantoea agglomerans* 299R exhibited a small but significant fitness advantage over an isogenic, auxin-deficient mutant when growth was compared *in planta*. Though enhanced carbon acquisition by IAA-producing cells has been proposed as a mechanism for this increased fitness (see Chapter 2), improved survival and replication under stressful leaf conditions could also account for the relative growth advantage enjoyed by wild-type 299R. Phyllosphere bacteria encounter a variety of rapidly fluctuating environmental challenges, including water limitation (Axtell *et al.*, 2002), UV exposure (Jacobs *et al.*, 2001; Sundin *et al*., 1999), oligotrophic growth conditions, and variable temperatures (Lindow *et al.*, 2003). Any IAA-mediated alleviation of such environmental stresses would therefore be expected to contribute to epiphytic fitness. Furthermore, transcription of *ipdC*, which encodes the rate-limiting step of IAA biosynthesis, was shown to be specifically upregulated under conditions of osmotic and matric stress in *Pa*299R (Brandl *et al.*, 1997).

We therefore sought to determine whether endogenous auxin production by *Pa*299R enhanced bacterial survival under three common phyllosphere stress conditions: UV exposure, osmotic stress, and oxidative stress.

Materials and Methods

Culture Conditions and Stress Treatments

Bacterial inocula were prepared by suspending freshly streaked, single colonies from selective LB plates into M9 liquid medium (Miller *et al*., 1972) supplemented with 2.5mM tryptophan and rifampicin (C_F=100µg/mL). Cultures were grown overnight at 28°C, washed once, and inoculated into M9 minimal media amended with varying concentrations of NaCl (for osmotic stress experiments) or H_2O_2 (for oxidative stress experiments). Bacterial survival was estimated by spiral plating at the indicated timepoints, incubated for 24-48 hours at 28°C, and enumerated by hand or laser counting.

For UV exposure experiments, overnight liquid inocula were prepared as described above, then diluted to $5x10^8$ cells/mL in fresh M9/Trp and grown for 2-3 hours, until OD_{600}=0.5. Cells were diluted to $2x10^3$/mL and plated onto LB+Rif plates at approximately 100 colonies per plate. Plates were incubated at 28°C for 2-3 hours to allow acclimation to plate conditions; the agar surface was then exposed without the plastic lid to a germicidal lamp (General Electric #G30T8;

irradiance at 1m/254nm/100 hours=125μW/cm^2) for varying amounts of time (0-120 seconds) to achieve different doses of UV radiation. Plates were then incubated at 28°C for 24-48 hours and the surviving colonies enumerated by hand or laser counting.

Induction of inhibitory levels of cellular stress was confirmed by correlation analysis of stress intensity and cell survival. Differential survival of IAA^+ and IAA^- strains was determined with multifactorial ANOVA analysis, with bacterial strain and stress condition as independent categorical variables and surviving cell number as the dependent variable. Where indicated, Tukey's post-hoc analysis was used to distinguish interactions between multiple variables.

Results and Discussion

Auxin production by P. agglomerans *299R has no measurable effect on bacterial stress resistance*

To test whether bacterial IAA production contributed to osmotic stress resistance, *Pa*299R and its auxin-deficient derivative MX149 were inoculated separately into minimal media containing 0, 0.17, 0.33, or 0.5M NaCl and their survival was monitored by plating. After two hours in culture, a significant negative correlation was observed between NaCl concentration and cell survival in both strains ($r=-0.9$, $n=12$, $p<0.001$), indicating that osmotic stress was induced in the cell cultures. But at a given salt concentration, cell survival was similar between 299R and MX149 (Figure 1a). A multifactorial ANOVA supported these observations, showing a significant effect of NaCl concentration on growth ($F=15.10$, $p<0.001$, d.f.=3), but no effect of bacterial strain on growth ($F=1.24$, $p=0.28$, d.f.=1) and no strain-by-concentration interactions ($F=0.18$, $p=0.91$, d.f.=3). Similar results were obtained in three replicate experiments (Figure 1). These results conform to data reported by Brandl *et al.* (1997), who saw no growth differences between 299R and a different IAA-deficient derivative, XYLE, when the two strains were co-cultured in 0.2M NaCl.

Oxidative stress resistance was tested in a similar experiment. *Pa*299R or MX149 bacteria were inoculated into minimal media containing 0, 0.02, 0.2, or 2.0M H_2O_2, and bacterial survival measured after two hours in culture (Figure 2). A significant negative correlation was observed between H_2O_2 concentration and cell survival in both treatments ($r=-0,9$, $n=12$, $p<0.001$). But multifactorial ANOVA suggested no significant overall effect of bacterial strain on cell survival ($F=4.44$, $p=0.05$, d.f.=1), and no strain-by-concentration interaction ($F=1.60$, $p=0.23$, d.f.=3).

Resistance to UV radiation was the final environmental stress condition tested. Unlike, Bianco *et al.* (2006), who irradiated shaken broth cultures, this experiment was designed to mimic conditions of *de novo* bacterial immigration onto a leaf: freshly plated bacteria were incubated briefly at 28°C to acclimate to the media surface, then placed under a UV lamp for varying durations to produce varying doses of net UV exposure. A UV survival curve was first constructed to confirm the irradiation of the lamp and determine optimum exposure times (Figure 3); exposure settings of 0, 40, 80, and 120 seconds were chosen for further experimentation (an estimated 0, 50, 100, and 150 J/m^2 of UV radiation). Survival of the two strains after exposure to each of these doses was then compared. (Due to differences in initial

inoculum densities in the experiment, data were expressed as each strain's percent survival relative to the inoculum.) Both 299R and MX149 cells exhibited dose-dependent impairment, evidenced by a significant negative correlation between UV exposure and cell survival ($r=-0.9$, $n=12$, $p<0.001$). However, at a given UV dosage, no significant difference was detected between cell survival of the two strains: multifactorial ANOVA confirmed a significant negative effect of UV dose on cell survival ($F=233.72$, $p<0.001$, $df=3$), but no significant strain effects ($F=3.02$, $p=0.9$, $df=1$) or strain-by-UV interactions ($F=2.68$, $p=0.06$, $df=3$).

Conclusions

Although exogenous IAA induces a variety of physiological changes that enhance stress resistance in *Escherichia coli* K12 and *S. meliloti*, endogenous production of IAA does not appear to enhance stress resistance in the phyllosphere epiphyte *Pantoea agglomerans.* When bacteria were exposed to moderately inhibitory doses of NaCl, H_2O_2, or UV radiation, no differences in cell survival were detected between wild-type *Pa*299R and the auxin-deficient mutant *Pa*MX149 (Table 1).

These results do not completely eliminate the possibility that IAA production regulates stress responses in 299R. Subsequent *in vitro* experiments have suggested that the greatest concentrations of IAA accumulate in media supernatant during late stationary-phase growth (data not shown); this suggests that endogenous IAA might have stronger physiological effects after 48 hours of inoculum growth than it does after 24, as studied here. More intense sampling and greater statistical power might also reveal subtle differences in bacterial survival between the two strains that were not evident in these experiments.

However, preliminary results suggest that endogenous IAA biosynthesis does not play a role in stress resistance in the phyllosphere epiphyte *Pantoea agglomerans.*

II. IAA biosynthesis by *Pantoea agglomerans* 299R cell aggregates exerts no measurable effect on the autofluorescence of substrate leaf epidermal cells

Introduction

Many hypotheses that attempt to account for the prevalence of bacterial auxin production posit that bacterial IAA modifies the plant host in some way. Monier *et al*. (2005) suggested that such modification might be directly observable by microscopy: they reported that when colonized by the leaf epiphyte *Pantoea agglomerans* strain 299R, leaf epidermal cells of *Phaseolus vulgaris* exhibited elevated autofluorescence (Figure 4e).

Though quantitative data were not provided, the authors reported that "almost all" epidermal cells colonized by "significant numbers" of 299R bacteria displayed elevated autofluorescence. Of the 299R aggregates observed in this study, 55% were located on leaf epidermal cells; in a small subset of ≈30 colonized epidermal cells, 87% reportedly exhibited autofluorescence

(Monier *et al.*, 2005). Though bacterial cell size was not quantified directly, modified plant epidermal cells reportedly harbored larger bacteria than unmodified cells—according to previous reports, an indication of higher bacterial metabolic activity (Monier *et al.*, 2003). And when leaves with established bacterial populations were re-inoculated with "immigrant" cells, newly arrived bacteria were more likely to survive if they landed on modified epidermal plant cells (94.3% survival when immigrant cells were 299R; 91% when immigrant cells were *P. syringae* B728a) than if they landed on unmodified epidermal cells (25% survival of 299R; 47.2% of B728a). This result suggested that cells with modified autofluorescence provide a more hospitable environment to bacteria—possibly as a result of enhanced nutrient leakage induced by bacterial IAA.

To test the putative association between *Pa*299R aggregates and modified plant epidermal cell fluorescence, *Pa*299R bacteria bearing the constitutively cyan fluorescent protein (CFP)-expressing plasmid pWM1009 (Miller *et al*., 2000) were inoculated onto bean leaves and visualized by epifluorescence microscopy; the distribution of bacterial cells across "modified" or "unmodified" epidermal substrate cells was recorded. To assess whether bacterial IAA production affected substrate cell fluorescence, the distribution of wild-type *Pa*299R was compared to that of its isogenic, IAA-deficient mutant derivative *Pa*MX149. If IAA were responsible for substrate cell modification, plant epidermal cells colonized by 299R aggregates would be expected to include a higher proportion of autofluorescent cells than plants colonized by MX149 aggregates.

Materials and Methods

Plant Inoculation and Harvest

Bacteria were freshly streaked onto LB plates amended with rifampicin (C_F=100mg/L) and kanamycin (C_F=50mg/L) and incubated for 48 hours at 28°C. Bacteria were scraped from plates, resuspended at $1x10^6$ cells/mL in 2L buckets filled with 10mM KPO_4 buffer, and used to dip-inoculate X-week-old, greenhouse-grown *Phaseolus vulgaris* plants (Blue Bush Lake 274 variety). Plants were assigned identification numbers to mask the treatment and prevent scoring bias during microscopy. Plants were immediately placed in a mist chamber at 22°C and maintained at 100% humidity for 4-5 days to allow bacterial growth.

For microscopic observation, five healthy leaves were randomly selected from each pot; 4 sections of 1x1cm were haphazardly cut from each leaf with sterile scissors (avoiding the midrib) for a total of 20 leaf sections per pot. A total of 56 leaf samples (28 each from MX149 and 299R) were observed across 5 separate inoculations.

Fluorescence microscopy

Harvested leaf segments were placed on 100µL of molten 1% water agar on a glass microscope slide, then gently but firmly covered with a cover slip daubed with Aquapolymount. Slides were kept in the dark at room temperature for 10 minutes, and then observed using a Zeiss AxioImager M1 microscope equipped with a CFP/YFP 51057 Chroma filter to observe CFP

excitation and a 650nm Melles-Griot short-pass filter to block leaf autofluorescence. Using 40-100x magnification, leaves were scanned for aggregates (defined as any CFP-labeled bacterial cluster that appeared to have more than 10 cells at 100x magnification). Potential aggregates were confirmed at 400x magnification, and the associated substrate epidermal cells characterized for autofluorescence.

Results and Discussion

Leaves of *P. vulgaris* plants were inoculated with the naturally IAA-producing leaf epiphyte *P. agglomerans* 299R or its isogenic, IAA-deficient mutant *Pa*MX149; each strain constitutively expressed CFP via the plasmid pWM1009 (Miller *et al.*, 2000). After 48-72 hours of growth under humid conditions, leaf samples were harvested and analyzed by microscopy. Bacterial aggregates of three or more cells were counted and scored for whether their substrate plant cell exhibited autofluorescence or not (Figure 4). Epidermal cells which fluoresced in the absence of bacterial aggregates were also noted.

A total of 250 bacterial aggregates were observed across 56 leaf samples (28 each of 299R and MX149) harvested from five replicate experiments. There was no significant interaction between the strain's IAA status and the frequency with which it was found on an autofluorescent cell versus an unmodified cell (X^2_{250}=1.09, p=0.298), which suggests that auxin production does not impact substrate plant cell autofluorescence (Table 2). Furthermore, contrary to the qualitative observation by Monier *et al.* (2001) that substrate cell autofluorescence occurred under the majority of large aggregates, only 30% of aggregates were found on plant cells with elevated autofluorescence.

One possible explanation for this discrepancy is that our operational definition of a "large bacterial aggregate" was too small; aggregate size may have to exceed a certain threshold before IAA production is sufficient to impact the substrate plant cell. Though the definition by Monier *et al*. of a large aggregate was vague, it was inferred to be on the order of ≥50-100 cells. Given that any cell cluster that appeared larger than 10 cells was included in this analysis—and that small clusters accounted for the majority of observations (Powell, *pers. obs*.)—this experiment would have missed distinct patterns of behavior exhibited by rare, larger aggregates. (A previous replicate of this experiment, in which aggregates were defined as any clump of ≈2-3 cells, also failed to show strain-dependent differences in substrate cell fluorescence.) Unfortunately, the size distribution of epiphytic bacterial aggregates was strongly right-hand skewed, with large cell clusters (>64 cells) making up only 0.7% of aggregates by 48 hours after inoculation (Monier *et al*., 2004). As a result, too few large bacterial aggregates were spotted in the course of the experiment to permit conclusive analysis of their behavior. Sampling intensity would have to be scaled up considerably to achieve sufficient statistical power.

As with the definition of a "large aggregate", the exact nature of the "enhanced autofluorescence" plant cell phenotype was also difficult to define. Leaf epidermal cells exhibited a variety of fluorescent phenotypes: fluorescent cells ranged from individual cells to large rafts of contiguous cells, and from elevated blue fluorescence across the plant cell (as depicted by Monier *et al*.) to a paler, fibrous-looking zone of fluorescence concentrated around

the margins of the plant cell (Figure 4a). In some cases, autofluorescence appeared to be out-of-focus light emanating from deeper cell layers. Effort was made to conform to the published description, but it was often difficult to score heterogeneous autofluorescent phenomena. Furthermore, many autofluorescent plant cells were observed in the absence of colonizing bacteria, or in uninoculated negative controls (data not shown).

Within the defined parameters of aggregate size and autofluorescence, the observed data suggest that bacterial IAA production plays no role in plant cell autofluorescence. A variety of alternative explanations could account for the distinct phenotype of colonized cells. Plant cell autofluorescence of various wavelengths can be induced by osmotic or other cellular stress (Weir, 2001) and increases strongly after cell death (Koga *et al*., 1988). In particular, infection by fungal or bacterial pathogens (Russo *et al.*, 1983; Holliday *et al*., 1981) and the resulting accumulation of phytoalexins may increase epidermal cell autofluorescence in assorted plant tissues. This could explain the variety of autofluorescent phenotypes observed in colonized and uncolonized epidermal leaf cells. It also calls into question the assumption by Monier *et al.* that large epiphytic aggregates induce leaf autofluorescence. Rather, the reverse may be true: large aggregates of leaf epiphytic bacteria may preferentially accumulate on stressed or fungally infected (and therefore autofluorescent) leaf cells, which presumably leak more nutrients and therefore support larger bacterial populations.

The possibility that modified, autofluorescent plant cells might support large bacterial aggregates (rather than the other way around) was not tested directly. But of the 302 autofluorescent plant cells observed in the experiment, 25% were colonized. In contrast, a tentative estimate suggests that far less than 10% of non-autofluorescent cells were colonized. (The total number of non-autofluorescent plant cells was not counted, but a conservative estimate suggests that there were at least 10-fold more uncolonized plant cells than colonized cells.). Based on this tentative calculation, an autofluorescent plant cell is significantly more likely to harbor a bacterial aggregate.

Ultimately, though there may be a positive association between the occurrence of enhanced-autofluorescent plant epidermal cells and large bacterial aggregates, causality remains open to interpretation. Furthermore, the autofluorescence of substrate epidermal cells exhibits no detectable association with bacterial IAA production.

III. The *iaaM* gene is not necessary for auxin biosynthesis by *P. syringae* pv. *syringae* strain B728a

Introduction

Microbial IAA production has been shown to enhance plant disease in a variety of bacterial and fungal pathogens. In gall-forming organisms, the hormone plays a well-established role in tissue hyperplasia and tumor vascularization (Lee *et al*., 2009; Gafni *et al*., 1995). Auxin's role in the

pathogenesis of non-gall-forming organisms, however, is still an area of active investigation (reviewed in Kazan *et al*., 2009).

One possibility is that IAA promotes disease by acting as an endogenous regulator of bacterial virulence factors. Relative to wild-type *Erwinia chrysanthemi* strain 3937, an IAA-deficient mutant showed reduced maceration of host leaf tissue accompanied by deficits in pectate lyase production; downregulation of the type-three secretion system (TTSS) and two related effector proteins; and altered expression of the global regulators *gacA* and *rsmA* (Yang *et al.*, 2007). Knocking out IAA biosynthesis in *Pseudomonas syringae* pv. *syringae* strain Y30-53.29 led to reduced production of syringomycin, an important virulence factor (Mazzola *et al*., 1994). Surprisingly, although these changes altered patterns of virulence and symptom development in IAA^- knockouts of both strains, the relationship between disease progression and bacterial population was not straightforward. In *E. chrysanthemi*, the auxin-deficient mutant displayed reduced disease symptoms but no reduction in population growth; in *P. syringae*, the mutant actually triggered earlier symptom development and experienced faster growth *in planta* (though it exhibited no growth advantage when inoculated epiphytically).

In addition to its potential role in regulating bacterial virulence, recent research has also implicated bacterial IAA in suppression of plant defenses. Exposing *Nicotiana tobacum* to auxin *in vitro* represses antifungal chitinase production (Shinshi *et al*., 1987) and pathogenesis-response (PR) genes (Jouanneau *et al*., 1991). Bacterial IAA production may therefore be a strategy to repress plant immune responses. For example, the *Pseudomonas syringae* type-III effector protein AvrRpt2 appears to promote accumulation of auxin, induction of IAA-regulated genes, and disease susceptibility in *A. thaliana*. Similarly, overexpression of IAA in the fungal pathogens *Fusarium oxysporum* and *F. arthrosporioides* enhanced disease in *Orobranche aegyptiaca* (Cohen *et al*., 2002).

More recent work has begun to elucidate details of the interactions between auxin and plant defense. Navarro *et al.* (2006) demonstrated that as part of its innate immune response to pathogen-associated molecular patterns (PAMPs), *Arabidopsis thaliana* upregulates miRNA393, a microRNA which targets the auxin F-box receptors TIR1, AFB2, and AFB3 for degradation. Pathogen challenge therefore elicits defensive downregulation of plant IAA signaling. This repression of auxin signaling contributed significantly to *A. thaliana*'s resistance to the compatible bacterial pathogen *P. syringae* pv. *tomato* DC3000: plants unable to repress auxin signaling (due to constitutive overexpression of AFB1) had more severe symptoms and carried bacterial loads 20-fold higher than did wild-type plants. Conversely, plants that constitutively repressed auxin signaling (due to overexpression of the defensive miRNA393) carried fourfold lower populations of DC3000 than did wild-type *A. thaliana*.

These findings implicate plant auxin signaling in susceptibility to bacterial pathogens. By extension, they also suggest that IAA production by bacterial pathogens may help overcome plant downregulation of auxin signaling. For example, coinoculation of DC3000—which does not produce significant quantities of endogenous IAA (Glickmann *et al*., 1998)—with the synthetic auxin 2,4-D yielded greater lesion formation in *A. thaliana* than did bacterial inoculation alone, though it did not significantly impact bacterial growth *in planta* (Navarro *et al*., 2006, *supplementary materials*).

To further understand how IAA affects plant-pathogen interactions, we investigated how IAA biosynthesis facilitates the survival and fitness of the foliar bean pathogen *Pseudomonas syringae* pv. *syringae* strain B728a. We were particularly interested in the potential roles of auxin in regulating expression of pathogenesis-related bacterial genes, mediating plant defense responses, and improving microbial fitness during epiphytic or endophytic life stages.

Like many bacterial pathogens (Spaepen *et al*., 2007; Kazan *et al*., 2009), B728a was expected to synthesize IAA via the indoleacetamide pathway, in which a monooxygenase (IaaM) converts tryptophan to indoleacetamide, which a hydrolase (IaaH) then converts to indole-3-aetic acid (Figure 5c). In addition to Mazzola *et al.*'s (1994) demonstration that interruption of *iaaM* abrogated IAA synthesis in the closely related *P. syringae* strain Y30, both indoleacetamide and indole-3-acetic acid are found in culture supernatant of B728a cells cultured with tryptophan (Figure 10). Additionally, a canonical *iaaM* gene (Psyr_1536) is present in the B728a genome: it exhibits 99% nucleotide sequence identity to the Y30 *iaaM* characterized by Mazzola and colleagues (1994), and is located in a canonical *iaaM/iaaH* auxin biosynthetic operon. A second tryptophan monooxygenase (Psry_4667), with only 47% nucleotide sequence identity, is also present in the B728a genome (Figure 5a-b).

We therefore sought to characterize the role of the indoleacetamide biosynthetic pathway in B728a by generating *iaaM* knockouts, intending to study the endophytic and epiphytic growth, virulence traits, and gene transcriptional patterns of IAA-deficient mutants. In previous work, knocking out *iaaM* reduced IAA production to background levels as effectively as a double *iaaM/iaaH* mutant, so the gene was believed to be a good target (Mazzola *et al.*, 1994). The epiphytic and endophytic transcriptional activities of the putative *iaaM* homologs were also investigated.

Materials and Methods

Cloning of auxin-deficient P.s.s. *B728a knockout mutants*

The intermediate cloning vector pENTR-MCSGent was generated by replacing the Kanamycin resistance cassette of pENTR/D entry vector (Invitrogen) with a Gentamycin resistance cassette. The resulting construct features a gentamycin cassette flanked by two unique multiple cloning sites used to insert 5' and 3' regions of the gene being targeted for knockout. The vector is also compatible with the LR-Clonase system (Invitrogen), enabling cassette transfer into the suicide knockout vector pLVCD (Marco *et al*, 2005) and subsequent mutagenesis of *P. syringae*.

A gene deletion knockout of the *iaaM* homolog Pss1536 (Figure 6) was generated by double-homologous recombination. 1Kb segments flanking the 5' and 3' ends of Pss1536 were amplified by PCR, then TOPO-cloned. Each flanking fragment was isolated by restriction digest with appropriate enzymes and sequentially cloned into the MCS sites of the pENTR-MCSGent entry vector, creating pENTR-D:Gent:1536_5'3', a knockout cassette comprising the gentamycin resistance gene flanked by the 5' and 3' regions of Pss1536. The cassette was mobilized into pLVCD via Clonase LR enzyme reaction as describe by the manufacturer (Invitrogen). The resulting pLVCD:1536-Gent_5'3' construct was verified by sequencing, then

electroporated into *E. coli* strain S17. *Pseudomonas syringae* knockouts were generated by biparental mating between the S17 pLVCD_1536-Gent_5'3' donor strain and the *Pss* B728a recipient. Putative knockouts were recovered on LB agar plates supplemented with rifampicin (100µg/mL) and gentamycin (20µg/mL), to select for B728a carrying the gentamycin insert. Surviving colonies were cultivated for several days in media amended with gentamycin, plated for single colonies on LB supplemented with gentamycin (indicating maintenance of the insertion cassette), then replica plated onto LB supplemented with tetracycline (15µg/mL) to confirm tetracycline susceptibility (indicating loss of the integrated plasmid). Putative knockout strains were verified by PCR to confirm excision of the Pss1536 gene; the resulting mutant was designated *Pss*Δ1536. A B728a gene-deletion knockout of the putative *iaaM* homolog Pss4667 (Figure 7) was generated using the same procedure, and designated *Pss*Δ4667.

Two separate single-crossover insertion knockouts of Pss1536 were also generated. In the first, an internal 1Kb fragment of the gene was amplified with a 5' ACC overhang for ligation into pENTR-dTOPO, to generate pENTR:1536_KO. The resulting mutant was designated *Pss*1536*1. In the second, the amplified Pss1536 fragment was only 500bp long, and the resulting construct was designated pENTR:1536_KO.2. The knockout cassettes were mobilized into pLVCD via Clonase LR enzyme reaction, as described by the manufacturer (Invitrogen) and the resulting pLVCD:1536-KO constructs verified by sequencing before electroporation into *E. coli* strain S17. *Pss*1536*2 knockouts were then generated by biparental mating, and putative mutants selected on LB agar amended with rifampicin and tetracycline. Strains were verified by PCR to confirm interruption of the Pss1536 gene, as well as the placement and orientation of the tetracycline cassette. (See Table 3 for a summary of knockout strains.)

Auxin Quantification

To quantify auxin production, bacterial strains were cultured in a darkened shaker in liquid KB amended with 2.5mM tryptophan and appropriate antibiotics. After 48 hours of growth at 28°C, samples were centrifuged at 10,000x*g* at 4°C for 5 minutes, and the supernatant collected.

For liquid auxin assays, culture supernatant or IAA standard solutions were mixed with freshly prepared Salkowski reagent (as described by Gordon *et al*., 1951) in a 1:3 (vol:vol) ratio and incubated in the dark at room temperature for 30 minutes. Absorption of each sample was promptly measured at 530nm with a spectrophotometer.

For thin-layer chromatography assays, indolic compounds were extracted from each sample as described by Brandl *et al*. (1996). Briefly, culture supernatants were adjusted to pH=2.5-3.0 with HCl, extracted twice with an equal volume of H_2O-saturated ethyl acetate, vacuum-dried in a darkened rotary-evaporator unit under moderate heat, and stored at -20°C until further processing. For analysis, the residue was resuspended in 10µL ethyl acetate and repeatedly spotted in 2µL droplets onto the same spot on the loading phase of a precoated silica gel TLC glass plate with a layer thickness of 0.25mm. The plate was placed in an equilibrated chamber with 100mL of EIA reagent (45% ethylacetate, 35% isopropanol, 20% ammonium hydroxide by volume) and monitored for solvent migration. When the solvent front of the mobile phase reached the last 2.5cm of the plate, it was removed and dried at 45°C for 5-10 minutes, until all trace of solvent had evaporated. The plate was then evenly sprayed with VanUrk-Salkowski reagent (Ehmann, 1977) using an atomizer, followed by heating at 100°C using a heat dryer held

approximately 12" from the plate surface. When maximal color intensity developed (and before the silica began to discolor), the plate was gently rinsed 3 times in distilled water, and dried at 45°C for 20-30 minutes; plates were scanned or photographed immediately for later analysis.

Cloning of promoter:reporter fusion constructs

Reporter constructs for each gene consisted of a transcriptional fusion of the promoter region (defined as noncoding DNA extending 5' from the gene of interest to the preceding ORF) to an *inaZ* reporter gene (Leveau *et al*., 2002). Briefly, the 5' promoter region of Pss1536 was amplified and restriction sites added by PCR (Table 3), then TOPO-cloned. The insert was isolated by restriction digest and gel purification, then ligated into the ice nucleation reporter plasmid pProbe-GI' to yield the reporter construct p1536(-500)-GI'. The construct was then electroporated into *P. syringae* strain LK-2, a Δ*inaZ*, ice-nucleation-deficient derivative of B728a.

The reporter construct for Pss4667 was generated in the same fashion as for Pss1536, but the promoter region was ligated into the pProbe-GI reporter plasmid, yielding p4667(-650)-GI. Both constructs were verified by PCR and direct sequencing.

Promoter Induction Assays

Single colonies of *P. syringae* from 2-day-old plates were inoculated into KB liquid media amended with natamycin, rifampicin, and appropriate antibiotics, and grown overnight at 28°C with 300rpm shaking. On the day of experiment, 2-week-old *Phaseolus vulgaris* (Blue Bush Bean variety) at the first emerging trifoliate stage of development were selected from the greenhouse.

For epiphytic induction assays, overnight liquid cultures of *P. syringae* were diluted to $1x10^6$ cells/mL in KPO_4 buffer. For each strain, three separate pots of *P. vulgaris* (five plants per pot) were dip-inoculated into the cell suspensions. Plants were incubated in a growth chamber at room temperature under 100% humidity with a 12-hour light/dark cycle. After 48 hours, three healthy primary leaves were harvested from each pot, and immersed together in tubes of 20mL of 10mM KPO_4 buffer. To remove epiphytic bacteria from the leaf surfaces, the tubes were sonicated for five minutes, vortexed for 10 seconds, and the leaves removed and discarded.

For endophytic induction assays, *P. syringae* were scraped from 2-day-old plates, diluted to $1x10^5$ cells/mL in KPO_4 buffer, and used to syringe-infiltrate *P. vulgaris* plants. Infiltrated areas were visible as an approximately 1.5cm-diameter dark circle of water-soaking; the margins of the infiltrated area were marked with a black Sharpie marker. Plants were left on the benchtop in a plastic tub under ambient light conditions and bottom watered until harvest. After 48 hours, leaves were severed at the petiole and rinsed three times in 15% H_2O_2 to surface sterilize, followed each time with rinsing in ddH_2O. Uniformly sized segments of inoculated leaf tissue were punched from leaves using the cap of a 1.5mL Eppendorf tube, and the resulting leaf samples macerated in their Eppendorf tube with a pestle in 500µL of KPO_4 buffer.

Mean bacterial reporter induction in inocula and leaf harvest samples was measured by ice nucleation assay (Loper *et al.*, 2002) and normalized to CFU counts derived from hand- or laser-

counting of spiral-plated samples. Quantitative differences in reporter induction were evaluated using Tukey's HSD test.

Results and Discussion

Knocking out Pss1536 or Pss4667 does not reduce IAA production by B728a

In an initial attempt to abolish auxin production by *P. syringae* B728a, double-homologous recombination was used to create a gene deletion knockout of the *iaaM* homolog and putative auxin biosynthetic gene Pss1536. *Pseudomonas syringae* pv. *syringae* had previously been found to produce up to 69.7 µg/mL IAA in liquid culture (Glickmann *et al.*, 1998); our results suggested comparable levels of IAA accumulation in B728a. However, a Salkowski assay indicated approximately equal IAA production in the wild-type and knockout strains (Figure 8). Because this standard chromogenic assay can react nonspecifically to indolic compounds other than IAA (Glickmann *et al*., 1995), thin-layer chromatography was also used to visualize bacterial production of individual indolic compounds. Again, roughly equal quantities of IAA were detected in both wild-type and Δ1536 strains. A band of the approximate retention factor and color of IAM appeared slightly reduced in the mutant relative to the wild-type (Figure 10a), though this qualitative observation was not quantitatively confirmed. This observation, however, would indicate that the mutant accumulated IAA despite reduced concentration of the putative IAM precursor, suggesting that either 1) *iaaH*, and not *iaaM*, was the rate-limiting enzyme, and sufficient IAM was present in the cell to sustain IAA production even if the dedicated *iaaM* monooxygenase gene was knocked out; or 2) an alternate biosynthetic pathway is responsible for IAA production.

To check whether a second, poorly conserved *iaaM* homolog might possess functionally redundant IAA biosynthetic activity, a ΔPss4667 gene deletion knockout was also generated. Like the Δ1536 mutants, the single-Δ4667 mutants appeared to produce IAA at concentrations similar to the wild-type strain (Figures 8,10). Though desirable, double-knockout was never generated.

Subsequent to these assays, several concerns arose regarding the *pENTR-D:MCS-Gent* construct used to generate the Δ1536 and Δ4667 deletion mutants. Despite seemingly normal PCR confirmation that gene excision had occurred, several laboratory members reported experiencing unusual difficulty recovering knockout clones from bacterial matings, possible read-through expression from the gentamycin cassette into neighboring genes, and phenotypic inconsistencies in the resulting knockouts—including inexplicably kanamycin-resistant clones, suggesting aberrant recombination between the cloning and entry vectors (Pers. Comm.—A. Burch, A. Parenguy). Between the unexpected maintenance of IAA production in the Δ1536 knockout and irregularities in the knockout vector, we elected to generate new mutants using a different approach.

The Pss1536 gene was mutated via single-crossover insertional mutagenesis, using homologous recombination between the B728a genome and a 1 Kb internal gene fragment cloned into the

suicide vector pLVCD to generate the strain *Pss*1536*1. The new mutant exhibited no reduction in IAA production, as measured by either Salkowski assay or TLC (data not shown).

One possible explanation for this result was that because the fragment used to target homologous recombination was a full 1Kb in length, recombination would have left the first 1.3 Kb of the gene intact (the full-length ORF is 1.7 Kb). If this truncated gene product were still functional, this might explain the persistence of IAA in the knockout mutant. To address this concern, the single-crossover mutant was redesigned using a 500bp fragment, such that gene disruption occurred after the first 750bp. The resulting *Pss*1536*2 knockout strain was again tested for auxin production and, once again, IAA levels were indistinguishable from wild-type using either liquid Salkowski assay (Figure 9) or TLC (Figure 10b).

One possible explanation for continued IAA production in the knockout is that the truncated, 750bp mutant transcript is functional. Alternatively, the putative *iaaM* homolog Pss_1536 may not be necessary for IAA biosynthesis in B728a. Functional redundancy with a weakly conserved monooxygenase, Pss_4667, could potentially complement loss of Pss_1536. Although knocking out Pss_4667 alone did not appear to alter IAA production, a 1536/4667 double-knockout could test this hypothesis.

Alternatively, IAA synthesis might not occur via the IAM pathway in B728a. This possibility was recently lent credence by Howden *et al*. (2009), who demonstrated that B728a is capable of synthesizing IAA via an indole-3-acetonitrile intermediate. Inactivation of the nitrilase homolog Psyr_0007 abolished the strain's ability to grow and produce IAA using indole-3-acetonitrile (IAN) as a sole nitrogen source, while complementation with Psyr_0007 under its native promoter restored growth and IAA biosynthesis to near wild-type levels. Because these *in vitro* assays were not conducted in tryptophan-rich media, the data do not directly address whether the IAN pathway is solely responsible for the *in vitro* IAA biosynthesis typically reported in B728a. But when supplied with 1mM IAN, the strain produced approximately 128µg/mL of IAA—almost twofold higher than the concentration of IAA reported from B728a supplied with 2.5mM tryptophan. This suggests that Psyr_0007 at least has the physiological capacity to generate the expected quantities of IAA solely via the IAN pathway. It is worth noting, however, that the Δ0007 knockout displayed significantly reduced *in vitro* growth relative to the wild-type strain, indicating that the gene may also play a more basic role in nitrogen acquisition and metabolism (Howden *et al.*, 2009).

The presence of an alternative IAN biosynthetic pathway in B728a is not surprising—similar pathways have been reported in other bacteria (Kobayashi *et al*., 1995; Spaepen *et al*., 2007). But the observation that the putative *iaaM* homolog makes no measurable contribution to IAA synthesis *in vitro* is highly unexpected, given the presence of a highly conserved, canonical *iaaMH* operon and previous results obtained with the closely related strain *P.s.s.* Y30 (Mazzola *et al.*, 1994). An undiagnosed technical problem with the mutants generated in this research remains a formal possibility. Another possibility is that the *iaaMH* operon is nonfunctional. For example, *P. syringae* pv. *tomato* strain DC3000 possesses a highly conserved nitrilase gene (PSPTO_0189) in an operon syntenous to that found in B728a (Howden *et al*., 2009). But unlike B728a, DC3000 possessed minimal nitrilase ability, could not use IAN a sole nitrogen source, and could not synthesize significant quantities of IAA. Clearly, even closely related strains with apparently highly conserved genetics can exhibit unexpected differences in auxin production.

Another possibility is that *iaaM* is responsible for IAA production in B728a, but only under an untested environmental condition. The nitrilase may be important under nitrogen starvation conditions or in basal media, for example, while iaaM/iaaH is induced only during growth on plants, or in some environmental conditions not tested in these simple *in vitro* experiments. Other strains have been shown to use multiple, distinctly regulated IAA biosynthetic pathways under different conditions: the gall-forming bacterial pathogen *Erwinia gypsophila*, for example, induces *iaaM* to synthesize IAA during pathogenesis, but induces an *ipdC* gene to synthesize IAA during epiphytic growth on the leaf surface (Manulis *et al*., 1998).

In part to investigate this possibility that Psry_1536 is induced under alternate growth conditions, a series of experiments was conducted to characterize the promoter activity of putative auxin biosynthetic genes.

Psyr1536 is modestly repressed on the leaf surface, while Psyr4667 is significantly induced

To determine whether the putative *iaaM* homologs Psyr1536 or Psyr4667 are epiphytically or endophytically induced *in planta*, transcriptional reporters were generated. The *inaZ*-deficient B728a derivative LK2 was transformed with the plasmid pPROBE-GI':p1536(-500), on which the Psyr1536 promoter drives expression of an ice nucleation reporter gene, or pPROBE-GI:p4667(-650), in which the Psyr4667 promoter drives reporter expression. *P. vulgaris* plants were inoculated with either one of the two reporter strains, with untransformed LK2 as a negative control, or with 31R1P6 (pJL24631-6) (which expresses weak but constitutive ice nucleation activity) as a positive control. Reporter induction was measured in the inocula and again from cells harvested after 48 hours' incubation on the leaf surface.

The LK2 reporterless negative control exhibited negligible ice nucleation activity in all treatments. Mean fold induction at 48 hpi was calculated for the remaining three strains and compared using Tukey's HSD test. Relative to the constitutive control, the Pss1536 promoter exhibited a small, marginally significant reduction ($p=0.02$, $df=4$), suggesting modest repression on leaves; in contrast, Pss4667 exhibited significantly elevated reporter activity relative to the control ($p<0.001$, $df=4$) (Figure 11a-b). Similar results were obtained in a second, independent experiment (Figure 11c).

A similar experiment was performed to determine whether either of the two genes were induced by endophytic growth *in planta,* and yielded similar results to the epiphytic growth experiments (Figure 12). When mean fold induction was compared using Tukey's HSD test, Pss1536 promoter activity was similar to the constitutive control ($p=0.14$, $df=4$), while the Pss4667 construct reported significantly elevated activity inside leaves ($p<0.001$, $df=4$).

As part of a separate study, gene induction data were also obtained by microarray profiling of 3 putative IAA biosynthetic genes in *Pss*B728a: the *iaaM* homolog Psyr_1536, the weak *iaaM* homolog Psyr_4667, and the nitrilase Psyr_0007 (Russell Scott, unpublished data). Scott *et al.* harvested mRNA from cells grown in basal media, epiphytically inoculated onto bean leaves, or perfused into the leaf apoplast; they then quantified cellular transcript abundance by generating and hybridizing cDNA to a Roche Nimblegen oligonucleotide microarray for *Pss*B728a. The

resulting data (Figure 13) generally support those generated by the ice-nucleation reporter constructs reported above. Relative to cells grown in basal media, wild-type B728a cells exhibited modest (2.3-fold) but statistically significant repression of Psyr_1536 on leaf surfaces ($t=4.97$, $p<0.001$, $df=10$), but no significant change when inoculated endophytically ($t=1.16$, $p=0.27$, $df=10$). Psyr_4667 was significantly upregulated nearly 7-fold on bean leaves ($t=-7.25$, $p<0.001$, $df=10$); however, an apparently similar level of endophytic upregulation was the result of a single outlier, and was not statistically significant ($t=-2.50$, $p=0.03$, $df=10$). The nitrilase Psyr_0007, which reportedly enables IAA production *in vitro* via the IAN pathway (Howden *et al*., 2009), was not significantly upregulated either epiphytically ($t=-0.55$, $p=0.59$, $df=10$) or endophytically ($t=-1.64$, $p=0.13$, $df=10$).

Conclusions

The role of bacterial auxin production by *Pseudomonas syringae* pv. *syringae* strain B728a remains murky, due to our inability to generate an IAA-deficient mutant strain. Repeated attempts to knock out the putative *iaaM* homolog Psyr_1536—by double homologous recombination and two different single-crossover insertional mutations—yielded apparently successful gene interruption, but no accompanying reduction in IAA biosynthesis as measured by Salkowski assay or thin-layer chromatography. This suggests that either the mutants suffer from undetected technical deficiencies, another gene (such as the weak homolog Psyr_4667) complements the activity of Psyr_1536, or the indoleacetamide pathway is nonfunctional despite the presence of a canonical *iaaMH* operon—and that IAA is therefore synthesized by an alternate pathway, such as IAN. Gene expression profiles generated via promoter-reporter fusion constructs and microarray analysis both hint that Psyr_1536, which exhibited low overall transcript abundance and modest repression on plant surfaces, may not play an important role in IAA production *in planta*. (Despite Howden *et al.*'s (2009) preliminary report suggesting that Psyr_0007 may facilitate IAA biosynthesis via the IAN pathway, microarray profiling also found little evidence that it is upregulated on or in plants.) Psyr_4667, however, displayed significant epiphytic upregulation. Only further study can confirm whether Psyr_4667 plays a role in IAA biosynthesis in *Pss*B728a, but the gene does appear to exhibit leaf epiphytic (and possibly endophytic) induction.

Acknowledgments

Many thanks to Steve Ruzin and Denise Schichnes, of the College of Natural Resources Biological Imaging Facility, for their instruction and advice on fluorescence microscopy. Thanks also to Russell Scott for sharing his preliminary microarray results regarding IAA biosynthetic gene transcription in *Pss*B728a. This work was supported by a National Science Foundation Graduate Research Fellowship.

LITERATURE CITED

Axtell, C.A., and G.A. Beattie. (2002) Construction and characterization of a proU-gfp transcriptional fusion that measures water availability in a microbial habitat. *Applied and Environmental Microbiology*. **68**(9): 4604-4612.

Bianco, C., and R. Defez. (2009) Medicago truncatula improves salt tolerance when nodulated by an indole-3-acetic acid-overproducing *Sinorhizobium meliloti* strain. *Journal of Experimental Botany*. **60**(11): 3097-3107.

Bianco, C., E. Imperlini, R. Calogero, B. Senatore, A. Amoresano, A. Carpentieri, P. Pucci, R. Defez. (2006) Indole-3-acetic acid improves *Escherichia coli*'s defences to stress. *Archives of Microbiology*. **185**: 373-382.

Brandl, M., and S. Lindow. (1998) Contribution of indole-3-acetic acid production to the epiphytic fitness of *Erwinia herbicola*. *Applied and Environmental Microbiology*. **64** (9): 3256-3263.

Brandl, M.T., and S.E. Lindow. (1997) Environmental signals modulate the expression of an indole-3-acetic acid biosynthetic gene in *Erwinia herbicola*. *Molecular Plant Microbe Interactions*. **10**(4): 499-505.

Chen, Z., J.L. Agnew, J.D. Cohen, P. He, L. Shan, J. Sheen, and B.N. Kunkel. (2007) *Pseudomonas syringae* type III effector AvrRpt2 alters *Arabidopsis thaliana* auxin physiology. *Proceedings of the National Academy of Sciences*. **104**(50): 20131-20136.

Cohen, B.A., Z. Amsellem, R. Maor, A. Sharon, and J. Gressel. (2002) Transgenically enhanced expression of indole-3-acetic acid confers hypervirulence to plant pathogens. *Phytopathology*. **92**(6): 590-596.

Ehmann, A. (1977) The Van Urk-Salkowski reagent—a sensitive and specific chromogenic reagent for silica gel thin-layer chromatographic detection and identification of indole derivatives. *Journal of Chromatography*. **132**: 267-276.

Feil, H., W.S. Feil, P. Chain, F. Larimer, G. DiBartolo, A. Copeland, A. Lykidis, S. Trong, M. Nolan, E. Goltsman, J. Thiel, S. Malfatti, J.E. Loper, A. Lapidus, J.C. Detter, M Land, P.M. Richardson, N.C. Kyrpides, N. Ivanova, and S.E. Lindow. (2005) Comparison of the complete genome sequences of *Pseudomonas syringae* pv. *syringae* B728a and pv. *tomato* DC3000.

Gafni, Y., M. Icht, B.Z. Rubinfeld. (1995) Stimulation of *Agrobacterium tumefaciens* virulence with indole-3-acetic acid. *Letters in Applied Microbiology*. **20**(2): 98-101.

Glickmann, E., and Y. Dessaux. (1995) A critical examination of the specificity of the Salkowski reagent for inolic compounds produced by phytopathogenic bacteria. *Applied and Environmental Biology*. **61**(2): 793-796.

Glickmann, E., L. Gardan, S. Jacquet, S. Hussain, M. Elasri, A. Petit, and Y. Dessaux. (1998) Auxin production is a common feature of most pathovars of *Pseudomonas syringae*. *Molecular Plant-Microbe Interactions.* **11**(2): 156-162.

Gordon, S.A., and R.P. Weber. (1951) Colorimetric estimation of indoleacetic acid. *Plant Physiology*. **26**:192-195.

Holliday, M.J., N.T. Keen, and M. Long. (1981) Cell death patterns and accumulation of fluorescent material in the hypersensitive response of soybean leaves to *Pseudomonas syringae* pv. *glycinea*. *Physiological Plant Pathology*. **18(**3): 279-287.

Howden, A.J.M, A. Rico, T. Mentlak, L. Miguet, and G.M. Preston. (2009) *Pseudomonas syringae* pv. *syringae* B728a hydrolyses indole-3-acetonitrile to the plant hormone indole-3-acetic acid. *Molecular Plant Pathology.* **10**(6): 857-865.

Jacobs, J.L., and G.W. Sundin. (2001) Effect of solar UV-B radiation on a phyllosphere bacterial community. *Applied Environmental Microbiology*. **67**: 5488-5496.

Jouanneau, J.P., D. Lapous, and J. Guern. In plant protoplasts, the spontaneous expression of defense reactions and the responsiveness to exogenous elicitors are under auxin control. *Plant Physiology*. **96**: 459-466.

Kazan, K., J.M. Manners. (2009) Linking development to defense: auxin in plant-pathogen interactions. *Trends in Plant Science*. **14(**7): 373-382.

Kobayashi, M., T. Suzuki, T. Fujita, M. Masuda, and S. Shimizu. (1995) Occurrence of enzymes involved in biosynthesis of indole-3-acetic acid from indole-3-acetonitrile in plant-associated bacteria, *Agrobacterium* and *Rhizobium*. *Proceedings of the National Academy of Sciences.* **92**(3): 714-718.

Koga, H., R.J. Zeyen, W.R. Bushnell, and G.G. Ahlstrand. (1988) Hypersensitive cell death, autofluorescence, and insoluble silicon accumulation in barley leaf epidermal cells under attack by *Erysiphe graminis* f. sp. *hordei*. *Physiological and Molecular Plant Pathology*. **32**(3): 395-409.

Lee, C.W., M. Efetova, J.C. Engelmann, R. Kramell, C. Wasternack, J. Ludwig-Muller, R. Hedrich, & R. Deeken. (2009) *Agrobacterium tumefaciens* promotes tumor induction by modulating pathogen defense in *Arabidopsis thaliana*. *Plant Cell*. **21**(9): 2948-2962.

Leveau, J.H.J, and S.E. Lindow. (2002) Bioreporters in microbial ecology. *Current Opinion in Microbiology*. **5**(3):259-265.

Lindow, S.E., and M.T. Brandl. (2003) Microbiology of the Phyllosphere. *Applied and Environmental Biology.* **69**(4):1875-1883.

Loper, J.E., and S.E. Lindow. (2002) Reporter gene systems useful in evaluating *in situ* gene expression by soil- and plant-associated bacteria. pp. 627-637. in: C.J. Hurst (ed.) Manual of Environmental Microbiology. 2nd Edition. ASM Press, Washington D.C.

Manulis, S., A. Haviv-Chesner, M.T. Brandl, S.E. Lindow, and I. Barash. (1998) Differential involvement of indole-3-acetic acid biosynthetic pathways in pathogenicity and epiphytic fitness of *Erwinia herbicola* pv. *gypsophilae. Molecular Plant-Microbe Interactions*. **11**(7): 634-642.

Marco, M.L., J. Legac, S.E. Lindow. (2005) *Pseudomonas syringae* genes induced during colonization of leaf surfaces. *Environmental Microbiology*. **7**(9): 1379-1391.

Mazzola, M., and F.F. White. (1994) A mutation in the indole-3-acetic acid biosynthesis pathway of *Pseudomonas syringae* pv. *syringae* affects growth in *Phaseolus vulgaris* and syringomycin production. *Journal of Bacteriology.* **176**(5): 1374-1382.

Miller, J.H. (1972) *Experiments in Molecular Genetics.* Cold Spring Harbor Laboratory, Cold Spring Harbor, NY.

Miller, W.G., A.H. Bates, S.T. Horn, M.T. Brandl, M.R. Wachtel, and R.E. Mandrell. (2000) Detection on surfaces and in Caco-2 cells of *Campylobacter jejuni* cells transformed ith new *gfp, yfp,* and *cfp* marker plasmids. *Applied and Environmental Biology*. **66**(12): 5426-5436.

Monier, J.M., and S.E. Lindow. (2003) *Pseudomonas syringae* response to the environment on leaves by cell size reduction. *Phytopathology*. **93**: 1209-1216.

Monier, J.M., and S.E. Lindow. (2004) Frequency, size, and localization of bacterial aggregates on bean leaf surfaces. *Applied and Environmental Microbiology*. **70**(1): 346-355.

Monier, J.M., and S.E. Lindow. (2005) Aggregates of resident bacteria facilitate survival of immigrant bacteria on leaf surfaces. *Microbial Ecology*. **49**: 343-352.

Navarro, L., P. Dunoyer, F. Jay, B. Arnold, N. Dharmasiri, M. Estelle, O. Voinnet, J.D.G. Jones. (2006) A plant miRNA contributes to antibacterial resistance by repressing auxin signaling. *Science* **312**: 436-439.

Russo, V.M., and A.J. Pappelis. (1983) Factors affecting the autofluorescence response in infected onion epidermal cells. *Transactions of the British Mycological Society*. **81** (1): 47-52.

Shinshi, H., D. Mohnen, and F. Meins. (1987) Regulation of a plant pathogenesis-related enzyme: Inhibition of chitinase and chitinase mRNA accumulation in cultured tobacco tissues by auxin and cytokinin. *Proceedings of the National Academy of Sciences*. **84**: 89-93.

Simon, R., U. Priefer, and A. Puhler. (1983) A broad host range mobilization system for *in vivo* genetic engineering: transposon mutagenesis in gram negative bacteria. *Nature Biotechnology*. **1**: 784-791.

Spaepen, S., J. Vanderleyden, and R. Remans. (2007) Indole-3-acetic acid in microbial and microorganism-plant signaling. *FEMS Microbiology Reviews*. **31**(4): 425-448.

Sundin, G.W., and J.L. Jacobs. (1999) Ultraviolet radiation (UVR) sensitivity analysis and UVR survival strategies of a bacterial community from the phyllosphere of field-grown peanut (*Arachis hypogeae* L.). *Microbial Ecology*. **38**: 27-38.

Weir, I. (2001) Analysis of apoptosis in plant cells. *Methods in Cell Biology.* **63** (1): 505-526.

Yang, S., Q. Zhang, J. Guo, A.O. Charkowski, B.R. Glick, A.M. Ibekwe, D.A. Cooksey, and C.H. Yang. (2007) Global effect of indole-3-acetic acid biosynthesis on multiple virulence factors of *Erwinia chrysanthemi* 3937. *Applied and Environmental Microbiology.* **73**(4): 1079-1088.

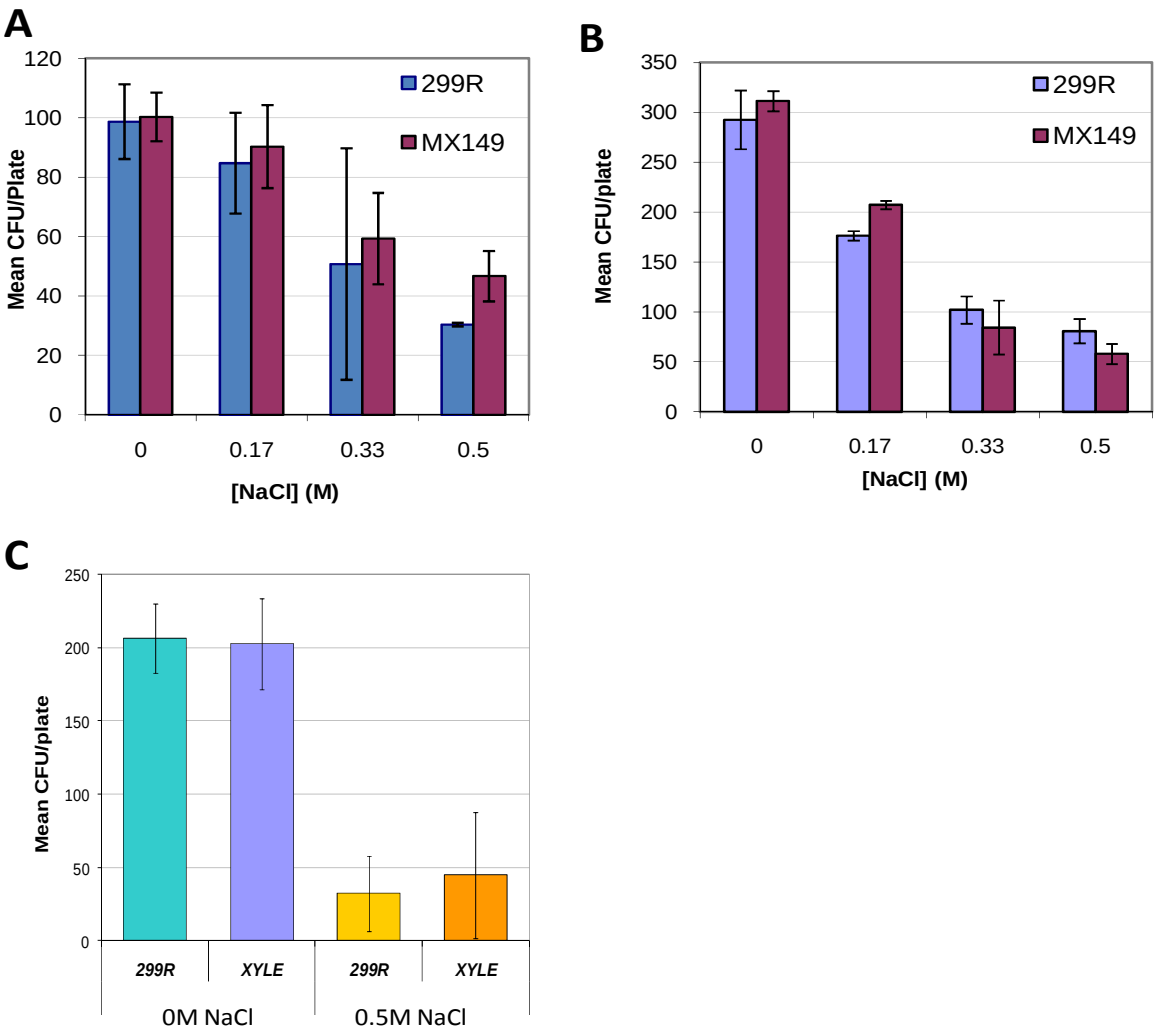

Figure 1. An *in vitro* growth experiment failed to show growth differences between wild-type *Pa*299R and its isogenic, IAA-deficient derivatives *Pa*MX149 or *Pa*XYLE when cultured under varying concentrations of NaCl (A). Replicate experiments produced similar results (B-C) (Each point represents the mean of 3 technical replicates ± 1 S.D.)

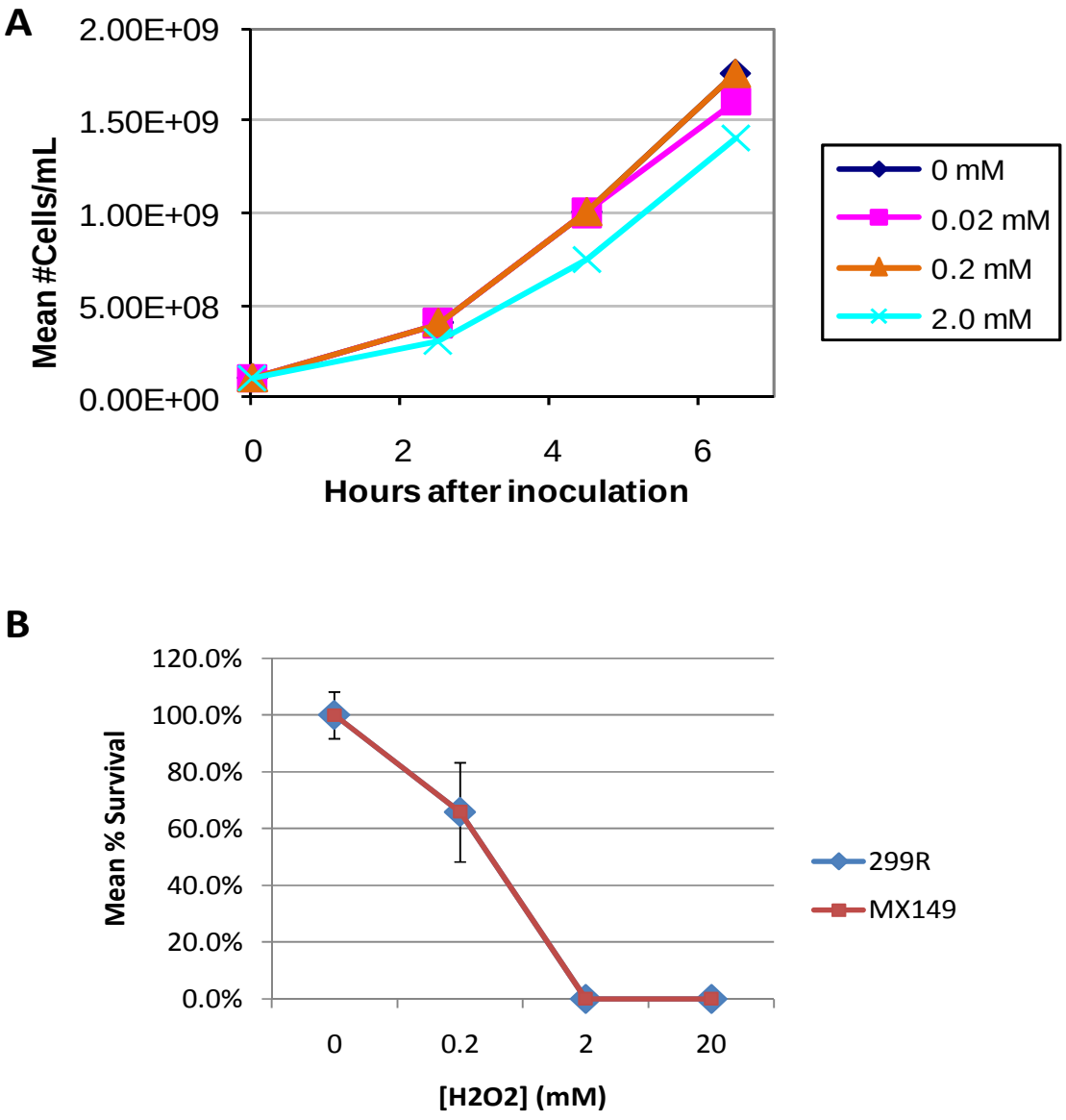

Figure 2. *Pa*299R survivorship when subjected to varying doses of hydrogen peroxide (A) and a comparison of survivorship of *Pa*299R and its isogenic, IAA$^-$ mutant derivative *Pa*MX149 at 2 hpi (lines overlap) (B). Each point is the mean of three technical replicates, ± 1 S.D.

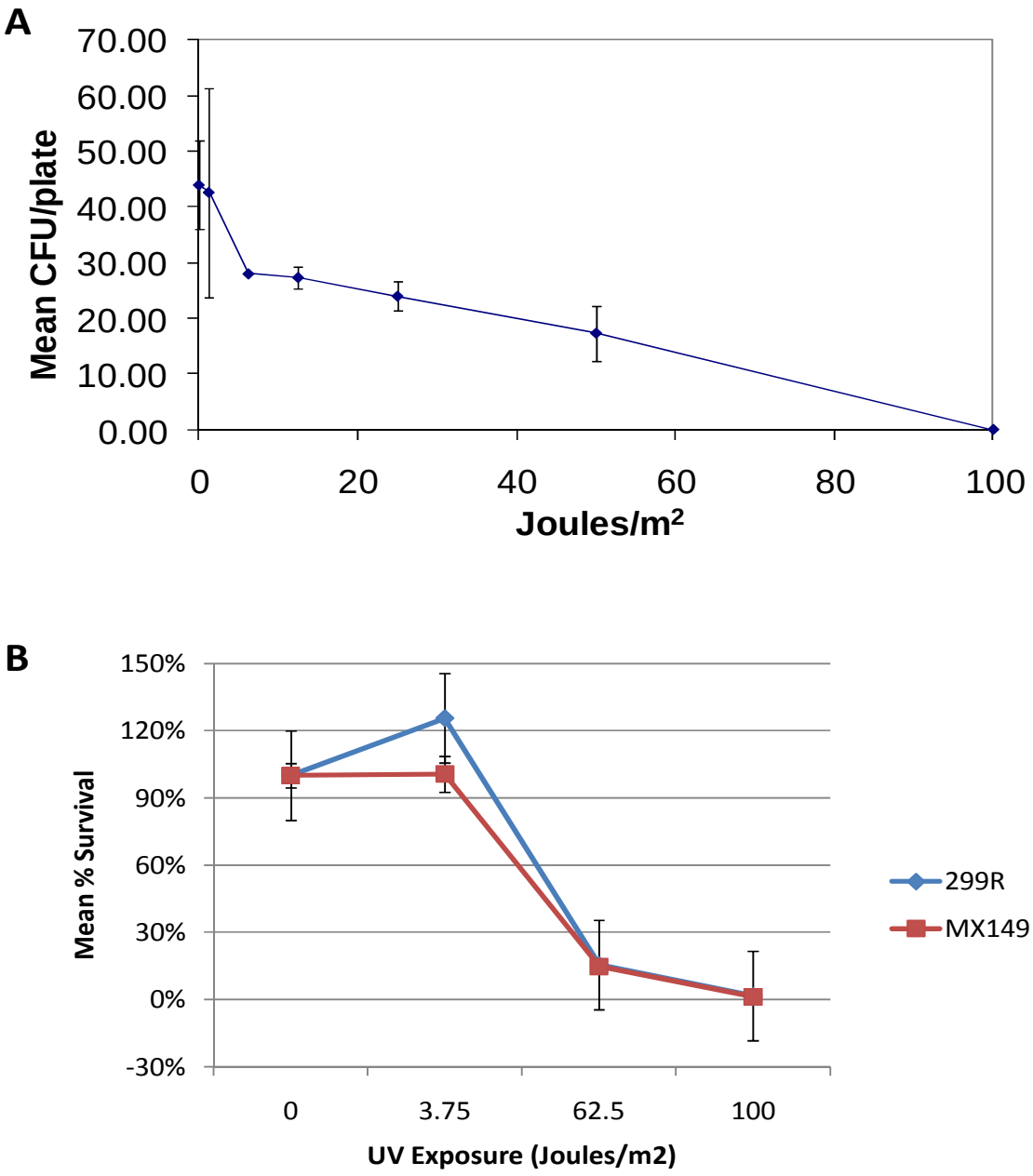

Figure 3. Preliminary experimental data characterizing *Pa*299R survivorship when subjected to varying doses of UVC radiation (A) and survivorship of Pa299R and an isogenic IAA- mutant (B). Each point is the mean of three replicate plates, ± 1 S.D.

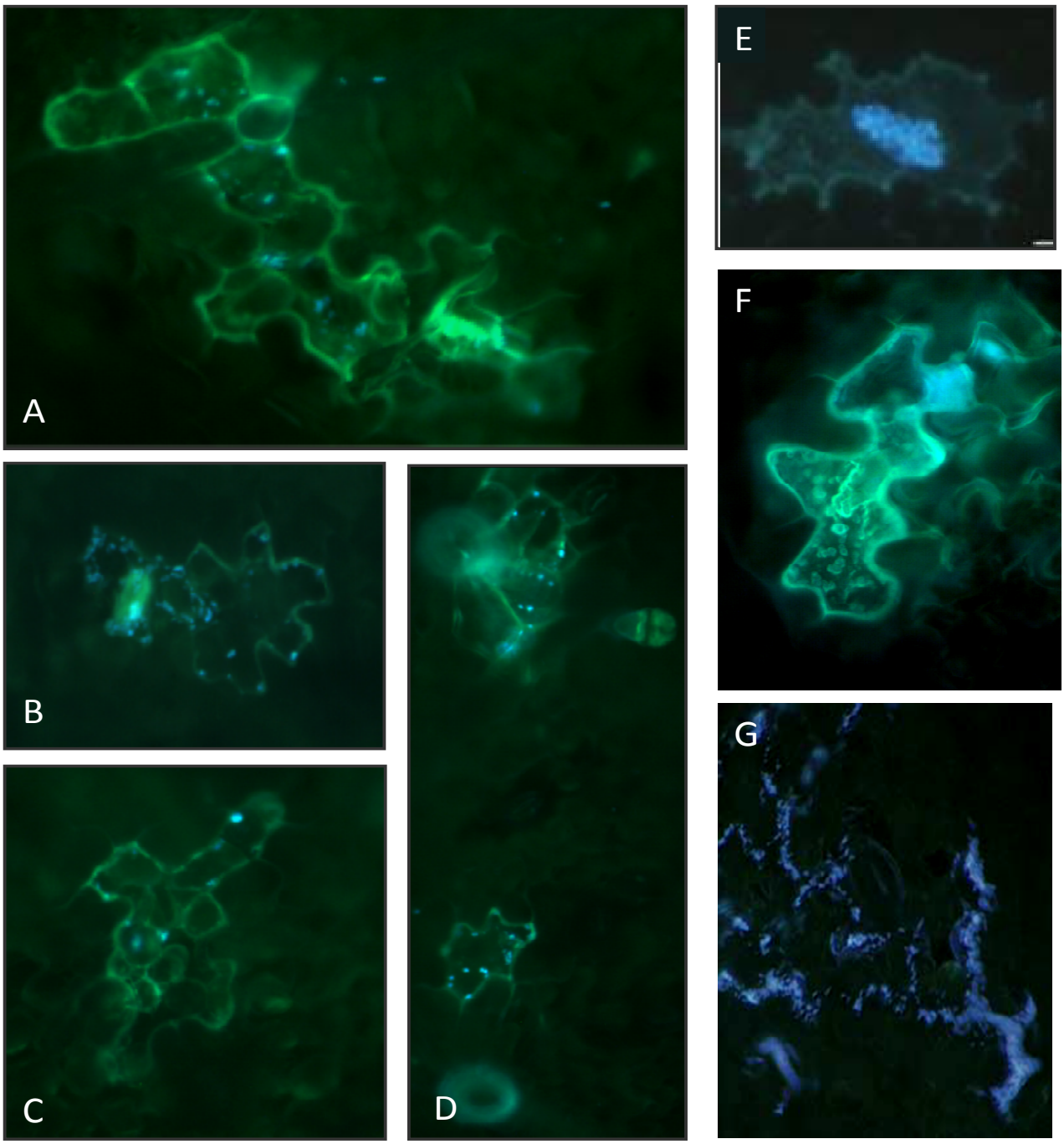

Figure 4. CFP-labeled epiphytic aggregates of *Pa*299R (pWM1009) (blue) on bean leaf epidermal cells exhibiting elevated autofluorescence (green) (A-D). These observations were similar to those described by Monier *et al*. (2005) (E). In addition to resident bacterial aggregates, cells with modified fluorescence profiles also sometimes showed evidence of fungal infection or other damage (*i.e.* granular surface irregularities) (F). Large aggregates could also be found on plant epidermal cells that did *not* exhibit increased fluorescence (G).

A

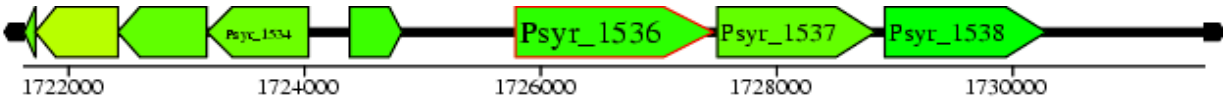

***Psyr_1536*:** putative iaaM homolog
Strong homology to Y30 *iaaM* (99% nucleotide identity)
Canonical *iaaM/iaaH* operon structure
**Likely role in IAA biosynthesis

B

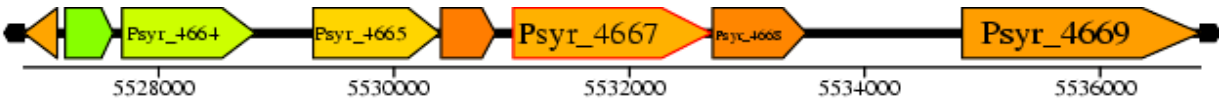

***Psyr_4667*:** putative iaaM homolog
Weak homology to Y30 *iaaM* (47% nucleotide identity)
Different operon structure
Less likely to play a role in IAA biosynthesis

C

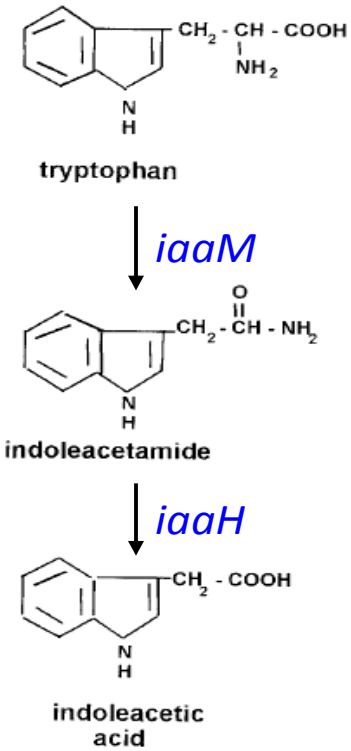

Figure 5. *P. syringae* pv. *syringae* B728a is believed to synthesize auxin via the indoleacetamide pathway, in which a monooxygenase (*iaaM*) and a hydrolase (*iaaH*) convert tryptophan to IAA (C). Nucleotide sequence analysis suggests the presence of two putative *iaaM* homologs in the *Pss*B728a genome: Psyr_1536 and Psyr_4667 (A-B).

ATGGATGACCATTTTAATTCACCCAGTATTGATATTTTGTACGACTACGGTCCCTTTCTG
AAAAAATGTGAGATGACGGGAGGCATAGGCAGCTATTCATCCGGAACGCCCACCCCTCGG
GTAGCGATAGTCGGTGCCGGCATCAGTGGGCTGGTCGCTGCAACTGAATTATTACGTGCG
GGAGTCAAGGACGTTGTTTTATATGAGTCGCGTGATCGAATCGGGGGGCGGGTATGGTCT
CAAGTGTTCGATCAGACTCGTCCACGTTACATTGCAGAAATGGGTGCGATGCGCTTTCCT
CCCAGCGCAACTGGCCTTTTCCACTACCTGAAAAAGTTTGGTATTTCAACGTCGACCACC
TTTCCGGATCCAGGTGTGGTGGACACGGAGCTGCATTACCGTGGTAAACGCTATTACTGG
CCAGCGGGCAAAAAGCCGCCCGCATTATTCAGGCGAGTTTATGAGGGGTGGCAGTCTTTA
TTGCGCGATGGTTACCTCCTTGAAGGCGGTTCTTTAGTTGCCCCGCTGGACATTGCCTCC
ATGCTCAAGTCGGGTTGTTTGGAAGAGGCAGCGATCGCATGGCAAGGATGGCTCAATGTA
TTCCGAGATTGTTCATTCTACAACGCGATTGTCTGTATTTTTACCGGCCCCCACCCGCCA
GGCGGTGACCAATGGGCTCGCCCTGAAGACTTTGAGCTGTTCGGCTCGCTTGGCATAGGC
TCGGGTGGTTTTCTGCCAGTCTTTCAGGCTGGCTTCACGGAAATACTCCGGATGGTCATC
AATGGATACCAAAGTGATCAGCGACTGATTCCGGACGGGATATCCAGTCTGGCCACGAGA
CTCGCTGATCAGGCATTTGACGGCAAAACGTTAAGGGAGCGCATTTGTTTTAGTCGGGTA
GGCCGCATTTCCAGAGACTCTGAAAAAATCATCATCCAGACAACAGCAGGAGAACAGGGC
TTATTTGATCGAGTGATTGTCACTAGCAGTAATCGAGCCATGCAAATGATTCATTGCCTC
ACGGACAGCGAGCGCTTCCTGAGTCGTGACGTCGCTCGTGCTGTCCGCGAAACCCACCTG
ACCGGATCATCGAAGCTTTTCATTCTCACCCGTACCAAATTCTGGATAAAAAACAAACTT
CCGACCACCATCCAGTCGGACGGCTTGGTGCGCGGCGTCTATTGTCTGGATTATCAGCCC
GATGAACCTGATGGTCACGGAGTTGTTCTGCTCAGTTACACGTGGGAAGACGACGCTCAA
AAAATGCTGGCGATGTCTGACAAAAAGACACGTTGTCAGGTACTGGTTAATGACCTCGCT
GCGATGCATCCGACGTTCGCCAGTTATCTCCTGCCTGTTGAGGGGGATTATGAGCGGTAT
GTATTGCACCATGACTGGCTCACCGATCCCCATTCTGCGGGCGCTTTCAAACTCAATTAC
CCCGGCGAGGATGTTTACTCGCATCGATTGTTCTTTCAACCGATGACAGCGAACAGTCCC
GATAAAGACACGGGGCTCTATCTGGCTGGCTGCAGTTGCTCTTTTGCCGGAGGGTGGATC
GAAGGTGCTGTCCAGACAGCATTGAACAGTGCCTGTGCCGTGCTGCGCAGCACCGGAGGG
CAGGTGTCAGAAGGCAACCCGCTTGACTGTATTAACGCCTCCTATCGCTATTAG

Figure 6. NCBI sequence of *P. syringae* pv. *syringae* B728a gene Psyr_1536 (104043210), amine oxidase and putative *iaaM* homolog.

ATGAAGAACAACCGTCACCCCGCCAACGGCAAAAAGCCGATCACCATGTTCGGCCCCGAC
TTCCCCTTCGCCTTCGATGACTGGATCGAGCACCCTAAAGGCCTGGGCAGCATTCCGGTG
GAGAACCACGGCGCTGAAGTGGCAATTATCGGTGCAGGGATAGCCGGTCTGGTGGCGGCC
TACGAATTGATGAAGATGGGCCTCAAGCCGGTGGTGTACGAAGCCTCGAAAATGGGCGGC
CGCCTGCGCTCGCAGGAGTTCGAAGGCGCCAAAGGCATCGTGGCCGAACTGGGCGGCATG
CGCTTTCCGGTGTCCTCGACGGCGTTCTTTCATTACGTCGACAAGCTGGGCCTTGAGTCC
AGGCCGTTCCCCAACCCGCTGACCGCGGCGTCTGGCAGCACCGTTATCGACCTGGAAGGC
ACCACCTACTACGCACAGATGCTCTCGGACCTGCCGGCGCTGTTTCAGGAAGTCGCCGAC
GCCTGGGCCGACGCACTGGAAAGCGGCTCGCAATTCGGCGACATCCAGCAGGCGATCCGC
GACCGCGATGTGCCGCGTCTCAAGGAACTGTGGAACAAGCTGGTGCCGTTATGGGACGAC
CGCACGTTCTATGATTTTGTCGCGACTTCCAAGGCCTTCGCCAAGCTGTCTTTCTTTCAC
CGCGAAGTATTCGGCCAGGTGGGCTTCGGCACCGGCGGCTGGGATTCGGACTTCCCCAAC
TCGATGCTGGAAATCTTCCGCGTGGTGATGACCAACTGCGATGAACACCAGCACCTGATC
GTCGGCGGCGTGCAGCAAGTGCCGGTCGGCTTGTGGAGCCATGTACCCGAGCATTGCGCG
CACTGGCCCAAGGGCACCAGCCTGTCGTCGTTGCACCGCGGTGCACCACGTCCCGGCGTG
AAGCGCATTGCGCGCGCCGAGGATGGCAGTTTTGCGGTGACCGACAATTGGGGCGACACC
CGGCAGTACGCCGCTGTGCTGACCACCTGCCAGAGCTGGCTGCTGACCACGCAGATCGAG
TGCGAAGAGTCGCTGTTCTCGCAGAAAATGTGGATGGCCCTGGACCGCACCCGCTACATG
CAGTCGTCAAAGACCTTCGTGATGGTCGACCGCCCGTTCTGGAAGGACAAGGACCCGGAA
ACCGGCCGCGACCTGATGAGCATGACCCTCACCGACCGGCTGACCCGTGGCACGTACCTG
TTCGATAACGGCGACGACAAGCCAGGCGTGATCTGCCTGTCCTACTCGTGGATGAGCGAT
GCACTGAAGATGCTCCCGCAGCCCATCGAGAAGCGGGTGAAGCTAGCGCTGGATGCCTTG
AAGAAGATCTACCCGAAAGTGGACATCGCCGCGCGGATCATCGGTGATCCGATTACCGTG
TCATGGGAAGCTGATCCGCACTTCCTGGGTGCGTTCAAGGGTGCGCTGCCGGGCCATTAC
CGCTATAACCAGCGCATGTACGCGCACTTCATGCAGCAGGATATGCCCAGCGAACAGCGC
GGCATGTTCATCGCCGGCGACGATGTCTCCTGGACACCGGCGTGGGTCGAAGGCGCTGTG
CAGACCTCACTGAACGCCGTGTGGGGGATCATGAACCACTTCGGCGGCAAGACTCACGCC
GAGAACCCCGGCCCCGGTGATGTGTTCCACGAAATCGGCCCGATAGCACTGGGCGACTGA

Figure 7. NCBI sequence of *P. syringae* pv. *syringae* B728a gene Psyr_4667 (104198922), tryptophan monooxygenase and weak *iaaM* homolog.

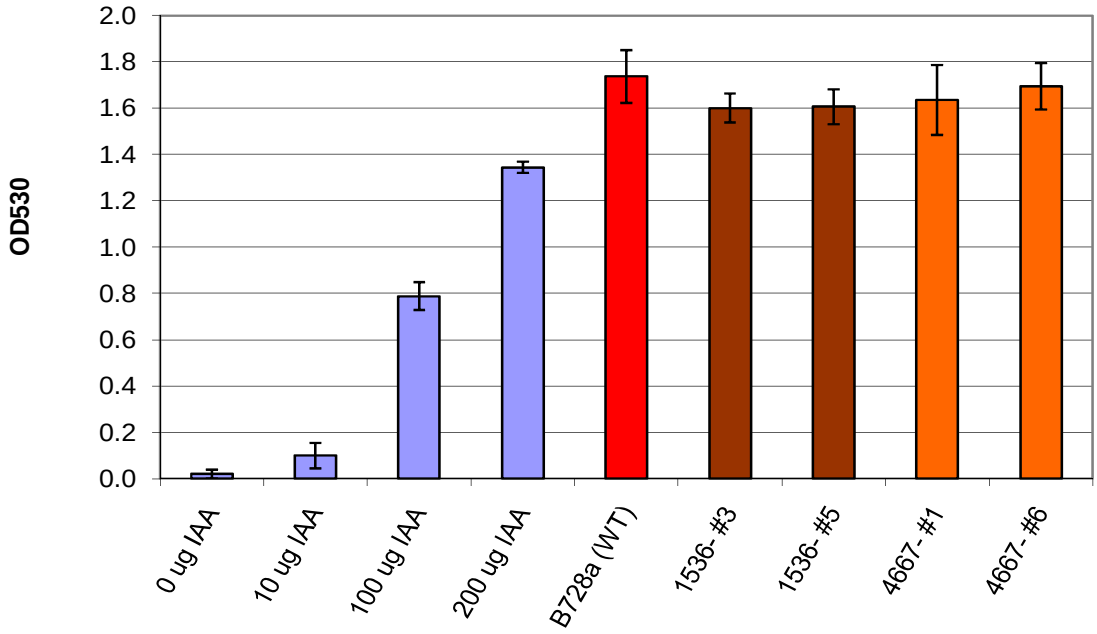

Figure 8. A Salkowski assay showed no significant difference between *in vitro* IAA production by wild-type *Pss*B728a, the Pss_1536 deletion mutant (clones # 3 and 5), or the Pss_4667 deletion mutant (clones # 1 and 6). Standard IAA controls of known concentration are shown for reference.

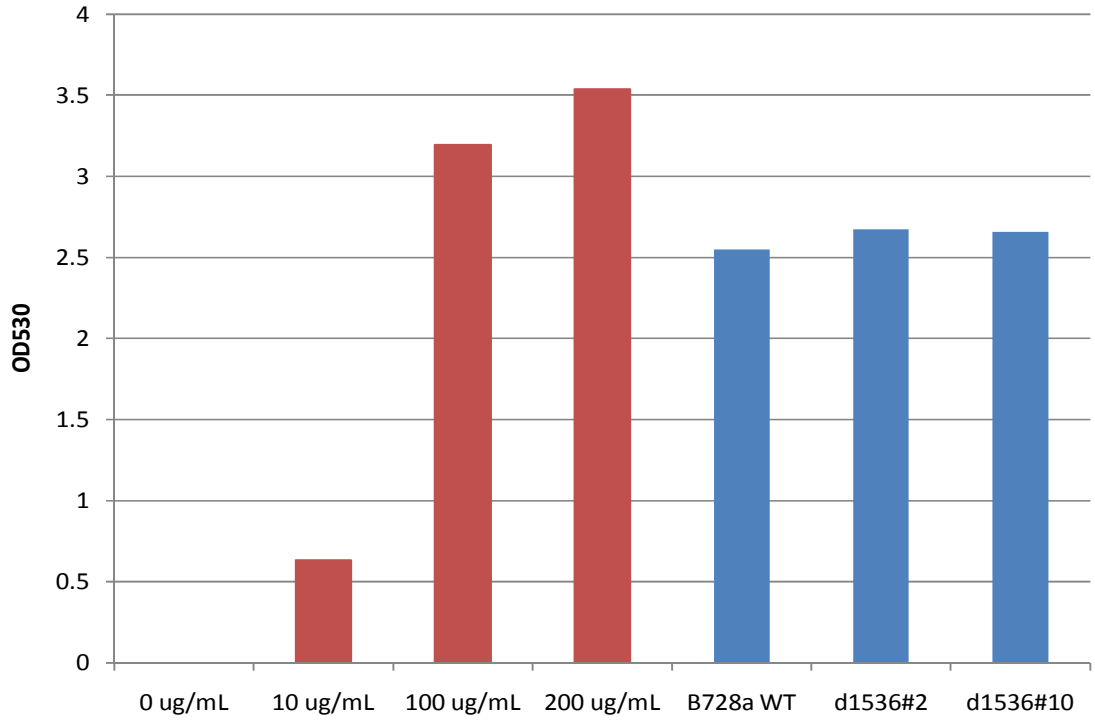

Figure 9. A Salkowski assay of Pss_1536 single-crossover insertion mutant *Psyr*1536*2 (clones # 2 and 10) shows IAA production similar to wild-type *Pss*B728a. Standard IAA controls of known concentration are shown for reference.

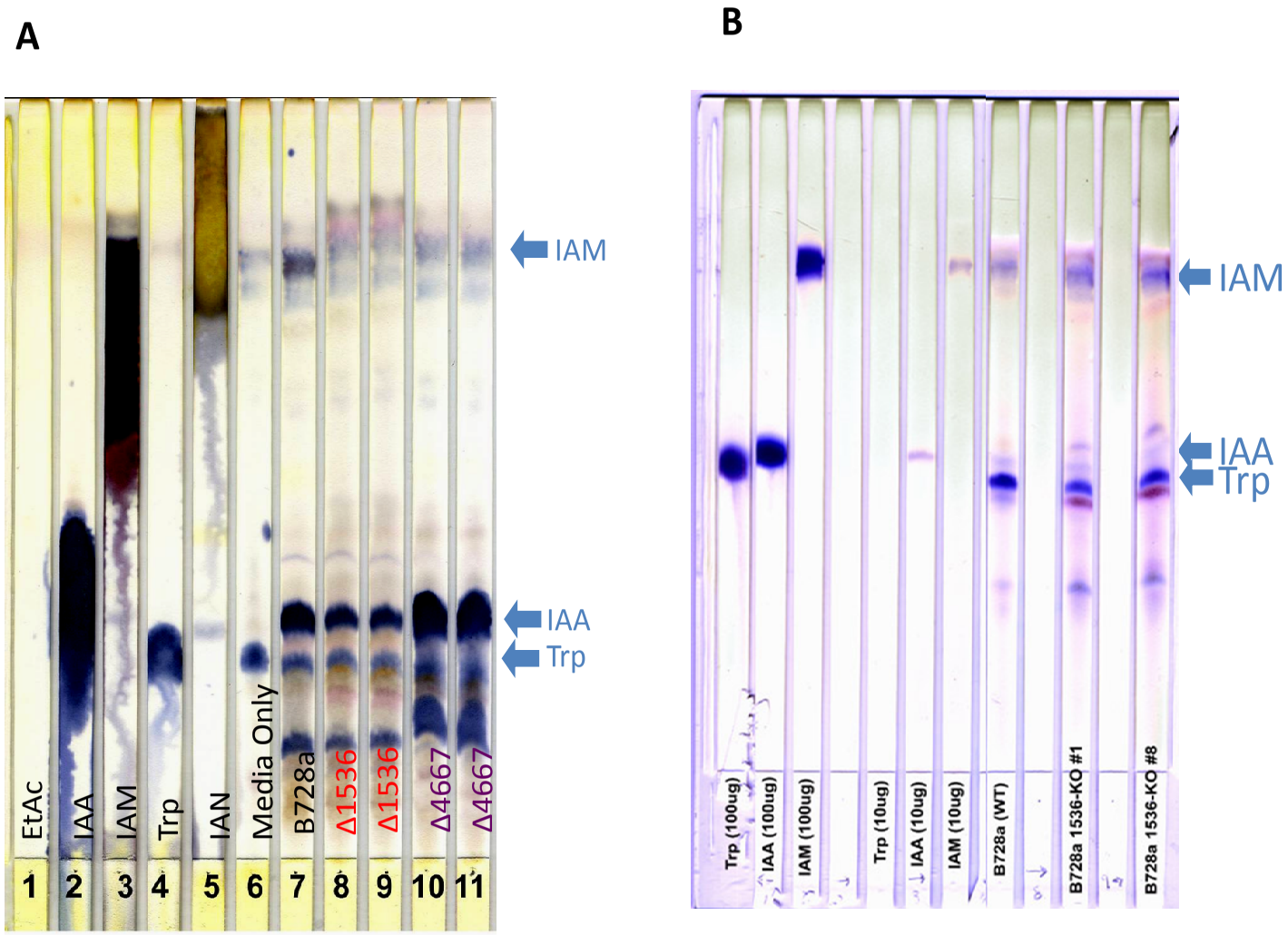

Figure 10. Production of IAA and other indolic compounds by putative IAA biosynthetic knockouts of *Pss*B728a. Results for gene deletion knockout Δ1536 (lanes 8,9), Δ4667 (lanes 10,11) (A) and single-crossover insertional knockout *Pss*1536*2 (clones #1, 8) (B) are shown.

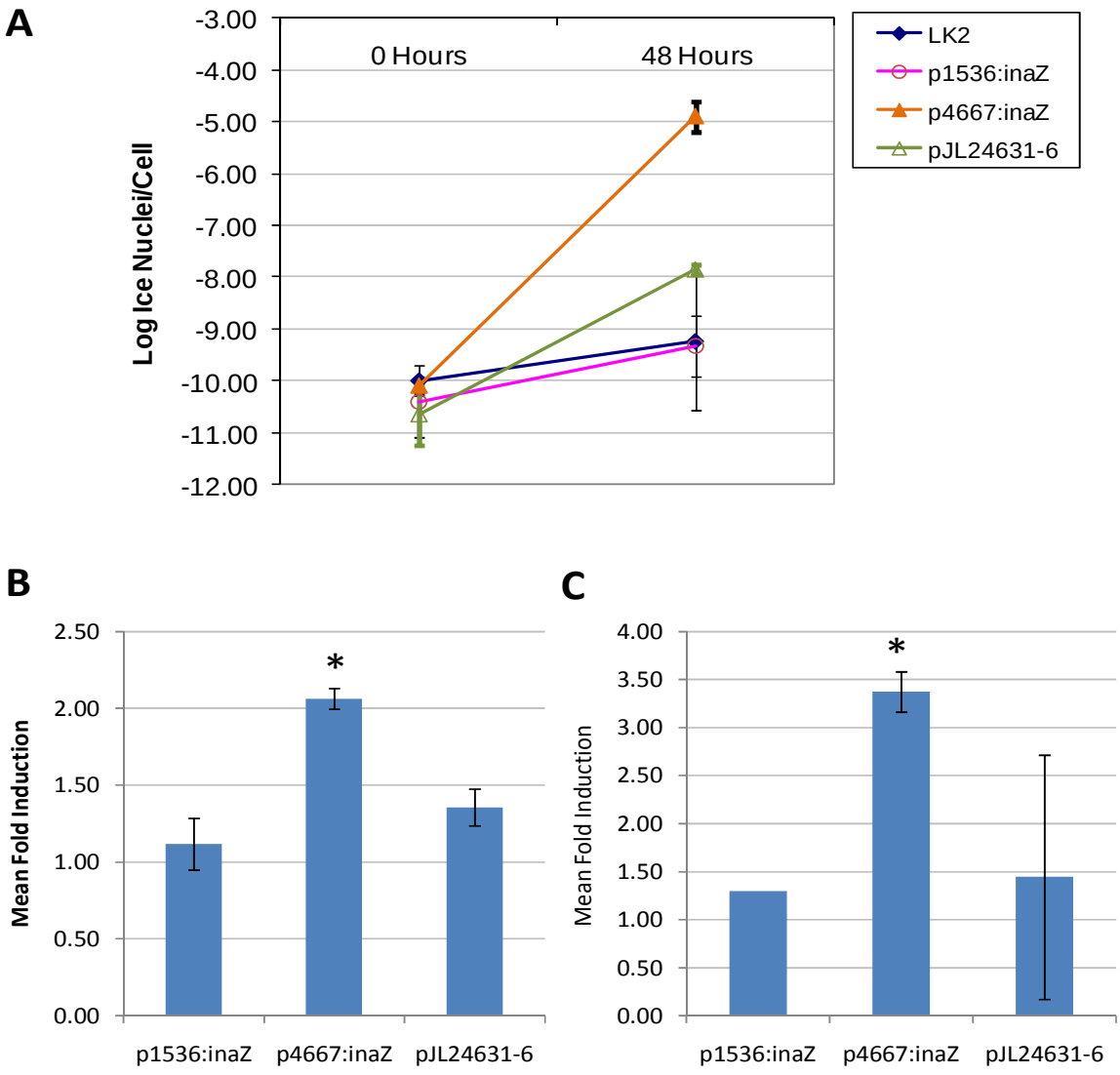

Figure 11. Leaf epiphytic induction of Ps_1536 and Ps_4667 promoter:reporter fusion constructs relative to an untransformed control (LK2) and a weak constitutive positive control (pJL24631-6) (A). Mean fold induction data from the same experiment (B) reveal significant induction of Ps_4667 and modest repression of Ps_1536 relative to the constitutive control (B). Similar data were obtained in a second experiment (C). Each point represents the mean of three samples ± 1 S.D; *=significant difference from the pJL24631-6 control ($p<0.001$).

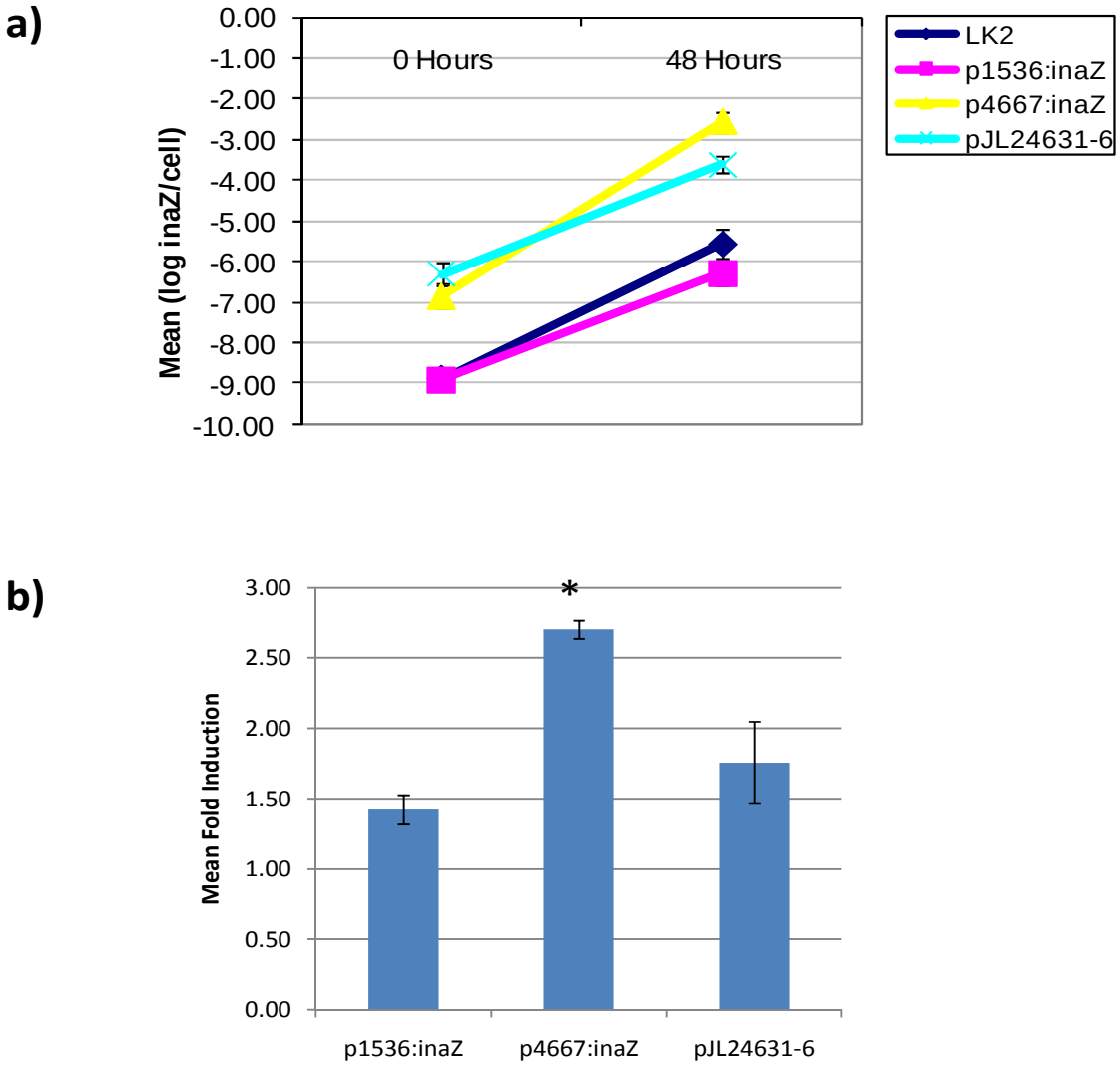

Figure 12. Leaf endophytic induction of Ps_1536 and Ps_4667 promoter:reporter fusion constructs relative to an untransformed control (LK2) and a weak constitutive positive control (pJL24631-6) (A). Mean fold induction data from the same experiment (B) reveal significant induction of Ps_4667 and modest repression of Ps_1536 relative to the constitutive control (B). Each point represents the mean of three samples ± 1 S.D; *=significant difference from the pJL24631-6 control ($p<0.001$).

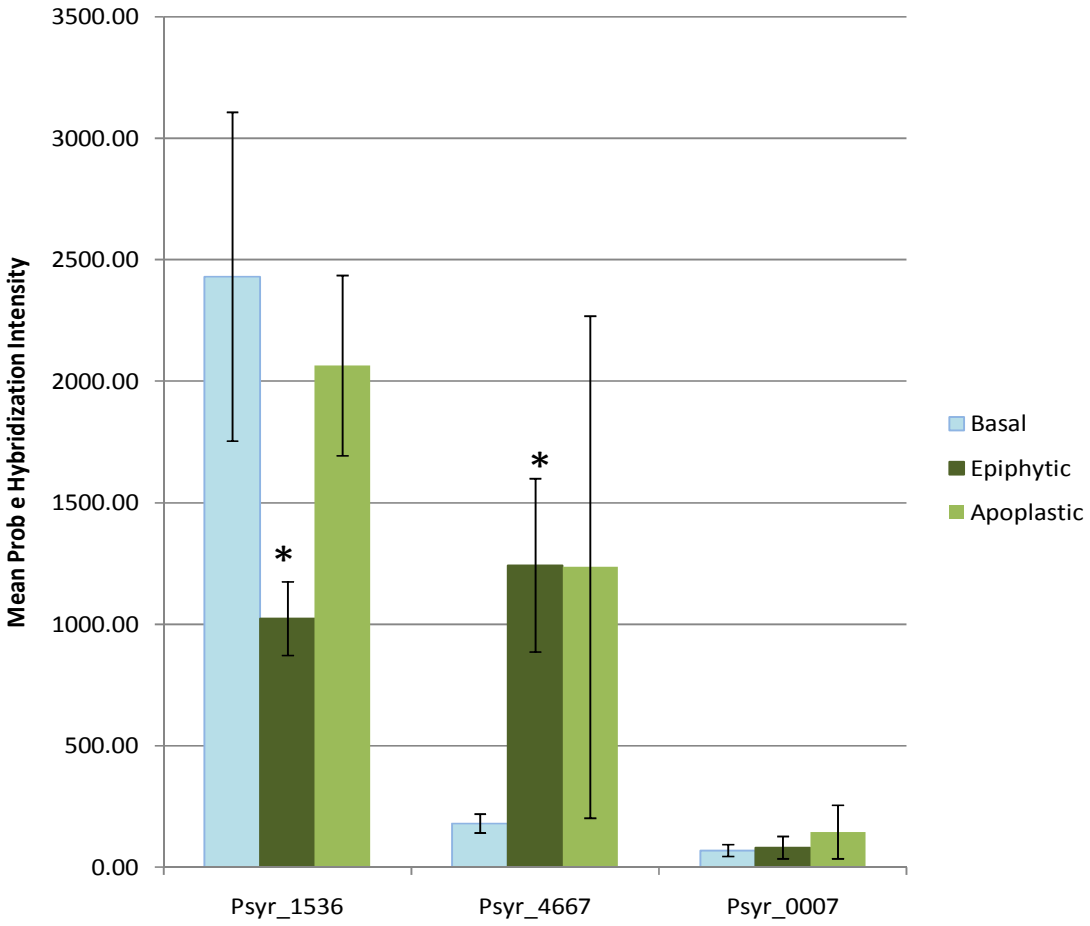

Figure 13. Microarray expression profiles of 3 putative IAA biosynthetic genes after *Pss*B728a were grown in basal media, on bean leaves, or inside the bean leaf apoplast. Each point represents the mean of 6 independent experiments ± 1 S.D; *=significant difference from basal media control ($p<0.001$).

	% Survival *E. Coli K12**		% Survival *P. agglomerans*	
Condition	**IAA+**	**IAA-**	**299R (IAA+)**	**XYLE (IAA-)**
Osmotic shock *0.2-0.5M NaCl*	72 ±1	52 ±1	10-90% *(no diff.)*	10-90% *(no diff.)*
UV Stress *Bianco=100 J/m^2, liquid Powell=62.5 J/m^2, plate*	81 ±2	46 ±5	15.5	14.8
Oxidative stress *Bianco=2.0mM H_2O_2 Powell=0.2mM*	97 ±6	56 ±2	65.8	65.9

*(Bianco *et al.*, 2006)

Table 1. Comparison of IAA-Induced Stress Resistance Data in *E. coli* K12 versus *P. agglomerans* 299R

Strain	Aggregate on Dark Cell	Aggregate on Fluorescent Cell	*Row Totals*
Pa*299R *(IAA$^+$)	88	33	***121***
Pa*MX149 *(IAA$^-$)	86	43	***129***
Column Totals	***174***	***76***	***250***

Table 2. Occurrence of bacterial aggregates on modified (blue-green autofluorescent) versus unmodified (nonfluorescent) epidermal cells of bean plants.

Organism/Strain	Description
E. coli S17	Donor strain for conjugative plasmid transfer via biparental mating; RP4-Tc::Mu-Km::Tn7 ; $Spec^R$/$Strep^R$ (Simon *et al*., 1983)
Pseudomonas syringae pv. *syringae* B728a	Parent strain; Rif^R (Feil *et al*., 2005)
*Pss*Δ1536	B728a derivative; Putative deletion knockout of Pss_1536; Rif^R/$Gent^R$ (this study)
*Pss*Δ4667	B728a derivative; Putative deletion knockout of Pss_4667; Rif^R/$Gent^R$(this study)
*Pss*1536*1	B728a derivative; single-crossover insertion knockout of Pss_1536; Rif^R/Tet^R (this study)
*Pss*1536*2	B728a derivative; single-crossover insertional knockout of Pss_1536; Rif^R/Tet^R (this study)

Table 3. Strains involved in generating auxin biosynthetic knockouts of *P. syringae* pv. *syringae* B728a

Chapter IV. Conclusions

The ability to biosynthesize indole-3-acetic acid (IAA), an important plant hormone, is common among plant-associated microbes (reviewed in Spaepen *et al*., 2007), in which it has been shown to enhance microbial fitness and influence a variety of host-microbe interactions. In this work, I have presented a series of investigations intended to elucidate mechanisms by which IAA production enhances the fitness of plant-associated bacteria.

The majority of the research discussed focuses on the phyllosphere epiphyte *Pantoea agglomerans* 299R, an enterobacterial species previously shown to induce IAA biosynthesis on leaf surfaces (Brandl *et al*., 2001). Past work demonstrated that wild-type 299R bacteria experience a small but significant growth advantage over auxin-deficient mutants *in planta* (Brandl *et al*., 1998). A variety of hypotheses could be invoked to account for this fitness benefit.

IAA and bacterial stress resistance

One possibility is that bacterial IAA acts endogenously to improve survival. Research by Bianco *et al*. (2006) showed that application of exogenous IAA to *in vitro* cultures of *E. coli* strain K12 increased both transcriptional activity of stress-related genes and survival under a variety of stress conditions. More recently, the same group reported that either exogenous or endogenous (transgenic plasmid-encoded) IAA production confers stress resistance in *Sinorhizobium meliloti* (Bianco *et al*., 2009), which suggests that native auxin production by bacteria may also confer stress resistance. Particularly given that matric and osmotic stress were shown to increase transcription of the *Pa*299R indolepyruvate decarboxylase (*ipdC*) gene, which encodes the rate-limiting enzyme in IAA biosynthesis (Brandl *et al*., 1997), the hypothesis that auxin production improves bacterial fitness by enhancing stress resistance in *Pa*299R seemed plausible.

However, our *in vitro* experiments (Chapter Three) to test whether endogenous auxin production enhanced bacterial resistance to harsh conditions likely to be encountered on the leaf surface—matric, osmotic, or UV stress—detected no significant differences in the survival of wild-type (IAA+) versus mutant (IAA-) strains. We therefore concluded that endogenous production of IAA by *Pa*299R does not enhance fitness via increased stress resistance under the *in vitro* conditions tested. This conclusion hints that water-stress-inducibility of the bacterial *ipdC* gene (and therefore of IAA production) may not serve as a direct physiological adaptation to withstand matric or salt stress *per se*; rather, water stress may act as a proxy indicator that the bacteria has arrived in a leaf environment, and should therefore commence IAA biosynthesis for adaptive purposes other than stress resistance.

This negative result was not entirely surprising, given that wild-type *Pa*299R experienced the greatest relative fitness benefit over IAA-deficient mutants during periods of bacterial population expansion on the leaf; in contrast, auxin production was found to confer little or no benefit during periods of population stability or decline (Brandl *et al*., 1998). If IAA actually functioned to maximize bacterial survival under stress, the opposite pattern would be expected: IAA-mediated fitness advantages would emerge during stressful periods of population contraction or stagnation, as auxin-deficient mutants became less able to resist physiological constraints

imposed by stressful phyllosphere conditions. The observation that IAA-mediated fitness benefits instead accrued primarily during periods of population growth therefore suggested that IAA did not improve fitness by preventing bacterial death, but rather by promoting bacterial proliferation.

IAA and modification of host cell autofluorescence

A second hypothesis for IAA-mediated bacterial fitness in the phyllosphere is that bacterial IAA acts upon the plant host, modifying the local foliar environment in a way that enhances microbial proliferation. Monier *et al*. (2005) suggested this hypothesis to explain their observation that recent immigrant bacteria were more likely to survive and replicate if they landed on a leaf epidermal cell already inhabited by a *Pa*299R colony—indicating that the presence of a large, preexisting population of auxin-producing cells rendered the environment more hospitable for subsequent growth. In advancing this hypothesis, the researchers also noted that many plant epidermal cells occupied by *Pa*299R colonies exhibited elevated cellular fluorescence under the microscope. They therefore suggested that plant epidermal cell autofluorescence arose in response to local IAA production by resident colonies of *Pa*299R bacteria.

As described in Chapter Three, we therefore sought to further characterize the relationship between bacterial auxin production by phyllosphere epiphytes and the autofluorescence of their substrate plant cells. These experiments suggested that *Pa*299R colonies were indeed more likely to be located on autofluorescent leaf epidermal cells than on nonfluorescent cells. However, a wild-type colony was no more likely to reside on an autofluorescent leaf cell than an auxin-deficient mutant colony, suggesting that bacterial IAA production did not cause elevated leaf cellular fluorescence.

Other aspects of bacterial colonization (*i.e.* other chemicals produced or secreted by the cell) may instead be responsible for eliciting altered fluorescence in substrate epidermal cells of the host plant. Alternatively, cause and effect may be reversed: cellular autofluorescence may be an independent phenomenon indicating that a cell was previously damaged or subjected to pathogen attack, making it inherently more hospitable to incoming bacteria (perhaps due to nutrient leakage from compromised membranes and cell walls). In either case, plant cell autofluorescence did not appear to be a particularly useful phenomenon for studying the adaptive role of bacterial IAA production.

IAA facilitates carbon acquisition by Pa299R

As an alternative approach to investigating whether microbial IAA improves bacterial fitness by modifying host plant behavior, we tested whether bacterial auxin status affected local carbon availability to bacterial cells (experiments described in Chapter Two). Researchers studying microbial hormone production have long posited a role for bacterial IAA in nutrient acquisition (Monier *et al*., 2005; Brandl *et al*., 1998). Furthermore, in the carbon-limited phyllosphere (Mercier *et al*., 2000), hormone-mediated increases in plant carbon exudation are consistent with the report of elevated *in planta* growth by IAA-producing *Pa*299R cells relative to IAA-deficient

mutants (Brandl *et al.*, 1998), and increased survival of immigrant cells that arrive near wild-type *Pa*299R colonies on the leaf surface (Monier *et al*., 2005). In conjunction with IAA's well-characterized ability to affect endogenous plant carbon metabolism and transport—particularly via the stimulation of apoplastic cell-wall invertases (Roitsch *et al.*, 2004)—these observations suggested a plausible role for IAA in facilitating microbial access to host plant carbon reservoirs.

To test this hypothesis, we transformed *Pa*299R and two of its IAA-deficient mutant derivatives, *Pa*MX149 and *Pa*XYLE, with plasmids bearing sugar biosensor constructs. These plasmids included the fructose-inducible GFP biosensor pFru46 (Leveau *et al.*, 2001a), and the sucrose-inducible biosensors p61RYice and p61RYtir (Miller *et al.*, 2001), which encode an ice-nucleation protein reporter or GFP reporter, respectively. By assaying the levels of fructose or sucrose detected by each strain *in planta*, we sought to determine whether IAA-producing bacteria experienced higher levels of carbon availability than isogenic knockout strains. As an additional test, IAA status was also manipulated by co-inoculating *Pa*MX149 mutants with or without exogenous NAA (a synthetic auxin).

As might be expected given that IAA production was reported to yield a relatively modest fitness benefit (roughly 7% more cells per generation [Brandl *et al*., 1998]), differences in carbon sensing between the two strains were subtle, but detectable. Sucrose sensing was significantly (12-16%) lower in the presence of exogenous NAA or endogenously produced bacterial IAA, as detected by the p61RYice reporter. (The p61RYtir reporter yielded inconsistent results, most likely due to its relatively weaker sensitivity to low concentrations of sucrose.) Conversely, fructose sensing increased significantly in the presence of exogenous NAA or bacterial IAA, with higher proportions of cells becoming induced sooner after inoculation onto the leaf.

In both sucrose and fructose sensing experiments, auxin-mediated differences in carbon availability were transient, typically occurring within the initial 1-7 hours after inoculation onto *Phaseolus vulgaris* leaves. This span coincides with the period of rapid population expansion typically observed in leaf-dwelling bacteria as newly arrived immigrants deplete existing carbon reservoirs on the phylloplane. At later time points (12-24 hpi), after initial carbon reservoirs became depleted, differences were generally not detected between the amount of carbon sensed by IAA^+ and IAA^- treatments. (In a single flow cytometry experiment, the pFru46 biosensor did report a subtle but significant carbon advantage persisting in IAA^+ bacterial strains at 24 hpi.)

These sugar sensing data generally support Brandl *et al*.'s (1998) finding that auxin-mediated fitness differences are positively correlated with periods of rapid population expansion. There is, however, a discrepancy in the timing between the two studies: Brandl *et al*.'s earliest collected timepoint was at 24 hpi, while our experiments indicate differences in sugar sensing at 7-9hpi. This difference could be due to the different types of data collected, with the IAA-dependent differences in sugar availability described in this study occurring earlier than the IAA-dependent growth differences detected by Brandl *et al*. It may also be that Brandl *et al*. would have detected larger growth discrepancies between IAA^+ and IAA^- strains, had they measured bacterial populations at an earlier timepoint.

IAA and bacterial carbon acquisition: a resource conversion strategy targeting plant cell wall invertase?

The observed trends in carbon sensing suggest that IAA decreases sucrose availability and increases fructose availability to bacteria in the *Phaseolus vulgaris* phyllosphere. In turn, this pattern implicates bacterial IAA in the stimulation of cell wall invertase—an extracellular plant enzyme that cleaves the disaccharide sucrose into its component monosaccharides, glucose and fructose (Roitsch *et al.*, 2003).

To test whether IAA-mediated changes in phyllosphere carbon availability were invertase-dependent, we inoculated biosensor bacteria onto wild-type *Arabidopsis thaliana* and three *A.thaliana*.cell wall invertase mutants (*cwinvX, cwinvX,* and *cwinvX)* under IAA^+ or IAA^- conditions (Chapter 2). The experiment yielded two important results: 1) using microscopic quantification of fluorescent fructose and sucrose biosensor bacteria, we found no difference in carbon status between IAA^+ and IAA^- treatments on wild-type *A. thaliana*, suggesting that bacterial IAA's ability to elicit changes in sugar availability is host-dependent; and 2) we found no consistent differences in sugar sensing among bacteria inoculated onto wild-type versus mutant *Arabidopsis*. Thus, although the experiment did not support the hypothesis that bacterial IAA modulates carbon availability by targeting plant invertases, neither did it rule it out; *Arabidopsis* simply turned out to be a poor model for auxin-mediated phyllosphere interactions. In the future, experiments testing whether invertase function is required for IAA-dependent carbon shifts should be executed in host plants, such as *P. vulgaris*, that are susceptible to manipulation by microbial IAA—perhaps using chemical inhibitors (Huang *et al*., 2007) or inducible gene silencing (Siemens, *et al*., 2010; Essmann *et al*., 2008) to inactivate cell wall invertases. In the meantime, invertase remains a plausible—but hypothetical—target of bacterial IAA.

Although the involvement of plant cell wall invertases in IAA-mediated carbon acquisition awaits further experimental confirmation, we proceeded to conduct preliminary experiments to assess whether resource conversion represented an adaptive strategy for *Pa*299R (Chapter 2). Expending cellular resources simply to transform one metabolizable carbon source (sucrose) into another (fructose and, presumably, glucose) would only make sense if the bacteria derive a growth advantage from this transformation. By monitoring the *in vitro* growth of *Pa*299R with sucrose, glucose, or fructose as a sole carbon source, we determined that such an advantage did exist: although net growth of the bacteria was similar on all three carbon sources after 24-48 hours of growth, *Pa*299R was able to induce growth more quickly on glucose and fructose than on sucrose, yielding higher growth at early time points. (Delayed growth on sucrose may be due to metabolite repression or to slow induction of the *scr* genes required for transport and metabolism of sucrose.)

In conclusion, IAA may foster quicker onset of phyllosphere growth by transforming less-accessible sucrose into more easily metabolizable glucose or fructose. Relative growth differences on the three sugars appeared particularly strong at low *in vitro* carbon concentrations; this observation is especially relevant given that 89% of phyllosphere epiphytes have access to only 0.15-4.6 pg of sugar (Leveau *et al*., 2001). Maximal growth benefits are therefore expected to accrue under exactly the sorts of oligotrophic conditions that prevail on the leaf surface.

Particularly in highly dynamic phyllosphere conditions, which can limit bacterial proliferation to brief windows of environmental opportunity (Lindow *et al*., 2003; Axtell *et al*., 2002), the ability to exploit local nutrients more rapidly than auxin-deficient competitors would be expected to significantly enhance bacterial fitness (Lenski, 1998).

Methodological considerations in working with single-cell bacterial biosensors

In using fluorescent bacterial biosensors to make nuanced measurements of subtle, population-wide phenomena, we gained extensive experience with the potential and limitations of these tools—particularly in complex environments. Though only briefly considered in the body of this dissertation, Appendix 1 contains an extended discussion of methodological and technical investigations pertaining to the quantification and analysis of fluorescent biosensors. This information may prove valuable to researchers considering similar approaches in their own research.

In short, although reporters such as *inaZ* can detect aggregate changes in gene expression across a population, they reveal little about differential patterns of reporter activity *within* a given population. In contrast, single-cell quantification of fluorescent bioreporters allows sensitive measurement of the distribution of reporter activity among individuals within a bacterial population (so long as the gene/trait is expressed at a level sufficiently high to detect at the single-cell level with reporters such as gfp).

Two primary methods enable quantification of cellular fluorescence of bacterial biosensors: flow cytometry and fluorescence microscopy. Each approach demands different compromises between precision and expedience. Assuming access to a flow cytometer specifically suitable for small-particle analysis, flow cytometry permits high-throughput analysis, massive sample sizes, and sensitive detection of a wide range of GFP expression among induced cells. However, in complex environmental samples, flow cytometry suffers from significant, highly variable background contamination (25.5-88.5% of putative cell events from leaf-wash samples were background particles), making it difficult to discriminate uninduced cells from background debris without some sort of secondary labeling. Variability in how each cell tumbles through the optical path of the machine's analytical module may also reduce resolution, introducing an additional source of error that can obscure subtle differences between two fluorescent populations. In contrast, epifluorescence microscopy enjoys consistently lower background contamination (typically <10% of putative cell events from leaf-wash samples), allowing greater confidence in determining the proportion of induced versus uninduced cells in the population, as well as sensitive detection of GFP expression among induced cells. However, this precision comes at the expense of throughput, as fluorescence microscopy is extraordinarily labor-intensive and time-consuming; this limits sample sizes to a fraction of those possible using flow cytometry—in turn restricting an experiment's statistical power.

In an effort to better distinguish inoculated bacteria from native microbes and other background leaf debris during flow cytometry, a variety of secondary fluorescent labeling approaches were tried. To complement the use of a GFP reporter, we first attempted to constitutively express red fluorescent proteins including mRFP1, dsRed.T3_S4T, and mCherry in the biosensor bacteria;

unfortunately, when co-expressed with GFP, these reporters exhibited a range of problems: most were too dim to detect reliably via flow cytometry, several exhibited spectral or other interference with GFP (particularly when strongly expressed), and at least one exhibited cellular toxicity in *Pa*299R. As an alternative, attempts to label cells by staining with the nonspecific, fluorescent membrane dye FM4-64 did little to improve flow cytometric detection. Cell labeling with strain-specific fluorescent antibodies could potentially improve bacterial detection, but the commercially available α-*P.agglomerans* antibody tested failed to bind *Pa*299R in an agglutination assay, so an effective antibody would first have to be identified.

In short, secondary labeling for flow cytometry proved to be a nontrivial challenge. Preliminary experiments did suggest that fluorescence *in situ* hybridization may hold some promise. After screening a variety of potential *Pa*299R FISH probes, moderate success was achieved: roughly 50% of constitutive GFP-expressing *Pa*299R recovered from a *P. vulgaris* leaf were successfully identified using the red-labeled (DH-480) Eh299R FISH probe. However, due to mixed data indicating some false positive labeling in a negative control treatment, as well as reports that cell permeabilization during FISH staining can result in diminished GFP reporter brightness (Remus-Emsermann *et al.*, 2010; Leveau *et al.*, 2001), FISH labeling was not integrated into standard experimental procedures in this study. Future researchers, however, may wish to explore further optimization of FISH staining protocols.

IAA in P. syringae pv. syringae B728a pathogenesis

In addition to extensive investigation of the adaptive function of bacterial IAA in the epiphyte *Pa*299R, experiments were also performed to explore the role of IAA production in the foliar pathogen *Pseudomonas syringae* pv. *syringae*. Previous research has indicated that IAA production by bacterial pathogens may act as an endogenous regulatory signal, inducing suites of pathogenesis-related genes (Yang *et al.*, 2007; Mazzola *et al.*, 1994). Additionally, given that auxin appears to promote disease susceptibility in plants by repressing the plant's defense response (Shinshi *et al*., 1987; Jouanneau *et al*., 1991; Navarro *et al*., 2006), IAA may also facilitate pathogenesis by impairing host defenses.

To investigate the role that bacterial IAA plays in *Ps*B728a pathogenesis, we knocked out the indoleacetamide monooxygenase (*iaaM)* gene (Pss_1536), which was presumed to be responsible for the ultimate step in IAA biosynthesis via the well-characterized indoleacetamide (IAM) pathway. Despite the generation of three different *iaaM* knockout strains (via double-homologous recombination, and via single-crossover insertional mutagenesis with two different insertion constructs), no reduction in *in vitro* IAA production was ever achieved, as measured by both Salkowski assay and TLC chromatography. Barring undiagnosed technical problems with these mutants, it appears that *iaaM* is not required for auxin biosynthesis in *Ps*B728a.

This result was quite surprising, given that the B728a genome contains a highly conserved, canonical *iaaMH* operon, and that *iaaM* inactivation was sufficient to knock out IAA production in the closely related strain *Pss* Y30. The apparent irrelevance of i*aaM* could be due to functional redundancy between *iaaM* and another, weakly conserved monooxygenase gene (Psyr_4667). Although Δ4667 single-gene mutants produced wild-type levels of IAA *in vitro*, a double-mutant

was never generated to test for redundancy. Alternatively, a non-indoleacetamide biosynthetic pathway may be responsible for IAA production in B728a. Howden *et al.* (2009) recently demonstrated that *Pss*B728a can synthesize IAA from an indole-3-acetonitrile precursor via the nitrilase Psyr_0007. Although it is unclear how important this pathway is in contributing to net cellular IAA production under physiologically relevant conditions (*i.e.* using tryptophan as a precursor), it is possible that the indoleacetonitrile pathway, and not IAM, accounts for IAA production in B728a.

Implications

Ultimately, the research described in this dissertation sought to clarify how bacterial IAA facilitates the survival and proliferation of phyllosphere bacteria. In pursuing this goal, we explored flow cytometric and fluorescent microscopic approaches to the quantification of single-cell fluorescent biosensors, and made preliminary forays into studying the role of IAA in foliar pathogenesis of *Pss*B728a. However, the main advances achieved here lie in understanding IAA production by plant epiphytic bacteria—specifically, by the model epiphyte *Pa*299R.

In demonstrating that bacterial IAA alters carbon availability in the phyllosphere, we have confirmed that bacterial auxin can affect nutrient acquisition from the host plant—bolstering a longstanding hypothesis regarding the adaptive function of microbial hormone production. Furthermore, the observed pattern of auxin-induced sugar conversion (decreased sucrose and increased fructose) implicates plant cell wall invertase as a plant molecular target of bacterial IAA, although it is important to point out that this evidence remains circumstantial. These results add to a growing body of research indicating that apoplastic invertases act as key mediators of source-sink partitioning within plants, as well as between plants and their resident microbial communities (Roitsch *et al*., 2003). Assuming that invertase activation occurs via ABP1-mediated induction of ATPases, rather than by TIR1-mediated signal transduction, these results could also suggest that experiments which monitor the effects of microbial IAA solely by tracking changes in plant transcriptional activity may overlook important physiological responses that occur at the plant plasma membrane.

Finally, the research conducted for this dissertation demonstrates the utility of microbial bioreporter systems in probing the underlying dynamics of plant source-sink relationships (Biemelt *et al*., 2005)—particularly in tracking sugar flux through the apoplastic compartment and onto the leaf surface. Our bioreporter observations suggest complex interactions between the environment, the host plant, and the relative success of bacterial survival strategies in the phyllosphere. Bacterial IAA production may, for example, be adaptive only on certain host plants (*i.e. P. vulgaris*, but not *A. thaliana*). Similarly, it may be adaptive only under high-light, long-day conditions, when high photosynthetic productivity leads to the relative saturation of phloem loading and elevated concentrations of apoplastic photosynthate; under these conditions, IAA-activated invertases would have abundant substrate to cleave—and the metabolic expense of synthesizing IAA would yield a greater carbon advantage to phyllosphere bacteria.

IAA-mediated interactions between plants and their resident microbes therefore appear both complex and environmentally contingent. In unraveling these interactions, this research increases

understanding of the interactions between bacterial IAA production, plant invertase activity, photosynthate partitioning, and cultivation conditions—and ultimately, how these factors can be manipulated to establish beneficial bacterial populations and impede plant pathogens in an agricultural context.

LITERATURE CITED

Axtell, C.A., and G.A. Beattie. (2002) Construction and characterization of a *proU-gfp* transcriptional fusion that measures water availability in a microbial habitat. *Applied and Environmental Microbiology*. **68**(9): 4604-4612.

Biemelt, S., U. Sonnewald. (2006) Plant-microbe interactions to probe regulation of plant carbon metabolism. *Journal of Plant Physiology*. **163**(3): 307-318.

Brandl, M., and S. Lindow. (1998) Contribution of indole-3-acetic acid production to the epiphytic fitness of *Erwinia herbicola*. *Applied and Environmental Microbiology*. **64** (9): 3256-3263.

Brandl, M.T., B. Quinones, & S.E. Lindow. (2001) Heterogeneous transcription of an indoleacetic acid biosynthetic gene in *Erwinia herbicola* on plant surfaces. *Proceedings of the National Academy of Sciences.* **98**(6): 3454-3459.

Huang, L., P.N. Bocock, J.M. Davis, and K.E. Koch. (2007) Regulation of invertase: a 'suite' of transcriptional and post-transcriptional mechanisms. *Functional Plant Biology*. **34**: 499-507.

Leveau, J.H.J, and S.E. Lindow. (2001) Appetite of an epiphyte: Quantitative monitoring of bacterial sugar consumption in the phyllosphere. *Proceedings of the National Academy of Sciences*. **98**(6): 3446-3453.

Lindow, S.E., and M.T. Brandl. (2003) Microbiology of the Phyllosphere. *Applied and Environmental Microbiology*. **69**(4): 1875-1883.

Mercier, J., and S.E. Lindow. (2000) Role of leaf surface sugars in colonization of plants by bacterial epiphytes. *Applied and Environmental Microbiology.* **66**(1): 369-374.

Miller, W.G., M.T. Brandl, B. Quinones, and S.E. Lindow. (2001) Biological sensor for sucrose availability: relative sensitivities of various reporter genes. *Applied and Environmental Microbiology*. **67**(3): 1308-1317.

Monier, J.M., and S.E. Lindow. (2005) Aggregates of resident bacteria facilitate survival of immigrant bacteria on leaf surfaces. *Microbial Ecology*. **49**: 343-352.

Remus-Emsermann, MNP, and J. Leveau. (2010) Linking environmental heterogeneity and reproductive success at single-cell resolution. *ISME Journal*. **4**(2):215-222.

Roitsch, T. (1999) Source-sink regulation by sugar and stress. *Current Opinion in Plant Biology*. **2**: 198-206.

Roitsch, T., M.E. Balidbrea, M. Hofmann, R. Proels, & A.K. Sinha. (2003) Extracellular invertase: key metabolic enzyme and PR protein. *Journal of Experimental Botany*. **54**(382): 513-524.

Appendix I. Methods for single-cell fluorescence quantification of bacterial biosensors: A critical evaluation of flow cytometry and epifluorescence microscopy applied to environmental samples

Abstract

Many environmental bioreporters permit measurement of mean reporter induction within a population. But in order to understand gene expression dynamics in complex environmental settings, knowledge of reporter induction at the single-cell level is crucial. In order to facilitate such single-cell analysis, two methods were investigated that might be used to quantify fluorescent reporter induction of individual bacterial biosensors: flow cytometry, and epifluorescence microscopy coupled with quantitative digital image analysis. For each technique, various methodological and analytical approaches were assessed, and the range and sensitivity of the approach was assessed. To facilitate fluorescence analysis by both techniques, secondary labeling of bacterial cells was also explored, including constitutive expression of the red fluorescent proteins mRFP1, mCherry, and dsRed.T3_S4T; cell labeling via FISH and antibody staining; and nonspecific cellular dyes. Though flow cytometry holds some limited utility in detecting large shifts in fluorescence among GFP-positive cell populations, it was found to suffer from high background and limited sensitivity to dim fluorescence—particularly of secondary red fluorescent proteins. In contrast, fluorescence microscopy provided lower background and sensitive detection, but was labor-intensive, slow, and provided only small sample sizes. Efforts towards secondary cell labeling were largely unsuccessful, but bear some promise for future applications.

Introduction

In order to measure the carbon concentrations available to leaf epiphytic bacteria, a method was required to measure the reporter activity of sugar-inducible bacterial biosensors washed from the leaf surface. To accomplish this, preliminary experiments exploited a sucrose-inducible *inaZ* ice nucleation reporter; unfortunately, these data could only provide information about average, population-wide exposure to leaf surface sugars.

Though population-level data are informative, detailed knowledge about the distribution of sugar availability among individual leaf-surface bacteria are crucial to understanding the role of IAA in determining bacterial fitness in a complex and dynamic leaf environment. For example, preliminary research suggested a small, auxin-dependent decrease in population-level sucrose sensing (Chapter 2). But did decreased sucrose availability at the population level represent a steep drop in sucrose acquisition by a few bacteria, or a modest drop in sucrose acquisition by many bacteria? Were changes in sugar acquisition experienced by slow-growing bacteria in low-carbon, oligotrophic conditions? Or by bacteria dwelling in carbon-rich "nutrient oases" and experiencing relatively rapid growth (Lindow, 2003)? The answers to these questions could reveal broad patterns in auxin-dependent sugar acquisition, which could in turn illuminate the mechanisms by which bacterial auxin biosynthesis confers evolutionary fitness.

In order to gain more precise information about the induction of individual biosensor cells on the leaf surface, a method was required to quantify GFP expression at the single-cell level. To this end, multiparametric flow cytometry and epifluorescence microscopy were assessed for their ability to measure sugar-inducible GFP expression in bacterial biosensors washed from leaves.

For both methods, bacterial biosensors were inoculated onto the leaf, allowed to interact with the phylloplane for an appropriate interval, then washed off. In microscopy experiments, this "washate" was dried onto microscope slides and the cells' GFP intensity visualized using an epifluorescence microscope, then quantified using image analysis software. In flow cytometry experiments, the dilute suspension of cells was instead fed through a precisely controlled flow chamber, where the instrument collected detailed data on each cell's GFP intensity and other spectral characteristics.

In principle, flow cytometry *should* be an ideal approach for analyzing population-wide data from environmental samples. As samples flow through the analytical chamber, each cell crosses an interrogation point, where it is excited with a laser. The cell's response to laser excitation is measured in several different parameters: forward-light-scattering (FSC) indicates the cell's size; sidescattering (SSC) indicates the cell's granularity or internal structural complexity; and the cell's fluorescence emission can be simultaneously measured in several different wavelengths (reviewed in Shapiro, 1995). High flow speeds allow rapid, massively high-throughput analyses. Millions of individual cells can be measured in minutes. The resulting datasets are readily analyzable, as they index detailed cellular data on millions of individual cells into a computer file. Furthermore, by incorporating multiparametric data on cell size, particle irregularity, and secondary (non-GFP) fluorescence, leaf surface debris and native leaf bacteria can in theory be excluded from analysis of GFP fluorescence intensity.

Flow cytometry is also a well-characterized, extensively used technique. As a result, there are abundant software tools and user facilities devoted to its use. Though the majority of these are geared towards immunological and mammalian applications, flow cytometry has also been applied to microbiological research—mostly for *in vitro* experimentation (Choe *et al*., 2005), but the literature also contains reports of its use with environmental samples such as activated sludge (Lenaerts *et al*., 2007), seawater (Manti *et al*., 2010), and plant surfaces (Rochat *et al*., 2010a, b). On first glance, it therefore seems that applying flow cytometry would be the speediest, best-supported, most precise approach to monitoring bacterial biosensor induction.

In contrast, epifluorescence microscopy is a powerful but inefficient approach. Although it has been used to monitor fluorescent bioreporters in the environment (Leveau *et al.*, 2001; Dulla *et al.*, 2008; Remus-Emsermann *et al*., 2010), it is a highly labor-intensive method and therefore precludes the large sample sizes permitted by flow cytometry. Where flow cytometry allows hundreds of millions of cells to be analyzed in an hour, microscopy requires days to analyze hundreds or thousands of cells. Similarly, although leaf debris and native bacteria can often be distinguished from biosensor cells in microscopic images, this segregation relies on subjective visual discrimination rather than the strictly quantitative parameters enabled by flow cytometric software. As such, it is both more labor-intensive and more difficult to maintain consistent standards across large experiments.

Microscopy, like flow cytometry, is widely used and well-supported on the UC Berkeley campus and many other research facilities. But though the facilities and software devoted to microscopic

analysis are sophisticated, they are not specifically designed to enable high-throughput, multiparametric particle analysis. For example, flow cytometry software automatically links the various fluorescence and light-scattering data collected from each individual particle; in contrast, microscopy requires laborious manual curation to properly align particles in multiple image exposures collected from different emission wavelengths. Once this is accomplished, measurement of GFP intensity is time-consuming, and subsequent data manipulation and re-analysis are difficult.

For all of these reasons, at the outset of this research flow cytometry seemed the obvious choice for the quantification of single-cell GFP intensity in recovered leaf bacteria. Needless to say, in practice the answer was not so simple. In the course of this research, both approaches were explored in an attempt to collect GFP fluorescence data from bacterial biosensors harvested from leaves. Though systematic, side-by-side comparisons of the two techniques were not performed, extensive experience with both nonetheless allows critical comparisons.

Each technique's ability to meet the following criteria was assessed:

> 1) Does the technique sensitively measure GFP fluorescence of bacteria? (How induced are the cells?)
>
> 2) Does the technique allow discrimination between biosensor bacteria and similarly sized debris and native leaf bacteria? (What proportion of cells is induced)?

As an extension of the second criterion, methods were also investigated to help distinguish the total population of bacterial biosensors recovered from leaves from other background particles. This was particularly necessary to measure weakly induced cells which emit only dim or no GFP fluorescence, as these are difficult to distinguish from native bacteria, debris, and other GFP-negative particles recovered from the leaf. While flow cytometry could, in principle, apply forward-scatter, sidescatter, and fluorescence gating to discriminate between particle subpopulations, in practice a more specific method was necessary.

Several different approaches were eveluated. Co-expression of a second, constitutive fluorescent marker in GFP biosensor cells was particularly appealing, as it would require minimal staining or post-harvest manipulation of samples. A variety of red-shifted fluorescent reporter constructs have been developed, including mRFP1 (Campbell *et al.*, 2002), mCherry (Shaner *et al.*, 2004), and dsRed.T3_S4T (Sorensen *et al.*, 2003); the ability of each to distinguish biosensor bacteria from background particles was tested. Fluorescence *in situ* hybridization (Amann *et al*., 1995) and cell-specific labeling with fluorescent antibodies (McCarthy *et al*., 2011) are also commonly used strategies to identify target cells from complex populations. Though more commonly used in cultured samples, counterstaining with cellular stains such as the membrane dye FM4-64 (Pogliano *et al*., 1999) or nucleic acid-specific DAPI (Sgorbati *et al*., 1996) can also be used to identify cells. Each of these approaches was evaluated for specificity, signal intensity, and spectral compatibility with GFP and the available optics.

Materials and Methods

Culture Conditions

For routine culturing, all bacteria were grown in LB liquid or agar medium, with antibiotics as appropriate (Kanamycin C_F=50µg/mL, Tetracycline=15µg/mL, Rifampicin=100µg/mL, Natamycin=43µg/mL). *E. coli* were grown at 37°C, *P. agglomerans* at 28°C.

Dose-response experiments with bacterial biosensors were conducted as described in Leveau *et al.* (2001). Briefly, biosensors were grown to mid-log phase in liquid M9 minimal medium (Miller *et al.*, 1972) supplemented with 0.2% casamino acids and 0.4% galactose. At the start of the experiment, cells were washed once with 10mM phosphate buffer (pH=7.0) and inoculated into fresh M9 amended with 0.2% casamino acids, 0.4% galactose, and fructose as appropriate; cell fluorescence was then measured at the indicated timepoints.

Plant Inoculation and Harvest

In plant inoculation experiments, a single, freshly streaked colony was inoculated into Minimal-A medium (Miller *et al.*, 1972) amended with appropriate antibiotics, 0.4% Galactose, and 2.5mM tryptophan. The inoculum was grown overnight with shaking at 300rpm, then resuspended at a final concentration of 10^7 cells/mL in 100mM KPO_4 buffer. Healthy, 2-3-week-old Blue Bush Bean plants with undamaged leaves were spray-inoculated until water ran off the ab- and adaxial surfaces of all leaves. Each plants was then loosely covered with a plastic bag fastened at the base with a rubber band (to maintain humidity) and placed in an illuminated growth chamber at room temperature.

After the designated incubation period (usually 7 or 24h), bacteria were harvested from leaves. For microscopy analysis, two healthy primary leaves were chosen from each pot, severed, and immersed in 20mL of KPO_4 buffer; for flow cytometric analysis 15-20 leaves were immersed in a beaker of 200mL KPO_4 buffer. Leaves were sonicated for 5 minutes, vortexed for 30 seconds, removed, and discarded.

Others have used filtration to concentrate cells isolated from environmental samples (Goyal *et al.*, 1980). However, preliminary attempts to use this method for leaf surface samples produced relatively high levels of background debris—particularly bacterial-sized, red autofluorescent particles presumed to be chloroplasts (data not shown). Cell concentration was therefore performed via centrifugation for all experiments shown.

To concentrate cells, leaf washate was centrifuged at 5000 x *g* for 10 minutes at 4°C. The supernatant was removed by pipetting, and the pellet resuspended in approximately 2mL of KPO_4 buffer. To remove leaf debris, each sample was syringe-filtered through a 5µm TMTP filter (Millipore Isopore filter, CAT# TMTP02500). Filtered samples were once again concentrated by centrifugation at 5000 x *g* for 10 minutes at 4°C. (At this step, microscopy samples were resuspended in 25µL KPO_4 buffer and stained with 4',6-diamidino-2-phenylindole [DAPI, C_F=2.5µg/mL] for 10 minutes in the dark at room temperature, then snap-frozen on dry ice before fixation.)

To fix, 1mL of 4% paraformaldehyde was added to samples, which were then stored overnight at 4°C, washed with KPO_4 buffer, and resuspended for analysis. To prevent sample degradation, all samples were analyzed via microscopy or flow cytometry within one week of harvest.

Flow Cytometry

The majority of flow cytometric analyses described were performed on one of two instruments. The first was a Beckman-Coulter EPICS XL flow cytometer equipped with a 488nm, 15mW argon laser. On this machine, GFP fluorescence was detected with a 525nm band pass filter (FL1), orange-red fluorescence using a 575nm band pass filter (FL2), and red fluorescence using a 620nm (FL3) band pass filter. Data were analyzed using EPICS-XL data acquisition and display software, version 1.5. The second instrument used was a Partec CyFlow small-particle analyzer equipped with 480nm and 405nm lasers. GFP fluorescence was detected with a 520nm band pass filter (FL1) and red fluorescence using 570nm long-pass filter (FL2). Data were acquired and analyzed using FloMax software. Additional samples were analyzed on a Beckman-Coulter EPICS Elite cell sorter and Cytopeia INFLUX cell sorter. Post-acquisition analysis and data visualization was performed in FCS Express (Version 3, DeNovo Software,).

To ensure sensitive detection of bacteria, gain settings were always adjusted to ensure optimum separation and identification of bacterial subpopulations. Except where indicated, fluorescence was collected using logarithmic signal amplification, and gain was set such that 99% of non-fluorescent control bacteria fell within the first decade of a single-parameter fluorescence histogram; cells exceeding this threshold were considered GFP-positive. For samples harvested from leaves, a constitutive GFP-positive control strain was used to identify the biosensor cell population in each experiment: by selectively gating on GFP-positive fluorescent events, the biosensor cell subpopulation was identified from a complex mix of particles on the FS/SS scatterplot. A gate was drawn around this putative biosensor population, and all subsequent analysis of leaf washate samples restricted to this defined subpopulation.

Microscopy

Fixed, DAPI-stained cell samples were diluted as appropriate, spotted onto ProbeOn Plus (Fisher Scientific, cat#22-230-900) slides in 20µL droplets, and air-dried in the dark at 37°C for 30-45 minutes. Samples were then covered with Aqua PolyMount anti-fade mounting reagent (Polysciences, cat#18606) and a #1 cover slip. Bacteria were viewed and photographed at 1000x magnification using a Hamamatsu digital camera attached to a Zeiss AxioImager M1 microscope. Samples were excited using a broad-spectrum mercury arc lamp, and visualized using standard DAPI and EndowGFP filter cubes. To ensure sensitive detection of bacteria, exposure times were adjusted to ensure that relative pixel intensity did not exceed ≈3500 in maximally induced samples (to avoid saturation) and negative control cells exceeded 100 (to ensure detection of dimly fluorescent cells). Typical exposure settings ranged from 200-300ms for DAPI and 3000-500ms for GFP; the same exposure settings were used throughout a single experiment. Optimum views, in which cells were abundant but not clumped together, were chosen to be photographed. For each treatment, 5-25 images were acquired using iVision software. For each view photographed, tandem DAPI and GFP images were captured using the Multi-D Acquire function.

Image Processing

Where specified, images were corrected for uneven illumination or optical irregularities across the image field using the iVision FlatField function (BioVision, 2010). Control images were acquired during microscopy by photographing one dark image with the shutter closed, and one empty image with the shutter open; images were acquired using the same exposure settings and filters as the experiment. Using these blank images, the iVision software creates an image mask

to correct any pixel variability detected in the blank image, then applies the mask to each data image. This FlatField image correction was performed by applying the "Image Ratios" function to every DAPI and GFP image in the experiment prior to subsequent GFP intensity analysis.

For all images, bacterial cells were identified by using the iVision Segmentation or Autosegmentation function to separate DAPI-stained cells from the background. The resulting segment mask was copied and pasted onto the corresponding GFP image. Where specified, the image mask was manually aligned with the underlying image. Mean GFP pixel intensity of each segmented cell object was quantified using the iVision "Measure Segments" function.

Where specified, images were corrected for background fluorescence by haphazardly selecting three dark background segments within the image. Mean pixel intensities were calculated for each background segment using the "Measure Segments" function, and a mean image background intensity was calculated from these values. Within an image, mean image background intensity was subtracted from the mean GFP pixel intensity of each segmented object, thereby generating a background-adjusted fluorescence value for each cell.

Pixel intensity data were imported into Statistica (Version 9.1, StatSoft), which was used to generate basic descriptive statistics, histograms, and normal probability plots.

For co-localization analysis, images were analyzed using the Imaris software. The co-localization function was used to analyze red and green fluorescence in separate channels, and the Pearson correlation constant calculated to assess the degree of pixel overlap.

Cell Staining

Where specified, fluorescence *in situ* hybridization was performed as described in Lenaerts *et al.* (2007). Briefly, bacterial samples were resuspended at 10^8 or 10^9 cells/mL and fixed overnight in 4% paraformaldehyde. Samples were washed 3 times in KPO_4 buffer, resuspended in 1mL of 1:1 PBS:ethanol mix to permeabilize cells, and stored at -20°C. To stain, samples were thawed, resuspended in 200µL of hybridization buffer (900mM NaCl, 20mM Tris/HCL (pH=7.5), 0.01% SDS, 0-50% formamide as appropriate), and split into 2 tubes of 100µL each. Probe was added to one sample (C_F=5ng/µL) and H_2O to the other as a negative staining control. Samples were incubated at 46°C for 3 hours, then centrifuged at 8000x*g* for 5 minutes and resuspended in 500µL of fresh hybridization buffer. Samples were incubated for 20 minutes at 48°C, then centrifuged at 8000x*g* for 5 minutes and resuspended in 500µL of fresh washing buffer (900mM NaCl, 20mM Tris/Hcl (pH=8.0), 5mM EDTA, 0.01% SDS). Samples were incubated for 20 minutes at 48°C, then centrifuged at 8000x*g* for 5 minutes and resuspended in 500µL of cold PBS. Samples were stored in the dark at -20°C for <48 hours before processing with flow cytometry or microscopy. Oligonucleotide probes were conjugated to a 5' fluorescein probe for validation screens (Bioneer, USA), or a 5' DY480XL red fluorescent probe for use with GFP biosensor cells (Biomers.net, Germany).

Where specified, FM4-64 staining was performed by adding stain to cell suspensions to a final concentration of 1.5µM, then incubating samples in the dark at room temperature for 15 minutes. Cells were washed three times to remove excess stain (leaf-wash isolates were washed only once, to minimize sample loss), then fixed with 4% paraformaldehyde.

For antibody binding assays, TetraCore polyclonal rabbit anti-*Erwinia herbicola* IgG antibody was tested for agglutination activity against *P. agglomerans* strain 299R (pKTbla). Bacterial cells were incubated at 28°C with or without antibody, then wet-mounted onto microscope slides and visualized at 400x or 1000x.

Results and Discussion: Flow Cytometric Analysis of Fluorescent Biosensors

In an attempt to optimize flow cytometric analysis of bacterial biosensors harvested from leaves, two different machines were evaluated: a standard Beckman-Coulter EPICS XL and a Partec CyFlow small-particle analyzer. (Limited tests were also performed using Cytopeia INFLUX and Beckman-Coulter EPICS Elite cell-sorters.) For each of the two systems, a sample *in vitro* experiment was analyzed—typically a dose-response curve with a fructose-inducible fluorescent biosensor—in order to test the machine's ability to resolve small particles and detect GFP fluorescence under optimum conditions. Bacterial samples harvested from leaves were then analyzed in order to test the machine's ability to resolve cells from complex environmental samples.

Resolution of standard BC-EPICS XL flow cytometers is sufficient for in vitro*, but not environmental bacterial samples*

To test the machine's ability to detect bacterial samples, an *in vitro* time course experiment was performed in which the fructose-inducible bacterial biosensor *P. agglomerans* 299R (pFru46) was cultured with various doses of fructose for seven hours, and samples collected at regular intervals. All samples were analyzed in parallel using a standard laboratory fluorimeter and the EPICS XL flow cytometer, and the results compared.

The two methods produced broadly similar results. Negative controls and 0 hpi inocula were GFP-negative, while positive controls exhibited right-shifted, GFP-positive peaks throughout the experiment (data not shown). At the highest dose of fructose, the *Pa*299R (pFru46) biosensor cells were strongly induced by 2-3 hpi, as indicated by the significant rightward shift of biosensor cells' fluorescence intensity in the sample GFP histogram; cells exposed to lower doses of fructose experienced a lesser, dose-dependent induction beginning at 5.5 hpi (Figure 1).

This indicated that under *in vitro* conditions, the flow cytometer was able to collect informative GFP fluorescence data from bacterial biosensors. Despite this apparent success, closer inspection of the FSC/SSC plots suggested that the machine would be unable to resolve bacterial cells in complex environmental samples (Figure 1c). Even at maximum gain settings in the FSC and SSC channels, bacteria were visible only as a dense cluster of cells near the origin, at the limit of detection. Under clean culture conditions, when the only particles entering the flow cytometer were the cells of interest, this was no great obstacle—an inclusive gate could be drawn around every particle analyzed because few background particles existed. But in samples with many small contaminating particles, the ability to detect and exclude subpopulations of smaller, larger, or more irregular particles from the population of biosensor cells could be critical.

To test whether the EPICS XL possessed sufficient resolution to measure fluorescence from environmental samples, bean leaves were inoculated with phosphate buffer, wild-type *P. agglomerans* 299R, constitutively GFP-expressing 299R(pKTbla), or the fructose-inducible

biosensor 299R (pFru46). Bacteria were allowed to interact with the phylloplane for an appropriate amount of time, then harvested and analyzed by flow cytometry.

The results confirm the EPICS XL's unsuitability for environmental samples. FSC/SSC plots of the plant-harvested samples displayed a broad smear of particles, clustered primarily around the origin (Figure 2). The cytometer did enable crude distinctions between GFP-positive samples and GFP negative samples: both the pKTbla and pFru46 strains displayed rightward-shifted fluorescence peaks in the GFP histogram, while the buffer and WT 299R negative controls lacked GFP-positive peaks (Figure 3). However, in the pKTbla sample, which should contain only GFP-positive cells, the fluorescent cells were barely distinguishable from a significant population of GFP-negative particles. Modifying gating of the total particle population to select different areas on the FSC/SSC plot did not improve the specificity of the GFP intensity results (data not shown). Native bacteria and leaf surface debris therefore interfered with resolution of the positive control cell population; the pFru46 treatment was similarly obscured.

In the absence of a second fluorescent label to help resolve the inoculated cell population from background cells and debris, the EPICS XL was unable to sufficiently resolve bacterial biosensor cells. The machine's inability to logarithmically amplify FSC and SSC signals was particularly crippling, as it prevented segregation of particle subpopulations based on size and structural irregularity. The machine's flow chamber and optical array, which are optimized for much larger mammalian cells, also may have impeded accurate detection and measurement of leaf-surface bacteria.

The Partec small-particle analyzer possesses sufficient resolution to analyze biosensor bacteria from complex environmental samples

In contrast to the EPICS XL, Partec's CyFlow analyzer possesses several design features intended specifically for use with small particles. The machine permits logarithmic gain amplification on all channels, including FSC and SSC, which enhances resolution of signals from tiny bacterial cells. Its precision flow chamber is designed to minimize positional variation of particles flowing through the interrogation point, reducing signal variability that arises from bacteria tumbling askew through the path of the laser and optical measurement array. The optics are tentatively suitable for dual-fluorescence detection: a standard 520nm band-pass filter (FL1) for visualizing GFP, and a 570nm long-pass filter (FL2) for visualizing red fluorescence.

In order to evaluate the machine, an *in vitro* dose-response timecourse experiment was performed, as with the EPICS-XL. Two different fructose-inducible fluorescent biosensors were tested: *P. agglomerans* 299R (pFru46), which employs the faster-maturing, short-half-life GFP variant AAV (Andersen *et al*., 1998), and pFru44, which uses the stable GFP variant ASV. Each strain was cultured with various doses of fructose for seven hours, and samples collected at regular intervals.

Negative controls and 0hpi inocula were GFP-negative, while the *Pa*299R (pKTbla) positive control was weakly fluorescent throughout the experiment (Figure 4). Both biosensor constructs exhibited dose-dependent responsiveness to fructose. However, fluorescence appeared to accumulate more rapidly in the stable-GFP pFru44 reporter—particularly in the 167 and 16.7µM treatments, which reached maximal induction 2 hours earlier than the pFru46 bioreporter cultured in the same concentration of fructose. Once maximal fluorescence was reached, GFP

fluorescence was also maintained more stably in the pFru44 bioreporter strain. In part due to this stability, the lowest dose of fructose (1.67µM) was weakly detectable with pFru44, but not with pFru46. These observations conform to previous reports which quantified the effects of promoter strength, cellular growth, and GFP half-life on reporter induction activity (Leveau *et al.*, 2001).

These results indicated that the Partec CyFlow had sufficient resolution to measure GFP fluorescence of bacterial biosensors grown in culture. Furthermore, inspection of the FSC/SSC plots suggested that the cytometer's optics enabled much clearer visualization of complex samples: in contrast to the barely-visible cluster of cells at the EPICS XL's scatterplot origin, the Partec's logarithmic signal amplification settings rendered a discrete population of cultured bacterial cells identifiable, even at moderate gain settings (Figure 4e-f).

To evaluate whether the machine's superior optics could be successfully applied to an environmental sample of leaf bacteria, a leaf inoculation experiment was performed. Bean leaves were inoculated with either phosphate buffer, wild-type *P. agglomerans* 299R, constitutively GFP-expressing 299R(pKTbla), or the fructose-inducible biosensor 299R (pFru46). Bacteria were allowed to interact with the phylloplane for an appropriate amount of time, then harvested and analyzed by flow cytometry. As predicted from the culture-based experiments, FSC/SSC plots of the plant-harvested samples were able to resolve bacterial subpopulations of approximately the same size and granularity as cultured samples using only moderate gain settings (Figure 5). Sensitive detection of GFP fluorescence was possible, with GFP-positive cells of the pKTbla-expressing positive control and pFru46 biosensor visible as distinct, rightward-shifted peaks in the FL1 channel (Figure 6).

Despite this improved detection of sample cells with the Partec CyFlow, background contamination remained a problem. Fluorescent background was extremely low: only 1% of recovered wild-type *Pa*299R cells were GFP-positive (Figure 7f). However, nonfluorescent background was high. When leaves were inoculated with the constitutively GFP-positive strain *Pa*299R(pKTbla), GFP-negative particles nonetheless comprised 25.5-88.5% of the population recovered from leaves, even when gating selectively on the putative bacterial subpopulation (Figure 7a-e). This demonstrated that even with superior optics, size and granularity alone were not sufficient to distinguish biosensor bacteria from leaf debris and native bacteria.

Based on these results, the Partec was used to monitor shifts in reporter activity among the induced, GFP-positive portion of the bacterial population. However, as a result of significant and variable GFP-negative background, it was impossible to use flow cytometry to study GFP induction patterns of weakly fluorescent cells, or calculate induced-versus-uninduced cell ratios within the bacterial population. Given that such ratios are important to interpreting fluorescence data for both the sucrose- and fructose-inducible bacterial biosensors, this limited the scope of flow cytometric experiments.

Conclusion: Despite improved particle resolution, GFP-negative background contamination remains a problem

Flow cytometry remains a promising but ultimately problematic technique for single-cell fluorescence quantification. Though standard flow cytometers appropriate for mammalian work often lack sufficient resolution to process bacterial samples—particularly complex environmental samples—cytometers specialized for small-particle detection, such as the Partec,

are powerful tools for study of single-cell biosensor induction. Unfortunately, even such high-resolution cytometers suffer from several technical limitations.

Perhaps because of the machine's sensitivity, spurious background particles comprise a large proportion of the data collected, impeding quantification of dimly fluorescent or GFP-negative biosensor cells. In principle, an appropriate combination of secondary cellular fluorescence and complementary optics should allow separation of biosensor cells from background particles, but such a combination was not attained in the course of this research.

Flow cytometry does offer limited utility for observing the fluorescence of *induced* cells, as GFP-positive populations are clearly detectable when recovered from the leaf surface. Others have therefore exploited bacterial biosensors with high baseline fluorescence to measure broad shifts in fluorescence of biosensors recovered from roots grown in a soil-free, artificial system (Rochat *et al*., 2010*a*-*b*).

Unfortunately, even within this limited application, flow cytometry suffers from tradeoffs between the range and resolution of fluorescence detection. When operated in linear acquisition mode, the machine can collect detailed information about fluorescence distribution within a narrow range of sensitivity. However, biosensors from environmental samples typically exhibit a wider range of induction than can be captured in the linear range. When operated in logarithmic acquisition mode, the machine has a broad range of sensitivity and can measure 1000- or 10,000-fold shifts in fluorescence, permitting analysis of the full range of reporter induction. However, because the machine has a fixed number of detectors, increased range comes at the expense of decreased sensitivity: as a fixed number of detectors monitor a broader spectrum of induction, each detector must bin together a broader cohort of fluorescent cells. This erodes informative, fine-scale differences in GFP induction, particularly at the upper range of induction. Flow cytometry, though useful for detecting broad changes in GFP-positive populations, can therefore be poorly suited to monitoring subtle shifts in reporter activity.

Mindful of these limitations, flow cytometry was employed in a limited capacity to probe the behavior of strongly induced biosensors on the leaf surface. But in order to address the behavior of weakly induced or GFP-negative populations—a central goal of this research—alternative methods were explored to quantify single-cell biosensor induction.

Results and Discussion: Developing a Methodology for Digital Image Analysis

Due to limited equipment availability and the technical challenges of applying flow cytometry to debris-laden environmental samples, microscopy was investigated as an alternative tool to characterize environmental populations of bacterial biosensors. But before actual experimental data could be analyzed, an image processing method was developed to quantify GFP induction.

In order to develop the most efficient and accurate method to analyze microscopy data, a sample dataset was constructed from fluorescence microscopy images of *P. agglomerans* MX149 cells bearing the pKTbla plasmid, which encodes weak but constitutive GFP expression. Representative photographs were chosen to represent the 0-hour inoculum (5 images), and samples washed from bean leaves at 1 and 3 hours after inoculation (7 and 5 images, respectively). The objective was to develop an analytical method that correctly identified each

cluster of fluorescent pixels as a discrete object (segmentation), measured the mean fluorescence of the object, and compiled the fluorescence data for all the objects in a given image; for accurate quantification of fluorescence induction within a bacterial biosensor population, each segmented object ideally represents an individual bacterial cell. Images were analyzed using various digital processing methods in order to assess how cellular fluorescence data were affected by digital image manipulations including: segmentation method, size- and eccentricity-based exclusion of image objects, segment mask alignment, correction for background fluorescence, and flat-field correction for uneven microscope illumination.

Digital image processing: Size-dependent exclusion of particles improves cell analysis

Because DAPI segmentation is fully or semi-automated, selection errors often occur. For example, the software can pick out small patches of fluorescence attributable to debris or out-of-focus cells; it can also highlight cell aggregates, mistakenly identifying a huge raft of clustered cells as a single large object. Both errors distort experimental data. In the case of cell aggregates, other researchers have noted a "halo" effect, in which densely clustered cells display artificially elevated fluorescence due to their proximity to other bright neighbors (G. Dulla, pers. comm.). This suggests that large segmented objects (representing clumps of cells) will tend to have higher fluorescence—an observation supported by the positive correlation between segment size and fluorescence (Figure 10). Similarly, very small objects (particularly single-pixel objects) disproportionately tend to be GFP-negative debris, as determined both by the size-fluorescence correlation and by visual inspection of segmented images.

As a result, segmented objects were subjected to size-dependent exclusion as a method of excluding both tiny debris and large clusters of cells. Optimal microscopic images, in which cells were abundant and discrete (*i.e.* not clustered together, but scattered as single cells), were chosen from the 0-hour inoculum samples. The images were manually segmented to ensure optimum segmentation, and the resulting distribution of object sizes plotted on a histogram (Figure 8). Typical *P. agglomerans* cells were defined as segmented objects between 40-300 pixels in size—a range of values that covered 99% of the segmented objects, and which conformed to visual inspections of cell size. As a result, only objects within this range were included in analyses of GFP intensity; larger or smaller objects were excluded to omit multicellular clusters and debris.

Despite its potential advantages, size exclusion is not without concern, as it has the potential to distort population-wide fluorescence data. In inoculum samples, where segmented objects were primarily single cells, size exclusion had little effect on the distribution of fluorescent cells in the population (Figure 9). But bacteria shrink when inoculated onto leaves (Monier *et al*., 2003). This suggests that lower bounds of cell size based on *in vitro* cultured cells could inadvertently result in omission of many shrunken bacterial cells when applied to samples harvested from leaves. This omission is of some concern: assuming that cell shrinkage is a result of cellular stress, systematic exclusion of smaller cells could bias results towards leaf surface bacteria in relatively hospitable environments, while excluding cells from stressful microhabitats with marginal resources. However, the tradeoff of excluding smaller-sized objects is that fewer pieces of debris are admitted as data. Visual inspection of segmented images suggested that size-exclusion successfully disqualified many pieces of leaf debris that would otherwise have entered analysis (data not shown). This observation was confirmed quantitatively by comparing histograms of fluorescence data analyzed with or without size exclusion (Figure 9b-c). When all particles were included in the analysis, the leftmost column of the histogram represents a large

population of GFP-negative particles; if only particles that fell within the cell size boundaries were included in the analysis, nonfluorescent particles make up a relatively smaller proportion of the total distribution.

Size exclusion of objects outside of the defined cellular range also minimized size-dependent variability in fluorescence. Regression of object fluorescence against object area suggested that, in samples including all segmented objects, fluorescence increased significantly with object size (Figure 10). When cells <40 pixels or >300 pixels were excluded, this correlation was abolished or dramatically reduced in both the inoculum and leaf surface samples. It is unclear whether this was due to the omission of small, nonfluorescent debris; the exclusion of large, disproportionately fluorescent aggregates; or a combination of both. In either case, size exclusion minimizes distortion of fluorescence data.

An object area of 40-300 pixels was therefore used as an inclusion criterion for all subsequent analyses. Segmented objects outside of this area range were excluded.

Digital image processing: Object eccentricity does not discriminate cells from leaf debris

In addition to the size of each segmented object in an image, the iVision software package can calculate the "eccentricity", of each segment—a standard measure of shape irregularity, in which 0 is a circle and 1 is a line segment (Cappelleri *et al.*, 2010). As a 2-dimensional approximation of the flow cytometric sidescatter measure, the eccentricity parameter was investigated as a possible method to identify and exclude non-cellular debris.

To test whether eccentricity was a good predictor of noncellular debris, object irregularity was plotted against mean GFP for the sample dataset of constitutively GFP-positive cells. As debris were expected to be more irregular in shape than the fluorescent bacterial cells, a negative correlation was expected between fluorescence and eccentricity. Contrary to this expectation, a weak *positive* correlation existed between object eccentricity and fluorescence in the 0-hour inoculums (Figure 11). This may suggest that irregularly shaped, multicellular clusters at the upper range of the size inclusion limit exhibited slightly elevated fluorescence—possibly as a result of the "halo" effect. However, there was no significant correlation between eccentricity and fluorescence in samples harvested from leaves—the context in which debris exclusion is most relevant. As a result, eccentricity was rejected as a diagnostic criterion for cell identification, and eccentricity data were not collected in subsequent analyses.

Digital image processing: Autosegmentation contributes to significant edge-effects when calculating cellular GFP fluorescence.

Segmentation, in which DAPI-stained cells are identified against a darkfield background, is the most labor-intensive step of digital image analysis. Using sliders to select portions of a pixel-intensity histogram for each image, the user modifies the brightness threshold such that the selection mask conforms tightly to fluorescent cell boundaries visible in the image. Automation of this step would reduce processing time from hours to minutes. It would also impose uniform processing for each image, rather than the variable, subjective selection employed during manual segmentation. The sample dataset was therefore analyzed using both manual segmentation and iVision's Autosegmentation function, which automatically defines a segmentation mask based on program defaults.

Visual inspection of the resulting segment masks showed obvious differences: manual segmentation produced small segments that conformed tightly to the contours of each cell, while autosegmentation produced large segments extending beyond the perimeter of the cell to include dimly illuminated ("halo") portions of the surrounding background (Figure 12). As a result of these larger segments, autosegmented images contained fewer segmented objects to analyze (Table 1), and a corresponding increase in the number of very large objects (>300 pixels) as individual cells with bloated segment masks were absorbed into large clumps (Figure 12) Attempts to adjust the autosegmentation default settings in order to improve selection criteria were unsuccessful (data not shown).

In addition to reducing the number of individual cells detected during image analysis, autosegmentation also affected the distribution of cellular GFP fluorescence calculated from each image. At 0, 1, and 3 hpi, mean cellular fluorescence estimates were 16-25% lower when generated by autosegmentation than from manual segmentation (Table 1), presumably because inclusion of surrounding low-intensity background pixels during autosegmentation reduced the mean fluorescence of each object (Figure 13, Table 1). The lower selection threshold for object autosegmentation may also have led to erroneous inclusion of dimly stained background particles. For example, at 1 hpi, 31% of autosegmented objects had an MPI<500, while only 12% of objects had an MPI<500 when the same image was subjected to manual segmentation (Figure 13). The higher proportion of GFP-negative objects suggests that autosegmentation defaults permit inclusion of weakly stained, noncellular debris that are excluded by stricter manual segmentation.

The bloated segment masks produced by autosegmentation clearly produced edge effects, in which selection of surrounding background pixels reduces the mean fluorescence intensity of each object. If such edge effects uniformly reduced the mean fluorescence of all cell objects, their impact might be discounted. But as an object's radius increases, its area increases exponentially while its circumference increases linearly; edge effects can therefore be expected to reduce the calculated fluorescence of small objects more than that of large objects.

To test whether the segmentation method contributed to size-dependent distortion of GFP fluorescence intensity, object size was plotted against mean pixel intensity for the three timepoints in the dataset. When the images were analyzed via autosegmentation, a significant positive correlation between size and fluorescence was detected in all three samples (Figure 14). In contrast, when segmentation was performed manually, no significant correlation was detected in either of the leaf washate samples; though a significant correlation persisted in the inoculum sample, it was much weaker than that generated by autosegmentation. This supports the hypothesis that autosegmentation distorts cellular GFP fluorescence in a size-dependent manner and that, though laborious, manual segmentation minimizes edge effects.

Unfortunately, manual segmentation requires imposing slightly different thresholds in each image in order to achieve the best segment mask. (Attempts to define optimal thresholds in one image, then manually apply uniform settings to all images, resulted in wildly different image masks from one image to another; data not shown.) Though this element of subjectivity would normally be frowned upon as introducing variability, in this case judicious manual input enhanced the uniformity of segmentation across images, increasing uniformity of fluorescent estimates by eliminating edge effects.

Digital image processing: Manual alignment of the segment mask further reduces edge effects in fluorescence quantification

After the initial segmentation mask is created using the DAPI image as a template, it is pasted onto the GFP image in order to quantify the distribution of fluorescence intensity across the total cell population. Although tandem DAPI and GFP images of each view are automatically acquired in rapid succession, image drift can occur between one photograph and the next—particularly at 1000x magnification. Unfortunately, manually aligning the pasted segment mask with the underlying GFP image is the second most labor-intensive step of image analysis. To test whether it was worth the effort, the sample dataset was analyzed with and without mask alignment and the results compared. (All data were analyzed using manual segmentation on the DAPI image.)

Based on visual inspection, the majority of images required small adjustments to image alignment. Quantitative analysis of the resulting data reveals that such alignments exert a small but significant effect on fluorescence intensity distribution. As with the autosegmentation analysis, mask misalignment resulted in size-dependent edge effects. The misaligned segment inadvertently selected a crescent of dark background pixels along the rim of the segmented cell, reducing the mean fluorescence of the segmented object; this effect was magnified in larger cells, yielding a positive correlation between object size and mean pixel intensity (Figure 15). Compared to the unaligned samples, manual alignment obliterated any marginally significant correlation between size and fluorescence in the leaf washate samples; though a significant correlation persisted in the inoculum sample, it was further weakened by manual alignment.

The lingering correlation between size and fluorescence intensity in the inoculum sample could be an artifact of segmentation. When creating segments in the DAPI image, cell boundaries were established slightly within the region defined by staining, so that the pasted segment would fall inside the region of GFP fluorescence and omit any edges. However, in cases where DAPI staining was very bright and GFP fluorescence was very dim, the selected segment may have exceeded the zone of GFP fluorescence; this would exacerbate edge effects in dim cells more than in large cells. Alternatively, this positive correlation may represent a biologically relevant relationship. Larger cells, for example, may not have undergone recent cell division. Assuming that these cells had accumulated larger quantities of GFP protein than smaller, recently-divided cells, it could explain the weak positive relationship between object size and fluorescence intensity.

Digital image processing: Correction for background fluorescence provides minor enhancements to data quality

Previously published work using digital quantification of biosensor fluorescence reported correction for image background fluorescence (Leveau *et al*., 2001), to adjust for variability in basal fluorescence between different images. However, collecting background values and calculating the corrections adds several hours to each analysis. To test whether this step was necessary, the sample dataset was analyzed with and without background correction and the results compared. (All data were analyzed using object size exclusion, manual segmentation, and manual mask alignment.)

Mean background fluorescence was calculated for all images in the sample set, as well as images of *Pa*MX149 (pKTbla)cells from a separate experiment (Figure 16). In both experiments, mean background fluorescence was similar in all images of leaf-harvest samples, but significantly higher in the inocula; variance was heteroscedastic, and increased with mean background fluorescence (Table 2). Increased background fluorescence in inoculum samples was probably attributable to higher cell density in the field of view, which seemed to create a diffuse halo effect.

For each image in the sample set, mean background fluorescence was subtracted from the GFP fluorescence of every object analyzed. Histograms of background-corrected and uncorrected data were compared (Figure 17). Corrected samples displayed a lower mean fluorescence, as the subtraction of background fluorescence caused a linear decrease in each sample's population mean. However, correction for background fluorescence made no perceptible alteration to the distribution of GFP fluorescence: uncorrected and background-corrected histograms exhibited identically shaped distributions (as established by visual inspection of histogram distribution and normal probability plots) as well as nearly identical standard deviations, despite the shift in mean fluorescence. This suggested that background correction had minimal impact on the distribution of GFP fluorescence within a population.

Given that inocula from both experiments had systematically higher mean background fluorescence than samples harvested from means (probably as a result of halo effects from images with more densely packed cells), background correction did have a moderating effect on the relative GFP intensity of the 0-hour sample relative to samples harvested from leaves. As a result, background-adjusted analyses suggested that bacteria experience a slight increase in fluorescence when inoculated onto leaves, as previously reported (Remus-Emsermann *et al.*, 2009), rather than the steep decrease in fluorescence indicated by the uncorrected data. Within the sample dataset, this normalizing effect between timepoints was the principal advantage of background correction. In other experiments, however, some leaf sample images were occasionally found to have significantly elevated background relative to other samples within the treatment, or between treatments (data not shown). As a result, background correction was included as part of routine fluorescence analysis, despite its minimal impact on data in the sample set.

Digital image processing: Flatfield correction for uneven illumination provides minimal enhancement to data quality

In addition to variation between the background fluorescence of different images, artifactual variation can occur due to uneven microscope illumination or variations in the digital camera's acquisition of pixels across the field of view. When banding patterns of light and dark areas were noted in a supposedly uniform, blank image, the possibility of such artifactual variation was investigated.

To test for background variation in camera acquisition, a blank image was acquired with the camera shutter closed. The raw pixel intensity data were then exported and analyzed for systematic variations in fluorescence intensity. To test whether vertical bands were present in the image, the mean pixel intensity of each column was calculated and plotted in a scatterplot against column order; to test whether horizontal bands were present in the image, the mean pixel intensity of each row was calculated and plotted against row order (Figure 18). The results

suggest systematic variation: though intensity varied within a narrow range (pixel intensities fluctuated between 55-75 units), a clear vertical band of brightness occurred at the left edge of the negative-control images, and a relatively bright horizontal band across the middle. Because these images were collected with the shutter closed, this suggests that background excitation of the digital detectors in the camera introduce pixel intensity variation across the image field.

Assuming that bacterial cells were scattered evenly and randomly across all images, this systematic bias in pixel fluorescence intensity would be applied equally across treatments (and therefore controlled for). However, while bacterial distribution across each image is fairly random, it is not even; particularly in leaf-surface samples, bacteria are often clustered in one portion of the image. With only 5-15 images collected for each treatment, stochastic cell distribution into inherently dimmer or brighter regions in the camera's field of view in one or more pictures could potentially introduce errors into analysis of fluorescence distribution.

To correct for this possibility, the iVision FlatField correction function was explored. Two images were collected—one with the camera shutter closed, in order to measure background excitation from dark currents in the camera detector, and another with the shutter open, in order to measure variations in pixel intensity due to uneven illumination of the field of view. (Images were captured using the same exposure settings and filters as the experimental samples.) Based on these calibration images, the FlatField function automatically corrected background variations in pixel intensity for each image in the sample set. To characterize the effect of flat-field correction on bioreporter data, cell segmentation analysis was performed on uncorrected and flat-field-corrected sample images, and the resulting GFP pixel intensity data distributions were compared.

When the cellular fluorescence distribution of uncorrected images was compared to that of flat-field-corrected images, no difference was evident in the basic shape of the distribution (Figure 19). Correction did result in a uniform, linear downward shift of approximately 200 fluorescence units, but this shift appeared consistent between all images. It therefore appears that flat-field correction exerted no significant effect on the data, despite some minor optical distortions evident in the image field. Combined with the extra labor and time required to conduct this step, flat-field correction was therefore not used in routine data analyses. However, positive and negative control images were collected for each experiment as a precaution, and future researchers who wish to pursue similar techniques should be attentive to the possibility of optical distortions that make it necessary to apply flat-field correction.

Digital image processing: Semi-automation of microscopy image processing improves efficiency of analysis

Based on the results presented above, microscopy images were processed using manual segmentation, size-dependent exclusion of segmented objects, manual mask alignment, and correction for background fluorescence. Even though the digital camera introduced slight, artifactual variations in background pixel intensity, FlatField image processing was rejected as having minimal impact on data quality; depending on the level of background noise in a given microscopy system, however, this correction may be worthwhile.

Due to the manual steps required to achieve optimal image analysis, this approach was inherently slow and labor-intensive, particularly when applied to datasets comprising hundreds of images.

To speed the process, iVision macros were scripted to automate as many steps as possible (Figure 20). As a rule of thumb, scripting enabled segmentation data to be gathered from image files at a rate of roughly 100 images/hour.

Results and Discussion: Digital Image Analysis of Fluorescent Biosensors

After establishing a standard image processing method, the microscopic approach was evaluated for its ability to describe the distribution of GFP fluorescence intensity in *in vitro*-grown and leaf-inoculated biosensor cells.

Microscopic image analysis sensitively resolves GFP fluorescence of cultured bioreporter cells

To test whether microscopy was able to detect bioreporter fluorescence variation, an *in vitro* timecourse experiment was performed in which the fructose-inducible bacterial biosensor *P. agglomerans* MX149R (pFru46) was cultured with various doses of fructose, and samples collected at regular intervals.

As previously reported (Leveau *et al*., 2001), the bioreporter strain experienced transient, dose-dependent induction of GFP in response to fructose (Figure 21). From an uninduced 0-hour inoculum, the 0µM and 1.67µM fructose samples remained negative throughout the timecourse. The 16.7µM sample experienced a modest elevation in GFP fluorescence at 1hpi, but returned to GFP-negative status by 3hpi, as the fructose inducer was consumed. The 167µM sample experienced strong, rapid induction by 1hpi which persisted at 3hpi; at both timepoints the cells exhibited an unexpectedly bimodal fluorescence distribution, but the basic results correspond to those described in the initial characterization of reporter construct (Leveau and Lindow, 2001). These results place the sensitivity of microscopic quantification in line with that achieved by flow cytometry. Furthermore, the full range of sample induction was detectable using uniform exposure settings and a linear display axis, suggesting that the microscope's sensitivity and linear range of detection are both appropriate for use with bacterial biosensors.

Microscopic image analysis minimizes background contributions from native bacteria and leaf debris

After establishing that microscopy was capable of detecting small variations in GFP fluorescence in *in vitro* samples, the technique's ability to resolve complex environmental samples was tested. Bean leaves were inoculated with either *P. agglomerans* MX149 as a negative control, constitutively GFP-expressing MX149 (pKTbla) as a positive control, or the fructose-inducible biosensor MX149 (pFru46). Bacteria were allowed to interact with the phylloplane for an appropriate amount of time, then harvested and analyzed by microscopy.

Negative control samples were uniformly nonfluorescent at all timepoints, with only a few scattered objects above background fluorescence at 3hpi. In contrast, the MX149 (pKTbla) samples were weakly GFP-positive, with a log-normal (1, 3hpi) or normal (10hpi) distribution (Figure 22). Unlike flow cytometry samples, in which nonfluorescent background particles comprised a highly variable but significant proportion of the collected data, contaminating debris were minimal in microscopic analysis. Even after a small rise in the number of GFP-negative particles at 10hpi, nonfluorescent cells represent only 7.5% of the total cell fraction (compared to

5% at 1 hpi, and 4.6% at 3 hpi); these GFP-negative objects could represent native leaf bacteria, foliar debris, or biosensor bacteria that had lost the reporter plasmid. Though the plasmid is stably maintained in *Pa*299R, approximately 5% of cells appear to lose the plasmid after 4 hours' growth in culture (Leveau *et al*., 2001); it is therefore reasonable to assume that 2.5% of cells could lose the plasmid between 3 and 10 hours after inoculation on the leaf surface.

A broader comparison of constitutively fluorescent cells harvested from leaves at multiple timepoints across several independent experiments revealed slight variability in the proportion of GFP-negative particles. In several cases, the nonfluorescent particles simply appear to be the lowest-expressing cells of a normally or log-normally distributed, weakly fluorescent population (Figure 23b,d,and e-g), and are therefore unlikely to represent background particles. In other samples, there appears to be a distinct peak of GFP-negative particles (Figure 23a, c, and h), suggesting background contamination with debris, native bacteria, or bioreporter cells which have lost the plasmid. However, even in populations with small background peaks, GFP-negative particles typically make up less than 10% of the total cell population, compared to 25-88% of all particles in positive control samples measured by flow cytometry. Microscopy therefore appears to be a superior technique with regard to excluding non-biosensor particles from analysis.

Microscopic image analysis improves sensitivity to variations in the distribution of GFP intensity among bacterial biosensors isolated from bean leaves

Though it is a labor-intensive method that limits the number of cells analyzed to a few hundred per treatment, microscopy ultimately provides the greatest sensitivity to variations in single-cell GFP induction of bacterial biosensors. Using a carefully validated method to quantify cellular fluorescence using digital image analysis, expected patterns of biosensor induction were confirmed in both *in vitro* cultures and plant-inoculated cells. Perhaps most importantly, contaminating, GFP-negative background particles comprised less than 10% of positive-control samples; though not completely clean, this offers a significant advantage over flow cytometry in discriminating weakly fluorescent or GFP-negative biosensor cells from leaf debris and native bacteria.

Results and Discussion: Secondary Red Fluorescence for Total-Cell Identification

Distinguishing biosensor cells from background particles was a persistent challenge in flow cytometry and, to a lesser extent, microscopy. Various methods of distinguishing the target cell population were therefore explored. All of these techniques—including expression of three different red fluorescent proteins, cellular dyes, FISH staining, and a cursory attempt at antibody labeling—attempted to use red fluorescence as a secondary label to identify the total population of inducible-GFP biosensor cells (Table 3).

Red fluorescent proteins: mRFP1 suffers from quenching interactions with GFP

To test whether constitutive co-expression of mRFP1 with inductible GFP would be a feasible strategy for analysis via microscopy or flow cytometry, an *E.coli* strain was constructed bearing both of the compatible plasmids p519mRFP1 and pKLN42<Tet>, which encode constitutive expression of mRFP1 and GFP, respectively.

Cells were first visualized via fluorescence microscopy. Bright red or green fluorescence were clearly visible in the single-expressing positive control strains (Figure 24). But although both red and green fluorescence were detectable in the dual-expression strain, green fluorescence looked dim relative to the single-fluorescent GFP positive control. Quantitative analysis of mean pixel fluorescence intensity supported this observation (data not shown).

The same fluorescent cell samples were analyzed in parallel using flow cytometry. Although the standard BC and Partec flow cytometers lacked sufficient resolution or optical capacity for red-green dual fluorescence imaging, the flow cytometry facility had recently acquired a Cytopeia cell sorter equipped with both 488nm and 567nm lasers, and therefore capable of exciting both mRFP1 and GFP. Unfortunately, flow cytometric analysis confirmed the results obtained during microscopy: the machine could detect red or green fluorescence in both single-expression strains, but the dual-expression strain exhibited only red fluorescence (Figure 25).

Microscopic and flow cytometric analyses therefore suggested that mRFP1 and GFP are incompatible when co-expressed in a bacterial cell. Plasmid incompatibility is an unlikely explanation, as the two replicons—RSF1010 for p519mRFP, and pBBR1 for pKLN42<Tet>—are known to be compatible (Antoine *et al*., 1992) and dual-plasmid transformed strains exhibited antibiotic resistance to standard concentrations of both Tetracycline and Kanamycin, indicating maintenance of both plasmids.

Some form of fluorescence quenching or energy transfer is a more likely explanation for the observed spectral incompatibility. Anecdotal reports from staff of the CNR Bioimaging Facility support this interpretation (pers. comm., Denise Schichnes). Although the emission and excitation spectra of the two proteins appear distinct, the original paper characterizing mRFP1 describes a distinct, nonexcitatory *absorption* peak around 500nm—near the GFP 510nm emission maximum (Figure 26; Campbell *et al*., 2002). mRFP1 absorption of GFP fluorescence could account for the GFP quenching observed in the presence of mRFP1, though not for the slight increase in red fluorescence of the dual-expression strain. Forster resonance energy transfer (FRET) has been reported between GFP-mRFP1 and GFP–mCherry pairs, and could account for this increased brightness (van der Krogt *et al.*, 2008). Such FRET transfer would normally only be expected between proteins in extreme molecular proximity (30-60Å, Gadella *et al.*, 1999), but at high levels of expression bacterial cells may be sufficiently suffused with protein that such proximity is achieved. Alternatively, *gfp* and *mRFP* may interact to form toxic aggregates (Campbell *et al*., 2002; Lauf *et al*., 2001).

The quenching interaction between mRFP1 and GFP posed a frustrating dilemma: flow cytometry theoretically permits linear compensation to normalize quenching or other spectral interactions, but is not sensitive enough to detect the quenched fluorescence; conversely, microscopy is sensitive enough to detect diminished GFP fluorescence in the dual-expression strain, but does not allow linear compensation, making GFP an unreliable reporter of induction in dual-labeled strains.

Red fluorescent proteins: mCherry exhibits incompatibility with GFP

Another of the red fluorescent proteins tested, mCherry, also exhibited incompatibility with GFP. As before, when viewed under a microscope strains consitutively expressing either *mChe* or *gfp* were brightly red or green fluorescent, respectively (flow cytometric observation was not

performed). But based on visual inspection, strains stably expressing both proteins did not exhibit dual fluorescence—instead, cells looked either red or green.

These qualitative observations were evaluated quantitatively: colocalization analysis was performed on the dual-expression strain *Pa*299R (pKTbla)(p519mChe), which constitutively expresses both GFP and mCherry (Figure 27a). Colocalization was weak in the 1% brightest pixels (Pearson's coefficient=0.10), though colocalization rose to 0.47 in the 10% brightest pixels, and 0.808 in the 75% brightest. (A Pearson's correlation coefficient of 1 indicates perfect overlap and -1 indicates mutual exclusion; 0.5 is typically considered the threshold for significant colocalization (Zinchuk *et al*., 2008).) This pattern was even more pronounced in the dual vector *Pa*299R (pFru46)(p519mChe), which expresses constitutive mCherry and a fructose-inducible GFP reporter (Figure 27b). When grown under inducing conditions (167µM fructose, sampled at 3hpi), the brightest 1-10% of pixels possessed a Pearson's coefficient of 0.16, and the brightest 75% a coefficient of only 0.20. For both dual-expression strains, red/green fluorescence scatterplots confirm that most cells are either bright red or bright green, while cells that exhibit both forms of fluorescence are much dimmer. The nature of this incompatibility was unclear, but others report similar difficulties co-expressing *mChe* and *gfp* in *Pa*299R (M. Remus-Emsermann, Pers. Comm.).

Red fluorescent proteins suffer from low brightness and optical incompatibility with flow cytometers

Microscopes, with their easily swappable filter sets, permit flexible combinations of excitation and emission wavelengths; by lengthening exposure times, they also permit easy visualization of even very dim fluorescence. In contrast, the flow cytometers available for this research possessed a fixed and narrow repertoire of excitation and detection capabilities, making it challenging to find secondary fluorescent markers compatible with the lasers and filter sets installed in each machine. Additionally, rapid flow rates are maintained through the analytical chamber in order to achieve high-throughput analysis during flow cytometry—meaning that each cell is subjected to an exposure time of mere microseconds, reducing the machine's sensitivity to dim fluorescence. This is particularly problematic given that red fluorescent proteins often exhibit relatively low fluorescence relative to GFP (Campbell *et al*., 2002)

Poor excitation capability was a major impediment, as 488nm lasers were the sole means of excitation for both the Partec and EPICS-XL flow cytometers. While this wavelength efficiently excites GFP, it barely tickles the edge of either the mRFP1 or mCherry excitation spectrum (Figure 28; Table 4). Given that both of these red fluorescent proteins suffer low brightness and quantum yield even under optimum excitation at 585nm (Table 3), the weak excitation afforded by a 488nm laser made any red fluorescent signal extremely difficult to detect.

It was therefore unsurprising that flow cytometric detection of red fluorescence was minimally successful. When mRFP1 was constitutively expressed in *E. coli* (Figure 29) or *Pa*299R (Figure 30) on the plasmid pVSP61_KANmRFP1, a high-copy-number vector with a strong promoter, cells could be left to grow on a plate until they looked aggressively fuchsia to the naked eye; under these conditions, cells exhibited significant red fluorescence in FL3 and weak spillover fluorescence in FL2 when viewed with a flow cytometer. Fluorescence was weaker, but still detectable, when cells were sampled during logarithmic growth in liquid culture (Figure 31).

However, red fluorescence could never be detected in cells recovered from plants using either the Partec or EPICS-XL (data not shown).

In an attempt to evaluate whether other types of biosensors might be more amenable to flow cytometric evaluation, additional experiments were performed with *Pseudomonas syringae* B728a biosensors in an attempt to replicate successful, published biosensor results achieved via microscopy (Dulla *et al*., 2008). As with the *Pa*299R biosensors, *Ps*B728a-based biosensors exhibited minimal red fluorescence when observed with the flow cytometer, whether cells were grown *in vitro* or harvested from plants (data not shown).

The Partec and EPICS-XL cytometers permit minimal user control over basic machine functions that influence sensitivity to fluorescence, such as laser intensity and flow speed. In attempt to improve detection of red fluorescence, cells were therefore viewed using an EPICS Elite cell sorter. This allowed the operating technician to elevate laser intensity (to maximize excitation of red fluorescence) and slow flow speed (to maximize each cell's transit time, and therefore exposure duration, as it passed through the detector). However, neither adjustment improved detection of red fluorescence (data not shown).

Attempts to view red fluorescence were repeated when the flow cytometry facility acquired a new Cytopeia INFLUX sorter, which boasted a second laser (575nm) dedicated to excitation of red fluorescence, as well as an expanded repertoire of detectors. Though the new sorter possessed overall sensitivity and resolution similar to the Partec, with strong discrimination of the leaf microbial subpopulations in FS/SS and good detection of GFP, it was only able to detect minimal red fluorescence of cells grown in liquid culture, even in strongly overexpressing red fluorescent strains (Figure 25). (In contrast, fluorescence of the same cells was easily detectible with microscopy). Red fluorescence was not detected in cells harvested from plants.

Based on these results, it was concluded that even under optimal excitation and detection conditions, a combination of small bacterial cell size, low absolute protein quantities, and the inherently low quantum yield and brightness of mRFP1 render the protein only marginally detectable by flow cytometry under optimum culture conditions, and undetectable in environmental samples.

Red fluorescent constructs exhibit cellular toxicity

Due to mChe and mRFP1's apparent quenching of GFP, low brightness, and spectral incompatibility with available flow cytometers, neither protein was suitable for flow cytometric applications. Reports of an improved red fluorescent protein suitable for flow cytometric applications were therefore intriguing. Sorensen *et al* (2003) described a dsRed derivative efficiently excitable at 488nm (the same wavelength as GFP) but with strongly right-shifted emission, making it compatible with standard flow cytometric optics. It was also reported to be brighter than other red fluorescent protein variants.

Promisingly, the *E. coli* host strain bearing pGMR7, a constitutive T3_S4T expression plasmid, exhibited robust red fluorescence based on visual inspection, microscopy (data not shown), and flow cytometric evaluation with the EPICS-XL (Figure 29). However, red fluorescence was weaker when the construct was transformed into the *Pa*299R biosensor strain (Figure 30). Additionally, the bacteria exhibited frequent, spontaneous inactivation or loss of red

fluorescence, even when freshly streaked from freezer stocks (Figure 32). Attempts to transform a high-copy-number vector with strong constitutive expression of *dsRed.T3_S4T* into *P. agglomerans* repeatedly failed to yield transformants. Though reportedly nontoxic in *E. coli, Salmonella enterica* (Sorensen *et al*., 2003), and *Pseudomonas fluorescens* (Dandie *et al.*, 2005), these observations suggested that T3_S4T was nonetheless toxic in 299R.

Though toxicity was much less pronounced, there was also evidence of reduced fitness in cells strongly expressing the *mCherry* protein. mCherry-expressing cells appeared to grow normally in culture, but when separate 299R strains expressing either constitutive *mChe* or *gfp* were coinoculated onto bean plants, the recovered green fluorescent cells grew normally, while recovered red fluorescent cells failed to form colonies. In contrast, platings of both inocula grew normally. (Pers. Comm., Adrien Burch) This suggests that though strong overexpression of *mRFP1* may not impair cell growth under culture conditions, it may reduce cell fitness under stressful conditions such as epiphytic growth on plants.

Though high-copy expression of *mChe* was unsuccessful under the experimental conditions tested here, mCherry may prove useful in other systems. In particular, a Tn7-based system for introducing targeted, single-copy genomic integrations of *mChe* has been successfully used to label several species of *Pseudomonas, Burkholderia,* and other bacteria for microscopic evaluation (Tecon *et al.*, 2009; Lambertson, pers. comm). When Tecon *et al*. used an *mChe*-marked *Burkholderia sartisoli* strain as a host for an inducible GFP biosensor of polycyclic aromatic hydrocarbons, they observed no apparent interference between red and green fluorescence, and reported no toxicity (2009). Their success may have been attributable to higher tolerance of their reporter strain to fluorescent protein accumulation; alternatively, genomic integration of the *mChe* gene may have relieved any plasmid incompatibility suffered here, or weak expression from the singly integrated gene copy may have proven less toxic. However, Emsermann *et al*. report that when a similar strategy was employed in *Pa*299R, Tn-7-mediated genomic integration of *mChe* yielded undetectably low fluorescence; only late stationary-phase cells exhibited detectable levels of red fluorescence (Pers. Comm.). So despite the promise of low-copy genomic integration in some bacterial strains, mCherry does not appear to be a feasible approach in *Pa*299R biosensor strains.

FISH staining: Design and optimization of a P. agglomerans*-specific FISH probe*

After unsuccessfully attempting to co-express a variety of red fluorescent proteins with GFP, we sought to avoid toxicity and incompatibility issues by exploring an alternative method to fluorescently label bacterial biosensors in a cell-specific manner. Unlike red fluorescent proteins, which exhibit restrictive spectral properties, synthetic fluorophores are available to suit a wide range of excitation and detection wavelengths. This made fluorescence *in-situ* hybridization an appealing possibility for secondary fluorescent labeling, as oligonucleotide probes can be conjugated to a variety of commercially available fluorescent tags.

Before testing the viability of FISH as a staining strategy to distinguish between inoculated biosensor cells and native leaf bacteria, an appropriate probe first had to be identified. Brandl *et al.* (2001) previously visualized *P.agglomerans* 299R during microscopy using the fluorophore-conjugated DNA oligo Eh299R. But based on reports of improved design algorithms for FISH probes (Kumar *et al*, 2005; Kumar *et al.*, 2006; Hugenholtz *et al*., 2001), the possibility of identifying a superior oligo sequence was also investigated.

Because no record existed of the 16S sequence used to design the original probe, *Pa*299R rDNA was re-sequenced using standard 16S primers 27F (5'-AGAGTTTGATCMTGGCTCAG-3') and 1525R (5'-AAGGAGGTGATCCAGCC-3'). The resulting sequence clustered with other strains of *P. agglomerans* and *P. anantis* when analyzed by BLASTn (Altschul *et al*., 1997) and comparison to the ARB database of bacterial 16s sequences (Ludwig *et al.*, 2004). The query sequence exhibited 99% similarity to other *Pantoea anantis* and *Pantoea agglomerans* entries, confirming the strain's identity. Interestingly, the existing Pa299R probe did not hybridize within the sequenced region, suggesting the presence of a second 16s gene in the 299R genome (Conville *et al.*, 2007), from which the original probe was presumably designed.

When the ARB 16s alignment and FISH probe design modules (Ludwig *et al.*, 2004) proved intractable, candidate probe sequences were generated and evaluated manually. Using the MegAlign function of the DNAStar sequencing software package (DNAStar, Inc.), the newly sequenced 16s gene was aligned with a reference sequence of *E. coli* K-12 DSM 30083 that was previously annotated to indicate experimentally determined regions of probe accessibility (Fuchs *et al.*, 1998). Due to the close phylogenetic relationship between *P. agglomerans* and its fellow enterobacter *E. coli* (Toth *et al.*, 2003), the reference sequence was expected to serve as a reliable template for identifying regions of the 16s structure that are accessible to FISH probe hybridization. Based on manual identification of accessible, homologous 16s regions within the 299R sequence, 7 candidate probes were designed (data not shown). The phylogenetic specificity of each probe was then checked using the ProbeMatch database (Loy *et al*, 2007), and probes with broad hybridization specificities were rejected. This analysis yielded one novel *P. agglomerans*-specific probe, named PAG299R-579, targeted to a putatively accessible region of the 16s rRNA subunit and with hybridization specificity concentrated in the *Erwinia* spp. and *Pantoea* spp..

In addition to the original Pa299R and newly designed PAG299R-579 probe, four additional candidate probes were identified based on published reports: PAG59 (Nakanishi *et al*., 2006), Enterobact D (Ootsubo *et al*, 2002), Ent* (Kempf *et al*, 2000), and Ent183 (Friedrich *et al*, 2003).

All six 5' fluorescein-conjugated oligonucleotide probes (Table 5) were tested for hybridization efficiency and specificity by staining the 299R target strain and an unrelated negative-control strain (*Pseudomonas syringae* B728a) under a range of hybridization stringencies. Cell fluorescence was then measured by flow cytometry with the Partec CyFlow. For each probe, the percentage of positively labeled cells was identified relative to an unstained control (Figure 33). Pa299R and PAG59 demonstrated the greatest hybridization specificity, identifying 6-10% of *Pa*299R cells under optimum hybridization conditions, but only 1% of the *Ps*B728a negative control cells. Cells labeled with these probes also exhibited the highest mean relative fluorescence (data not shown). The remaining probes exhibited only weak hybridization to the target strain.

Based on these results, subsequent FISH experiments were conducted using the previously published Pa299R probe.

FISH staining: FISH staining of bacteria from leaves provides modest power to distinguish inoculated populations from background particulates

To determine whether FISH staining could distinguish bacterial biosensor cells from background debris, the 5' DY480XL-conjugated Pa299R probe was used to stain bacteria harvested from bean leaves (Table 3). Sample fluorescence was then quantified via flow cytometry.

When constitutively GFP-expressing *Pa*299R (pKTbla) cells were stained with the Pa299R probe, the proportion of green cells that were also red rose from 10.4% in the unstained control to 57.6% (Figure 34). Similar values were achieved in an independent replicate experiment (data not shown), suggesting that approximately 50% of biosensor cells recovered from leaves can be identified by FISH staining. Based on staining of a mock-inoculated negative control sample, the FISH probe produced minimal background staining of native leaf bacteria and debris. However, background staining did occur in a B728a-inoculated negative control, with 7.3% labeled positive in the stained sample, compared to 0.4% in the unstained control. These results were roughly in line with those of *in vitro* staining experiments, where staining of B728a negative control samples labeled approximately 10-17% as many cells as staining of the target 299R samples.

By applying more stringent gating, it would be possible to measure GFP expression among only the most brightly FISH-labeled cells, thereby omitting weakly stained false positive events. Kalyuzhnaya *et al.* (2006) adopted this approach when using flow cytometry to identify methylotrophic bacteria from lakewater sediment samples, selecting only the brightest 0.2-2% of stained cells. However, while this approach would omit most background contamination, by omitting dimly stained cells it would also systematically exclude a large proportion of the biosensor cell population. Given that rRNA hybridization intensity is positively correlated with bacterial growth (Leveau *et al.*, 2001), systematic exclusion of dimmer, less active cells contradicts the basic aim of single-cell biosensor monitoring, which is to examine the distribution of reporter activity across the *entire* cell population. The conditions experienced by cells at the environmental margins—the same dimly stained cells that would be excluded by stringent gating of FISH-stained samples—may be the exact conditions most relevant to research. So although FISH offers modest success at distinguishing biosensor cells from background, it demands difficult tradeoffs.

In addition to questions regarding the functional specificity of the available FISH probe under environmental conditions, concerns also arose regarding the effect of FISH staining on GFP fluorescence. FISH protocols, which require permeabilization of bacterial cells, have been reported to reduce GFP fluorescence by up to fourfold (Remus-Emsermann *et al.*, 2010; Leveau *et al.*, 2001). In our leaf inoculation experiment, FISH staining reduced the fluorescence of GFP-positive control cells to an average of 79% that of unstained controls. The possibility that FISH staining could reduce sensitivity to bioreporter fluorescence is therefore a concern in both flow cytometry and microscopy.

Labeling with fluorescent-conjugated antibodies

Given the equivocal results yielded by FISH labeling, we explored fluorescent-conjugated antibodies as an alternative method to achieve cell-specific fluorescent labeling. A commercially available polyclonal rabbit α-*Erwinia herbicola* antibody (TetraCore) was identified. To test whether the antibody would bind to the *Pa*299R biosensor strain, an agglutination assay was conducted: cultured, constitutively fluorescent bacterial cells were incubated with the antibody *in vitro*, spotted onto a microscope slide, and then inspected with a fluorescence microscope for the

appearance of cross-linked cell rafts that indicate antibody binding. No cell clumps were consistently visible (a single cluster formed in the 0.03ng/µL treatment, but was not repeatable), suggesting that the antibody failed to bind to the biosensor strain (Figure 35). This may be a result of imprecise naming of bacterial species; *P. agglomerans* was formerly called *Erwinia herbicola*, but was reassigned to *Pantoea* on the basis of 16S sequence (Kado, 2006). The antibody may therefore have specificity for *E. herbicola* rather than *P. agglomerans.* TetraCore was unable to provide information regarding which strain of *E. herbicola* was originally used to generate the antibody, but the polyclonal anti-*E. herbicola* product they carry appears unable to bind *Pa*299R.

Although future identification of an antibody specific for the biosensor strain could enable fluorescent labeling, experiments were discontinued upon discovering that the most immediately available antibodies did not possess the required specificity. The technique certainly bears further exploration if an appropriate commercial antibody reaches the market. Alternatively, *Pa*299R-specific polyclonal or monoclonal antibodies could be custom-generated for this purpose.

Nonspecific Cell Stains: FM4-64, DAPI

Difficulties with endogenous expression of red fluorescent constructs prompted investigation of other methods to distinguish bacterial biosensors from background particles. As an alternative, we first explored the possibility of fluorescent-conjugated molecular labels such as anti-*Pa*299R antibodies and FISH oligo probes, hoping that these approaches might yield both improved fluorescence and high specificity for the target cells. Unfortunately, neither approach appeared promising. We therefore went on to explore whether FM3-64, a nonspecific cellular stain, would aid in discriminating biosensor signals from background noise.

FM4-64 is a red-fluorescent, amphiphilic styryl dye commonly used to stain bacterial membranes (Doctor *et al.*, 2002). It is a nonspecific stain, so it was unclear how useful it would be in distintinguishing between biosensor cells and debris. If the majority of background particles represent dust and non-membraneous debris, then FM4-64-stained particles would be highly enriched for experimental biosensor cells. If, however, background particulates comprise native leaf bacteria or membraneous cell debris, then FM4-64 staining would not usefully discriminate between signal and noise.

We first conducted an *in vitro* experiment to determine whether FM4-64 staining would aid in biosensor cell identification under ideal conditions. *Pa*299R cells or *Pa*299R (pKTbla) cells grown in liquid culture were stained with FM4-64 and compared to unstained controls using flow cytometry. In both strains, the red-fluorescent cell population went from <2% in the negative controls to 90-97% in the stained samples (Figure 36). This demonstrated that FM4-64 staining was visible by flow cytometry, and could effectively identify target cells in pure culture.

To test whether FM4-64 staining would be useful in environmental samples, bacteria were spray-inoculated onto bean leaves, harvested after 24 hours, and split into stained and unstained treatments. Unfortunately, in this experiment FM4-64 staining did not have the clear-cut discriminatory power observed in *in vitro* experiment: when analyzed by flow cytometry, red fluorescence of stained samples was only modestly higher than unstained samples (Figure 37).

Nonspecific staining of biosensor cells was therefore abandoned as a flow cytometric approach. Another nonspecific bacterial stain, DAPI, was employed to counterstain fluorescent bioreporter cells for microscopy, based on standard protocols communicated by others using similar techniques (A. Burch, M. Remus-Emsermann, Pers. Comm.). However, DAPI was never evaluated experimentally in a flow cytometric context.

Conclusion: Secondary fluorescence was a lost cause, at least in my experimental system

Constitutive expression of three different red fluorescent constructs (*mRFP1*, *mCherry*, and *dsRed_T3.S4T*) was plagued by dim fluorescence, cellular toxicity, spectral or expressional incompatibility with GFP, and the optical constraints of the available flow cytometers. Other labeling techniques, including a commercially available α-*P. agglomerans* antibody and the FM4-64 membrane dye, lacked sufficient specificity to recognize or distinguish the biosensor cell population from background. FISH labeling of leaf surface samples offered some ability to resolve bacterial cells from background debris, but suffered from background staining and additional concerns about the possibility of lost GFP fluorescence as a result of the labeling process. Although these approaches to secondary fluorescence might succeed with further optimization or in a different experimental system (particularly FISH staining, if slight loss of GFP intensity is not a concern), such optimization extended beyond the scope of the present research.

Conclusions

Single-cell quantification of bacterial biosensors remains a challenging endeavor. Although both flow cytometry and microscopy can be applied to the task, each approach suffers unique strengths and weaknesses. Flow cytometry with high-resolution machines such as the Partec CyFlow or Cytopeia offers high throughput, massive sample sizes, and quick processing times; however, it is hampered by high levels of background leaf debris as well as tradeoffs between high linear sensitivity and logarithmic detection range when characterizing the distribution of fluorescence within a population. In contrast, microscopy provides high sensitivity, sufficient range of detection, and lower levels of GFP-negative background; unfortunately, it is massively labor-intensive, slow, and provides relatively tiny sample sizes—weakening the statistical power of any resulting analysis.

In the research detailed throughout this dissertation, the two techniques were therefore employed to complement each other as best as possible: microscopy was used to make detailed observations of fluorescence distribution within smaller samples, while (when possible) flow cytometry was used to make broader observations about GFP-positive or brightly FISH-stained subpopulations using larger sample sizes. For each technique, methods were established to maximize accuracy and throughput.

In the future, flow cytometry might be of greater use in experimental systems that employ bioreporter cells with high basal fluorescence, particularly to detect relatively large changes in cellular GFP fluorescence. Rochat *et al*. (2010*a*) recently exploited this approach to characterize the strength of GFP bioreporter induction on roots of different plant species. Unfortunately, the p61RYtir and pFru46 sugar biosensors used in this research have low basal expression under

non-inducing conditions—traditionally a good characteristic for discriminating between induced and uninduced cells, but in this case making it difficult to distinguishing dim, uninduced cells from debris.

Both flow cytometry and, to a lesser extent, microscopy would benefit from a method that allowed constitutive secondary labeling to identify the total biosensor cell population. Such labeling would overcome difficulties resolving dimly fluorescent or GFP-negative biosensor cells from leaf debris and native bacteria. Unfortunately, a variety of techniques ranging from constitutive expression of three different red fluorescent proteins, FISH labeling, membrane dyes, and a cursory attempt at antibody labeling, proved inadequate for this task.

Some of these strategies for red fluorescence could eventually prove useful in a different experimental system. For example, despite concerns surrounding individual probe specificity, FISH staining could prove a generally useful technique for secondary cell labeling in flow cytometry. This is particularly true if probe brightness and specificity could be further maximized, or if systematic exclusion of dimly stained cells is an acceptable compromise within the given experimental system. FISH is already broadly applied for cell identification in microscopy (Leveau *et al*., 2001), though reports of diminished fluorescence as a result of the staining process suggest that the technique may be most suitable when used with a brightly fluorescent bioreporter, or when strongly induced subpopulations are of primary interest.

Similarly, single-copy genomic integration of *mCherry* could make a useful marker for microscopy with pseudomonads—though given the incompatibility observed here between the two fluorescent proteins, it would be prudent to confirm that low levels of mCherry expression do not interfere with quantitative detection of GFP reporter activity. Additionally, dsRed.T3_S4T possesses enhanced brightness and desirable spectral qualities relative to other red fluorescent proteins, making it attractive as a potential marker for flow cytometry. Although it proved toxic to the *Pa*299R strain used throughout these experiments, researchers have reported it to be nontoxic in other bacterial species.

Unfortunately, such optimization falls to future efforts, as it extended beyond the scope of the present research.

Acknowledgments

Great thanks to Steve Ruzin and Denise Schichnes, of the College of Natural Resources Biological Imaging Facility, for their instruction and advice on fluorescence microscopy and the IVision software package; also to Mietche Remus-Emsermann for his helpful suggestions on microscopic image analysis of biosensor cells. Thanks to the Arkin laboratory for the generous use of their Partec flow cytometer, and to Denise Wolf and Jolyn Twelves for instruction on its operation. Thanks also to Hector Nolla of the CNR flow cytometry core facility, for technical advice and assistance operating the cell sorters. Dr. John Morrissey (University College Cork), provided samples of the PGMR7 dsRED.T3_S4T construct, and Dr. Jan Van der Meer kindly provided the S17 (miniTn7PtacmCherry) constructs. This work was supported by a National Science Foundation Graduate Research Fellowship.

LITERATURE CITED

Altschul, S.F., T.L. Madden, A.A. Schaffer, J. Zhang, Z. Zhang, W. Miller, D.J. Lipman. (1997) Gapped BLAST and PSI-BLAST: a new generation of protein database search programs. *Nucleic Acids Research.* 1;25(17):3389-402.

Amann, R.I. W. Ludwig, and K.H. Schleifer. (1995) Phylogenetic identification and *in-situ* detection of individual microbial cells without cultivation. *Microbiological Review*. **59**(1): 143-169.

Andersen, J.B., C. Sternberg, L.K. Poulsen, S.P. Bjorn, M. Givskov, & S. Molin. (1998) New unstable variants of green fluorescent protein for studies of transient gene expression in bacteria. *Applied Environmental Microbiology*. **64**(6): 2240-2246.

Antoine, R., and C. Locht. (1992) Isolation and molecular characterization of a novel broad-host-range plasmid from *Bordetella bronchiseptica* with sequence similarities to plasmids from Gram-positive organisms. *Molecular Microbiology*. **6**(13): 1785-1799.

BioVision Technologies, Inc. (2010) IVision (image analysis software). http://www.biovis.com/ivision.htm.

Bitplane AG, Inc. (2010) Imaris (image analysis software), version 7.2 http://www.bitplane.com/.

Brandl, M.T., B. Quinones, & S.E. Lindow. (2001) Heterogeneous transcription of an indoleacetic acid biosynthetic gene in *Erwinia herbicola* on plant surfaces. *Proceedings of the National Academy of Sciences.* **98**(6): 3454-3459.

Brandl, M.T., and S.E. Lindow. (1997) Environmental signals modulate the expression of an indole-3-acetic acid biosynthetic gene in *Erwinia herbicola*. *Molecular Plant Microbe Interactions*. **10**(4): 499-505.

Campbell R.E., O. Tour, A.E. Palmer, P.A. Steinbach, G.S. Baird, D.A. Zacharias, R.Y. Tsien. A monomeric red fluorescent protein. (2002) *Proceedings of the National Academy of Sciences* **99**(12): 7877-7882.

Cappelleri, D.J., A. Halasz, J. Sul, T.K. Kim, J. Eberwine, & V. Kumar. (2010) Toward a fuly automated high-throughput phototransfection system. *Journal of the Association for Laboratory Automation.* **15**: 329-341.

Choe, J., H.H. Guo, G.van den Engh. (2005) A dual-fluorescence reporter system for high-throughput clone characterization and selection by cell sorting. *Nucleic Acids Research* **33**(5): e49.

Conville, P.S., & F.G. Witebsky. (2007) Analysis of multiple differing copies of the 16s rRNA gene in five clinical isolates and three type strains of *Nocardia* species and implications for species assignment. *Journal of Clinical Microbiology.* **45**(4): 1146-1151.

Dandie, C.E., E.Larrainzar, G.L. Mark, F. O'Gara, J.P. Morrissey. Establishment of DsRed.T3_S4T as an improved autofluorescent marker for microbial ecology applications. (2005) *Environmental Microbiology* **7**(11): 1818-1825.

De Novo Software. (2009). FCS Express (flow cytometry analysis software), version 3. http://www.denovosoftware.com/site/FCSExpress.shtml

Doctor, R.B., R.Dahl, L. Fouassier, G. Kilic, & J.G. Fitz. (2002) Cholangiocytes exhibit dynamic, actin-dependent apical membrane turnover. *American Journal of Physiology – Cell Physiology.* **282**: C1042-C1052.

Dulla, G., and S.E. Lindow. (2008) Quorum size of *Pseudomonas syringae* is small and dictated by water availability on the leaf surface. *Proceedings of the National Academy of Sciences.***105**(8): 3082-3087.

Friedrich, U., H. Van Langenhove, K. Altendorf, and A. Lipski. (2003) Microbial community and physicochemical analysis of an industrial waste gas biofilter and design of 16s rRNA-targeting oligonucleotide probes. *Environmental Microbiology*. **5**: 183-201.

Fuchs, B.M., G. Wallner, W. BBeisker, I. Schwippl, W. Ludwig, R. Amann. (1998) Flow cytometric analysis of the *in situ* accessibility of *Escherichia coli* 16s rRNA for fluorescently labeled oligonucleotide probes. *Applied and Environmental Microbiology* **64**(12): 4973-4982.

Gadella, T.W.J., G.N.M. van der Krogt, T. Bisseling. GFP-based FRET microscopy in living plant cells. *Trends in Plant Science* **4**(7): 287-291

Goyal, S.M., and C.P. Gerba. (1980) Simple method for concentration of bacteria from large volumes of tap water. *Applied Environmental Biology*. **40**(5): 912-916.

Hugenholtz, P., G.W. Tyson, L.L. Blackall. (2001) Design and evaluation of 16S rRNA-targeted oligonucleotide probes for fluorescence *in situ* hybridization. From *Methods in Molecular Biology, vol. 172: Steroid Receptor Methods: Protocols and Assays.* Edited by: B.A. Lieberman. Humana Press Inc., Totowa, NJ.

IPLab User's Guide, Version 3.6 (2002) Scanalytics, Inc., Fairfax USA.

Kado, C.I. (2006) Erwinia and related genera. From *The Prokaryotes*. Edited by: M. Dworkin, S. Falkow, E. Rosenberg, K. Schleifer, & E. Stackebrandt. Springer. New York, NY.

Kalyuzhnaya, M.G., R. Zabinsky, S. Bowerman, D.R. Baker, M.E. Lidstrom, L. Chistoserdova. (2006) Fluorescence *in situ* hybridization-flow cytometry-cell sorting-based method for separation and enrichment of Type I and Type II methanotroph populations. *Applied and Environmental Microbiology.* **72**(6): 4293-4301.

Kempf, V.A., K. Trebesius, and I.B. Autenrieth. (2000) Fluorescent in situ hybridization allows rapid identification of microorganisms in blood cultures. *Journal of Clinical Microbiology*. **38**: 830-838.

Kumar, Y., R. Westram, P. Kipfer, H. Meier, W. Ludwig. (2006) Evaluation of sequence alignments and oligonucleotide probes with respect to three-dimensional structure of ribosomal RNA using ARB software package. *BMC Bioinformatics*. **7**:240.

Kumar, Y., R. Westram, S. Behrens, B. Fuchs, F.O. Glockner, R. Amann, H. Meier, W. Ludwig. (2005) Graphical representation of ribosomal RNA probe accessibility data using ARB software package. *BMC Bioinformatics.* **6**: 61.

Lambertsen, Lotte. How to use the mini-Tn7 transposon, version 1. http://www2.biocentrum.dtu.dk/cbm/research/paper_supplementary/tn7/tn7howto.pdf. Accessed May 5, 2011.

Lauf, U., P. Lopez, and M.M. Faulk. (2001) Expression of fluorescently tagged connexins, a novel approach to rescue function of oligomeric DsRed-tagged proteins. *FEBS Letters*. **498**(1): 11-15.

Lenaerts, J., H.M. Lappin-Scott, and J. Porter. (2007) Improved fluorescent in situ hybridization method for detection of bacteria from activated sludge and river water by using DNA molecular beacons and flow cytometry. *Applied and Environmental Microbiology*. **73**(6): 2020-2023.

Leveau, J.H.J, and S.E. Lindow. (2001) Appetite of an epiphyte: Quantitative monitoring of bacterial sugar consumption in the phyllosphere. *Proceedings of the National Academy of Sciences.* **98**(6): 3446-3453.

Leveau, J.H.J., & S.E. Lindow. 2001) Predictive and interpretive simulation of green fluorescent protein expression in reporter bacteria. *Journal of Bacteriology*. **183**(23): 6752-6762.

Lindow, S.E., and M.T. Brandl. (2003) Microbiology of the Phyllosphere. *Applied and Environmental Microbiology*. **69**(4): 1875-1883.

Loy, A., F. Maixner, M. Wagner, M. Horn. (2007) probeBase—an online resource for rRNA-targeted oligonucleotide probes: new features 2007. *Nucelaic Acids Research*. **35**: D800-D804.

Ludwig, W., O. Strunk, R. Westram, L. Richter, H. Meier, Y. Kumar, A. Buchner, T. Lai, S. Steppi, G. Jobb, W. Forster, I. Brettske, S. Gerber, A. W. Ginhart, O. Gross, S. Grumann, S. Hermann, R. Jost, A. Konig, T. Liss, R. Lubmann, M. May, B. Nonhoff, B. Reichel, R. Strehlow, A. Stamatakis, N. Stuckmann, A. Vilbig, M. Lenke, T. Ludwig, A. Bode, K. Schleifer. (2004) ARB: a software environment for sequence data. *Nucleic Acids Research* **32**(4): 1363-1371.

Manti, A., T. Falcioni, R. Campana, D. Sisti, M. Rocchi, V. Medina, S. Dominici, S. Papa, W. Baffone. (2010) Detection of environmental *Vibrio parahaemolyticus* using a polyclonal antibody by flow cytometry. *Environmental Microbiology Reports.* **2**(1): 158-165.

McCarthy, M., and S.C. Culloty. (2011) Optimization of two immunofluorescent antibodies for the detection of *Escherichia coli* using immunofluorescent microscopy and flow cytometry. *Current Microbiology*. **62**(2): 402-408.

Miller, J.H.. (1972) *Experiments in Molecular Genetics*. (Cold Spring Harbor Laboratory Press, Cold Spring Harbor, NY).

Monier, J.M., & S.E. Lindow. *Pseudomonas syringae* responds to the environment on leaves by cell size reduction. *Phytopathology*. **93** (10): 1209-1216.

Nakanishi, Y., A. Adandonon, I. Okabe, Y. T. Hoshino, N. Matsumoto. (2006) An oligonucleotide probe for the detection of *Erwinia herbicola* and *Erwinia ananas*. *J. Gen Plant Pathol.* **72**: 328-333.

Ootsubo, M., T. Shimizu, R. Tanaka, T. Sawabe, K. Tajima, M. Yoshimizu, Y. Ezura, T. Ezaki, and H. Oyaizu. (2002) Oligonucleotide probe for detecting Enterobacteriaceae by in situ hybridization. *Journal of Applied Microbiology*. **93**: 60-68.

Pogliano, J., N. Osborne, M.D. Sharp, A. Abanes-DeMello, A. Perez, Y.L. Sun, and K. Pogliano. (1999) A vital stain for studying membrane dynamics in bacteria: a novel mechanism controlling septation during *Bacillus subtilis* sporulation. *Molecular Microbiology*. **31**(4): 1149-1159.

Remus-Emsermann, MNP, and J. Leveau. (2010) Linking environmental heterogeneity and reproductive success at single-cell resolution. *ISME Journal*. **4**(2):215-222.

Rochat, L., M. Pechy-Tarr, E. Baehler, M. Maurhofer, C. Keel. (2010*a*) Combination of fluorescent reporters for simultaneous monitoring of root colonization and antifungal gene expression by a biocontrol pseudomonad on cereals with flow cytometry. *Molecular Plant-Microbe Interactions*. **23**(7): 949-961.

Rochat, L., M. Pechy-Tarr, M. Maurhofer, C. Keel. (2010*b*) Combined use of fluorescent reporters and flow cytometry for simultaneous monitoring of bacterial growth and gene expression on plant roots. In *Handbook of Hydrocarbon and Lipid Microbiology,* ed. K. N. Timmis. © Springer-Verlag Berlin, Heidelberg, 2010.

Sgorbati, S., S. Barbesti, S. Citterio, G. Besbatti, and R. De Vecchi. (1996) Characterization of number, DNA content, viability and cell size of bacteria from natural environments using DAPI/PI dual staining and flow cytometry. *Minerva Biotecnologica*. **8**: 9-15.

Shaner, N.C., P.A. Steinbach, R.Y. Tsien. (2005) A guide to choosing fluorescent proteins. *Nature Methods*. **2**(12): 905-909.

Shaner, N.C., R.E. Campbell, P.A. Steinbach, B.N.G.Giepmans, A.E.Palmer, R.Y. Tsien. Improved monomeric red, orange and yellow fluorescent proteins derived from *Discosoma* sp. Red fluorescent protein. (2004) *Nature Biotechnology* **22**(12): 1567-1572.

Shapiro, H. (1995) *Practical Flow Cytometry*, 3rd edition. Wiley-Liss, New York, NY.

Sörensen, M., C. Lippuner, T. Kaiser, A. MiBlitz, T. Aebisher, D. Bumann. Rapidly maturing red fluorescent protein variants with strongly enhanced brightness in bacteria. (2003) *FEBS Letters* **552**: 110-114.

StatSoft, Inc. (2010). STATISTICA (data analysis software system), version 9.1. www.statsoft.com.

Tecon, R., O. Binggell, and J.R. van der Meer. (2009) Double-tagged fluorescent bacterial bioreporter for the study of polycyclic aromatic hydrocarbon diffusion and bioavailability. *Environmental Microbiology*. **11**(9):2271-2283.

Toth, I.K., K.S.Bell, M.C. Holeva, & P.R.J. Birch. (2003) Soft rot erwiniae: from genes to genomes. *Molecular Plant Pathology*. **4**(1): 17-30.

Van der Krogt, G.N.M., J. Ogink, B. Ponsioen, & K. Jalink. (2008) A comparison of donor-acceptor pairs for genetically encoded FRET sensors: Application to the Epac cAMP sensor as an example. *PLoS ONE*. **3**(4): e1916.

Zinchuk, V., and O. Zinchuk. (2008) Quantitative colocalization analysis of confocal fluorescence microscopy images. *Current Protocols in Cell Biology*. **39**: 4.19.1 - 4.19.16.

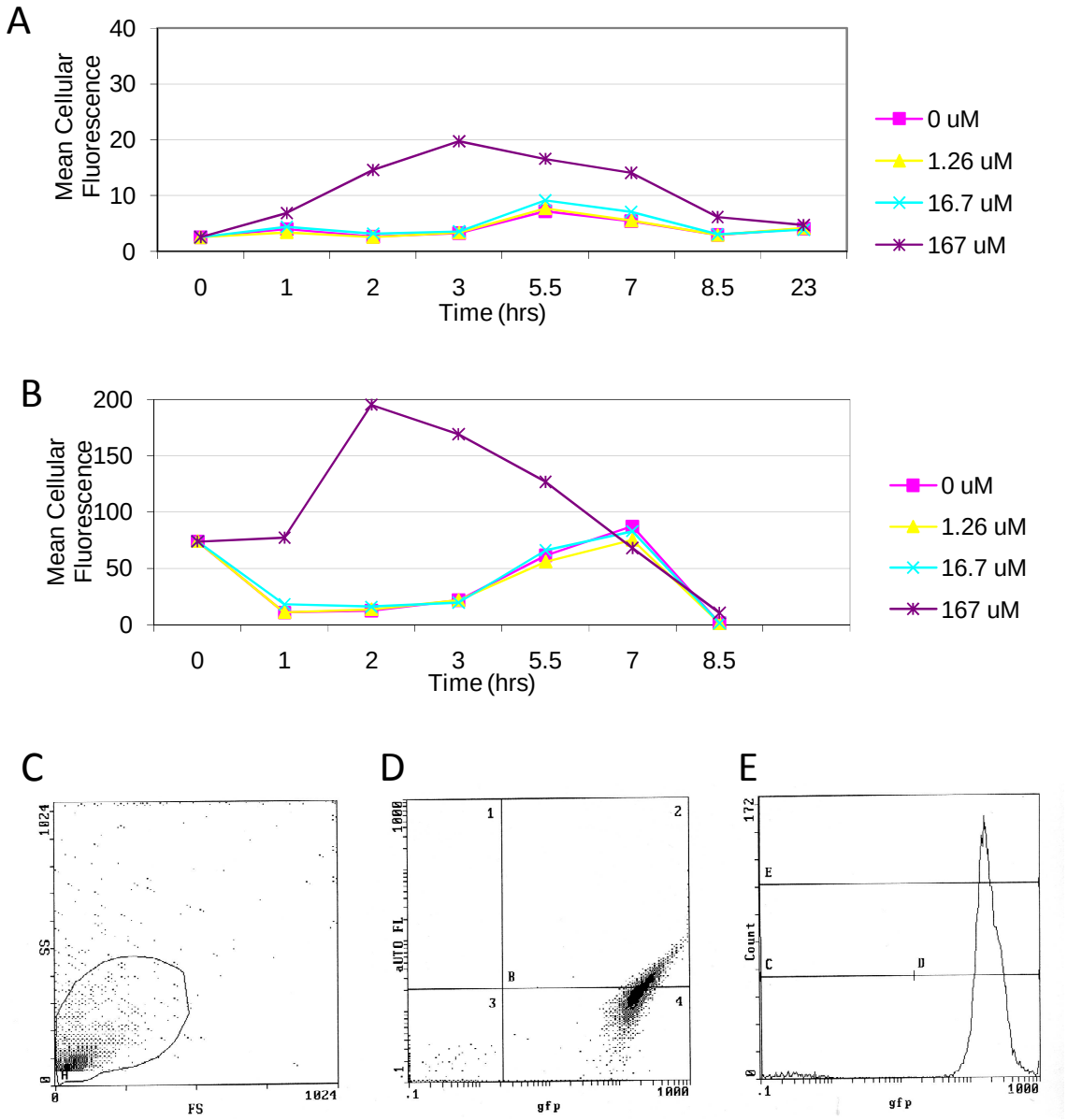

Figure 1. A fructose dose-response curve of the *P. agglomerans* 299R (pFru46) fructose biosensor, as measured by a fluorimeter (A) and a standard flow cytometer (B) over 9 hours of incubation *in vitro*. Sample cell-fluorescence data are also shown from flow cytometric analysis of the 2Hpi, 167µM treatment (C-E). The Forward Scatter (FS=particle size) versus Sidescatter (SS=particle granularity) plot shows all particles detected(C). The GFP-fluorescence scatterplot (D) and histogram (E) show the distribution of GFP intensity within the gated,GFP-positive subpopulation.

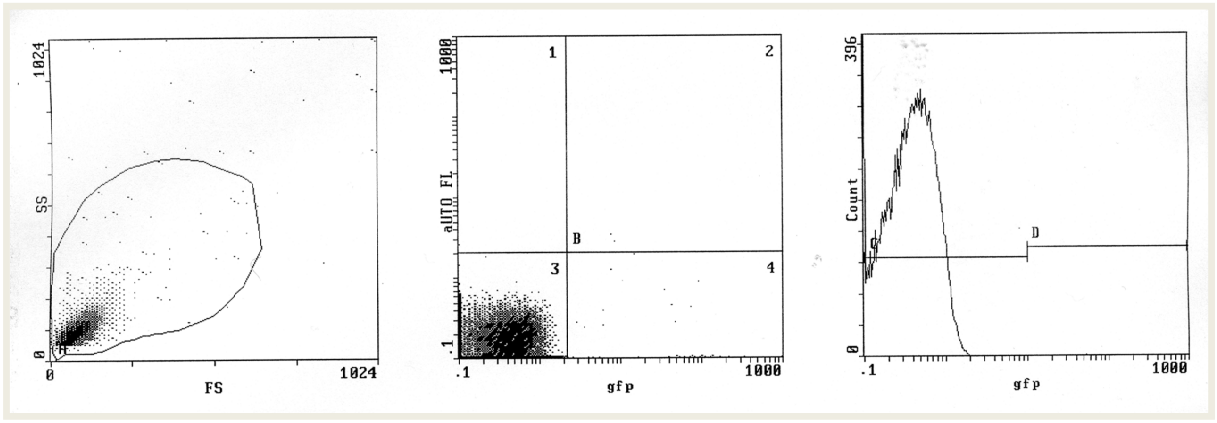

***p61RYice* (GFP-)**

0.1% GFP positive
Mean RFL1 0.226
104,448 events counted

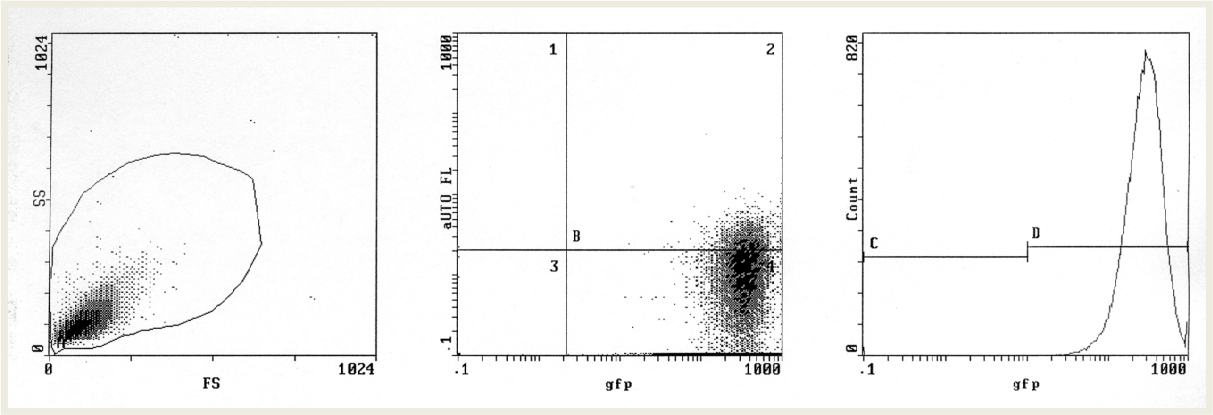

***pKT-bla* (GFP+)**

99.9% GFP positive
Mean RFL1 283.3
103,936 events counted

Figure 2. Sample flow cytometric analyses of bacteria harvested from leaves and analyzed using a Beckman-Coulter EPICS XL flow cytometer. Forward scatter (FS; particle size) versus Sidescatter (SS; particle granularity) plots depict all collected particles; GFP histograms show the distribution of fluorescence intensity within the gated population. Data were collected from plants inoculated with buffer only (A), wild-type 299R (B), or constitutive GFP-expressing 299R (pKTbla) (B).

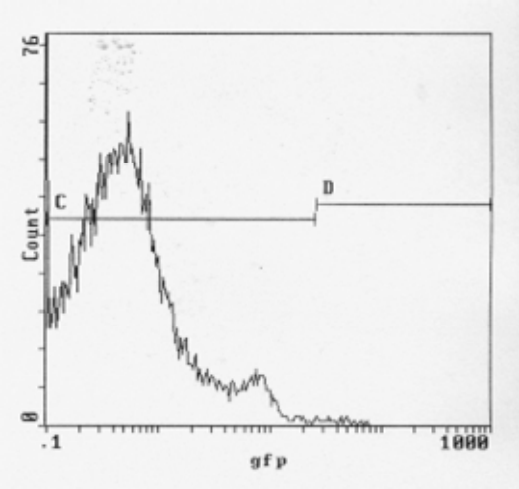

KPO4 0.45%+, Mean=41.0
21,849 events

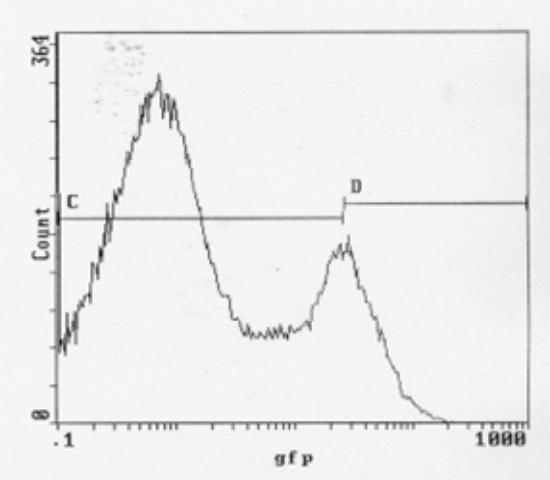

pKT-bla 9.49%+, Mean=45.2
152,496 events

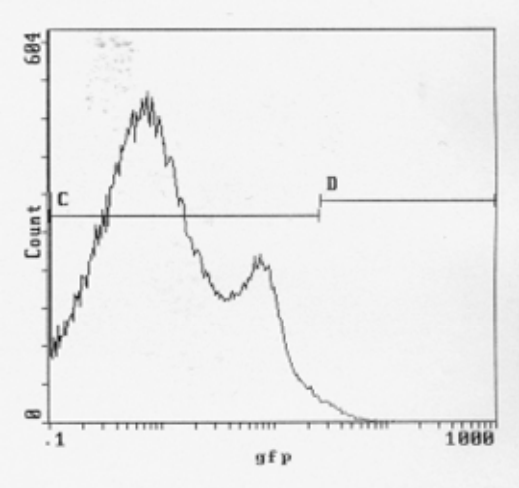

299R WT 1.0%+, Mean=39.5
203,776 events

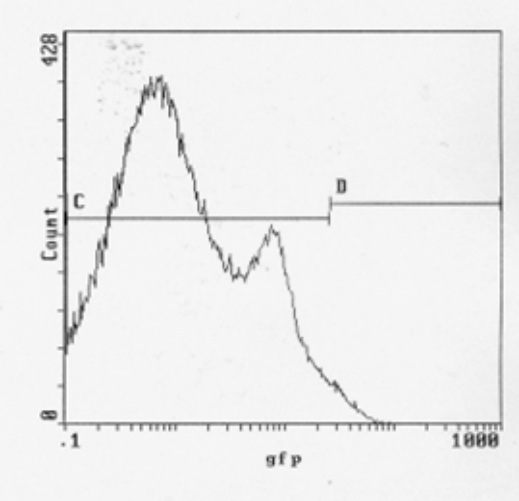

ipdC:GFP 1.55%+, Mean=38.4
170,490 events

Figure 3. Sample flow cytometric analyses of bacteria harvested from leaves and analyzed using a Beckman-Coulter EPICS XL flow cytometer. Forward scatter (FS; particle size) versus Sidescatter (SS; particle granularity) plots depict all collected particles; GFP histograms show the distribution of fluorescence intensity within the gated population. Data were collected from plants inoculated with buffer only (A), wild-type 299R (B), or constitutive GFP-expressing 299R (pKTbla) (B).

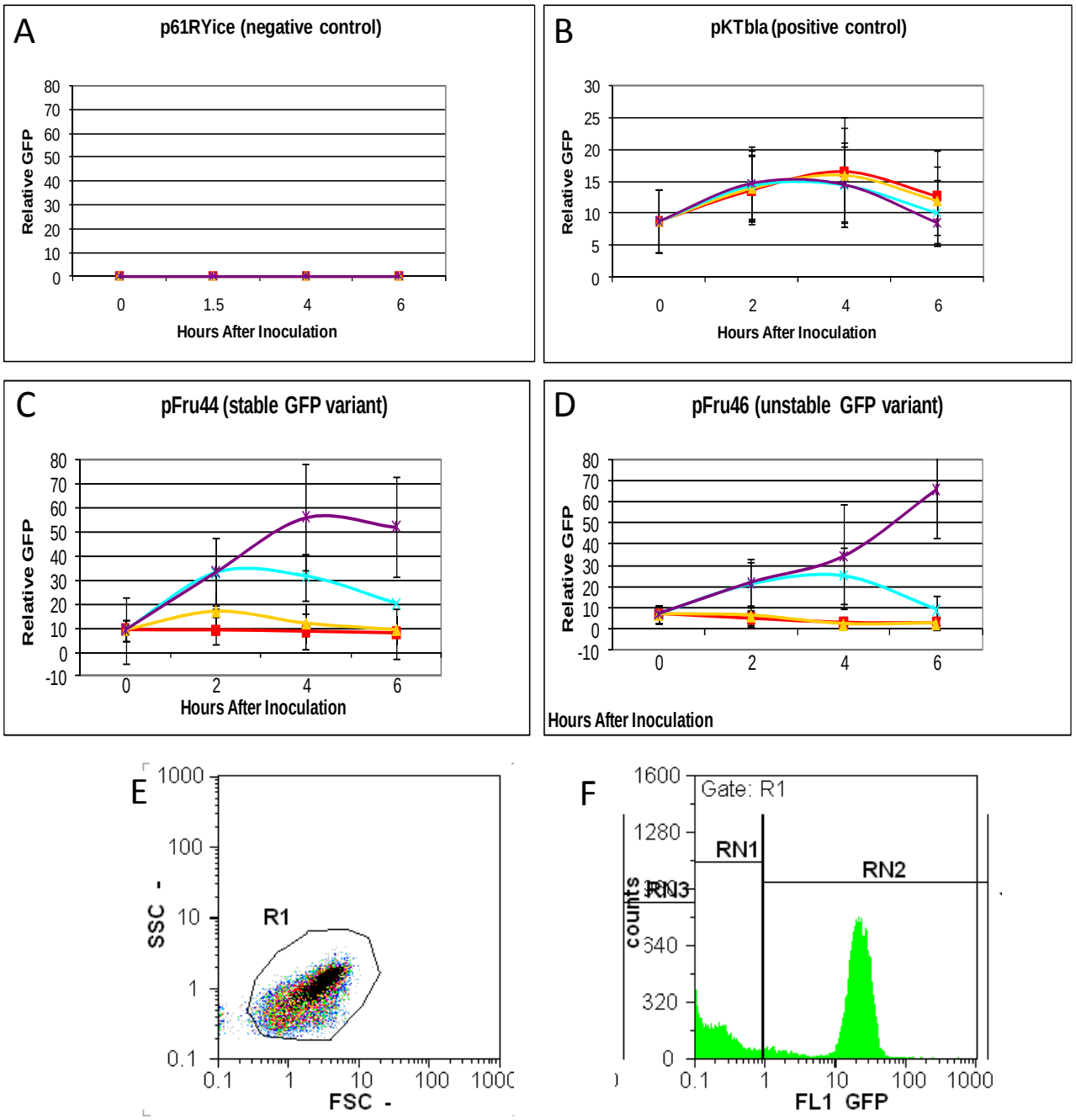

Figure 4. A fructose dose-response curve of the *P. agglomerans* 299R fructose biosensor, as measured by the Partec small-particle analyzer. The nonfluorescent ice-nucleating biosensor 299R (p61RYice) was used as a negative control (A) and the constitutively GFP-positive strain 299R (pKTbla) as a positive control (B); biosensor responsiveness was measured using 299R (pFru44) (C), which carries a stable GFP variant, and 299R (pFru46) (D), which carries an unstable GFP variant. A sample FSC/SSC plot (E) and GFP distribution histogram (F) are shown from the 2hpi, 167uM fructose treatment.

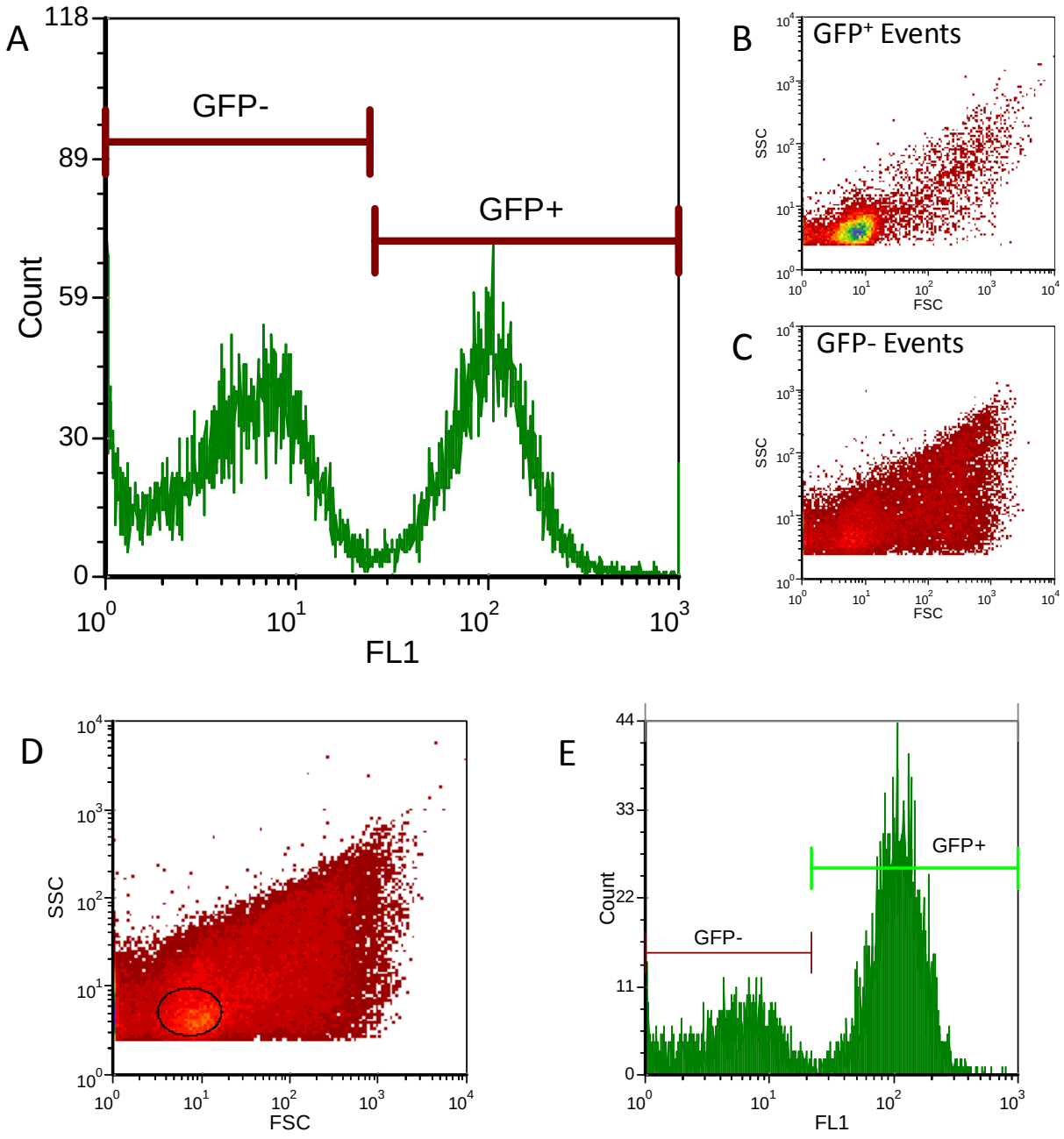

Figure 5. Sample flow cytometric analysis of constitutively GFP-positive *Pa*299R (pKTbla) bacteria harvested from leaves. GFP fluorescence among the entire leaf particle population was divided into GFP-negative and GFP-positive particles (A). In order to identify the bacterial subpopulation among leaf-surface particles, FSC/SSC intensity plots were constructed for the GFP-positive (B) and GFP-negative particle subpopulations (C), and an elliptical gate drawn to select the densest population of GFP-positive particles (D). Subsequent fluorescence analysis was restricted to this putative bacterial subpopulation (E).

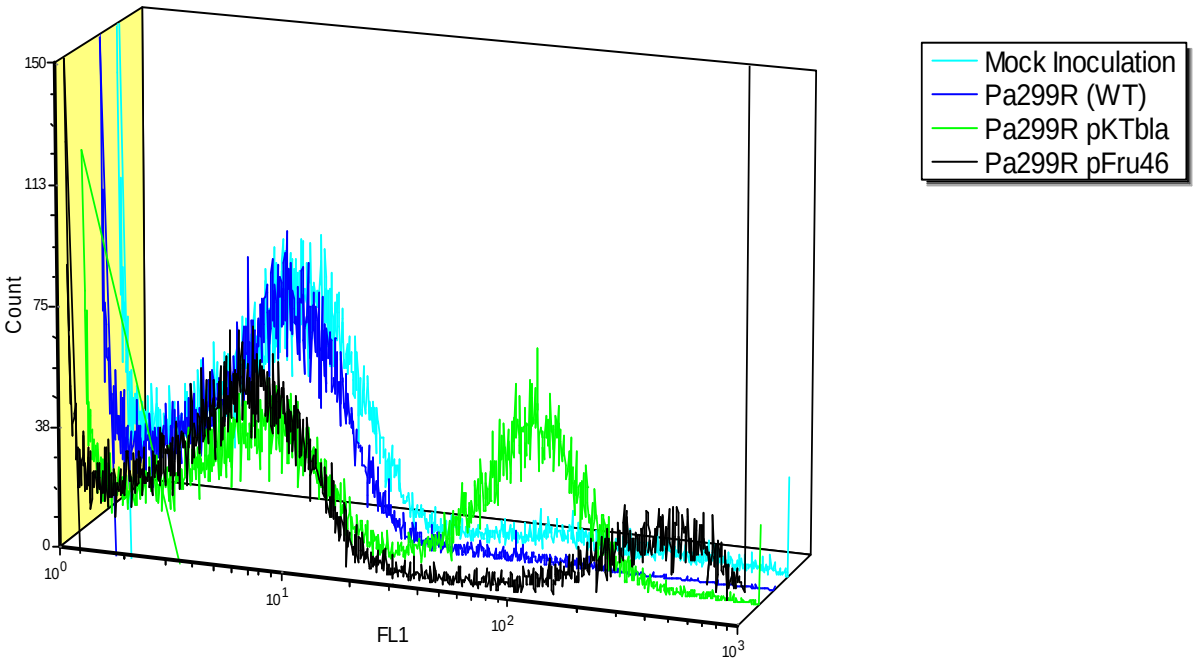

Figure 6. Sample flow cytometric analyses of bacteria harvested from leaves and analyzed using the Partec CyFlow. Data were collected from plants inoculated with (from back to front) buffer only, wild-type 299R , constitutivelyGFP-expressing 299R (pKTbla), or 299R expressing the fructose-inducible GFP construct (pFru46). Superimposed histograms show the distribution of GFP fluorescence intensity within the gated subpopulation of putative bacteria.

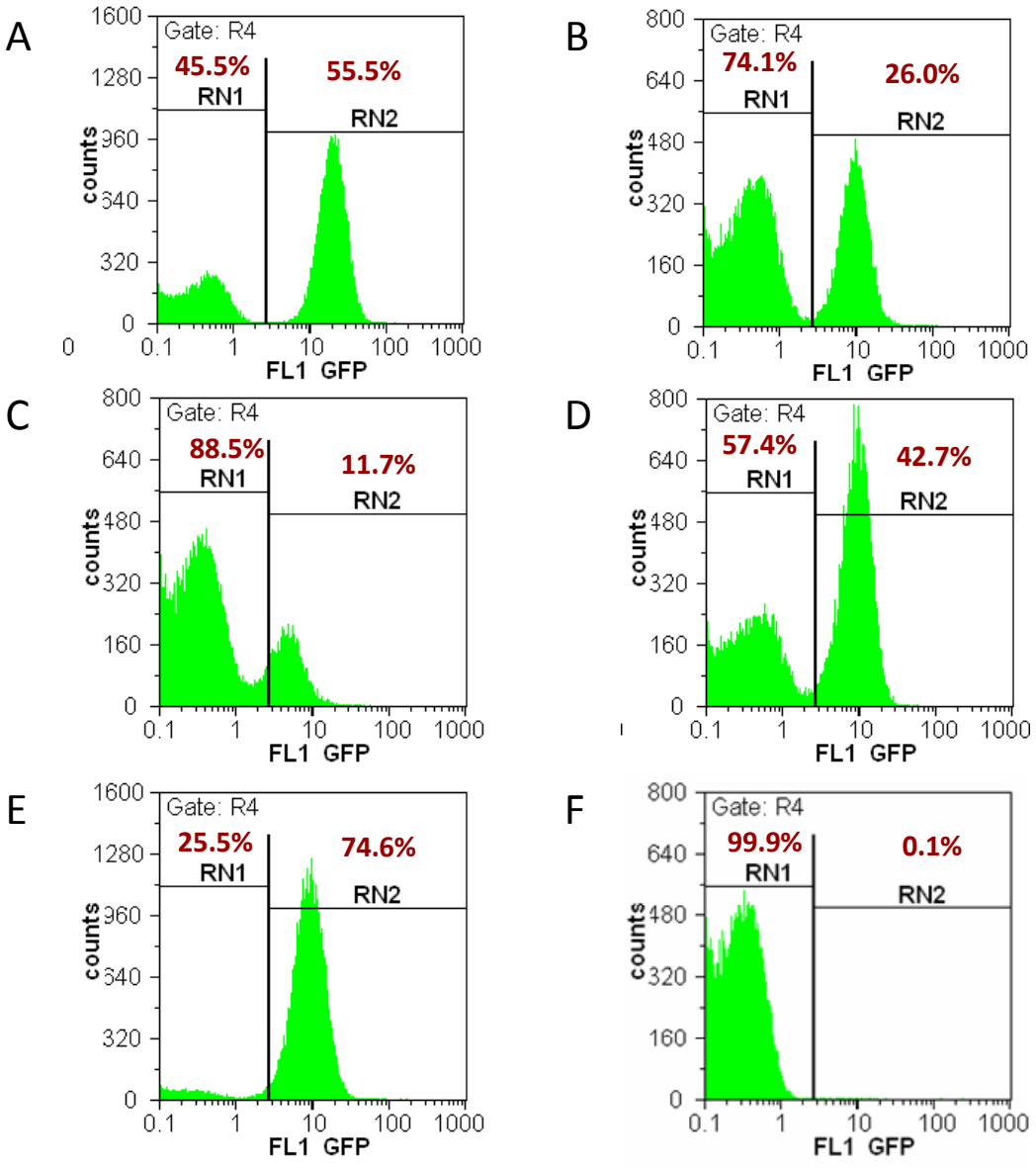

Figure 7. Native leaf bacteria and other debris comprise variable but significant GFP-negative background populations in environmental samples. The positive control strain 299R (pKTbla) was inoculated onto bean leaves in five independent experiments (A-E); histograms depict the distribution of GFP intensity in the recovered cell populations. One sample of 299R WT negative-control bacteria harvested from leaves is shown as a reference (F). The percentage of GFP-negative (RN1) and GFP-positive (RN2) particles in each population are also indicated.

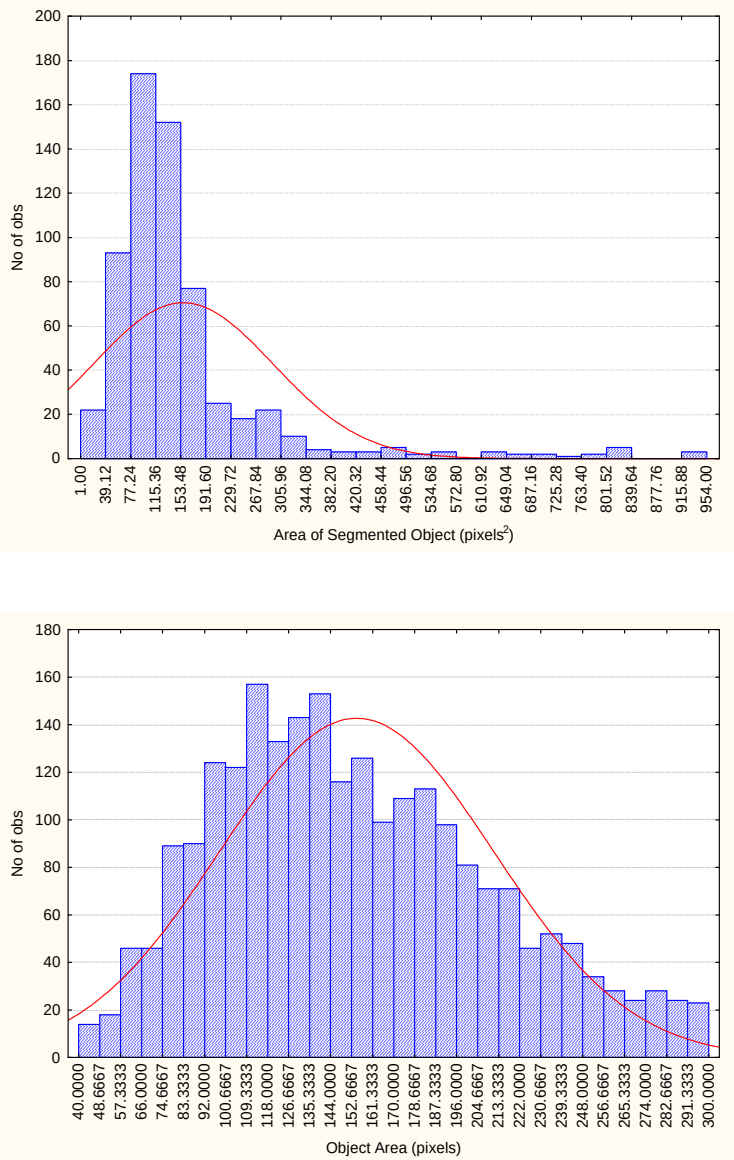

Figure 8. A histogram of object sizes was generated from two sample images of constitutively GFP-positive *Pa*MX149 (pKTbla) cells. Individual biosensor cells range between approximately 40 and 300 pixels in size.

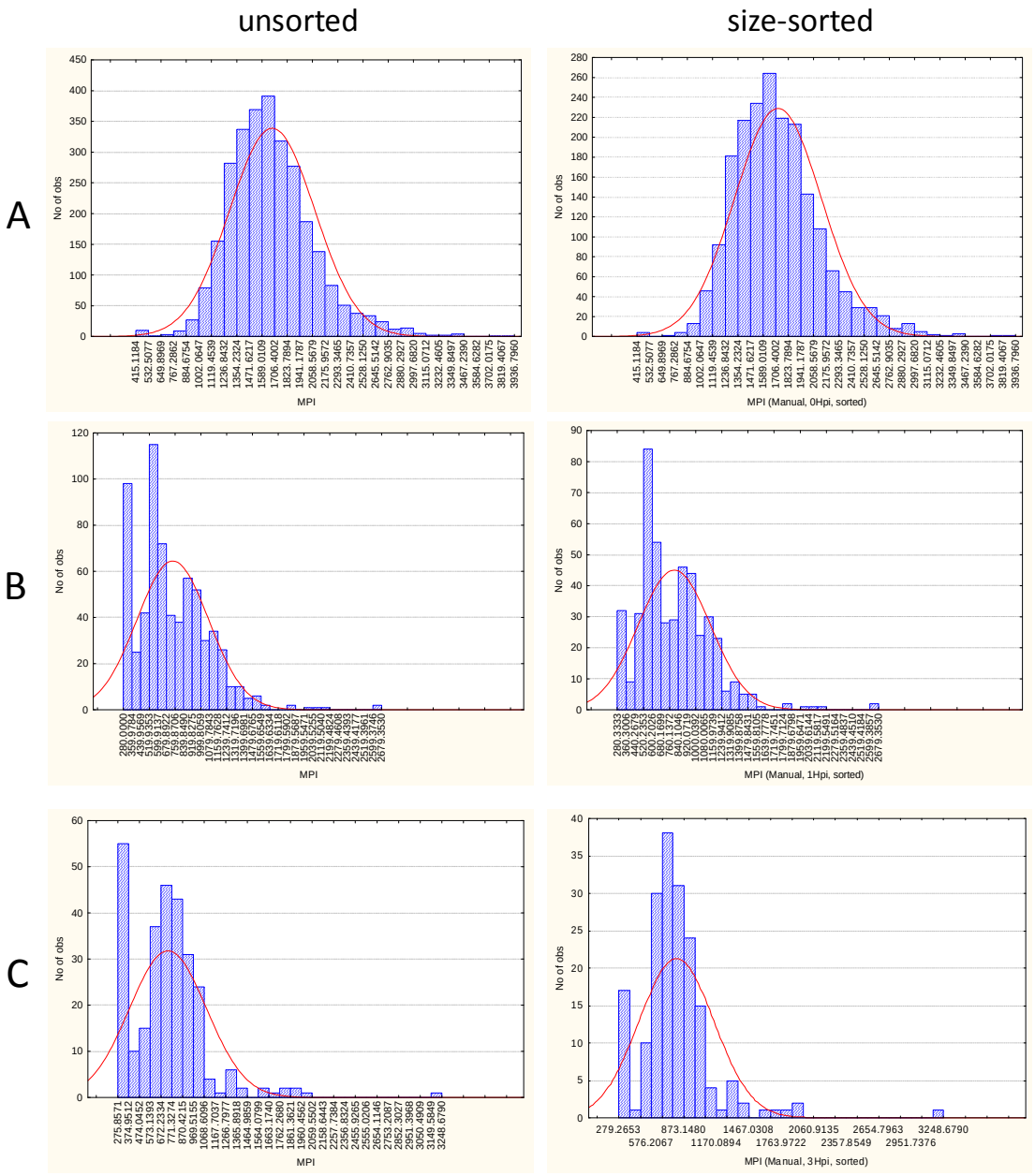

Figure 9. The distribution of cellular GFP fluorescence in MX149 (pKTbla) cells with constitutive GFP expression. Samples of 0-hour inoculum (A) and cells washed from bean leaves at 1Hpi (B), and 3Hpi (C) were analyzed via manual segmentation. The distribution of the total object analysis (unsorted, L) was compared to the distribution when all objects of less than 40 pixels or greater than 300 pixels were omitted (size-sorted, right). Red lines indicate a calculated normal distribution.

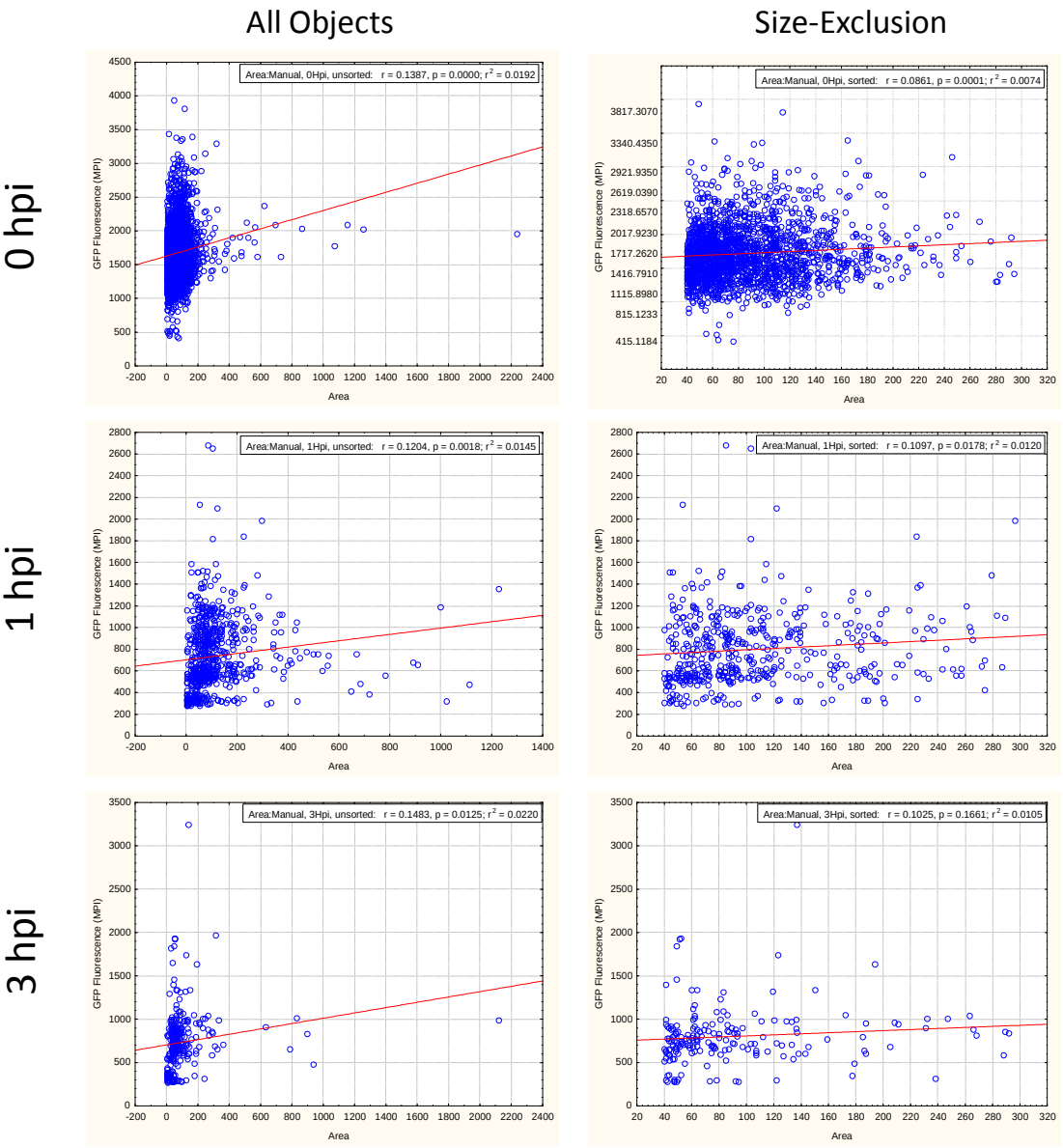

Figure 10. Size-based exclusion of segmented objects abolishes size-dependent variation in fluorescence. For *Pa*MX149 cells expressing constitutive GFP, scatterplots of object GFP fluorescence intensity versus object area are shown for 0-hour inoculum, and cells washed from bean leaves at 1 hpi and 3 hpi. The same data were analyzed by either including all objects (left), or excluding objects <40 pixels or >300 pixels (right). For each sample, the regression line, correlation coefficient (r), p-value (p), and r^2 are shown.

A

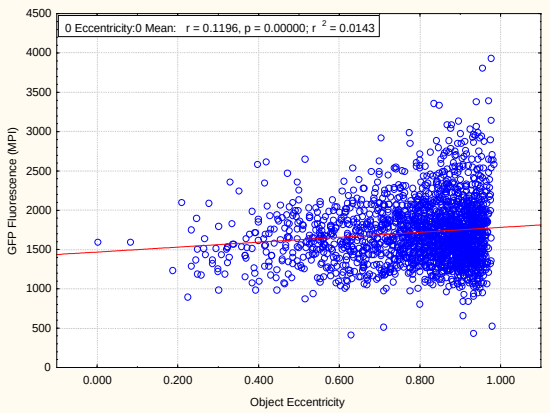

B

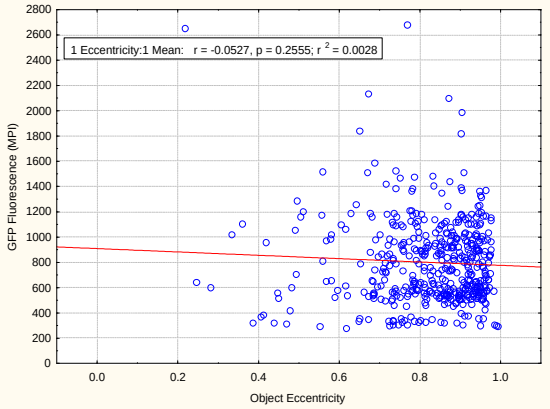

C

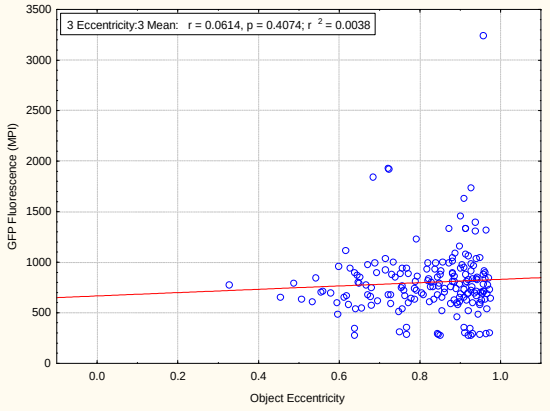

Figure 11. Segmented object eccentricity is a poor criterion for identifying noncellular debris in leaf wash samples. For *Pa*MX149 cells expressing constitutive GFP, scatterplots of object GFP fluorescence intensity versus object irregularity are shown for 0-hour inoculum (A), and cells washed from bean leaves at 1Hpi (B) and 3Hpi (C). For each sample, the correlation coefficient and p-value (r, p) and the r^2 value are shown.

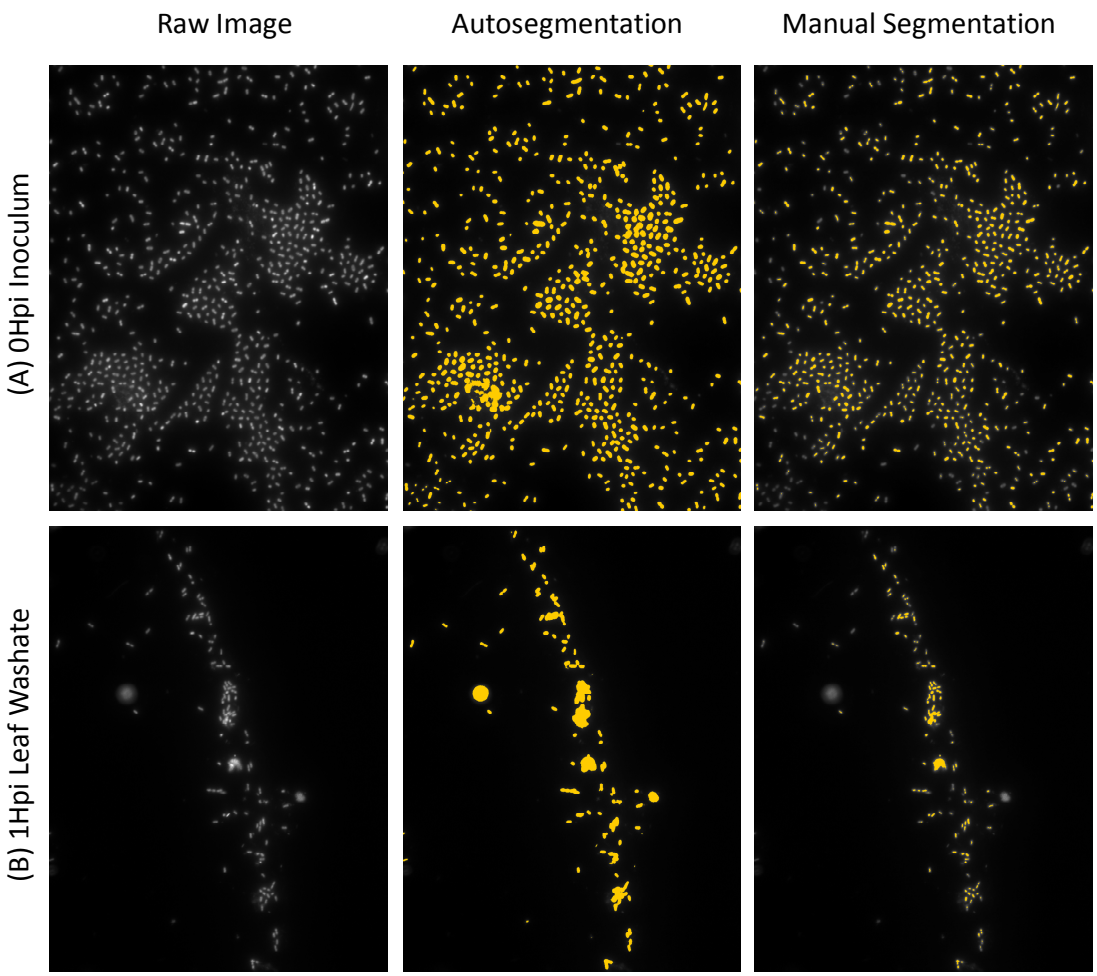

Figure 12. Different segmentation methods alter software estimates of cell-object boundaries in images of MX149 (pKTbla) cells with constitutive GFP expression. Sample DAPI-stained images are presented from 0Hpi cell inoculum (A) and 1Hpi cells washed from bean leaves (B). Cells were identified using either the autosegmentation function or manual segmentation.

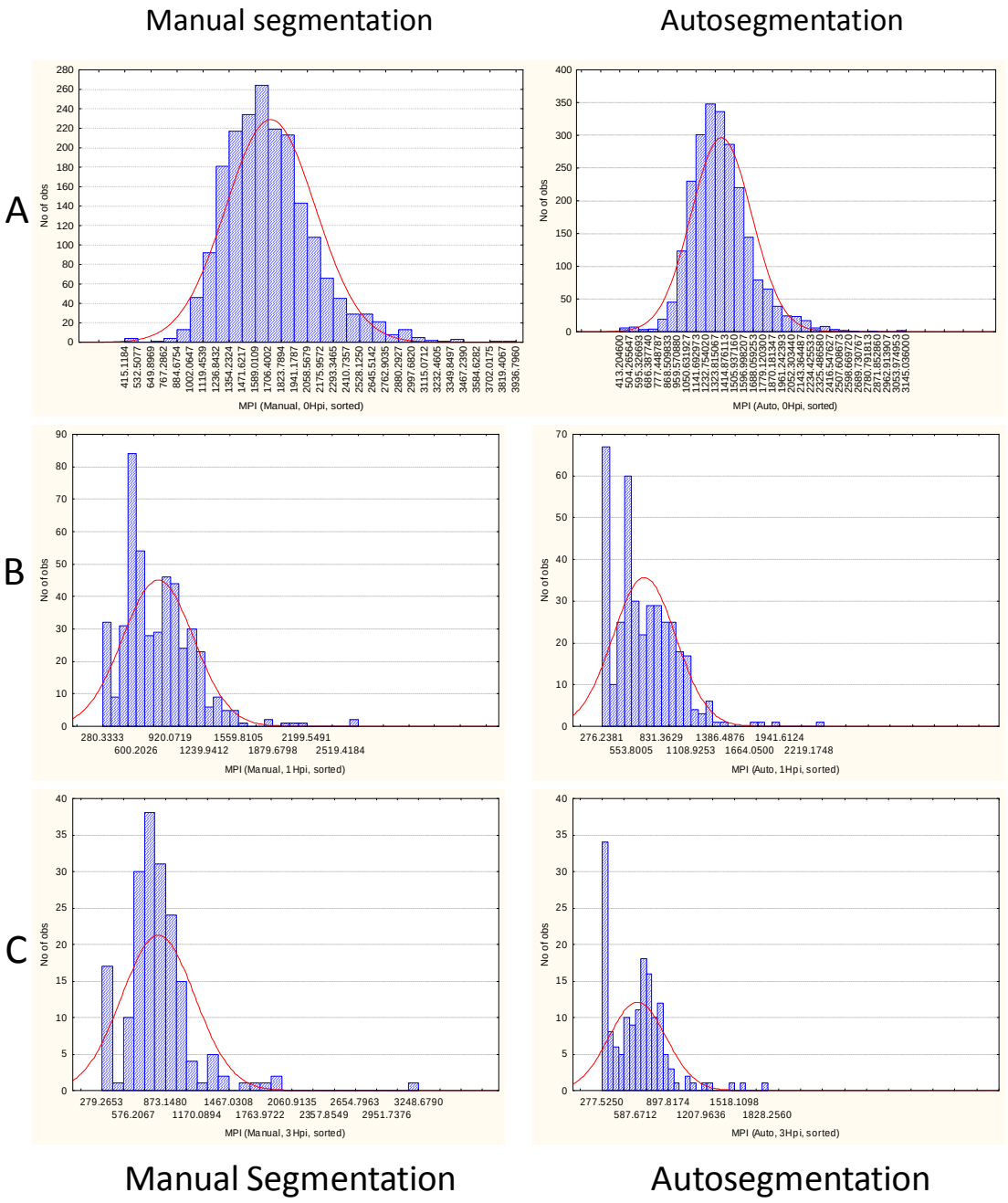

Figure 13. Histograms depicting the distribution of cellular GFP fluorescence in MX149 (pKTbla) cells with constitutive GFP expression. Samples of 0-hour inoculum (A), and cells washed from bean leaves at 1Hpi (B) and 3Hpi (C) were analyzed via manual segmentation (left) and autosegmentation (right) in IVision software. Red lines depict a calculated normal distribution.

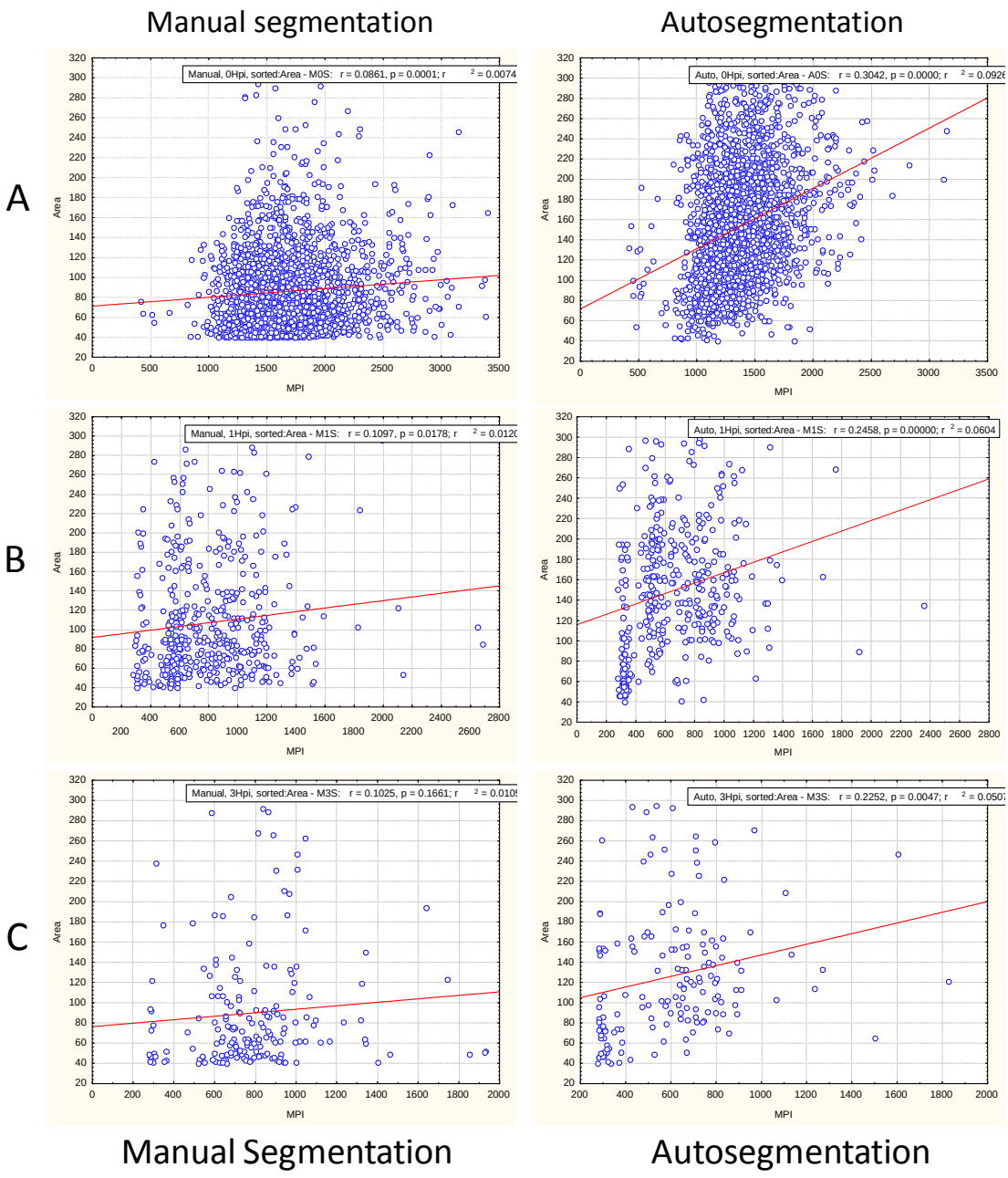

Figure 14. Autosegmentation contributes to significant edge-effects when calculating cellular GFP fluorescence. Scatterplots of area versus GFP fluorescence in MX149 (pKTbla) cells with constitutive GFP expression. Samples of 0-hour inoculum (A), and cells washed from bean leaves at 1Hpi (B), and 3Hpi (C) were analyzed via manual segmentation (left) and autosegmentation (right) in IVision software. Correlation and regression statistics for each sample are shown at the top right.

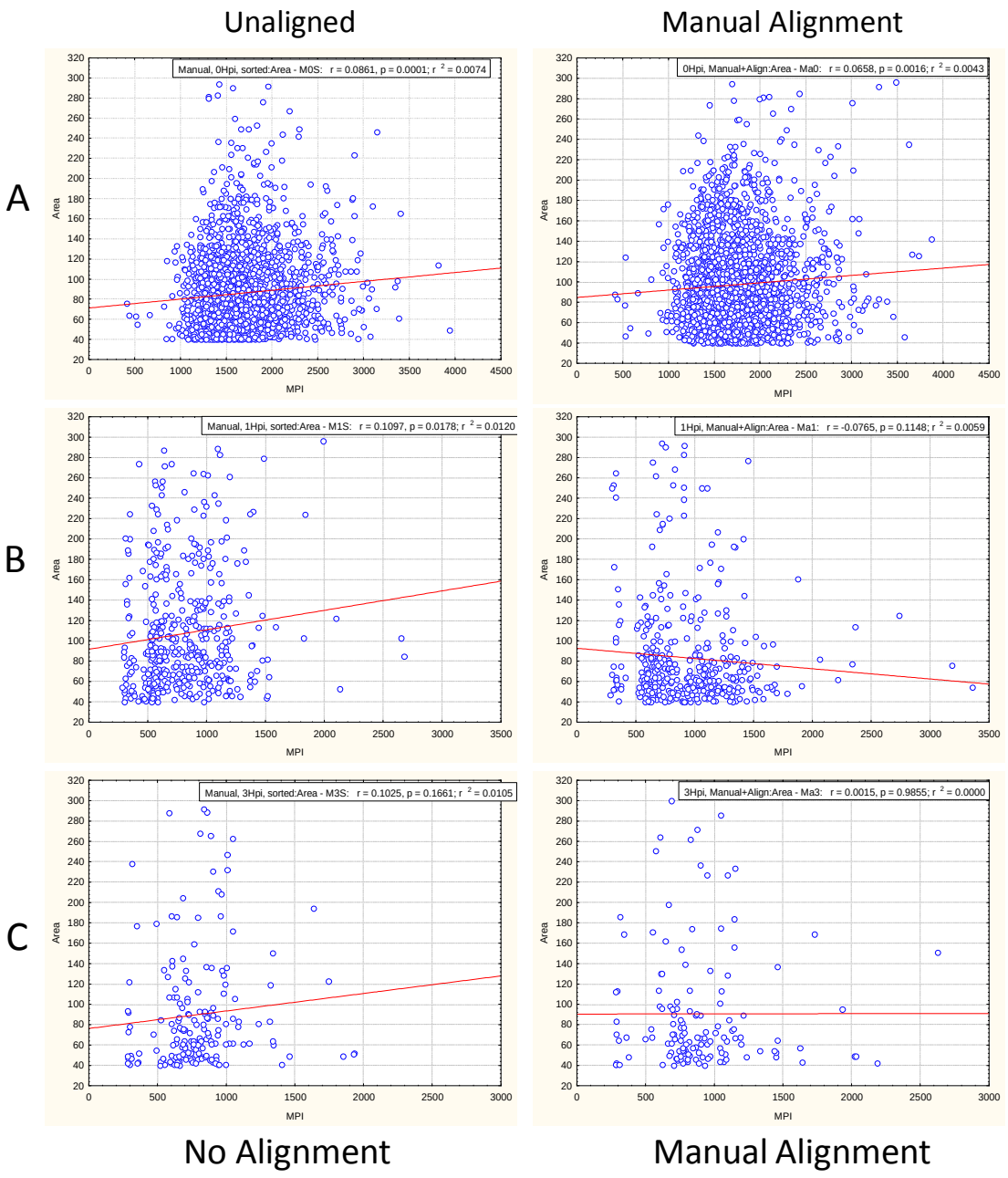

Figure 15. Manual alignment of the DAPI-generated segment mask over the GFP image reduces edge-effects when calculating cellular GFP fluorescence. Scatterplots of area versus GFP fluorescence in MX149 (pKTbla) cells with constitutive GFP expression. Samples of 0-hour inoculum (A), and cells washed from bean leaves at 1Hpi (B), and 3Hpi (C) were analyzed without (left) and with (right) alignment.

A

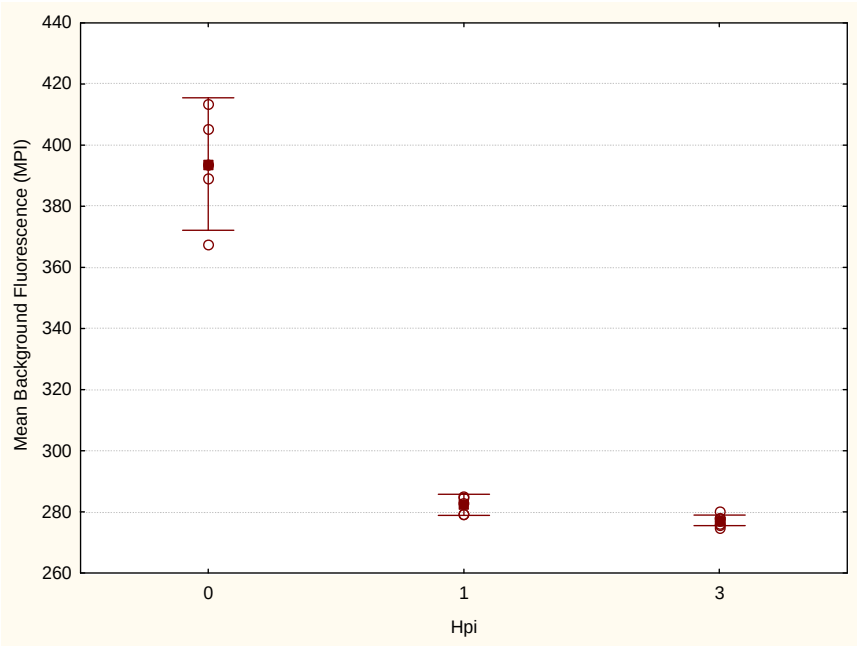

B

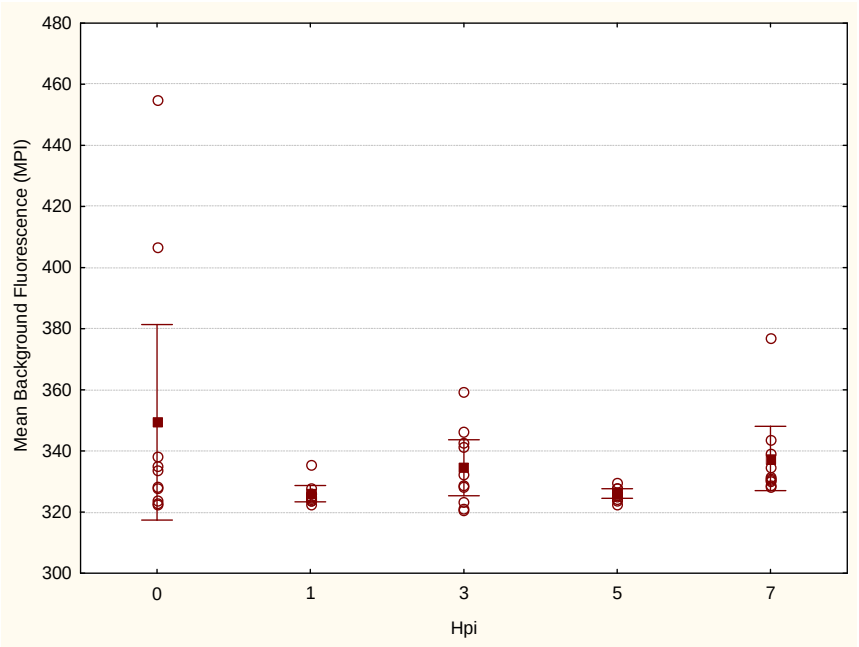

Figure 16. Variation in mean background fluorescence in microscopic images of *Pa*MX149 (pKTbla) cells with constitutive GFP expression. Box-and-whisker plots from the sample image dataset (A) and a second, independent experiment (B) display mean background fluorescence at a given timepoint (solid squares), 95% confidence intervals, and the distribution of individual datapoints (open circles).

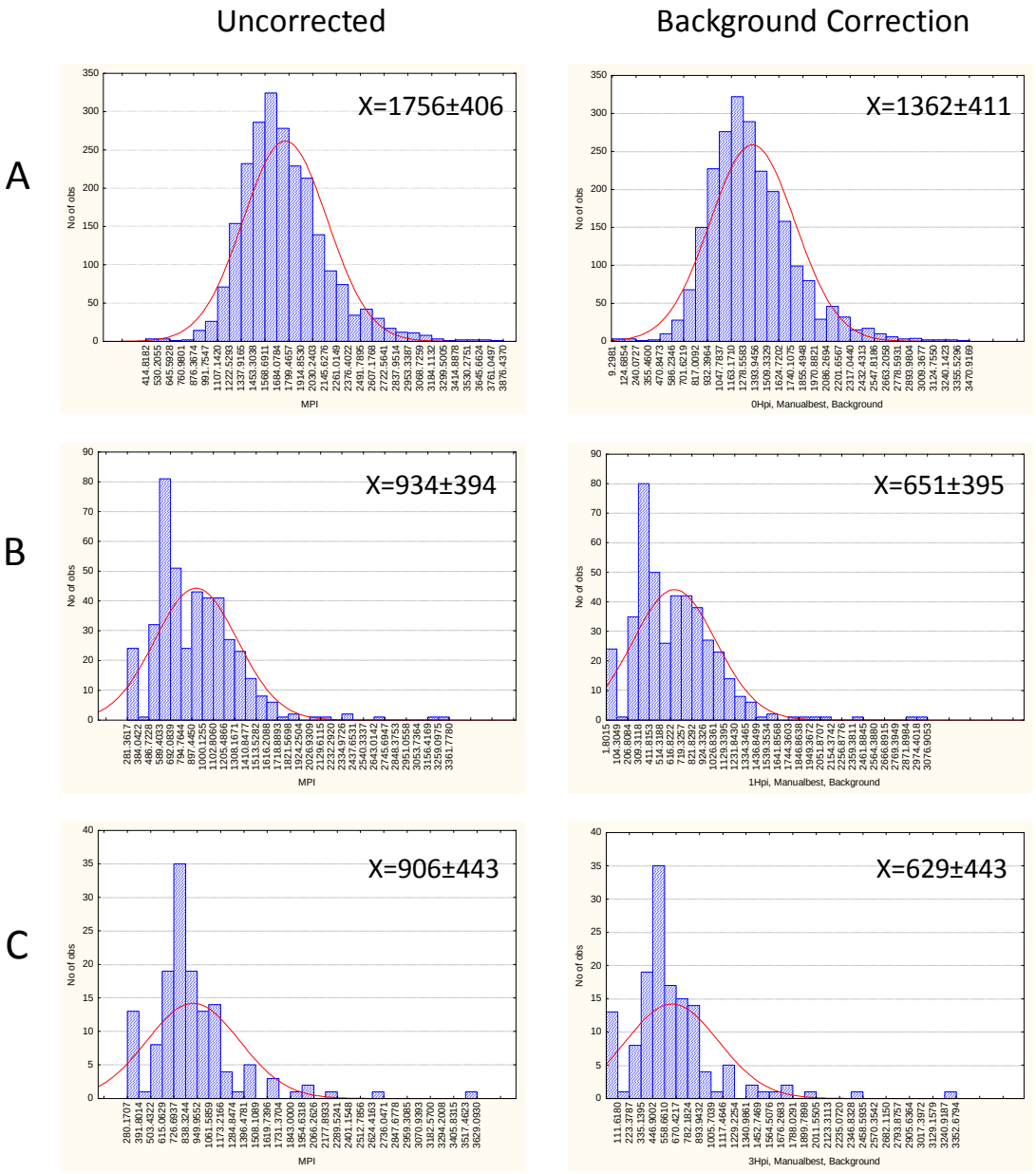

Figure 17. Background correction for variations in basal fluorescence between images causes a linear, downward shift in mean fluorescence in the inoculum population. Histograms display the distribution of GFP fluorescence within populations of *Pa*MX149 (pKTbla) cells with constitutive GFP expression. Samples of 0-hour inoculum (A), and cells washed from bean leaves at 1Hpi (B), and 3Hpi (C) were analyzed without (left) and with (right) correction for background fluorescence. Mean fluorescence ± standard deviation is indicated for each histogram.

A

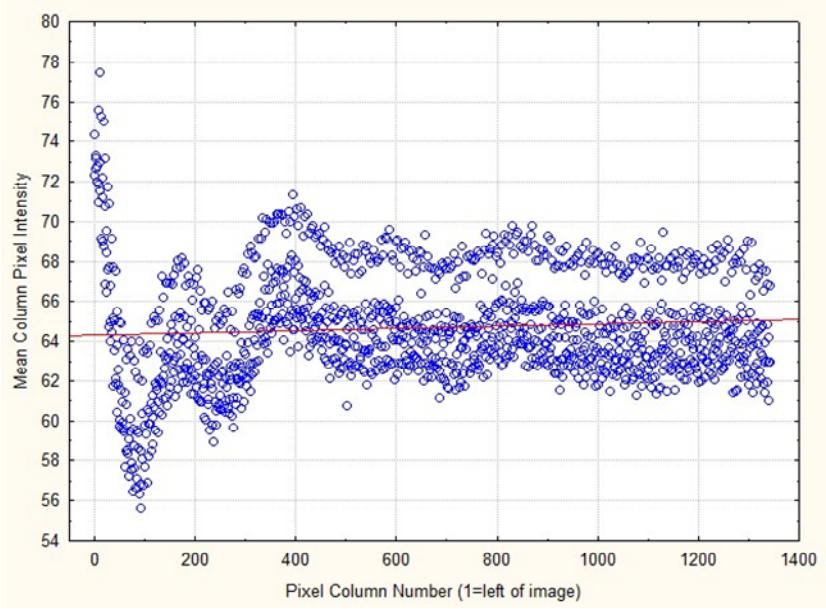

B

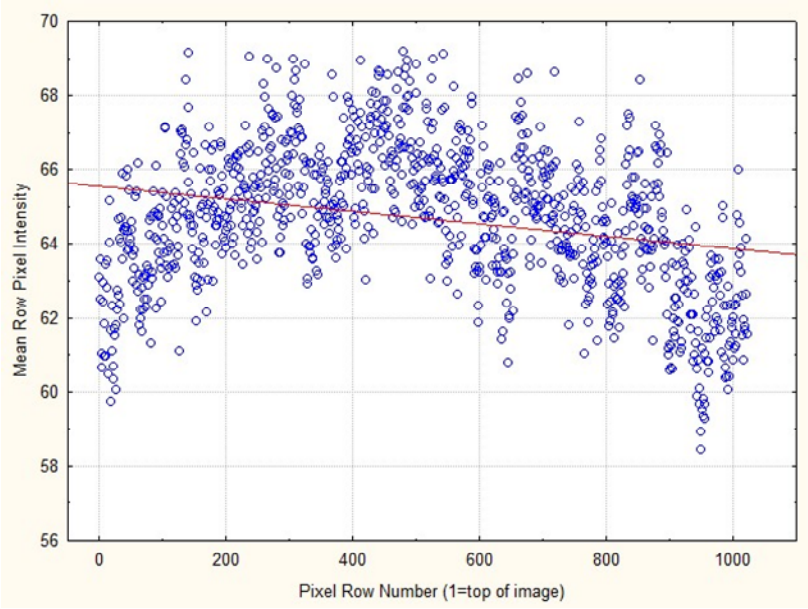

Figure 18. Mean pixel intensity of each column (A) or row (B) of a uniformly dark image. Plots suggest systematic , artifactual image bias, including a narrow bright vertical band followed by a dark vertical band at the left of the image, and dark horizontal bands at the top and bottom of the image.

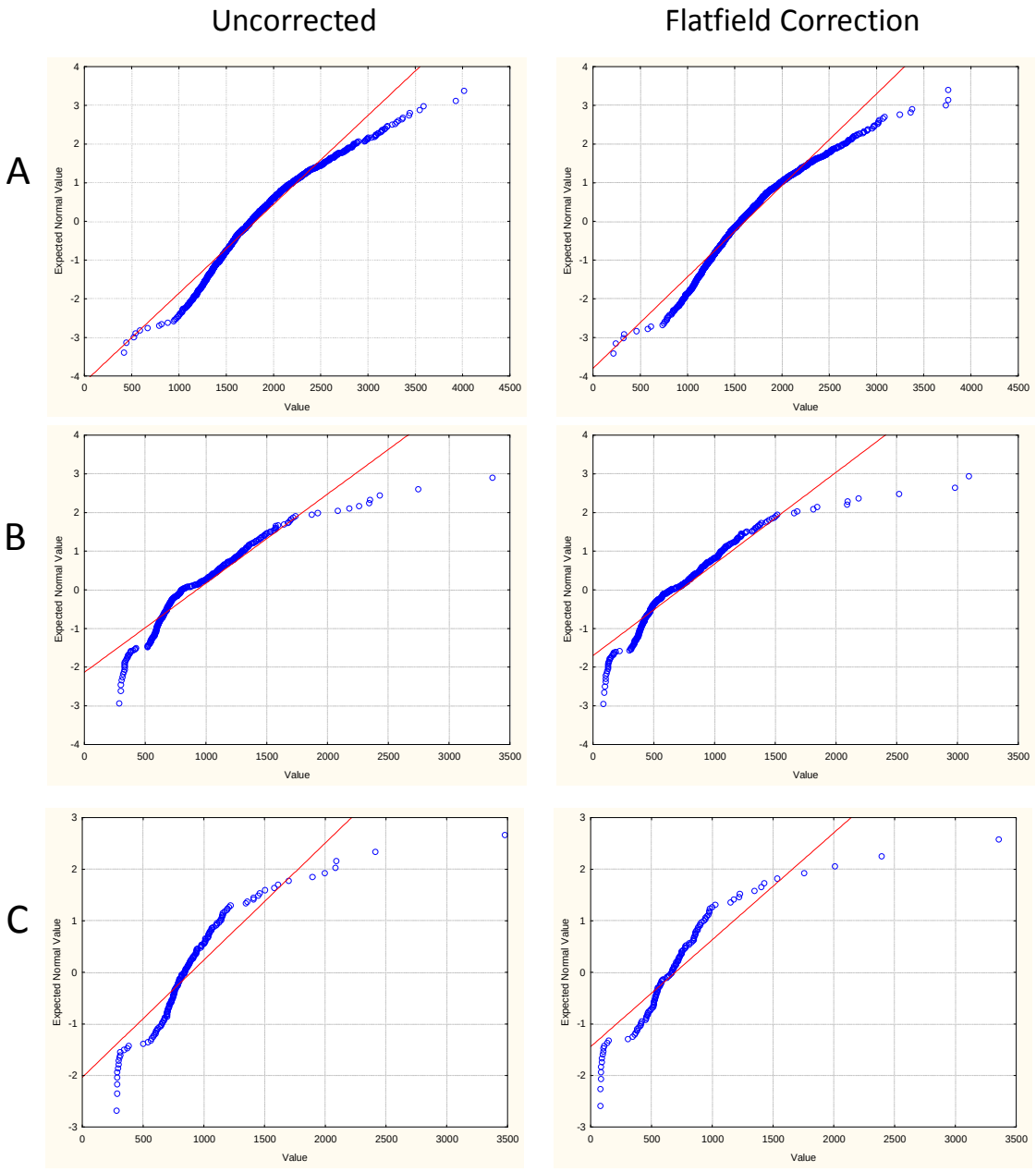

Figure 19. Flatfield correction for uneven microscope illumination has little effect on the distribution of GFP fluorescence intensity within the population. Normal probability plots of MX149 (pKTbla) cells with constitutive GFP expression. Samples of 0-hour inoculum (A), and cells washed from bean leaves at 1Hpi (B), and 3Hpi (C) were analyzed without (left) and with (right) flatfield correction.

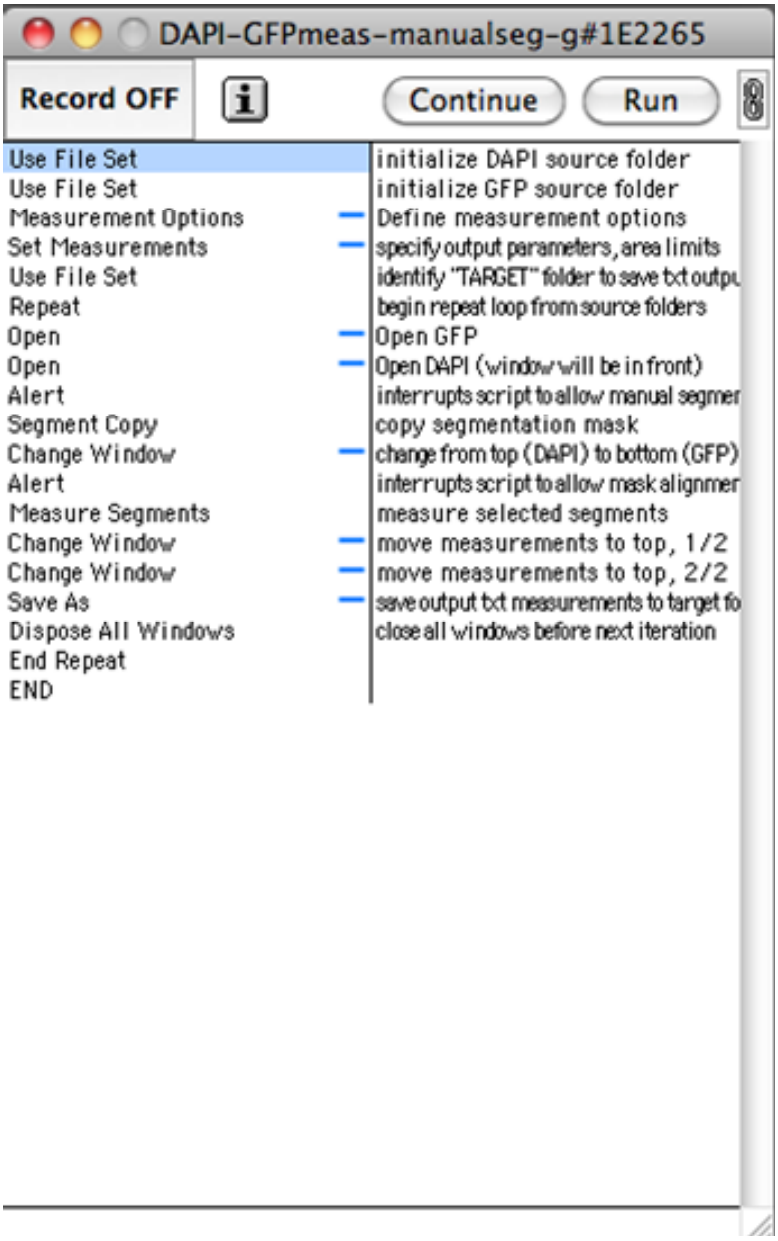

Figure 20. Automated macro for image processing in iVision.

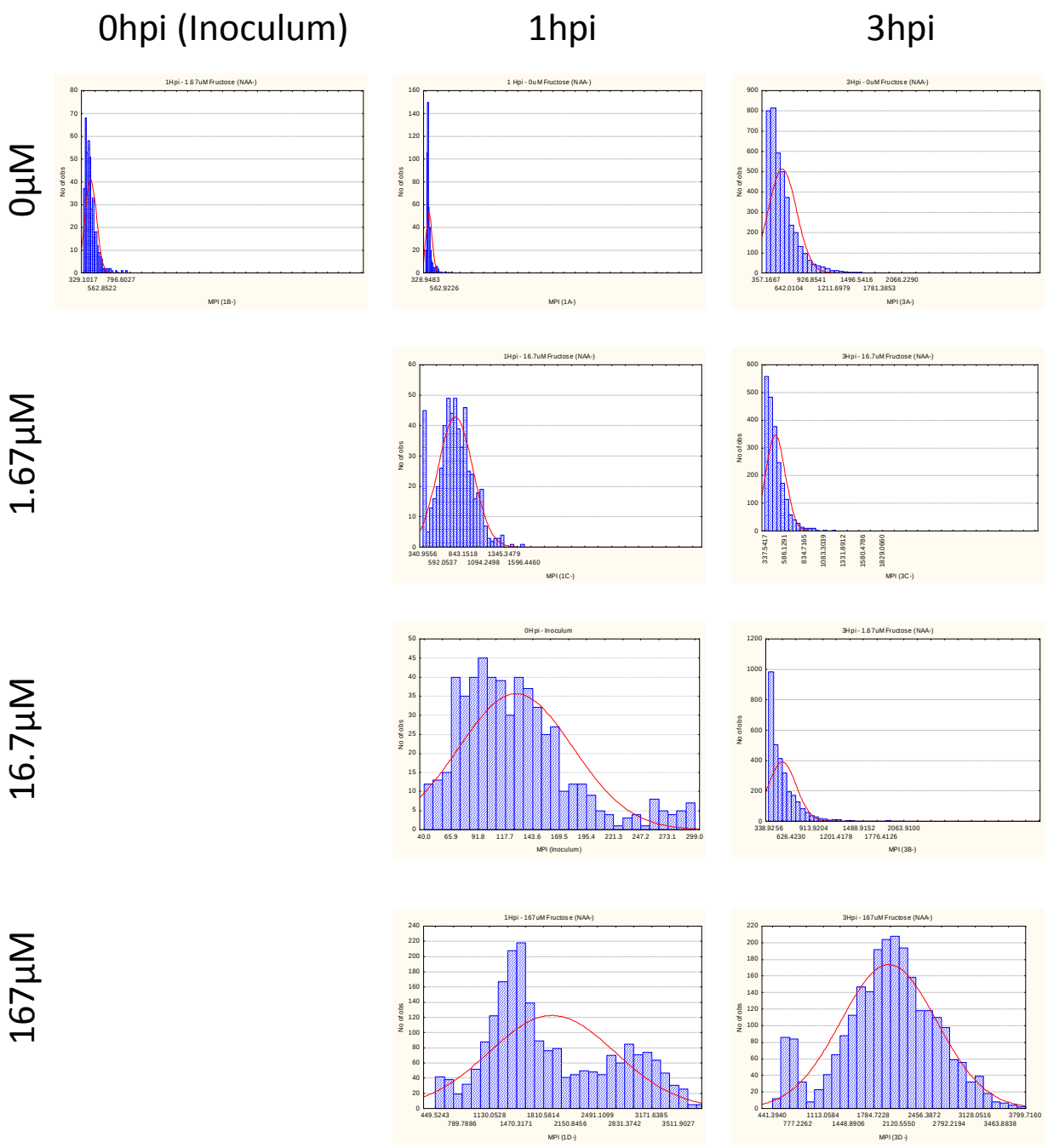

Figure 21. Fructose dose-response curve as imaged by fluorescence microscopy and quantitative digital image analysis. *Pa*299R (pFru46) cells were cultured in varying concentrations of fructose (indicated at left) and GFP reporter activity sampled at 1 and 3hpi (indicated above).

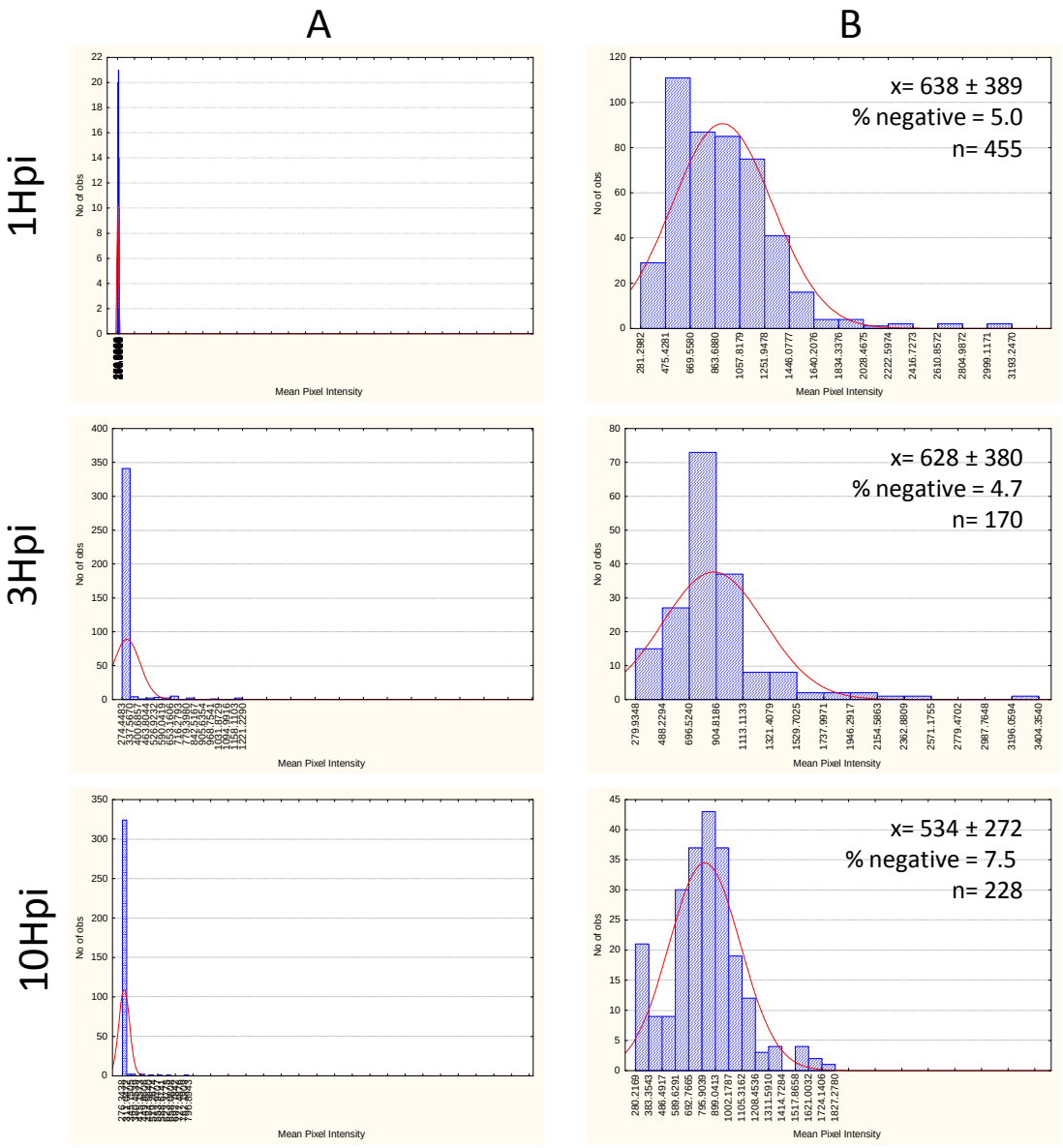

Figure 22. Sample fluorescence microscopy analyses of bacteria harvested from leaves at 1, 3, or 10 Hpi. GFP histograms display the distribution of fluorescence intensity within each population. Data were collected from plants inoculated with nonfluorescent *Pa*MX149 (A), or constitutive GFP-expressing 299R (pKTbla)(B). For 299R (pKTbla) samples, the mean (x) ± S.D, sample size (n), and percent of the population that was GFP-negative are indicated at top right. (GFP- cells are defined as MPI<93, which is the threshold defining the lowest 5th percentile of cellular fluorescence in the 1 hpi sample.)

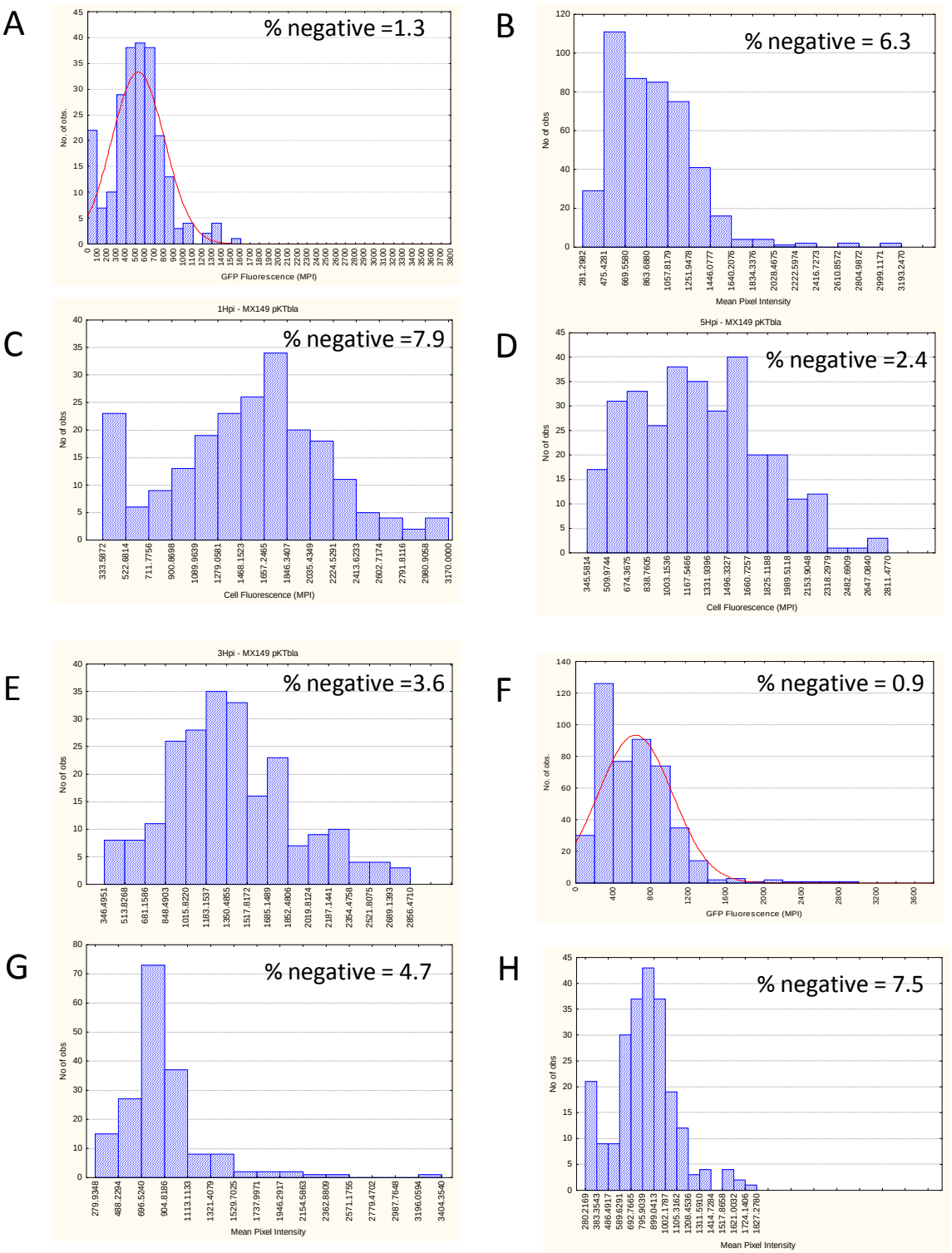

Figure 23. Constitutively positive *Pa*MX149 (pKTbla) samples recovered from bean leaves in multiple experiments or timepoints. The percentage of GFP-negative (contaminating) particles is also indicated.

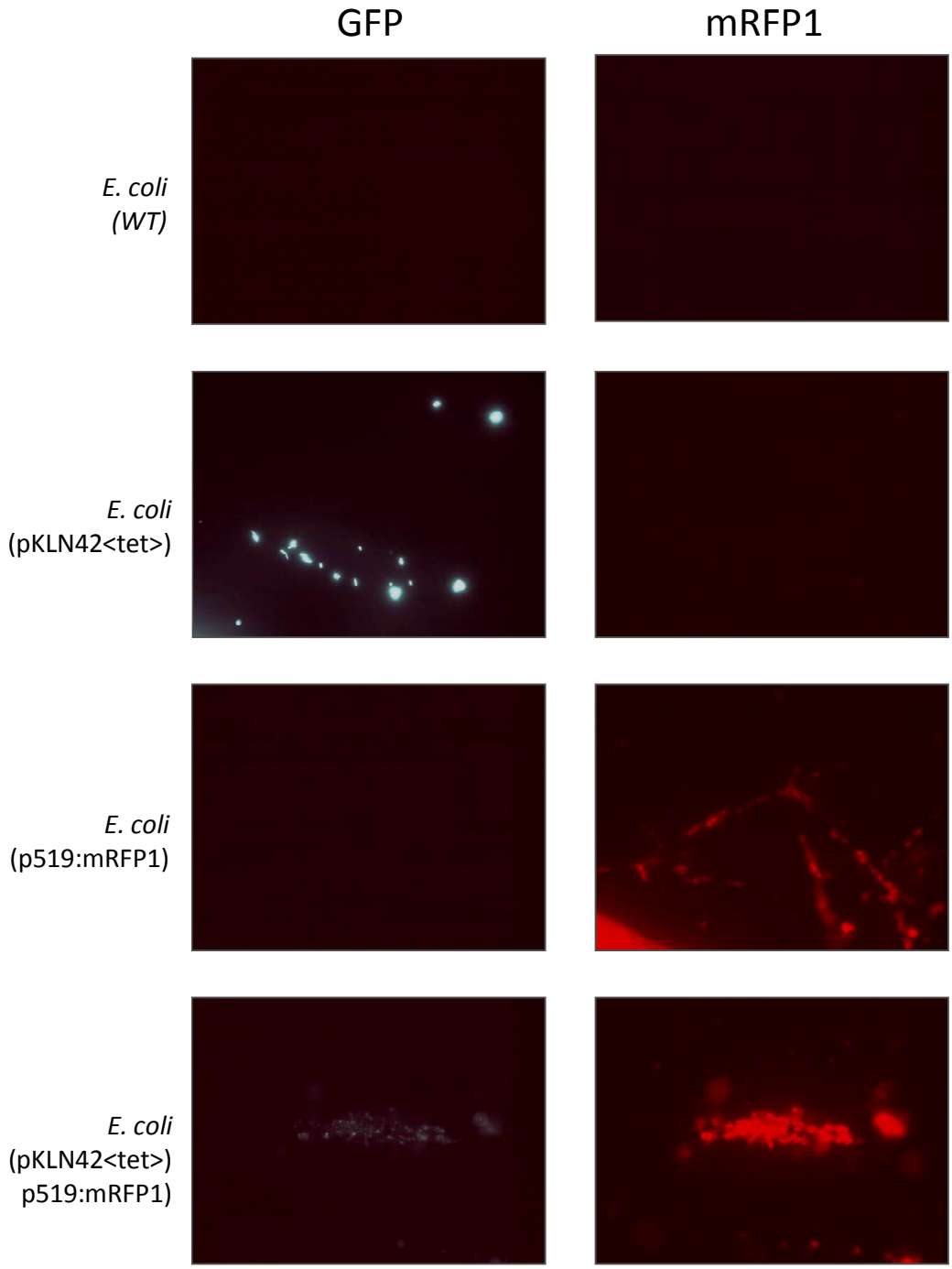

Figure 24. Evaluation of single- and dual-fluorescentce bacterial strains for mRFP1/GFP fluorescence using fluorescence microscopy. Bacteria expressing GFP (pKLN42<tet>), mRFP1 (p519:mRFP1), or both plasmids were photographed using GFP or dsRED filters and equal exposure settings.

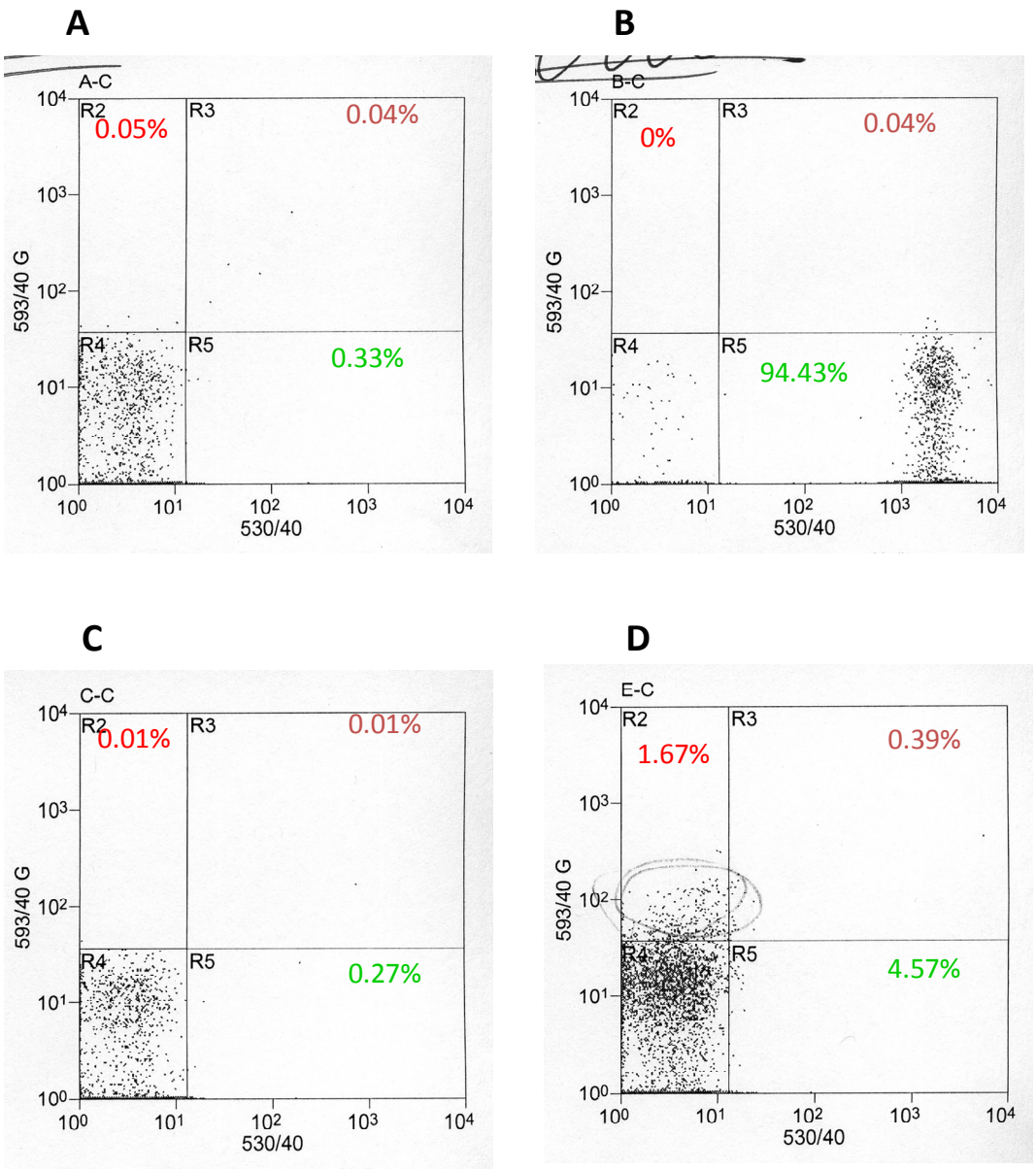

Figure 25. Evaluation of fluorescent bacterial strains for dual mRFP1/GFP fluorescence using the Cytopeia cell sorter, with dual excitation for GFP (488nm) and mRFP1 (575nm). Scatterplots depict relative fluorescence intensity of GFP (530/40; x-axis) versus mRFP1 (593/40; y-axis). The percentage of gated bacteria falling into the GFP-positive, mRFP1-positive, and dual-positive domains is also indicated. Results are shown for wild-type *E. coli* (A), constitutively green *E.c.*(pKLN42) (B), constitutively red *E.c.*(p519mRFP1) (C), and dual red/green *E.c.*(pKLN42/p519mRFP1)(D) strains.

A

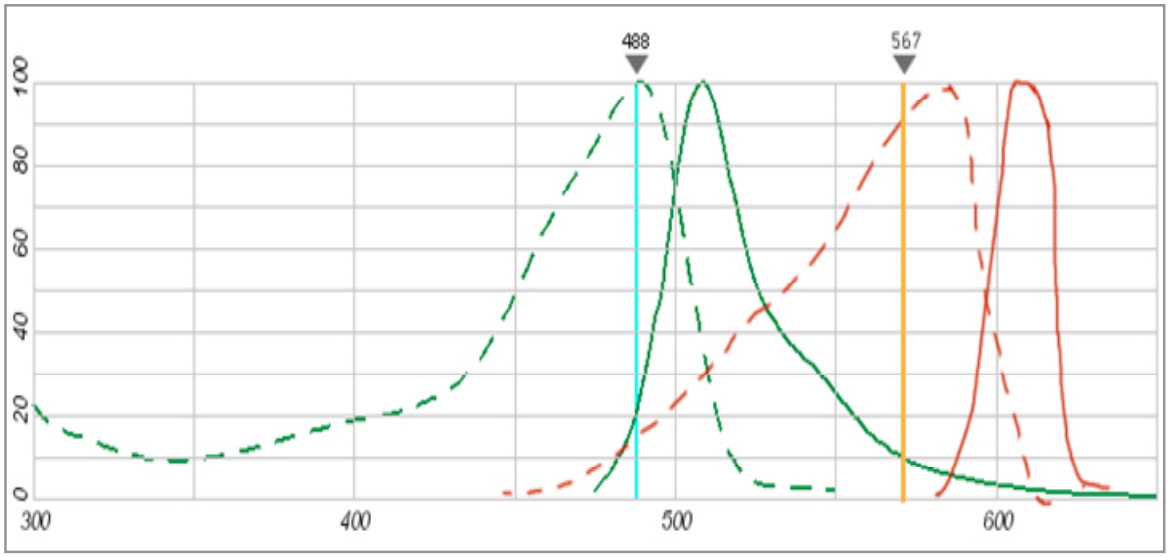

B

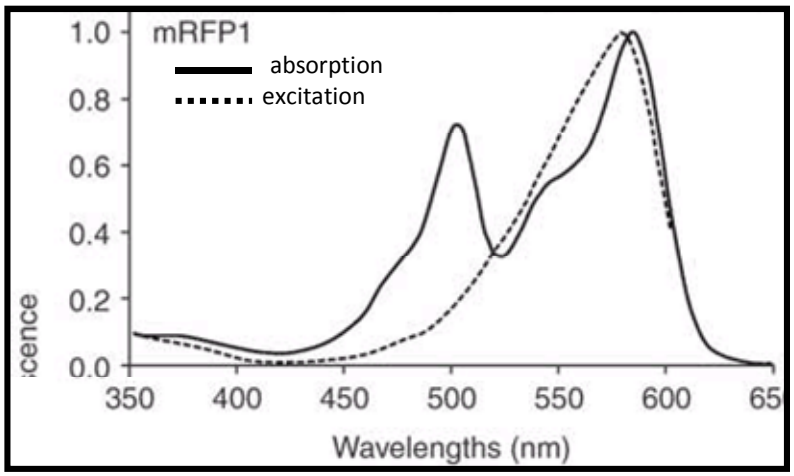

GFP:

*exc*λ=470nm

*em*λ=510nm

mRFP1:

*exc*λ=584nm

*em*λ=607nm

Figure 26. Excitation (dashed lines) and emission (solid lines) spectra of GFP (left) and mRFP1 (right) do not appear to overlap (A). However, mRFP was reported to have a nonexcitatory absorption peak at 500nm (figure from Campbell *et al*., 2002) that could explain GFP quenching observed in dual-expression biosensors (B).

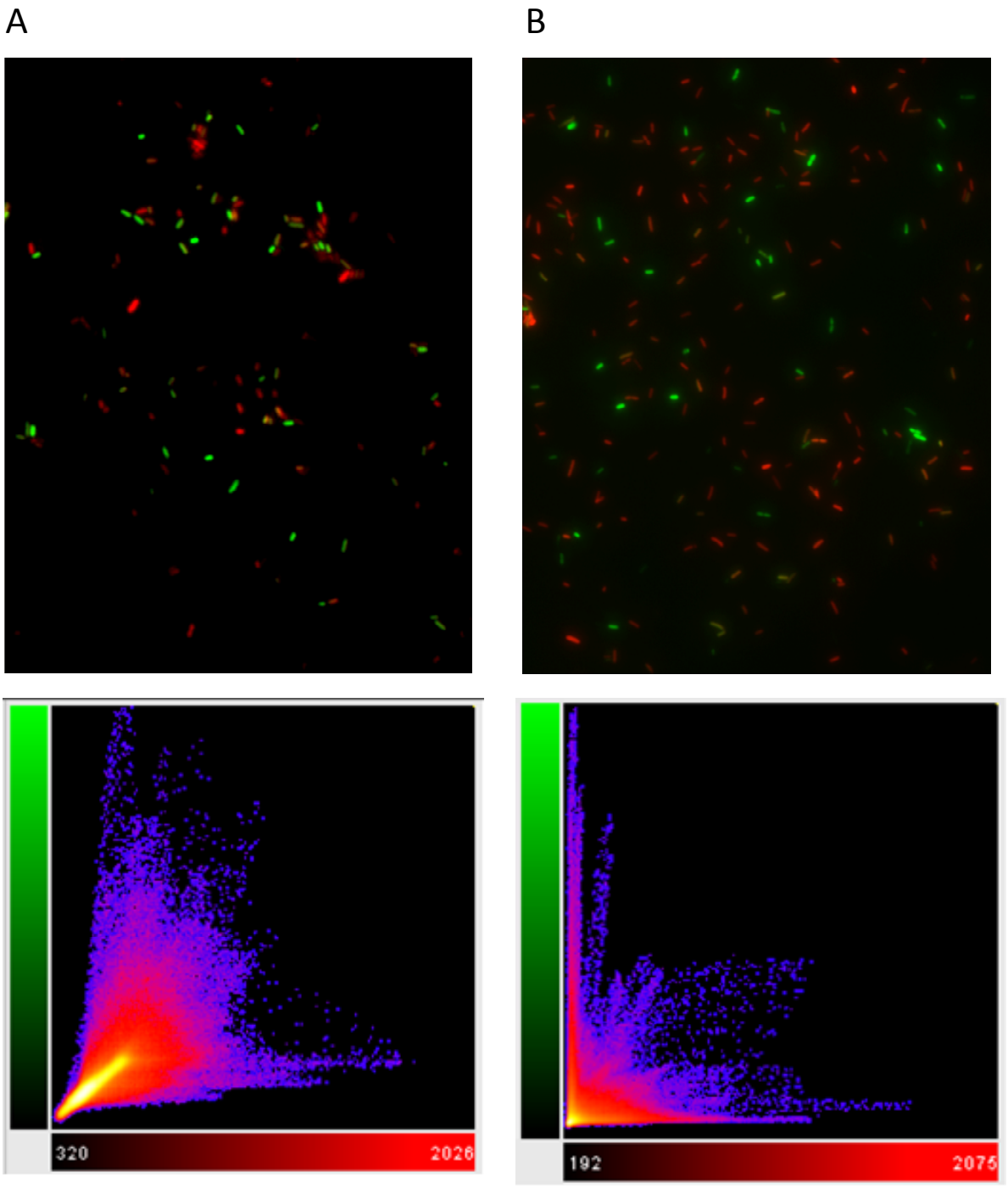

Figure 27. Microscopic image analysis of dual-fluorescent *Pa*299R strains constitutively expressing mCherry and GFP (p519mCherry/pKTbla) (A) or constitutive mCherry and a fructose-inducible GFP construct, grown under inducing conditions (p519mCherry/pFru46) (B). Colocalized images (top) display red and green fluorescence, with colocalized fluorescence in yellow. The same data as scatterplots (bottom) display the red (x-axis) and green (y-axis) fluorescence of each cell detected.

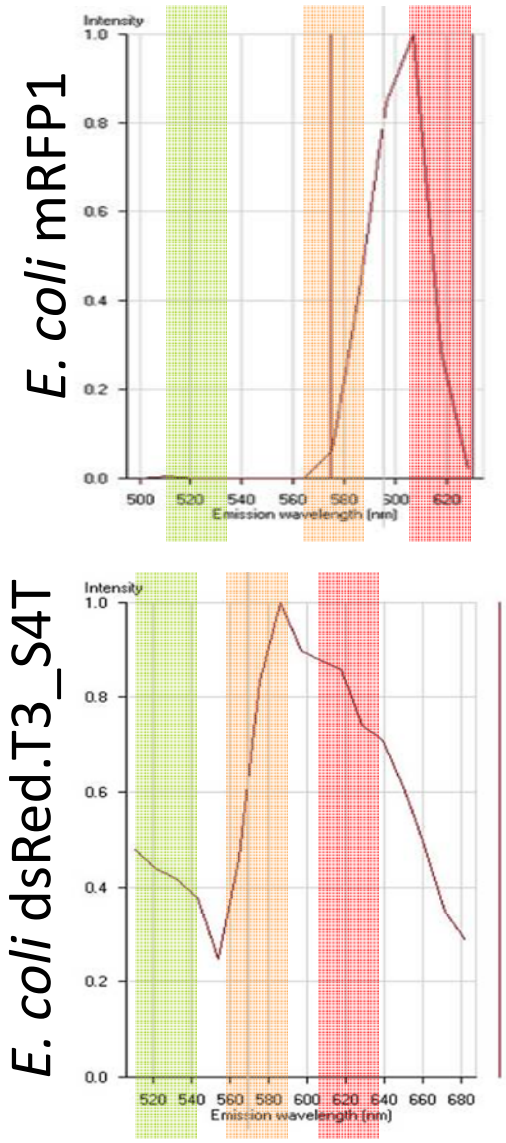

Figure 28. Emission spectra of mRFP1 and dsRed.T3_S4T as collected by confocal microscopy at excitation 488nm. From left to right, approximate detection ranges of the EPICS-XL flow cytometer for FL1 (green), FL2 (orange), and FL3 (red) are indicated as colored overlays.

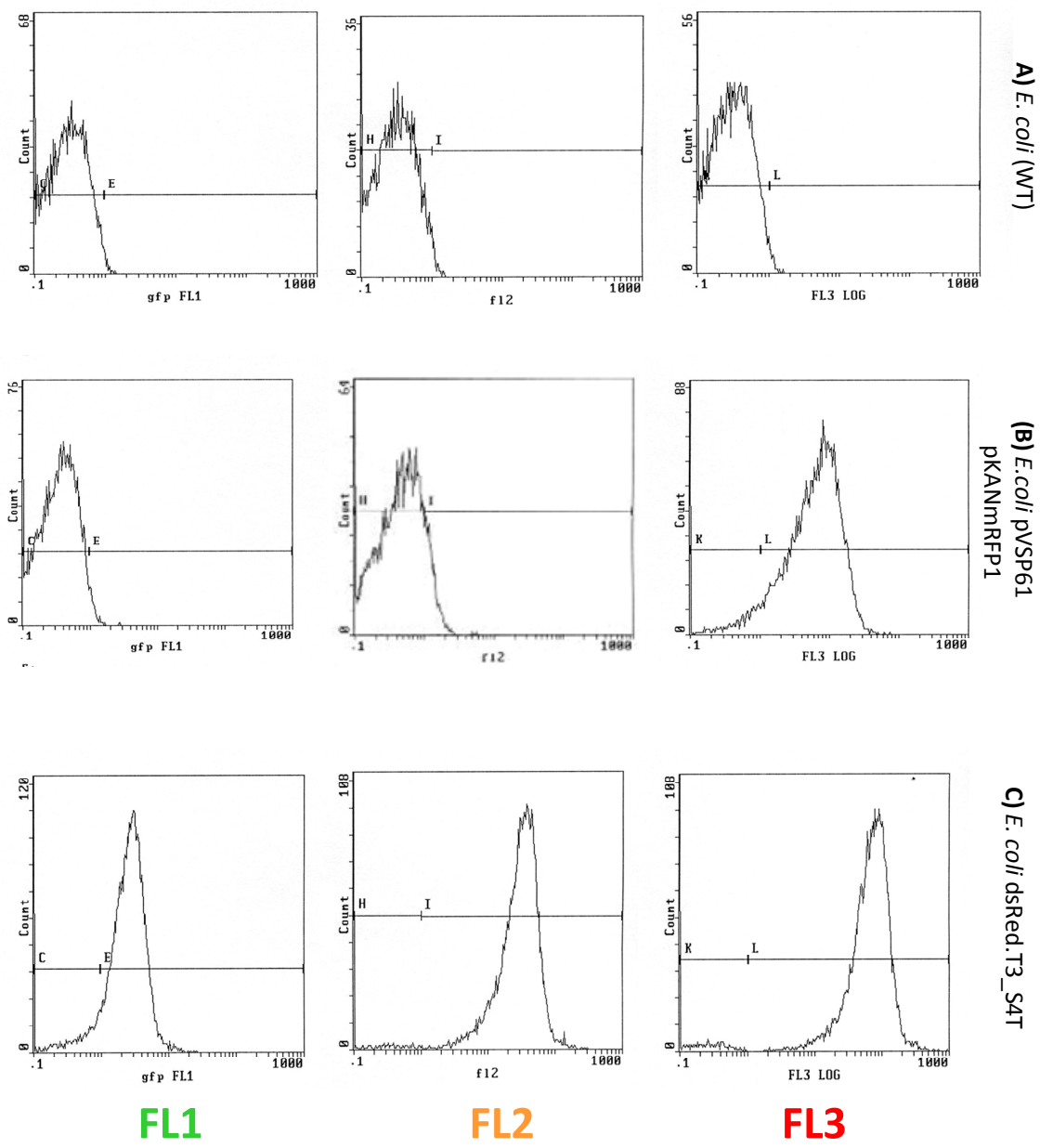

Figure 29. Cellular fluorescence among cultured *E. coli* cells expressing red fluorescent constructs, as detected by EPICS-XL flow cytometer. Fluorescence intensity histograms are displayed for FL1 (green), FL2 (orange), and FL3 (red) channels. Wild-type *E. coli* is shown as a negative control (A); *E. coli* expressing mRFP1 (B) or the dsRed derivative T3.S4T (C) are also shown.

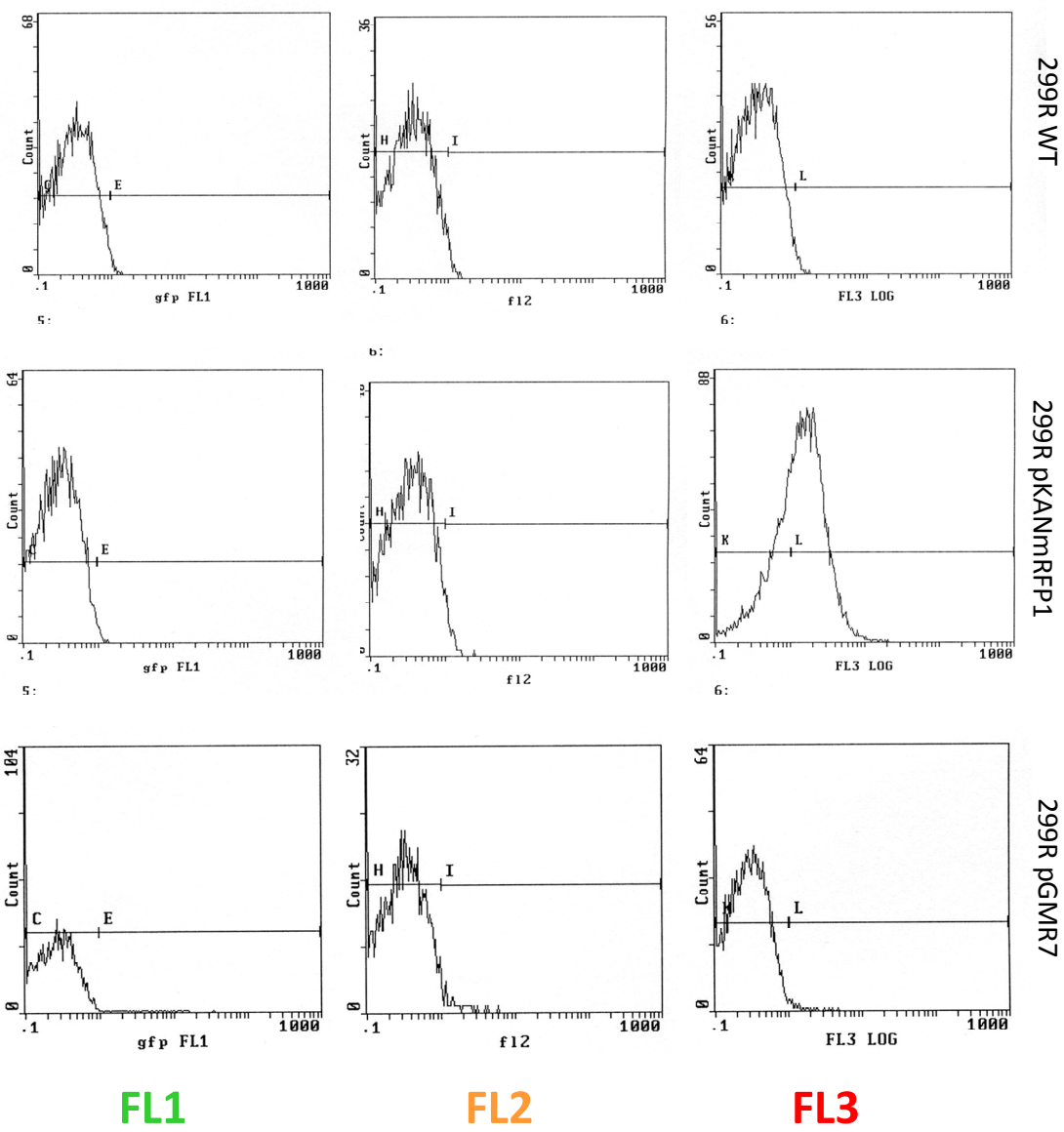

Figure 30. Cellular fluorescence among cultured *P. agglomerans* 299R cells expressing red fluorescent constructs, as detected by EPICS-XL flow cytometer. Fluorescence intensity histograms are displayed for the FL1 (green), FL2 (orange), and FL3 (red) channels. Wild-type 299R is shown as a negative control (A); *Pa*299R expressing mRFP1 driven by a strong promoter (B) or the dsRed derivative T3.S4T (C) are also shown.

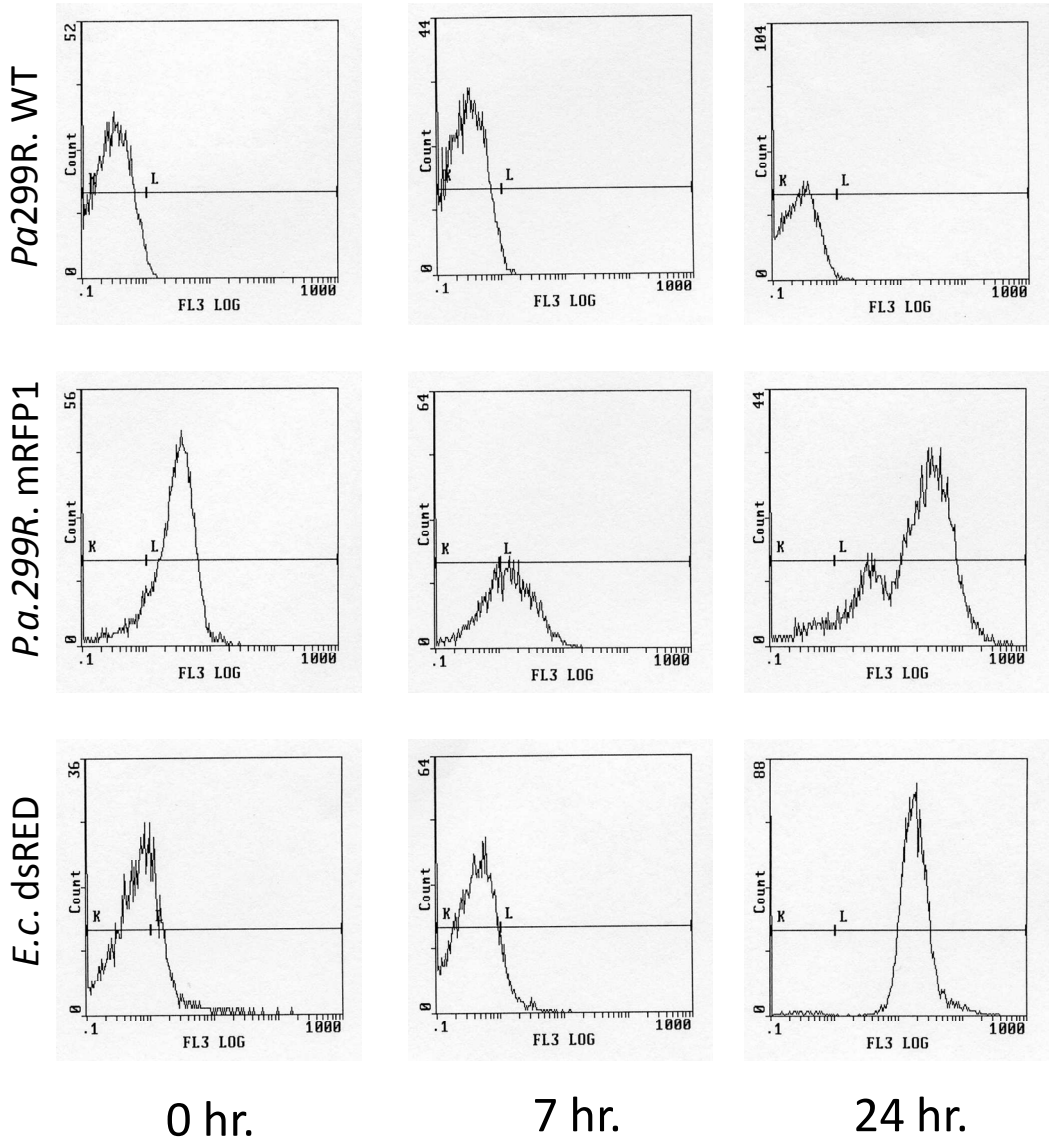

Figure 31. Fluorescence intensity accumulates over time in *P. agglomerans* 299R cultures expressing red fluorescent constructs, as detected by EPICS-XL flow cytometer.

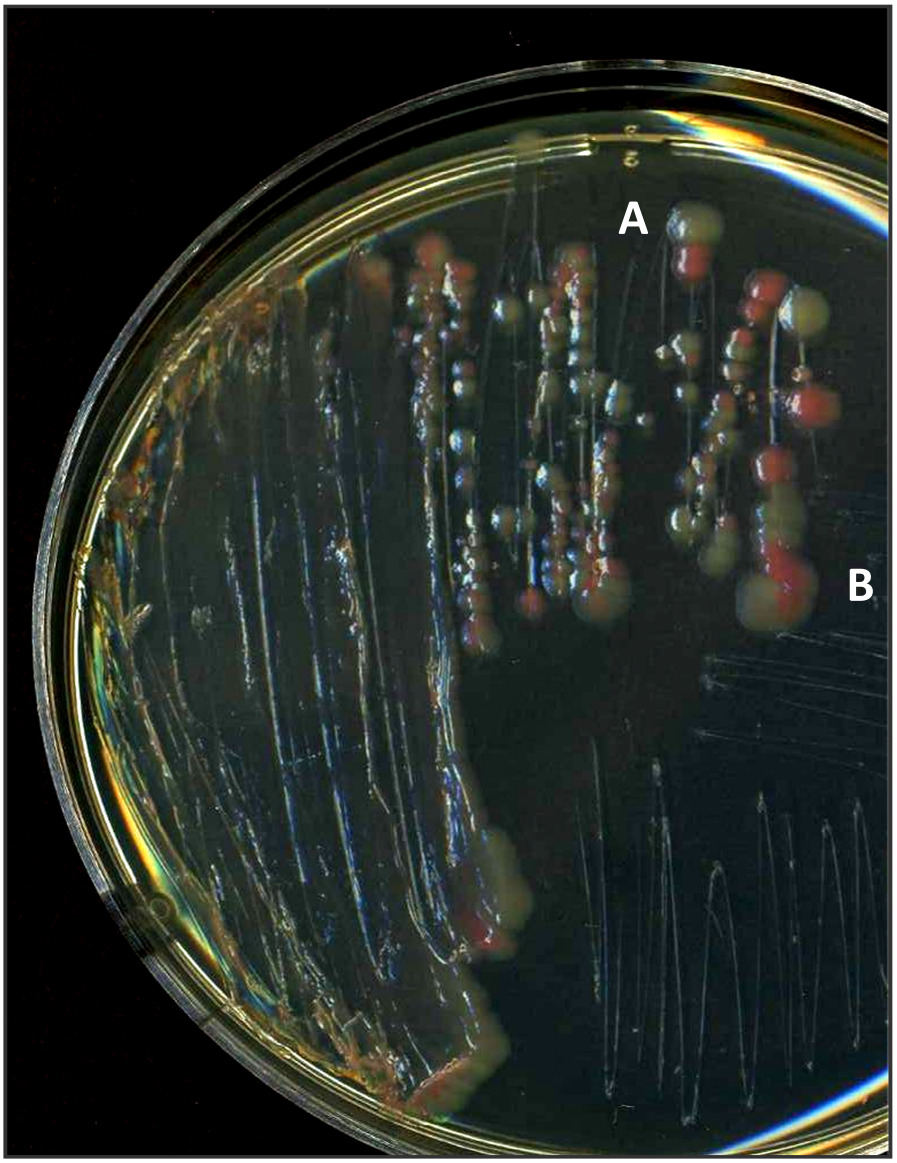

Figure 32. *P. agglomerans* 299R cultures expressing dsRed.T3.S4T. often experienced spontaneous loss or inactivation of the red fluorescent plasmid, even in cultures recently streaked from frozen stocks. Mixed (A) and sectored colonies (B) are indicated.

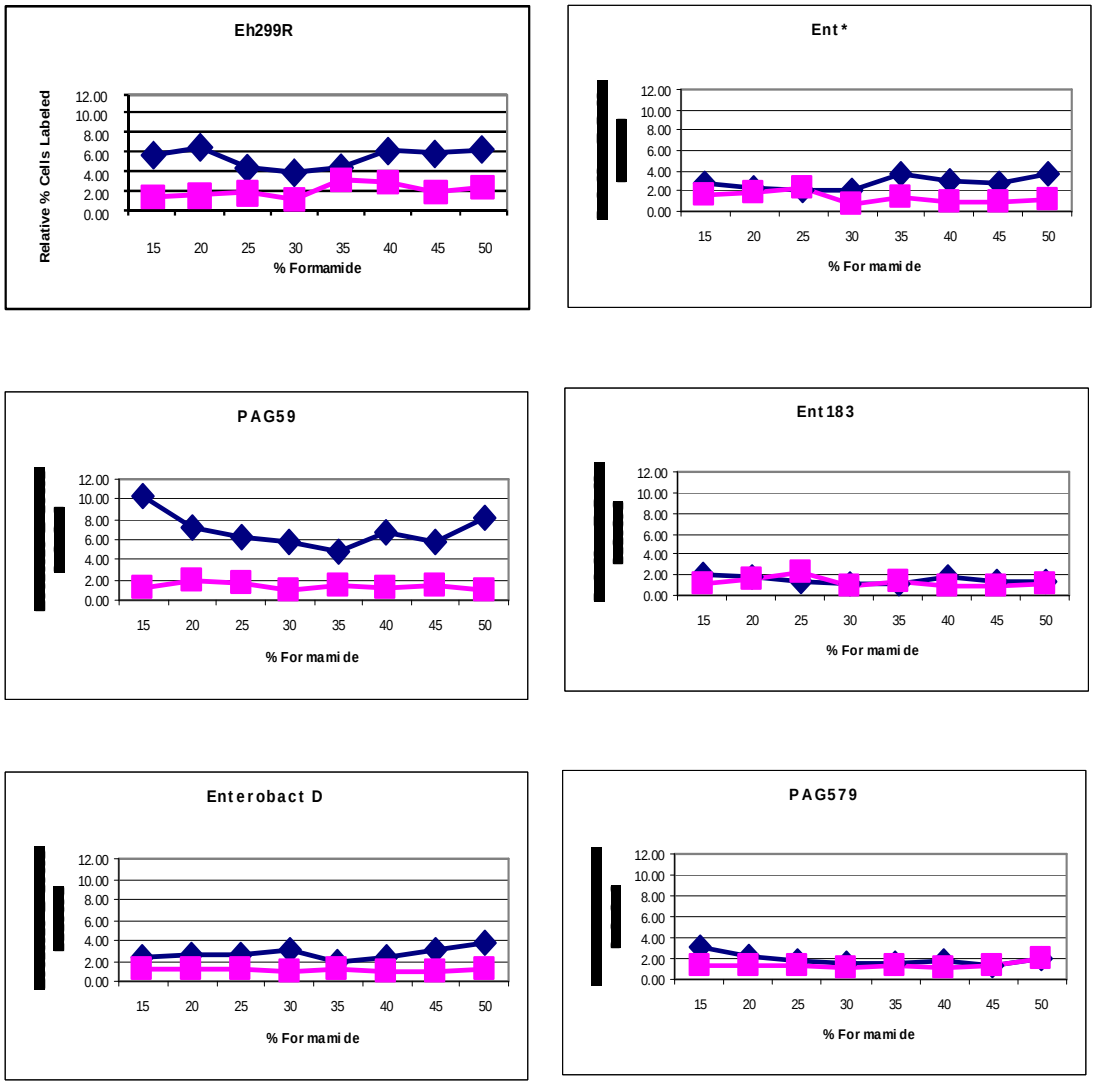

Figure 33. FISH hybridization efficiency of 6 candidate probes under a range of fixation stringencies. Probes were hybridized to cultured cells of either the target strain, *P. agglomerans* 299R (blue diamonds), or *Pseudomonas syringae* B728a (purple squares) as a negative control. Graphs indicate the percentage of positively labeled cells as determined by flow cytometry.

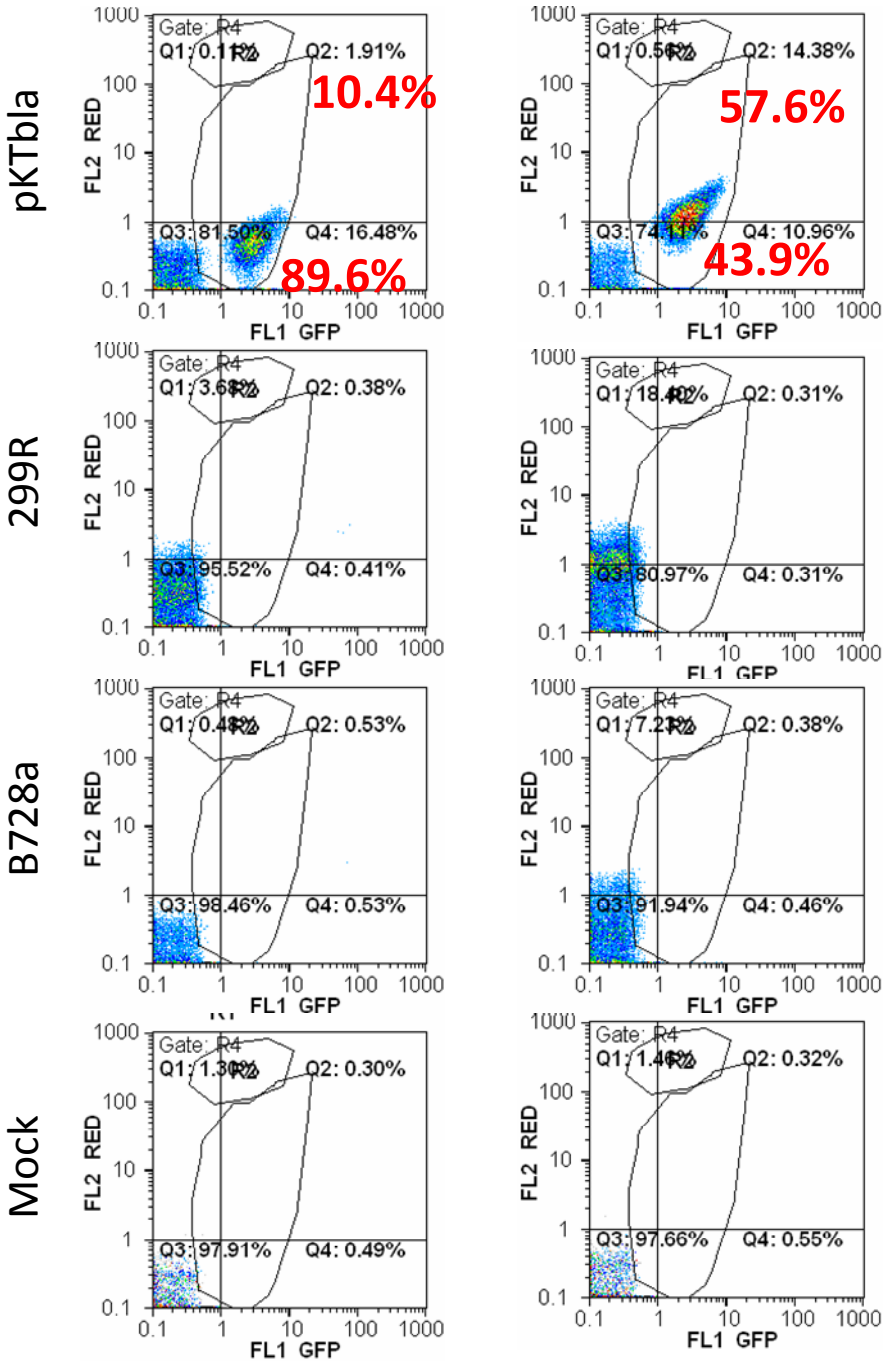

Figure 34. FISH staining of leaf-harvested bacterial samples with the *Pa*299R-specific , red-fluorescent conjugated probe Pa299R. Scatterplots of green (FL1) versus red (FL2) fluorescence are shown for unstained (left) or FISH stained (right) bacterial samples harvested from bean leaves. The % of red-fluorescent target cells is also indicated for the *Pa*299R (pKTbla) treatments.

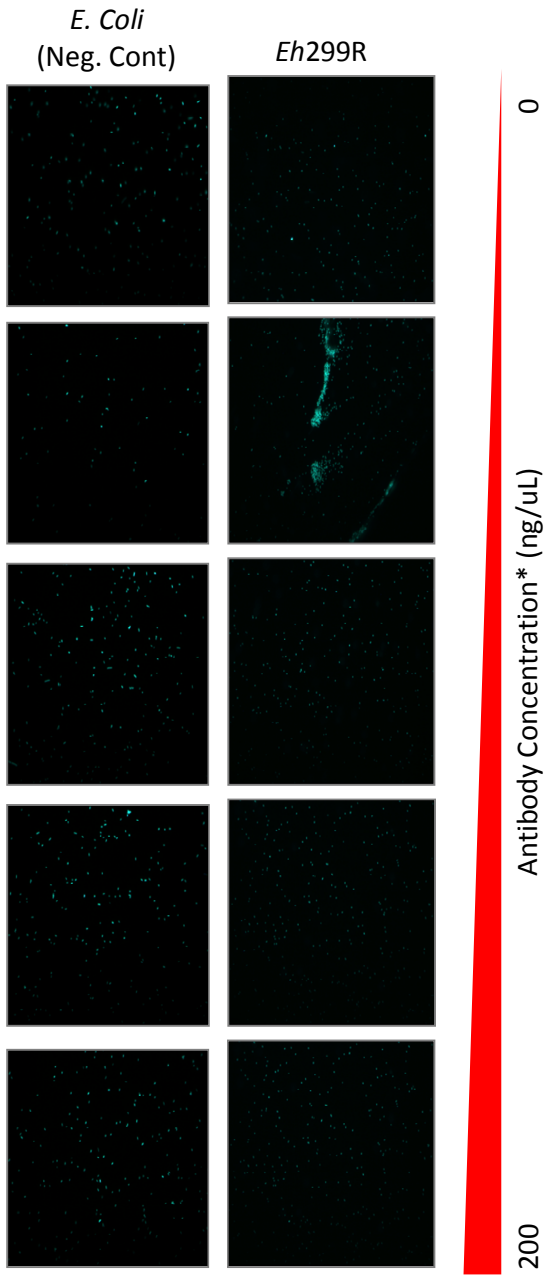

Figure 35. Agglutination assays were conducted by incubating *Eh*299R or a negative control strain in various concentrations of rabbit anti-*Erwinia herbicola* antibody. No consistent agglutination was observed.

A

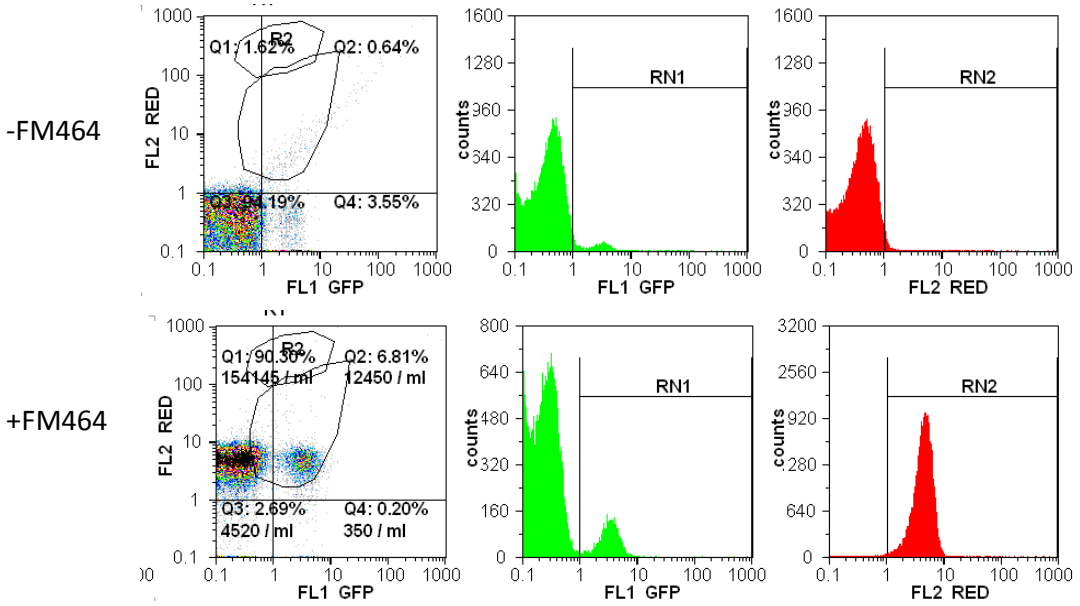

B

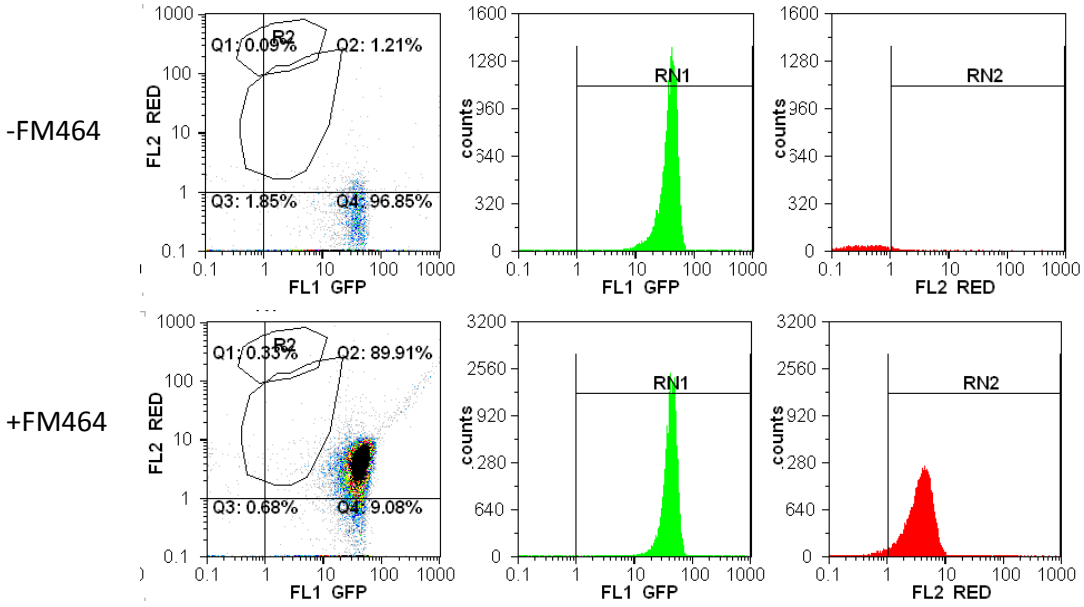

Figure 36. FM464 staining of *Pa*299R (A) or constitutively GFP-positive *Pa*299R (pKTbla) (B). Scatterplots and single- parameter histograms of green (FL1) and red fluorescence (FL2) are shown for unstained (-FM464) and stained (+FM464) samples of *in vitro* cultured cells.

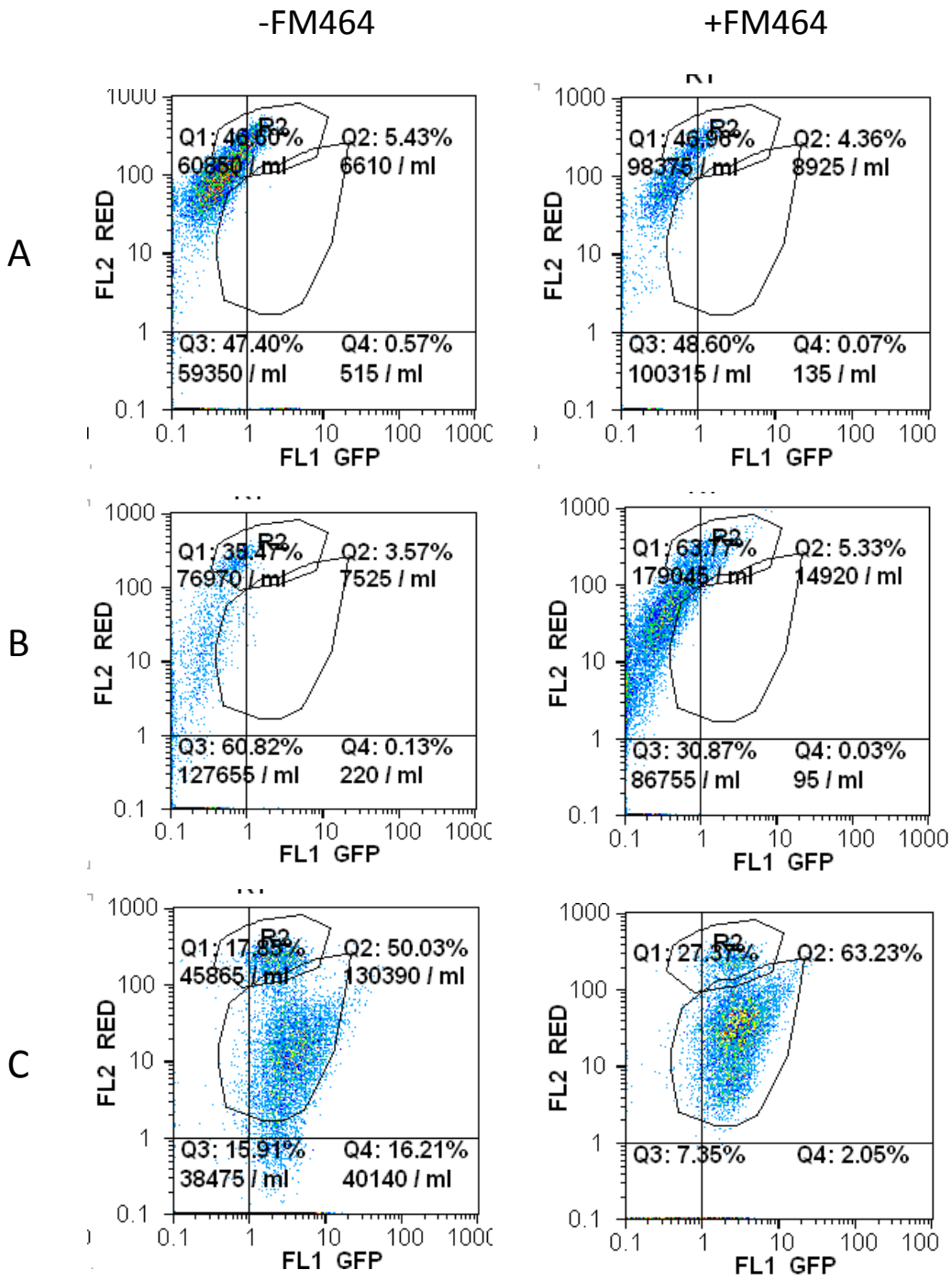

Figure 37. FM464 staining of samples harvested from bean leaves inoculated with a mock treatment (A), *Pa*299R (B), or constitutively GFP-positive *Pa*299R (pKTbla) (C). Scatterplots of green (FL1) and red fluorescence (FL2) are shown for unstained (-FM464) and stained (+FM464) replicates of each sample. Similar results were obtained in 2 independent experiments.

Hpi	Segmentation Method	n	Mean Cellular Fluorescence (MPI)	Minimum	Maximum	S.D.
0	Auto	2342	1376.1	413.2	3145.0	287.1
	Manual	1963	1718.5	415.1	3936.8	401.6
1	Auto	376	668.4	276.2	2358.0	291.7
	Manual	467	799.4	280.3	2679.3	330.8
3	Auto	156	604.8	277.5	1828.3	265.3
	Manual	184	801.1	279.3	3248.7	341.5

Table 1. Mean fluorescent pixel intensity (MPI) in auto- versus manually segmented images of *Pa*MX149 (pKTbla) cells

A

Hpi	n	Mean MPI	Minimum MPI	Maximum MPI	Variance	S.D.	S.E.
0	5	393	367	413	305.10	17.47	7.81
1	5	282	279	285	7.81	2.79	1.25
3	7	277	274	280	3.47	1.86	0.70

B

Hpi	n	Mean MPI	Minimum MPI	Maximum MPI	Variance	S.D.	S.E.
0	10	349	322	454	1998.65	44.70	14.13
1	10	326	322	335	13.61	3.69	1.16
3	10	334	320	359	162.43	12.74	4.03
5	10	326	322	329	4.63	2.15	0.68
7	10	337	328	377	216.49	14.71	4.65

Table 2. Descriptive statistics for mean background fluorescence of microscopy images taken of *Pa*MX149 (pKTbla) cells from the sample image dataset (A) and a second, independent experiment (B)

Fluorescent Material	Excitation maximum (nm)	Emission maximum (nm)	Reference
GFP	488	507	Shaner *et al*., 2005
5-FAM (5'-conjugated fluorophore)	492	518	*n/a*
DsRed.T3_S4T	560 (excites efficiently at 488)	589	Sorensen et al, 2003
mRFP1	584	607	Campbell *et al.*, 2002
mCherry	587	610	Shaner *et al.*, 2004
FM4-64 (membrane dye)	506	750	*n/a*
DY-480XL (5'-conjugated fluorophore)	500	630	*n/a*

Table 3. Properties of red fluorescent proteins, dyes, and fluorophores

Flow Cytometer	Excitation (nm)	Detection of GFP Fluorescence	Detection of Red Fluorescence
Beckman-Coulter EPICS XL	488	425nm bandpass	575nm bandpass (FL2) 620nm bandpass (FL3)
Partec CyFlow particle analyzer	488	425nm bandpass	575nm bandpass (FL2) 620nm bandpass (FL3)
Beckman-Coulter EPICS Elite cell sorter	488	425nm bandpass	575nm bandpass (FL2) 620nm bandpass (FL3)
Cytopeia INFLUX cell sorter	488, UV, 405, 567, and 632	11 different detectors	11 different detectors

Table 4. Optical properties of flow cytometers used in this work.

Probe	Sequence (5′ → 3′)	MT (°C)	Source
Eh299R	GAG TTC CCG CCA TCA CG	56.2	Brandl *et al.*, 2001
PAG59	TGT GCT ACC GTC CGA CTT	56.1	Nakanishi *et al.*, 2006
Enterobact D	TGC TCT CGC GAG GTC GCT TCT CTT	64.0	Ootsubo *et al.*, 2002
Ent*	CCC CCT CTT TGG TCT TGC	56.3	Kempf *et al.*, 2000
Ent183	CTC TTT GGT CTT GCG ACG	53.7	Friedrich *et al.*, 2003
Pag299R-579	TTA ACA GAC CGC CTG CGT	57.0	This work

Table 5. Candidate FISH probes for fluorescent labeling of *P. agglomerans* 299R.